THE DEVELOPMENT OF AN ULTRASONIC

DOPPLER BED-LOAD VELOCIMETER

MARK DORON LAZARUS

BSc (Electrical Engineering)
University of Cape Town

A Thesis submitted in full fulfilment of the requirement for the degree of Master of Science in the Department of Electrical Engineering, University of Cape Town

September 1989

Electrical Engineering Department
University of Cape Town
South Africa

DECLARATION

I hereby declare that this dissertation is my own work except where specific acknowledgement is made, and that it has not been submitted before for any degree or examination at any other University.

Signed by candidate

Mark Doron Lazarus

30 September 1989

DEDICATION

To my Parents.

ABSTRACT

A instrument has been developed for measuring the velocity of solid particles adjacent to the pipe wall in a solids-liquid pipeline. It has been based on the Doppler shift principle and employs ultrasonic methods for detecting the bed-load particle velocity. Its application is in the mining industry for measuring the bed-load velocity of high concentration slurries such as in tailings and backfill hydraulic pipelines.

Analyses have been conducted to investigate methods for increasing the accuracy of detecting the bed-load particle velocity. These methods have been implemented in the design of the transducer and the electronic circuitry. The system was tested using a simulation test-rig, hydraulic test-loops and at two industrial mining locations.

ACKNOWLEDGEMENTS

I would like to thank the following people:

Dr. R.M. Braun, the supervisor of this thesis, for his assistance and ideas.

Prof. J.H. Lazarus, my father, who provided assistance with the Hydraulic transportation concepts.

Miss. M. Vogel for her loyal and committed support and encouragement throughout my thesis.

Mr. S. Schire, Mr. D. Kenyan, Mr. I. Von Guerard, Mr. G. Bertuzzi and Mr. D. Botha for their technical assistance.

Rossing Uranium, Namibia; ERGO, Transvaal; Chamber of Mines for their respective sponsorship and for allowing me to conduct tests at their sites.

To my family and friends who supported me in their various ways.

The CSIR for the financial funding I received.

TABLE OF CONTENTS

LIST OF FIGURES **Page**

LIST OF TABLES

NOMENCLATURE

ABBREVIATIONS:

DDRR	Doppler Dynamic Range Reduction
F-V	Frequency to Voltage converter
PDF	Probability Density Function
PSD	Power Spectral Density
Rx.	Receiver
S/N	Signal to noise ratio
Tx.	Transmitter
UDBV	Ultrasonic Doppler bed-load Velocimeter
V-I	Voltage to current converter
V	Volts
v	velocity
ZCC	Zero crossing counter

NOMENCLATURE:

$a(z)$	Axial Intensity Distribution	
A	Surface area of backscattering target	
A_V	Doppler Gain	
AI	Axial Index	dB
AI_F	Focused Axial Index	dB
AI_R	Axial Index of the Rx.	dB
AI_T	Axial Index of the Rx.	dB
A_T	Comparator trigger volatge	V
$b(\theta)$	Directivity Intensity Distribution	
c	Ultrasonic velocity	m/s
C_A	Pre-amp input shunt capacitance	pF
C_M	Vibrational stiffness responsible for the restoring force in the mechanical resonance of the crystal	pF
C_0	Electrical capacitance of the crystal	pF
c_{SL}	Ultrasonic velocity in slurry layer	m/s

c_{TW}	Ultrasonic velocity in transducer window material	m/s
c_{PW}	Ultrasonic velocity in pipe-wall material	m/s
d	Effective transmission axial path length	mm
d_{PW}	Pipe-wall thickness	mm
$d_{PW(E)}$	Effective pipe-wall thickness	mm
d_S	Conductivity probe spacing	mm
D	Demodulated Doppler signal amplitude	
D(t)	Demodulated (after filtering) Doppler signal	
D_{BED}	Bed-load Doppler signal amplitude	
$D_M(t)$	Multiplicative (synchronous) demodulated Doppler signal	
D_{SUS}	Suspended-load Doppler signal amplitude	
DF_{BED}	Bed-load Doppler signal amplitude after DDRR filter	
DF_{SUS}	Suspended-load Doppler signal amplitude after DDRR filter	
$DI(\theta)$	Directivity Index	dB
$DI_R(\theta)$	Directivity Index of the Rx.	dB
$DI_T(\theta)$	Directivity Index of the Tx.	dB
$DI_F(\theta)$	Focused Directivity Index	dB
DR	Doppler Dynamic Range	
DR'	Doppler Dynamic Range after DDRR filtering	
f_{BW}	3dB Doppler signal bandwidth due to finite beamwidth broadening effects	Hz
f_{DB}	3dB Doppler signal bandwidth due to combination of broadening effects	Hz
$f_{D(BED)}$	Doppler frequency from bed-load particle velocities at a height of h	Hz
$f_{D(RMS)}(h)$	RMS Doppler frequency	Hz
$f_{D(SUS)}(h)$	Doppler frequency from suspended-load particle velocities at a height of h	Hz
f_{DV}	3dB Doppler signal bandwidth due to particle velocity fluctuation, ignoring broadening effects	Hz

$f_D(max)$	Maximum detectable Doppler frequency	Hz
f_R	Receiver frequency	Hz
f_S	Series resonant frequency	kHz
f_S'	Loaded series resonant frequnecy	kHz
f_T	Transmitter frequency	Hz
f_{TT}	3dB Doppler signal bandwidth due to finite transit-time broadening effects	Hz
f_Z	Expected frequency measurement of the F-V (ZCC)	Hz
f_{3dB}	3dB bandwidth of a crystal	kHz
h	Height up from the pipe soffit of moving particles	mm
h_{BED}	Actual height of bed-load layer (beginning of suspended-load layer)	mm
h_{MAX}	Maximum height of insonified volume within pipeline	mm
h_E	Effective height up from the pipe soffit of moving particles	mm
H	Defined height up from pipe soffit of begining of suspended-load	mm
H_E	Effective height up from pipe soffit of begining of suspended-load	mm
I_B	Required current to be delivered by the current buffer	mA
J_1	First order Bessel function	
k	Wave number	
k_C	fraction of the carrier signal	
k_D	Doppler constant relating Doppler frequency to particle velocity	
k_σ	Standard deviation constant: Ratio of standard deviation to mean Doppler frequency	
k_T	Threshold voltage constant of comparator	
$k_p(H)$	Penetration constant (ratio of $P_{SUS}(H)$ to $P_{BED}(0)$)	
k_S	Scaling constant	
Ios	Offset output current (usually set to 4mA)	
Iout	Output current (0/4-20mA)	mA

I_z	Axial intensity at a radial distance of z	
I_0	Maximum axial intensity	
L_M	Equivalent mass of vibrating crystal	mH
N	Number of calculations on spreadsheet	
p	Position of a cross-correlation function peak	
$P_{BED}(h)$	Relative backscattering power from the bed-load at h where h < H	
$P_{SUS}(h)$	Relative backscattering power from the suspended-load at h where h ≥ H	
r	Crystal radius	mm
R	Received signal amplitude	
R(t)	Received signal	
R_A	Input shunt resistance of pre-amp	Ω
R_B	Received Breakthrough signal amplitude	
$R_B(t)$	Received Breakthrough signal	
R_D	Received Doppler signal amplitude	
$R_D(t)$	Received Doppler signal	
R_{LOSS}	Energy dissipation within a crystal	Ω
R_{RAD}	Ultrasonic radiation	Ω
R_{TOT}	Total of energy dissipation and ultrasonic radiation within a crystal	Ω
TL_F	Focused Total Intensity Index	dB
S	Surface Backscattering strength from a target	
$S_D(f_D)$	Overall Doppler PSD due to the detection of a fluctuating velocity including broadening effects	
$S_{DV}(f_D)$	Doppler PSD due to the detection of a fluctuating velocity neglecting broadening effects	
$S_{DB}(f_D)$	Doppler PSD due to all the broadening effects	
t_D	Delay time of delay circuit module	ms
t_M	Width of monostable pulse	ms
T(t)	Tx. signal	
TL_F	Focused Total Intensity Index	dB
TL_P	Peak Total Intensity Index	dB
v	Particle velocity	m/s

v_{BED}	Mean bed-load velocity, defined for $v_{M2} < v_M < v_{M3}$	m/s
$v_{BED}(h)$	Mean bed-load velocity at a height of h, defined for $v_M > v_{M3}$	m/s
v_M	Mean particle velocity	m/s
v_{MAX}	Maximum velocity to be detected (=5m/s)	
v_{M1} v_{M2} v_{M3} v_{M4}	Mean mixture transition velocities	m/s
$v_{SUS}(h)$	Mean suspended-load velocity at a height of h	
V_{FV}	Output volatge from the F-V converter	V
V_{PP}	Peak to peak voltage out of oscillator	V
V_{RMS}	RMS voltage out of the oscillator	V
V_{VI}	Output volatge from the current to voltage converter	V
V_{VI}	Output voltage from the velocity scaling circuit	V
z	Axial distance	mm
z_R	Axial distance from the Rx. crystal face	mm
z_T	Axial distance from the Tx. crystal face	mm
α	Attenuation constant	
β	Ratio of the total 3dB bandwidth to the mean Doppler frequency	
β_{TT}	Transit-time spectral broadenind width expressed as a ratio of the mean Doppler frequency	
β_{BW}	Beamwidth spectral broadened width expressed as a ratio of the mean Doppler frequency	
σ_D	Standard deviation of Doppler signal due to all the causes of spectral spreading	
$\sigma_{DF(BED)}$	Standard deviation of DF_{BED} signal	
$\sigma_{DF(SUS)}$	Standard deviation of DF_{SUS} signal	
σ_{TT}	Standard deviation of Doppler signal due to transit time broadening	
θ	Crystal beamwidth measured from the normal	°
θ_R	Orientation angle of the Rx. (angle between normal of Rx. crystal face and particle velocity)	°

Θ_T	Orientation angle of the Tx. (angle between normal of Tx. crystal face and particle velocity)	°
δf_D	Total 3dB bandwidth of the Demodulated Doppler signal	Hz
δx	Insonified volume dimension in the direction of the particle velocity	mm
$\delta\varphi_R$	Rx. particle angle	°
$\delta\varphi_R^-(H)$	Rx. -3dB particle angle where $\delta\varphi_R^-(H) < \delta\varphi_R'(H)$	
$\delta\varphi_R^+(H)$	Rx. -3dB particle angle where $\delta\varphi_R^+(H) > \delta\varphi_R'(H)$	
$\delta\varphi_R'(H)$	Rx. particle angle for $TL_F(H,\delta\varphi_R'(H)) = TL_p(H)$	
$\delta\varphi_T$	Tx. particle angle	°
$\delta\varphi_T^-(H)$	Tx. -3dB particle angle where $\delta\varphi_T^-(H) < \delta\varphi_T'(H)$	
$\delta\varphi_T^+(H)$	Tx. -3dB particle angle where $\delta\varphi_T^+(H) > \delta\varphi_T'(H)$	
$\delta\varphi_T'(H)$	Tx. particle angle for $TL_F(H,\delta\varphi_T'(H)) = TL_p(H)$	
φ	Half angle beamwidth	°
$\varphi(t)$	Phase of demodulated Doppler signal	rad
ϵ	Accuracy in terms of an error term of determining the mean Doppler frequency	
ϵ_r	Improved error term using a larger response time	
λ	Wavelength in transmission medium	mm
τ_D	Unit delay time of cross-correlation function	μs
τ_F	DDRR Filter response time	s
τ_{TT}	Transit time (time taken for particles to travel across the insonified volume in the direction of the particle velocity)'	s
σ_{BW}	Standard deviation of Doppler signal due to finite bandwidth broadening	

CHAPTER 1

INTRODUCTION

An instrument was developed for measuring the velocity of solid particles adjacent to the pipe wall in a solids-liquid pipeline. The instrument is suitable for high concentration slurries.

In the mining industry, solids are often transported in the form of a slurry hydraulically in pipelines with water as the carrier medium for the slurry. Mine tailings and backfill slurries are two examples of the type of material conveyed hydraulically. The hydraulic transport of these materials is most economical when the slurry concentration is as high as possible and the solids are conveyed in the dense phase flow or stabilised flow regimes [Ref. 23]. In these regimes a bed-load (consisting of stationary or sliding particles supported by the pipe) invariably exists.

The instrument is based on the Doppler shift principle and employs ultrasonic methods for detecting the bed-load velocity. For this reason the instrument is referred to as an Ultrasonic Doppler Bed-load Velocimeter (UDBV), or simply as a Velocimeter. Doppler ultrasonic flowmeters are presently commercially available for measuring the average flow velocity of low concentration slurries. However, the present bed-load Velocimeter specifically measures the velocity of those particles close to the pipe wall (usually on the pipe soffit too, hence the term bed-load) and is thus specifically applicable for high concentration, dense phase or stabilised flow slurries.

Reasons for measuring the velocity of bed-load particles rather than the convention of measuring mean mixture velocities (with a flowmeter) are:

- To detect incipient pipe blockage by monitoring the particles which deposit and stop moving. Blockage can then be prevented by increasing the pump speed.

- To optimize the pipeline energy efficiency by reducing the pump speed if the bed-load particles travel too fast.

- To decrease wear of the pipeline internal surface by reducing the pump speed if the bed-load particles travel too fast.

The bed-load velocity measurement from the UDBV can be used in a feedback control loop to the hydraulic system pumps to automatically prevent pipe blockage and to decrease the energy and wear rate of the pipeline.

The UDBV may also be used for determining the extent of a stationary bed or for determining the local pipe wall particle velocity by positioning the transducer at various points around the pipe. In certain hydraulic situations, such as flow with a stationary bed, pipe blockage can sometimes more effectively be prevented in this way. In addition, information of this kind is important for the theoretical and analytical study of pipe blockage, as is currently being undertaken in the Hydraulics Laboratory of the Civil Engineering Department at U.C.T.

Chapter two of the dissitation presents a Literature Review of work conducted on the Doppler technique for measuring velocity. This is discussed mainly in the context of flow rate measurement of water and blood flow since this information is widely available in the literature.

A list of requirements that the UDBV system should satisfy are presented in Chapter three. Chapter four briefly discusses the advantages and disadvantages of alternative methods of measuring bed-load velocities. The conclusion is drawn that the ultrasonic Doppler technique is the most suitable.

Chapter five presents relevant published theory necessary for the subsequent system design and analysis of Chapter six. Chapter six discusses the entire system design with emphasis on optimising the focusing technique for detecting bed-load particle velocities. The causes of the Doppler broadening are discussed and analysed so that they may be reduced to increase the accuracy of the system. The electronic circuitry is also presented in Chapter six. Results obtained with the UDBV are presented in Chapter seven. Conclusions are drawn in Chapter eight.

A research paper presented at the BHRA, Hydraulic Transport of Solids in Pipes Conference (Stratford-upon-Avon, UK, October 1988) is reproduced from the Conference Proceedings in Appendix A. The title of the paper is: "The Development of an Ultrasonic Doppler Bed load Velocimeter".

CHAPTER 3

REQUIREMENTS OF THE SYSTEM

The UDBV instrument should satisfy certain requirements for it to be used effectively as a measuring instrument of the bed-load particle velocity. These requirements are:

3.1 THE BED-LOAD VELOCITY SHOULD BE MEASURED

The instantaneous velocity of the bed-load particles is measured rather than the mean mixture flow velocity. If however, the transducer is placed in a position situated radially around the pipe wall, then the velocity of the particles closest to the pipe wall is measured.

3.2 NON-INTRUSIVE TRANSDUCER

By attaching the transducer to the outside of the pipe wall, it is non-intrusive into the flowing slurry. This requirement is important and ensures the pipe wall requires minimal or no modifications. Installation is quick and simple and maintenance costs are kept low. Also, the absence of an obstruction to the flowing medium avoids pressure loss, possible pipe blockage and transducer wear.

3.3 LINEARITY, REPEATABILITY, HIGH ACCURACY

As an effective control sensor, the following three requirements must be satisfied by the UDBV:

CHAPTER 2

LITERATURE REVIEW

In conducting a literature review, one must distinguish between Ultrasonic Flowmeters / Velocimeters which are based on the Doppler shift priciple and those which are based on a different principle (eg. the Sing-Around or Travel Time Difference method and the Beam Deflection method) because all techniques are often categorized under the term 'Ultrasonic Flowmeters'.

The Ultrasonic Flowmeter based on the Doppler Shift principle is relevant to this thesis, as this technique bases its flow velocity measurement on the velocity of particles travelling within the fluid, unlike most other techniques.

According to Lynnworth, the Doppler effect has been known since 1842 [Ref. 27, p411]. Despite the wide interest in ultrasonic flowmetry (not necessarily based on the Doppler shift priciple) throughout the 1950's, and the simultaneous existence of Doppler radar velocimeters, little work on ultrasonic Doppler flowmeters was reported before almost the turn of that decade. By 1957 Satomura [Ref. 37] and in 1961, Franklin [Ref. 15] had reported the use of the ultrasonic Doppler effect in several medical and biological studies of blood flow or tissue movement.

Some industrial pipeline applications have been extensions of earlier oceanographic technology, where Doppler methods had been developed for ship navigation. The earliest available documents on applications of ultrasonic Doppler principles and methods include the patents of Chilowsky and

Langevin in 1923 [Ref. 8] and the patent in 1932 by Chilowsky [Ref. 9]. These patents relate, respectively, to measuring submarine motion from an observation point and measuring the speed of a marine vessel with respect to the sea bottom or to the sea itself.

Marine applications such as ship navigation, provided one of the first important uses for ultrasonic Doppler technology. In 1961 Chalupnik and Green presented an Ocean-Current Meter based on the Doppler shift principle to measure flow rates in ocean water and other liquids containing sufficiently high concentration of scatterers [Ref. 7]. Their operating frequency was chosen to be 10MHz. In 1962, Koczy, Kronengold and Loewenstein [Ref. 21] conducted practical experimental analyses and tests on the Ocean-Current Meter previously developed by Chalupnik and Green.

In 1964, Green presented a paper titled 'The Spectral Broadening of Acoustic Reverberation in Doppler - Shift Fluid Flowmeters' [Ref. 16]. Green's analyses is restricted to a low concentration of scatterers and four factors contributing to spectral broadening of the Doppler shifted signal (and hence uncertainties in interpretation of the Doppler shifted signal) are considered for a general fluid flowmeter.

By the end of the 1970's, published analyses on blood flow applications, which have relevance for this thesis, have dealt with the velocity distribution effect across the blood vessel [Refs. 5, 11, 14, 33, 35], spectral broadening effects [Refs. 5, 14, 30, 35], received power spectrums [Refs. 1, 5, 14, 35], Doppler signal processing procedures, specifically the zero crossing detection method [Refs. 1, 5, 11, 14, 33, 35], Doppler shifted power spectrums [Refs. 1, 5, 11, 14, 33, 35], noise limitations [Ref.14], errors in velocity determination [Ref. 5]

In the later half of the 1970's, the Doppler flowmeter for the measurement of fluid flow rates became more widely recognized for its industrial potential too, especially for multiphase scattering fluids in pipes where transmission techniques had not yet been adequate (slurries, sewage, carbonated beverages) [Ref. 27, p444].

Published papers dealing with industrial applications and analyses of the Doppler flowmeter have dealt with the basic principles of operation [Refs. 27, 32, 36, 39], advantages of ultrasonic flowmeters over other techniques for measuring flow rates [Refs. 27, 28], transducer design [Ref. 27], Doppler spectrum analyses [Ref. 25], effect of pipe wall, fluid density and velocity of sound [Ref. 24, 35], effect of particle sizes and concentration [Ref. 32], installation [Ref. 39], accuracy of determining the flowrate [Ref. 36] and comparisons of output readings of flow rate with a Doppler flowmeter compared with the readings obtained with a Magnetic Flowmeter [Ref. 32].

(i) The output reading must be linearly dependent on the (bed-load) velocity being measured over a velocity range from 0 to 5 m/s.

(ii) The output must be repeatable and consistant for typical slurries.

(iii) The accuracy in determining the bed-load velocity must be as high as possible within a particular response time.

3.4 DETECTION OF THE VELOCITY OF TYPICAL BED-LOAD PARTICLES

The transducers detect signals from typical bed load particles encountered in waste tailings and backfill pipelines in the mining industry. Typical particles range in size from 20μm to several millimetres. Typical concentrations of tailings and backfill lines range from 15% to 40% by volume. Typical bed-load concentrations range from 50% to 60% by volume.

3.5 INDEPENDENT OF THE PROPERTIES OF THE TRANSPORTING FLUID

The system is independent of the properties of the transporting fluid such as the speed of sound, density or temperature of the fluid.

3.6 CALIBRATION FACILTY

The relationship between the output of the UDBV and the bed-load velocity can only be determined with certainty if all the system parameters that affect the Doppler frequency are known. Since all the effective parameters are not known, an

alternative method of measuring the bed-load velocity is provided (the cross-correlation method) for calibration of the UDBV.

3.7 SHORT AND VARIABLE RESPONSE TIME

The instrument has a short response time (<0.2s) compared with the response time of the pipeline pumps so that an effective control system can be implemented. The response time can also be varied and set to a discrtete value between 0.2s to 8s so that an accuracy and response-time compromise can be reached.

3.8 ZERO TO 20 mA OR 4 TO 20 mA OUTPUT

As an industry standard control sensor which may require remote sensing, the output is in the form of either a 0 to 20 mA or a 4 to 20 mA output current, signifying a measured bed load velocity ranging from a stationary condition to a predetermined maximum velocity.

3.9 DOPPLER SIGNAL INDICATOR

A Doppler Signal Indicator must provide visual information about the state of the Doppler signal. It is used to aid in the set-up the UDBV and to indicate the state of the bed-load (ie. stationary, approaching settling or sliding)

3.10 TUNEABLE TRANSMITTER FOR OPTIMUM S/N RATIO THROUGH PIPE-WALL

The transmitter frequency is tuneable to allow for optimization of ultrasonic energy into the pipe for various pipe wall materials and various wall thicknesses.

3.11 MINIMUM MAINTENANCE

Maintenance of both the transducer and the electronic system is kept to a minimum by ensuring that:

(i) The transducer is non-intrusive so that no abrasion or corrosion due to the slurry can occur.

(ii) Operating conditions for the electronic system are set up once, without the need for recalibration or retuning due to drift or errors caused by temperature variations and other environmental variations.

CHAPTER 4

POSSIBLE SOLUTIONS TO SATISFY THE REQUIREMENTS

4.1 INTRODUCTION

In Chapter 3 a number of requirements were presented that a well designed Velocimeter should satisfy for measuring the bed-load (or wall) particle velocity within a fluid filled pipeline. Methods by which solid particle (eg. bed-load) velocities may be measured fall into two main groups, naimly Doppler shift methods and the Cross-correlation method.

The Doppler shift method is usually constructed using either ultrasonic, Laser or microwave energy [Ref. 42]. Each method is briefly mentioned and their respective advantages and disadvantages for the present application is discussed.

4.2 DOPPLER METHODS

The well known Doppler shift principle can be used as the basis of a bed-load particle Velocimeter. Energy is transmitted from a source at a constant frequency and directed into the flow (or bed-load particles) being monitored.

Solid particles travelling in the slurry backscatter the transmitted energy. It can be arranged so that part of the reflected energy is from the bed load particles and is detected by a receiver.

A measurement of the Doppler shift frequency of the reflected energy provides an indication of the bed-load particle velocity.

Doppler Velocimeters may be constructed using either light (laser), microwaves, or ultrasound as an energy source.

4.2.1 Laser Doppler Velocimeter

A great deal of effort has been channelled into the development and application of the Laser Doppler Velocimeter (LDV) during the last fifteen years. One of the reasons for the great interest shown in this measurement technique is that it is capable of achieving non-intrusive point velocity measurements in the range 0.1 m/s to 100 m/s with an extremely high accuracy, claimed to be better than 0.5% of measured value. Futhermore, no calibration is required [Ref. 42].

Disadvantages of the LDV are:

(i) It requires an optically transparent pipeline.

(ii) It is too expensive, fragile and difficult to set up for routine velocity measurements in an industrial situation.

Since most hydraulic tailings lines are steel, and because the mining environment is hostile, the LDV is an unacceptable method for detecting bed-load velocities for the present case.

4.2.2 Microwave Doppler Velocimeter

Microwave are another suitable source for the Doppler Velocimeter, and possess advantages over the LDV of being:

(i) low cost,
(ii) compact,
(iii) suitable for use in hostile environments,
(iv) the pipeline does no need to be optically transparent.

However, a disadvantage is that even if calibrated, a Microwave Doppler Velocimeter (MDV) can only be used for reliable particle velocity measurements in situations where both particle size and moisture content are constant [Ref. 19]. Since these are neither known nor kept constant, this method is unacceptable.

4.2.3 Ultrasonic Doppler Velocimeter

The ultrasonic Doppler technique for particle velocity measurement employs two piezoelectric crystals to transmit and receive an ultrasonic beam into and from the particles within the pipeline. The technique is refered to as the Ultrasonic Doppler Velocimeter (UDV). The UDV is chosen as the technique for measuring bed-load velocities because it best satisfies all the requirements presented in Chapter 3. A full discussion of the implementation of the Ultrasonic Doppler technique to satisfy the requirements presented in Chapter 3 will follow in the subsequent sections of this dissitation.

4.3 CROSS-CORRELATION METHOD

The cross-correlation method of velocity measurement is an established concept but has only recently become commercially available for industrial situations. [Ref. 42].

The cross-correlation technique has the following advantage over the UDV, LDV and the MDV:

(i) It is independant of fluid properties such as temperature, density and pressure.

It has the following two advantages over the LDV and the MDV:

(i) The transducers used need cause little or no obstruction to the flow since ultrasonic transducers may be used.

(ii) The system does not need to be recalibrated for different flow, slurry or pipe conditions.

Disadvantages of the method are:

(i) Determining cross-correlation functions requires a dedicated processor to process the output signals. Intricate algorithms must be employed to ensure reliability and accuracy.

(ii) The response time is inherently much slower than the Doppler techniques due to the complicated processing required with large amounts of data to determine and then analyse the cross correlation function.

However, its main advantage of providing a velocity indication independant of the uncertain system parameters warrants its application in the present thesis as a method of calibrating the ultrasonic Doppler bed-load velocimeter. This will be discussed more fully in Chapter 6.

4.4 CONCLUSIONS

Different methods for measuring bed-load particle velocity have been presented. In conclusion, the most suitable method that will satisfy all the requirements presented in Chapter 3, is the Ultrasonic Doppler Velocimeter (UDV), which is renamed the Ultrasonic Doppler Bed-load Velocimeter (UDBV) since the bed-load velocity is measured.

CHAPTER 5

THEORY TO BE USED IN THE SYSTEM DESIGN

5.1 BASIC PRINCIPLE AND OPERATION OF THE (CW) ULTRASONIC DOPPLER FLOWMETER

The well known Constant Wave (CW) Ultrasonic Doppler flowmeter, the principle on which this project is based, can only accurately be used in situations where the solids concentration is low. The flowmeter provides a measure of the mean flow rate of the fluid within the pipeline. This technique is to measure the average flow rate of particle scatterers travelling within the fluid and relies on the assumption that the particle scatterers are travelling at the same velocity as the flow of the fluid.

A flowmeter system of this kind can be described as follows (adapted from Refs. 27, 28, 36, 39). See Fig. 5.1.

The system usually employs two piezoelectric ceramic crystals mounted outside the pipe wall by means of a mounting structure (wedge) which acts as an ultrasonic window between the crystals and the pipe wall. One crystal acts as the transmitter and is excited by a constant sinusoidal signal from an oscillator, thereby sending out an ultrasonic beam into the pipe containing the moving particle reflectors. The other crystal acts as the receiver of the reflected ultrasonic beam and is arranged so that the intersection (or insonified volume) of the transmitted and received beams is across the pipeline.

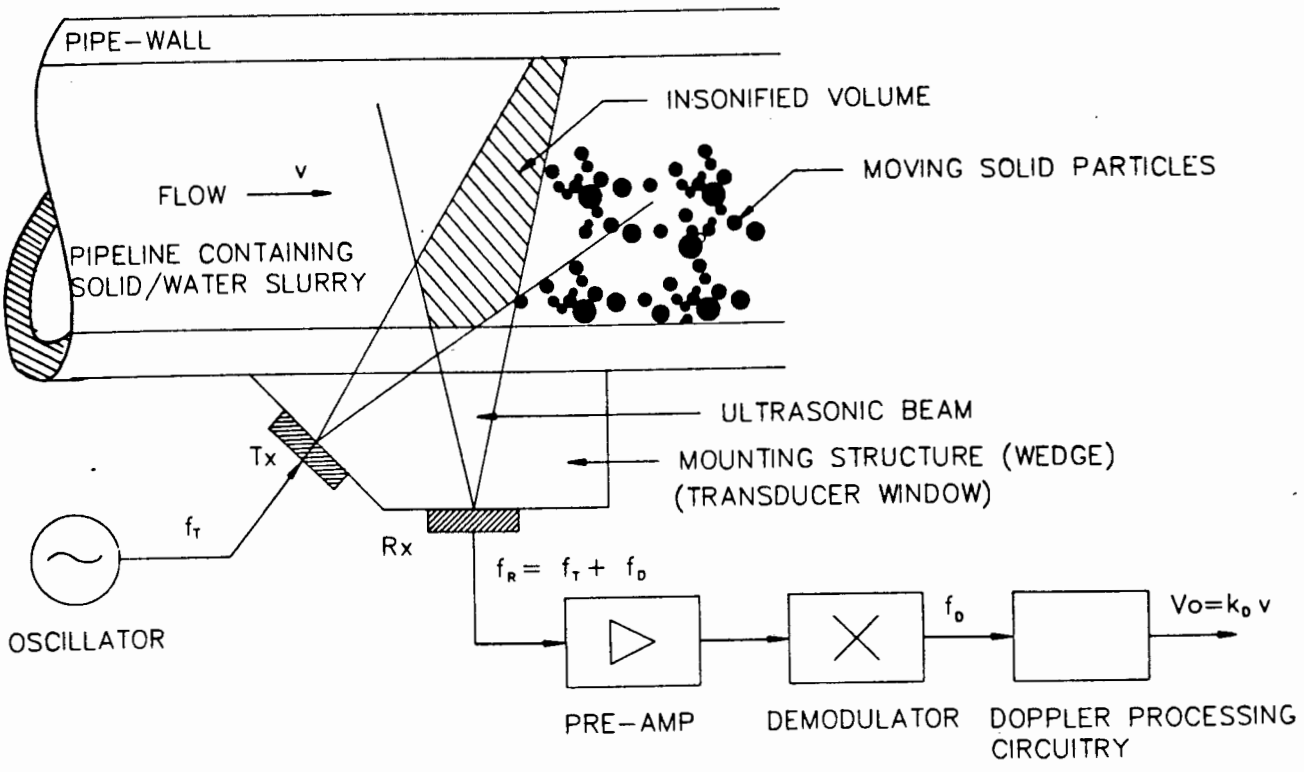

Fig. 5.1 A general flowmeter

The particle reflectors within the insonified volume, travelling in the fluid, reflect and backscatter the beam, part of which returns to the receiving crystal. The velocity of the particles cause part of the received signal to be Doppler shifted from the transmitted signal. The amount by which the received signal is Doppler shifted is proportional to the velocity of the particles.

The Doppler shifted received signal is pre-amplified and then demodulated so that any Doppler shifted component can be extracted. The frequency of the demodulated Doppler shift signal is then electronically processed and converted to a voltage (or current) to give an indication of the particle velocity.

5.2 HYDRAULIC TRANSPORT TERMS AND CLASSIFICATION OF HYDRAULIC FLOW REGIMES

5.2.1 Relevant Hydraulic Transport Terms Defined

A hydraulic transport system is defined as a system in which solids are transported in a moving liquid in a closed pipe. The pipeline may be constructed of steel, PVC, asbestos cement or concrete etc. The most common material is steel. Lined pipes to reduce wear (both erosive and corrosive) may be coated with rubber, polyurethane, plastics or ceramics.

The most commonly transported solid materials, to date, are quartz such as clay, sand and gravel, mineral slurries such as ore and tailings [Ref.23].

Hydraulic terms referred to later in this thesis are defined as follows [adapted from Ref. 24]:

(i) Solids (Load)

The solids, also referred to as the load, refers to the transported material which may be in the form of fine sediment, large particles, lumps or capsules. The size of particles transported ranges from a few microns to several millimeters.

(ii) Slurry (Mixture)

The slurry, which is also referred to as the mixture, is a mixture of solid particles and fluid ranging from suspensions of course, fast-moving particles, possibly with bed-load, to suspensions of fine highly concentrated particles moving slowly. The mean mixture velocity, averaged over the entire cross-

section of the pipeline is referred to as the mean mixture velocity [v_M]

(iii) Suspended Particles (suspension)

This term is used to describe mixtures or parts of mixtures in which no solid load is carried along the bed.

(iv) Bed-load

The bed-load is defined as that part of the solid particles which either is in contact with the pipe bottom or is in contact with particles which are themselves in contact with the pipe bottom. The bed-load is supported by the pipe either directly or by granular contact. The bed-load may be transported by means of a sliding bed or rolling particles or layers of rolling particles or a combination of sliding and rolling. The bed-load may also be stationary or move sporadically.

The velocity of the bed-load is defined by v_{BED} and the depth of the bed-load layer up from the pipe soffit is defined by h_{BED}, which is set to a constant [H] for all flow regimes for later analysis. The value of h_{BED} is difficult to predict in theory.

(v) Suspended-load

The suspended-load is defined as that part of the solid particles which travel above the bed-load layer. The average velocity of these particles is defined by v_{SUS}. Since a particle velocity profile exists across the cross-section of the pipeline for a particular flow regime, the value of v_{SUS} is a function of the

height [h] up from the pipe soffit: $v_{SUS}(h)$, where $h > h_{BED}$

(vi) Saltation

Saltation is a term used to describe the motion of particles which are carried in the fluid by a series of leaps and jumps. The particles are picked up by fluid turbulences and deposited further on downstream, on the bottom of the pipe or on the bed-load layer and the process is continuously repeated. At very low velocities the bed formation tends to be rippled (ie. dune shaped) and most of the saltation occurs from the crests of the ripples.

(vii) Transport Volumetric Concentration

The transport or in-situ volumetric concentration is defined as the volume of solids in a section of pipe divided by the volume of solids plus liquid in that same section of pipe.

5.2.2 Classification of Hydraulic Flow Regimes

Classification of flow regimes appears necessary because of the complex nature of solids-liquid flow. The relevance is for a clearer understanding of the conditions in which the Velocimeter of this project is functional. This is necessary so that a design can be undertaken which accounts for the various flow conditions. It must be bourne in mind that the Velocimeter is to be designed to measure only the bed-load particle velocity. Measurement of the suspended-load particle velocity constitutes a false measurement.

Table 5.1 shows a method of classifying the different flow regimes which may exist when transporting a solid-water slurry hydraulically in pipes [adapted from ref. 24]. There are two broad categories of flow, sometimes referred to as non-settling (or fully suspended flow) and settling slurries. A bed may or may not exist in the settled regime. It is important to realize that several regimes can exist simultaneously, particularly were the sediment is well graded.

In general, the type of regime found in a pipe depends on the physical properties of the mixture (mean mixture velocity and concentration), the properties of the solids (size, shape, density and size variation), the properties of the fluid (density and viscosity) and the properties of the pipeline (diameter, slope and roughness).

The flow regimes which have been classified for a range of mean mixture velocities (v_M). The regimes change when mean mixture velocity is increased (due to increasing hydraulic energy gradient ie. increasing power output of pumps) for a specific particle size, shape and density in a specific pipe with the transport volumetric concentration held constant.

On the left of the table v_M is low and a stationary bed exists. Movement towards the right in Table 5.1 indicates increasing mixture velocity. On the extreme right of the table, v_M is high and a pseudo-homogeneous flow exists with the solids almost uniformly distributed.

NO SOLIDS MOVEMENT	STATIONARY BED WITH SALTATION	SLIDING BED WITH SUSPENSION	HETERO-GENEOUS FLOW	PSEUDO-HOMOGENEOUS FLOW
no solids movement	upper layers move by rolling and saltation	fully moving bed with suspension	solids not uniformly distributed	solids almost uniformly distributed
$v_{SUS} = 0$	$v_{SUS} > 0$ $v_{BED} = 0$	Bed exists $v_{BED} > 0$	No bed exists	
h_{BED} is a maximum	h_{BED} is decreasing	$h_{BED}=H$	h_{BED} is defined by H	

v_{M1} v_{M2} v_{M3} v_{M4}

Mean mixture velocity [v_M] increasing ⟶

Table 5.1 Flow Regimes for a Range of Mean Mixture Velocities

The mean mixture transition velocities between the regimes presented in Table 5.1 can be designated as follows:

v_{M1} = Mean mixture transition velocity between regimes with stationary bed and suspended-load movement by saltation.

v_{M2} = Mean mixture transition velocity between stationary bed and fully moving (sliding) bed. Particles above the bed-load become suspended.

v_{M3} = Mean mixture transition velocity between moving bed and heterogeneous flow. (This velocity is also known as the limit deposit velocity).

v_{M4} = Mean mixture transition velocity between the regimes when flow behaves as two-phase and when flow behaves as single-phase (ie. transition between heterogeneous and pseudo-homogeneous flow)

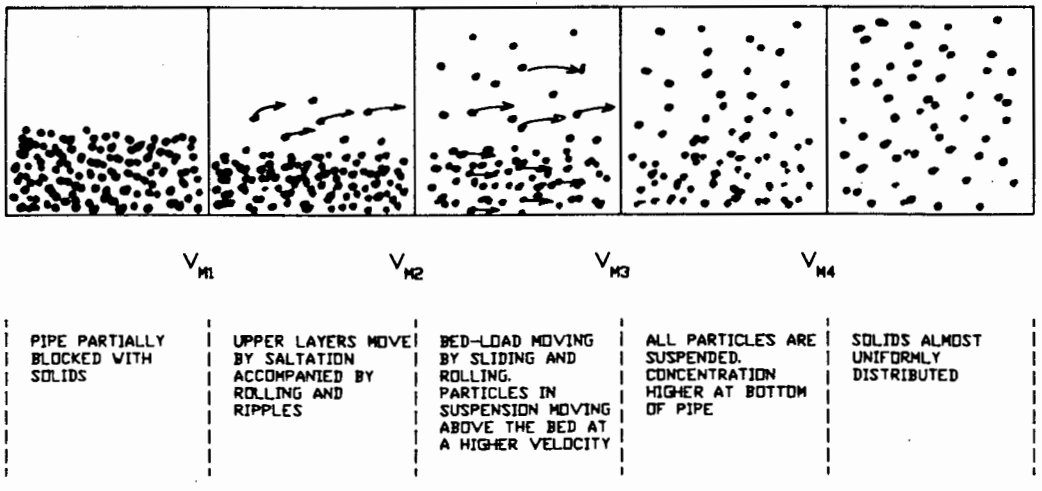

Fig. 5.2 Graphical representation of the various flow regimes

Each flow regime is discussed in more detail below. The Velocimeter measurement for each flow regime is also discussed.

(i) Stationary Bed with No Solids Movement ($v_M < v_{M1}$)

When the mean mixture velocity (v_M) is not high enough to dislodge particles from the bed, the pipe can be considered to be blocked with solids. Possibly a few odd particles will be in suspension. The hydraulic energy gradient required to maintain the flow will be high since the area of flow is reduced due to the partial blockage of the pipe. If more solids are fed into the pipe at a velocity less than v_{M1} then the entire pipe can become blocked.

The depth of the bed-load layer [h_{BED}] is a maximum in this flow regime since all the particles are settled.

The Velocimeter output must be zero corresponding to a zero bed-load velocity condition.

(ii) Part Stationary Bed with Saltation and Rolling Movement

($v_{M1} < v_M < v_{M2}$)

As v_M is increased a few particles begin to move by rolling along the bed and ripples may form which travel downstream. Only saltating particles are lifted into the stream. The bed-load remains stationary ($v_{BED} = 0$) and at times a suspended-load particle velocity exists (ie. $v_{SUS} > 0$). According to Bagnold [Ref.2] "The bed grains are seen to jump upwards into the fluid from seemingly random rest positions. The jumping grain subsequently becomes accelerated in the direction of flow....gravity ultimately pulls it back to the bed". The effect of a bouncing particle when landing is to cause further dislodgement of particles. Saltation is usually accompanied by rolling and ripple movement. See Fig. 5.3 for a velocity profile in this flow regime.

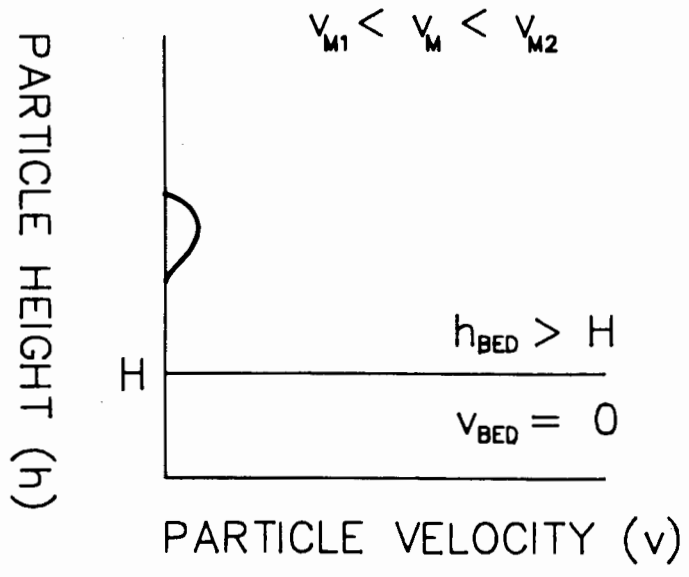

Fig. 5.3 Velocity profile for $v_{M1} < v_M < v_{M2}$

As v_M approaches v_{M2}, the depth of the bed [h_{BED}] decreases. When v_M is just below v_{M2}, the bed-load is stationary, but on the verge of moving.

Since the Velocimeter must detect the bed-load velocity, which in this case is stationary, the Velocimeter's output must be zero irrespective of whether suspended-load particles are moving.

(iii) Fully Moving Bed with Suspension ($v_{M2} < v_M < v_{M3}$)

If the particles are graded then the larger particles tend to remain on the bed but slide and roll due to fluid drag. The smaller particles saltate and some are fully suspended.

See Fig. 5.4 for an example of a velocity profile for this regime.

At mean mixture velocities below v_{M3}, particles tend to deposit but do not form a deposit. They are transported by sliding and rolling while the majority are in heterogeneous suspension.

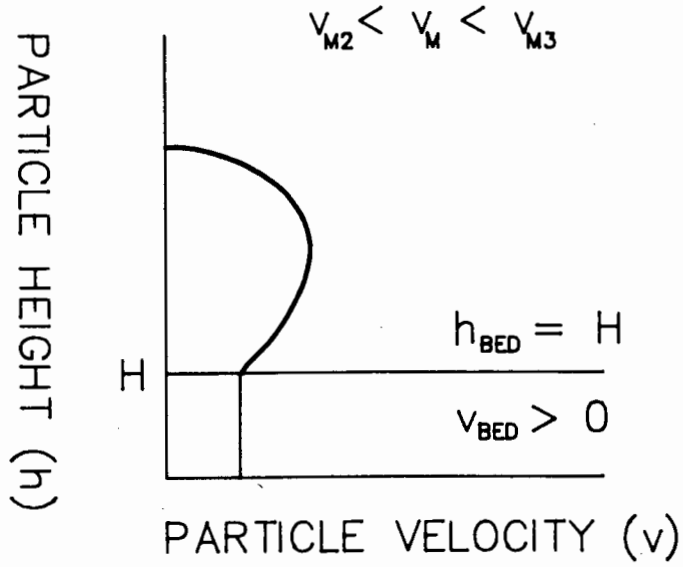

Fig. 5.4 Velocity profile for $v_{M2} < v_M < v_{M3}$

In this regime a bed-load layer physically exists and all the individual solid particles within the bed-load layer can reasonably be assumed to travel at the same mean velocity defined by v_{BED}. In this regime the value of h_{BED} can be assumed to have a constant height defined by H. The UDBV should be designed to measure the mean velocity of the particles extending up to a maximum height of H.

(iv) Fully Suspended Heterogeneous Flow ($v_{M3} < v_M < v_{M4}$)

All the particles are suspended although the distribution is asymmetrical. The concentration increases towards the bottom of the pipe. This is an important regime for most pipelines and is normally identified with economical operation with minimum hydraulic energy requirements. See Fig. 5.5 for an example of a velocity profile in this flow regime

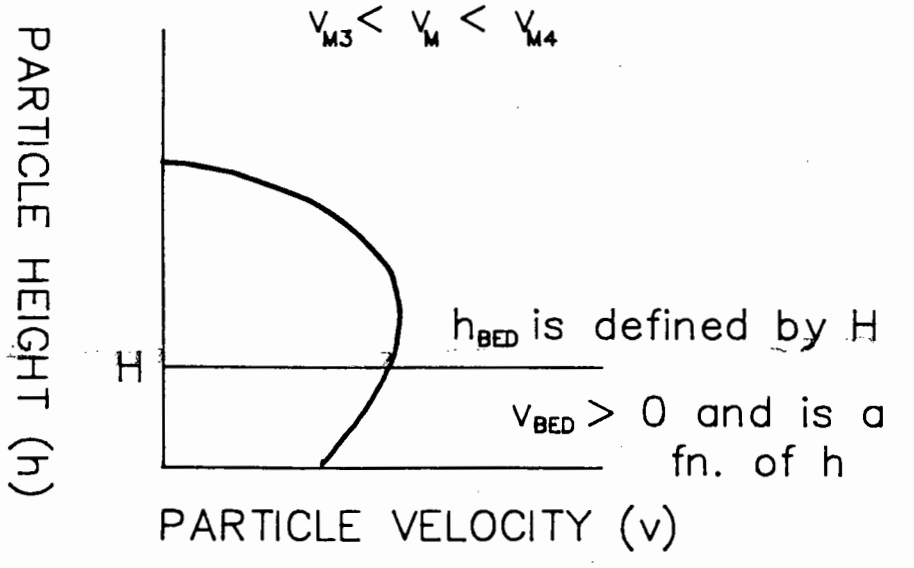

Fig. 5.5 Velocity profile for $v_{M3} < v_M < v_{M4}$

In this regime the velocity of the particles that extend up to H do not all travel at the same velocity ie. h_{BED} is a function of h (see Fig. 5.5 above). For simplicity of analysis in later sections, h_{BED} is defined by H.

The UDBV is not specified to measure the bed-load velocity in this regime. It will however measure the velocity of those particles closest to the pipe wall.

(v) Pseudo-Homogeneous Flow ($v_M > v_{M4}$)

The solids are fully suspended and the flow behaves as a single-phase fluid. The concentration of solid particles is virtually symmetric across a section of pipe but not necessarily uniform.

No bed is present and in this case the Velocimeter measures the velocity of those particles closest to the pipe wall.

5.3 THE DOPPLER EFFECT AND THE DOPPLER EQUATION

5.3.1 The Doppler Effect Applied to Particle Velocity Measurement

The UDBV relies on the Doppler effect to measure the velocity of the bed-load slurry particles. The Doppler equations describe the relationship between the frequency of sound waves travelling between moving objects and the frequency of sound waves reflected off moving objects. In this section, the Doppler equations are expressed in a form so that they may be used to relate the Doppler frequency to the velocity of particles travelling in a pipe.

In its basic form, the Doppler principle states that if a receiver (Rx.) moves relative to a transmitter source (Tx.) of sound waves as in Fig. 5.1, then the frequency detected

by the receiver is not the same as that transmitted by the source, and the received frequency (f_R) is given as follows:

$$f_R = f_T + \frac{v_R}{c} f_T \qquad (5.1)$$

where f_T is the transmitter frequency, v_R is the velocity of the receiver in the direction of the transmitter and c is the ultrasonic velocity in the medium.

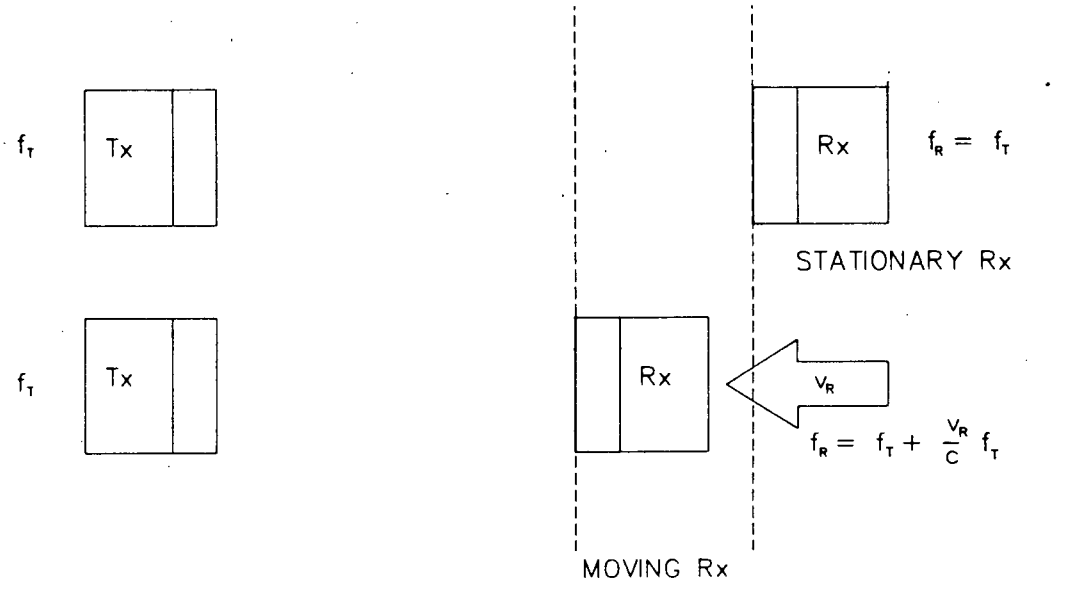

Fig. 5.6 The frequency detected from a moving receiver

The Doppler shift freqency (f_D) is defined as the absolute difference between the received frequency and the transmitted frequency:

$$f_D = |f_R - f_T| = \frac{v_R}{c} f_T \qquad (5.2)$$

If the Tx. is moving then the Doppler effect will cause the received frequency to equal that given in Eqn. 5.3:

$$f_R = f_T + \frac{v_T}{c} f_T \tag{5.3}$$

where v_T is the velocity of the Tx. in the direction of the receiver.

The Doppler shift frequency will then be as follows [Ref.1, p25]:

$$f_D = \frac{v_T}{c} f_T \tag{5.4}$$

The above analysis can be extended to describe reflection of ultrasound from a moving particle reflector simply by combining Eqns. 5.2, 5.3 and 5.4. The reflector is considered first to be a moving Rx. which detects Doppler shift sound waves at a frequency f_R given by Eqn. 5.1. This reflector then behaves as a moving Tx., radiating waves at an already Doppler shifted frequency f_R which are then detected by a stationary Rx. The frequency f_R' seen by this Rx. is, from Eqn. 5.3 given in Eqn. 5.5:

$$f_R' = f_R + \frac{v_T}{c} f_T \tag{5.5}$$

where f_R is given in Eqn. 5.1. Substituting f_R as given in Eqn. 5.1 into Eqn. 5.5 then yields Eqn. 5.6:

$$f_R' = f_T + \frac{v_R}{c} f_T + \frac{v_T}{c} (f_T + \frac{v_R}{c} f_T) \tag{5.6}$$

Since $|v_R| = |v_T|$ we can represent them both by v, the target velocity, and because $v << c$ the terms $\left[\frac{v}{c} \right]^2$ can be neglected, Eqn. 5.6 may be simplified to:

$$f_R' = f_T + \frac{2v}{c} f_T \qquad (5.7)$$

and the Doppler frequency (f_D) is:

$$f_D = \frac{2v}{c} f_T \qquad (5.8)$$

If the Tx. and Rx. are not orientated at the same angle (θ) to the moving particles, then respective components of their beams in the direction of the particles must be separately added as in Eqn. 5.9.

$$f_D = \frac{v\ (\cos \theta_T + \cos \theta_R)}{c} f_T \qquad (5.9)$$

where θ_T and θ_R are the angles of the Tx. and Rx. beams relative to the direction of the moving particle reflectors as illustrated in Figure 5.7.

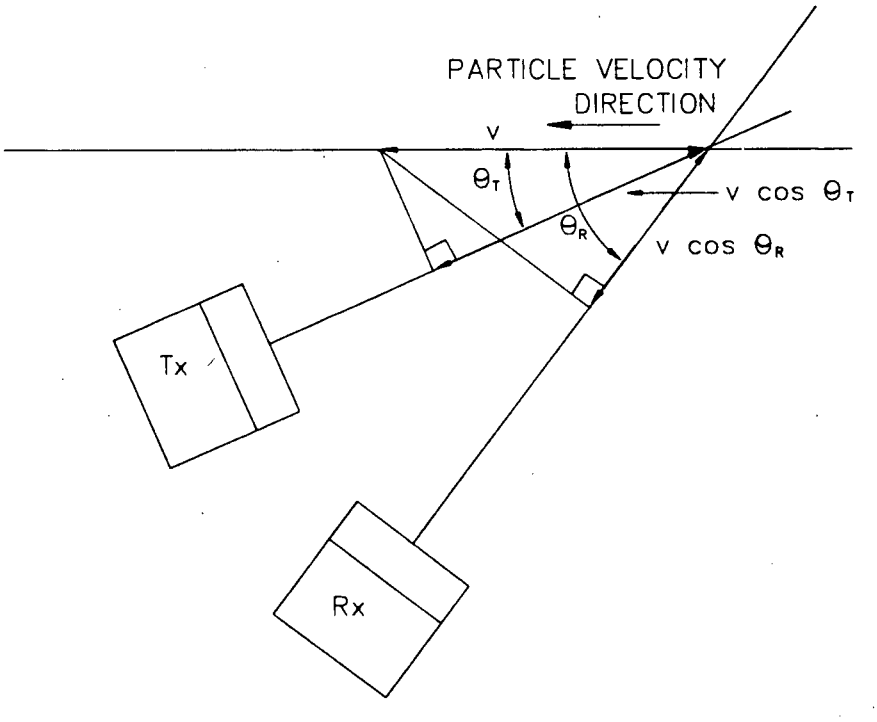

Fig.5.7 Particle velocity direction is not in the direction of the Tx. and Rx. beams

Eqn. 5.9 can be simply expressed by Eqn. 5.10 as follows:

$$f_D = k_D \cdot v \qquad (5.10)$$

where $k_D = \dfrac{f_T\ (\cos\ \theta_T + \cos\ \theta_R)}{c_{TW}}$

Eqn. 5.10 is referred to as the Doppler equation. The constant k_D is referred to as the Doppler constant. The ultrasonic velocity in the medium is expressed by the constant c_{TW} in Eqn. 5.10 and in all Eqn.s referring the Doppler equation to signify that the ultrasonic velocity is the velocity within the transducer window material.

5.3.2 Limitations of the Doppler Equation

Eqn. 5.10 describes how ultrasonic reflections from a moving reflector are shifted from the transmitted frequency. However, the practical solution to which this expression relates is extremely restricting. A single Doppler frequency can be produced only if an infinitely wide plane target moves at a constant velocity through a monochromatic ultrasonic beam which extends over an infinitely wide beamwidth [Ref. 1, p26]. If any of these conditions are not satisfied then the Doppler freqency spectrum cannot consist of a single spectral line.

For example, if either the beam or the target is finite in extent, which they are in practice, then the Doppler spectrum can be shown to be broadened, which degrades the accuracy with which the mean Doppler frequency can be determined.

Also if the moving reflectors are moving at different rates within the insonified volume than more than one Doppler frequency is present. The Doppler spectrum is then the convolution of all Doppler frequencies with their associated powers.

5.3.3 Refraction Effect on the Doppler Equation

As the transmitted and received beam propagate through the transmission path (see Section 6.3.2 for a definition and discussion of the transmission path), they encounter media having different sound velocities. For example, the sound velocity in an Epoxy Resin transducer window is 2400m/s and the velocity within a Steel pipe-wall is 5600m/s. As the beam travels from one medium to another having a different velocity, the beam will refract according to Snell's Law of refraction (see, for example, Ref. 20).

Contrary to intuition, the refraction effect has no affect on the Doppler equation. The Doppler equation (5.10) is defined completely in terms of the transducer window material properties, namely the sound velocity (c_{TW}) and the orientation angles of the Tx. and Rx. within the transducer window (θ_T and θ_R) according to the Doppler equation and is independent of refraction effects. This is because the Doppler Equation is a function of the ratios $\cos \theta_T/c_{TW}$ and $\cos \theta_R/c_{TW}$ which are constant even if the beam travels from one medium to another having different sound velocities.

If it can be shown that the above ratios are constant as the beam travels through the transmission path then it proves that the Doppler equation is defined completely in terms of the transducer window properties. When a beam refracts as it passes through two differing mediums then, according to Snell's law of refraction, the ratio $\cos \theta_1/c_1$ defined

within the one medium equals cos θ_2/c_2 defined within the second medium. Therefore Snell's Law proves that the above ratios, once defined within the transmission medium (ie. the transducer window material) are constant even if refraction occurs.

5.4 REPRESENTATION OF THE RECEIVED SIGNAL

It is important to analyse the received signal and to represent it mathematically so that appropriate demodulation techniques can be considered for extracting the wanted Doppler signal.

In practice, Doppler signals do not return in isolation, but are combined with a usually larger 'breakthrough' signal. The breakthrough signal is due to both an ultrasonic and electronic coupling of signals from the transmitter to the receiver. Its frequency is equal to that of the transmitted signal. The ultrasonic breakthrough is due to echoes from reflections at the interfaces within the transmission path (see Section 6.3.2)

The electronic breakthrough is due to coupling on the circuit boards and between the coaxial cable connected between the electronic circuitry and the transducer.

The ratio of the amplitude of the breakthrough signal to the Doppler signal is mainly dependant on:

(i) The operating transmitter frequency..

The frequency choice near resonance affects the electronic and ultrasonic matching conditions and therefore affects the

response and sensitivity of the system which ultimately affects the ratio.

Also, variations in the transmitter frequency affects the ratio of the transmitted to reflected ultrasonic energy at the interfaces within the ultrasonic transmission path. Unwanted reflections (contributing to the breakthrough signal amplitude) occur at the interface between the transducer window material and the pipe wall, between the pipe wall and the lining material (if present) and also where the beam enters the slurry.

(ii) The pipe-wall material and the lining material if present.

The acoustic impedance mismatch (ultrasonic velocity times density) between the transducer window and the pipe-wall and between the pipe-wall and pipe-lining affects the strength of the reflected ultrasonic beam from these interfaces, which contributes to the breakthrough signal amplitude.

(iii) The bed load particle material, size and concentration.

These factors will affect the reflectivity and therefore strength of the Doppler signal.

Simply, the received signal can be expressed as the sum of two signals, namely a large breakthrough signal $[R_B(t)]$, added to a smaller Doppler shifted signal $[R_D(t)]$, due to reflections from the moving particles within the pipe. The Doppler shifted signals are frequency displaced from the breakthrough signal by the Doppler difference frequency [f_D or the angular Doppler frequency, w_D] as defined by the Doppler equation.

The received signal can be represented by R(t) as follows:

Suppose the signal transmitted by the transmitting crystal is described by T(t) as in Eqn. 5.11.

$$T(t) = T \cos w_T t \qquad (5.11)$$

where T is the fixed amplitude and w_T is the transmitted angular frequency = $2\pi f_T$

The received signal, R(t), is the sum of the $R_B(t)$ and $R_D(t)$ as in Eqn.5.12 below

$$R(t) = R_B(t) + R_D(t) \qquad (5.12)$$

where $R_B(t) = R_B \cos (w_T t + \theta_B)$ (5.13)

and $R_D(t) = R_D \cos (w_T t + w_D t + \theta_D)$ (5.14)

to give:

$$R(t) = R_B \cos (w_T t + \theta_B) + R_D \cos (w_T t + w_D t + \theta_D) \qquad (5.15)$$

where R_B and R_D are the amplitudes of the breakthrough and Doppler signals respectively, w_D is the mean Doppler angular frequency ($=2\pi f_D$), θ_B and θ_D are the phase of the breakthrough and Doppler signals respectively relative to the transmitted signal at t = 0. θ_B is arbitrarily chosen to be zero.

For simplicity of the analysis, both R_D and w_D are represented as constants. However in reality, R_D will fluctuate due to the variations in the strength of the reflected signal from the moving particles. Also, w_D will not be a discrete freqency but rather a spectrum of frequencies due to the range of velocities of the detected

moving particles and due to the Doppler broadening causes discussed later in Section 6.5. These affects can be analysed after the following initial analysis.

R_B and R_D can be represented vectorially as in Fig. 5.8. The vector R_B (of fixed amplitude R_B) represents the breakthrough signal and rotates at an angular frequency of w_T about the origin. The Doppler shifted component is similarly represented by the much smaller amplitude vector R_D which rotates at an angular frequency of $w_T + w_D$, or at w_D relative to vector R_B.

The vector R_D is located at the tip of R_B so that the resultant received signal is represented by the vector sum R. Because vector R is rotating at a slightly different frequency to vector R_B, the amplitude of the resultant [R] will vary at the Doppler difference frequency [w_D] similar to an AM system.

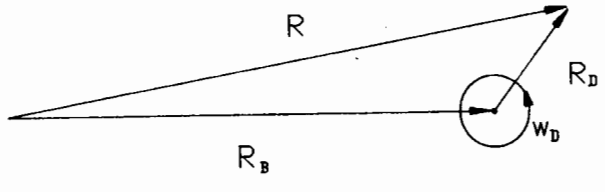

Fig.5.8 Vectorial representation of the received signal

The received signal can be expressed in the form of Eqn.5.16 [Ref. 1, p 280].

$$R(t) = [R_B + R_D \cos(w_D t + \theta_D)] \cos\left[w_T t - \frac{R_D}{R_B} \sin (w_D t + \theta_D) \right] \quad (5.16)$$

which has the form:

$$R(t) = [R_B + R_D(t)] \cos \Phi(t) \tag{5.17}$$

$$\text{with } R_D(t) = R_D \cos (w_D t + \theta_D) \tag{5.18}$$

$$\text{and } \Phi(t) = w_T t + \varphi(t) \tag{5.19}$$

$$\text{where } \varphi(t) = - \frac{R_D}{R_B} \sin (w_D t + \theta_D) \tag{5.20}$$

5.5 THE DOPPLER SPECTRUM AND BROADENING EFFECTS

5.5.1 Introduction

The relationship between the detectable (bed-load) particle velocity and the Doppler spectrum will be explained. It is important to determine this relationship since the Doppler spectrum must be electronically processed and provide information about the bed-load velocity.

5.5.2 Relationship between Particle Velocity and Doppler Spectrum

The velocity of the detectable (bed-load) particles can be expressed by a time-mean value [v] in this section. The particle velocity fluctuates about this mean value due to such factors as turbulence, interparticle collisions and wall to particle collisions. This velocity can be expressed by a PDF [$P_V(v)$] with a peak at the mean velocity [v] and a

standard deviation [σ_V] depending on the extent of the velocity fluctuation.

In the absence of spectral broadening effects [Ref. 12, p203], the instantaneous particle velocity and the instantaneous Doppler frequency are linearly related according to the Doppler equation. The statistics of the Doppler frequency and the particle velocity (eg. mean and standard deviation) are therefore equal except for the Doppler scaling constant. It follows that the ratio of the standard deviation [σ_V] to the mean of the particle velocity [v] will equal the ratio of the standard deviation [σ_{DV}] to the mean of the Doppler frequency [f_D] detected from the moving particles, as described by Eqn. 5.21.

$$\sigma_V/v = \sigma_{DV}/f_D \qquad (5.21)$$

The power spectral density [PSD] of the demodulated Doppler signal [expressed by $S_{DV}(f_D)$ neglecting broadening effects] is interpreted as being equivalent to the probability density function [PDF] of the instantaneous Doppler frequency [Ref. 12, p203] except for an amplitude scaling constant. This PDF is also identical to the PDF of the particle velocity except for a Doppler scaling constant.

The PSD of $S_{DV}(f_D)$ has a peak at the mean Doppler frequency [f_D], and a 3dB bandwidth determined from a result from Schultheis [Ref. 38] which has been restated by Denbigh [Ref. 10], who states that the standard deviation of the instantaneous Doppler frequency equals half the 3dB bandwidth of the signal for a Gaussian PDF. This implies that the 3dB bandwidth of the Doppler signal due to particle velocity fluctuation, ignoring broadening effects [f_{DV}] equals twice the standard deviation of the Doppler frequency [σ_{DV}] as expressed by Eqn. 5.22.

Solving Eqn. 5.21 for α_{DV} and substituting into Eqn. 5.22, yields the following expression for f_{DV}:

$$f_{DV} = 2 \cdot f_D \cdot \sigma_V / v \qquad (5.23)$$

Using the Doppler equation to express f_D in terms of v, the 3dB Doppler width [f_{DV}] can be expressed in terms of the particle velocity standard deviation [σ_V] as in Eqn. 5.24:

$$f_{DV} = 2 \cdot k_D \cdot \sigma_V \qquad (5.24)$$

5.5.3 Possible Doppler Broadening Causes

As discussed above, the demodulated Doppler frequency is not a discrete frequency as defined by the Doppler equation but rather consists of a spread of frequencies. This spread of frequencies can be treated as being due to two seperate effects. The first cause is due to the fact that the detectable particle velocity is not constant but rather fluctuates about a mean value. This effect has been discussed above. The second effect is due to the combination of all the spectral broadening components.

Because of the broadening effects, the PDF of the Doppler frequency is wider than the PDF of the particle velocity (hence, the term "broadening"), and the spread of the Doppler spectrum cannot be interpreted simply as the result of particle velocity fluctuations. Greater broadening causes greater uncertaintity in processing the Doppler spectrum to determinine the mean Doppler frequency. It is important to analyse the effects so that they may be minimised with a well-designed Velocimeter.

The PSD of the Doppler signal due to the combined broadening components are expressed by $S_{DB}(f_D)$. Possible causes of the broadening components of the Doppler spectrum cited in the literature include:

(i) Mean Particle velocity profile within insonified volume [Ref. 5, 11, 12, p209-210, 14, 16, 35].

(ii) Transit-time effects [Ref. 10, 12, p205-207].

(iii) Beam angle spreading due to finite beamwidth [Ref. 10, 16].

(iv) Brownian motion of individual scatterers [Ref. 12, p203, 16].

(v) Transducer motion [Ref. 16].

It must be bourne in mind that the above broadening components cited from the literature apply either to the case of measuring a fluid flow rate which contains a low concentration of scatterers or to the case of Laser Doppler Anemometry. Although there are factors in common, the literature does not discuss the present case, namely that of measuring specifically the bed load particle velocity, which is of a relatively high volumetric concentration.

The broadened Doppler spectrum can be analysed by determining the PDF or the PSD for each broadening effect individually. The Doppler spectrum is then the convolution of each PSD. Each broadening component presented and discussed in the literature is discussed in the following sections in the context of measuring bed-load particle velocities.

5.5.4 Particle Velocity Profile Effect Broadening

Velocity profile broadening occurs if the insonified volume covers a region of the particle flow where there is a mean velocity gradient [adapted from Ref. 12, p209]. The range of velocities detected will cause a corresponding range of Doppler frequencies.

Many references of this type of broadening effect appear in the literature on Doppler Ultrasonic Blood Flowmeters. For example see [Ref. 5, 11, 14, 34]

Simply, the Doppler frequencies are related by the Doppler equation to the local particle velocity across the pipeline. The power of the Doppler frequency due to particles travelling at a particular height up from the pipe soffit depends on the backscattering power from the particles at this height. From a knowledge of the velocity profile and the relative backscattering power from each layer of particles at the particular height, the PSD can be determined.

No further detailed discussion is necessary since Section 6.7 in Chapter 6 on measuring bed-load particle velocities discusses techniques to reduce the probability of detecting Doppler signals from particles travelling above the bed-load as suspended-load particles. If the design strategy discussed in Section 6.7.5 of Chapter 6 is implemented then the velocity profile effect broadening is negigable and so can be ignored. This also implies that broadening causes that are due only to detecting bed-load particle velocities need be considered in the succeeding sections on broadening.

5.5.5 Transit Time Broadening

Finite transit time broadening of the Doppler Spectrum is defined by the 3dB bandwidth [f_{TT}] of the demodulated Doppler signal due to this broadening effect. This Doppler broadening effect has been analysed in detail for the case of Laser Doppler anemometry [Ref. 12].

Finite transit time broadening arises because signals from individual scattering particles last only for the time required to traverse the scattering (insonified) volume. [Ref 12, p205]. This time is expressed by τ_{TT}. It depends on the insonified volume dimensions in the x-direction [δx] and the velocity of the particles in the x-direction [v]:

$$\tau_{TT} = \delta x/v \qquad (5.25)$$

When the ultrasonic beam is scattered from several particles simultaneously, fluctuations in phase of the received signal will occur. This fluctuation in phase will cause the Doppler spectrum to be spread.

This broadening effect can be understood by considering the PDF of the Doppler frequency. The origin of the uncertainty in frequency in the case of multi-particle scattering can be explained (Ref. Lumley et al 1969, Edwards et al 1971, mentioned in Ref. 12,p 205] by the fluctuations in phase, and hence frequency, of the combined Doppler signal as signals from particles leaving the scattering volume at arbitrary times are lost and replaced by signals from newly-entering particles. If the Doppler signal has a phase $\varphi(0)$ at t = 0, then at later times t = τ, $\varphi(\tau)$ becomes more and more uncorrelated with $\varphi(0)$ as some particles leave the scattering volume and others arrive. Eventually, when τ exceeds the transit time, all members of the original set of particles have left the scattering volume and $\varphi(\tau)$ is

completely uncorrelated with $\varphi(0)$. Thus the frequency uncertainty is seen to be related to the transit time which depends on the scattering volume dimensions.

From Durst [Ref. 12, p206], the Doppler spectrum due to this broadening effect is Gaussian if the scattering (insonified) volume is defined by two focused intersecting beams. The PDF of the Doppler signal will have a standard deviation [σ_{TT}] related to the transit time as follows:

$$\sigma_{TT} = 1/(\sqrt{2}\,\tau_{TT}) \qquad (5.26)$$

Using a result presented above in Section 5.5.2 that the standard deviation of the instantaneous Doppler frequency equals half the 3dB bandwidth of the signal for a Gaussian PDF, it follows that:

$$f_{TT} = 2\cdot\sigma_{TT} = 2/(\sqrt{2}\,\tau_{TT}) \qquad (5.27)$$

Substituting Eqn. 5.25 into Eqn. 5.27 yields the following expression for the 3dB transit time broadening:

$$f_{TT} = 2\cdot v/(\sqrt{2}\,\delta x) \qquad (5.28)$$

This finite transit time broadening effect is analysed in detail in Section 6.5.2 for the present UDBV system design.

5.5.6 Beamwidth Broadening

The finite beamwidth of the Tx. and Rx. crystals within the transducer cause a spread of Doppler frequencies to be detected with a 3dB bandwidth defined by f_{BW}. This broadening (spreading) effect exists because θ_T and θ_R as defined by the Doppler equation are spread by an amount related to the beamwidth of the crystals. Reflections and

hence Doppler shifted signals are received from particles lying within the intersection of the beamwidths of the Tx. and Rx. (ie. within the insonified volume) and not only from particles lying specifically at the focused point of intersection of the beams defined by θ_T and θ_R. This broadening effect is dependent on the geometry of the intersection of the beams and is analysed in detail in Section 6.5.3 for the present UDBV system design.

5.5.7 Brownian motion Broadening

The analysis of Brownian motion of the particle scatterers as been analysed by Green [Ref. 16]. According to Green, this cause of spectral broadening is negligable for most practicle Doppler flowmeters. In the case of the Velocimeter under consideration, this effect is negligable and ignored.

5.5.8 Transducer Motion Broadening

The effect of transducer motion on the broadening of the Doppler spectrum has also been analysed by Green [Ref. 16]. To prevent Doppler spreading due to this cause, care must be taken to ensure that the transducer is properly mounted on the pipeline. This especially applies to the case where hydraulic pumps which cause noise vibrations are located close to the transducer. It is assumed that the transducer is securely mounted ontó the pipeline so that this effect can be ignored.

5.5.9 Doppler Spectrum due to Broadening and Particle Velocity

The overall Doppler PSD [$S_D(f_D)$] due to the detection of fluctuating particle velocities and including the broadening effects is the convolution of:

(i) the Doppler PSD due to the detection of a fluctuating velocity with the broadening effects ignored [$S_{DV}(f_D)$] and

(ii) the Doppler PSD of the combined broadening components [$S_{DB}(f_D)$].

From, for example, Durst [Ref. 12, p204], the addition of independant random functions regardless of their PDFs is the sum of the variances of each random function's PDF. Since $S_{DV}(f_D)$ and $S_{DB}(f_D)$ are independent functions, the variance of the PDF of the instantaneous Doppler frequency is the sum of the variances of all the component PDFs.

Since the variance of each component is linearly related to the square of the 3dB bandwidth, the total 3dB bandwidth of the demodulated Doppler signal [δf_D] can be expressed in terms of each 3dB broadening component as in Eqn. 5.29:

$$\delta f_D^2 = f_{DV}^2 + f_{DB}^2 \qquad (5.29)$$

where f_{DB} is the 3dB bandwidth due to the combination of the broadening causes that have an effect on the Doppler signal and f_{DV} is defined by Eqn. 5.24 above. The only two broadening components that do have an affect on the Doppler signal are due to finite transit time broadening, with a 3dB bandwidth equal to f_{TT} and the beamwidth broadening with a 3dB bandwidth equal to f_{BW}, so that f_{DB} can be expressed as follows:

$$f_{DB}^2 = f_{TT}^2 + f_{BW}^2 \qquad (5.30)$$

The ratio of the total 3dB Doppler bandwidth [δf_D] to the mean Doppler frequency [f_D] is expressed by the constant β.

$$\beta = \delta f_D / f_D \qquad (5.31)$$

This constant is derived for the particular focusing parameters of the present UDBV design in Section 6.5.4. Its value is important in predicting the accuracy of the system as will become clear in Section 6.5.5.2.

5.6 DOPPLER SPECTRAL PROCESSING

5.6.1 Introduction

The demodulated Doppler signal must be processed and its frequency converted to a voltage. Currently utilised Doppler flowmeters for measuring the flow rate of blood in arteries produce flow estimates by passing the Doppler signal through a zero-crossing counter (ZCC) [Ref. 5, 11, 14, 15].

Since this method is simple to implement, has a relatively fast response time and its theory is well documented, it was chosen as the present method of Doppler processing.

5.6.2 Zero Crossing Counter

According to Atkinson et al [Ref. 1, p114], "Relating zero crossings to frequency in the practical situation is quite

difficult but nevertheless this principle forms the basis for the most popular type of Doppler shift processor currently in use".

The ZCC counts the number of zero crossings [N] of the signal and converts this number to a voltage [V_{FV}]. This process is realized with a frequency to voltage converter (F-V) circuit as in Section 6.8.10 hence the subscript FV. Ideally, the number of zero crossings should equal twice the mean Doppler frequency ie. $N = 2 \cdot \bar{f}_D$. However, this is not the case in practice, and the relationship between N and $\bar{f}_D$ follows in the subsequent section.

5.6.3 Number of Zero Crossings

The theory of operation of a zero crossing detector is based on a theoretical analysis by Rice [Ref. 34] who analysed the problem by predicting the expected number of zero crossings from the spectral content of the signal. The zero crossing rate is predicted from the probability density of finding a zero crossing event in a given time interval. Flax et al [Ref. 14] have adapted this theory to determine the relationship between the Doppler spectrum and the zero crossing frequency and show that for a Doppler power spectrum [$S_D(f_D)$] the zero crossing rate [N] is given by Eqn. 5.32:

$$N = 2 \left[\frac{\int_0^\infty f_D^2 \, S_D(f_D) \, df_D}{\int_0^\infty S_D(f_D) \, df_D} \right]^{1/2} \qquad (5.32)$$

provided there is no constant phase relation between components at different frequencies.

According to Denbigh [Ref. 10], the RHS of Eqn. 5.32 is equal to two times the second moment (radius of gyration) of the Doppler PSD or the root mean square (RMS) value of the input Doppler frequency. The expected instantaneous frequency provided by the ZCC [f_Z] is given by Eqn. 5.33:

$$f_Z = N/2 = (\bar{f_D}^2)^{1/2} = f_{D(RMS)} \quad \text{instead of } \bar{f_D} \qquad (5.33)$$

5.6.4 Operation in the Presense of Noise

Eqns. 5.29 and 5.30 above assume that the Doppler signal does not possess any noise. However, in practice noise is present so allowances must be made to reduce the occurance of false triggering of the ZCC. This consists of a comparator threshold and a positive feedback hysteresis arrangement at the input of the ZCC. The value of the threshold is adjustable so that under different noise conditions it can be adjusted so that it exceeds the noise level.

5.6.5 Accuracy and Response Time

The mean value of the instantaneous ZCC frequency [f_Z] cannot be obtained instantaneously. A determination of a true mean value requires an infinite integration time. An infinite number of measurements of instantaneous frequency would have to be obtained and averaged in order to obtain such a value [Ref. 10].

The problem of a finite measurement time has been examined by Berger [Ref. 3] in the context of airborne Doppler systems using radar, and the analysis is based upon theoretical studies carried out by Schultheiss et al [Ref. 38].

If the instantaneous frequency of a finite bandwidth signal fluctuates about a mean value as in Fig. 5.8 then the key points from Schultheiss are listed directly below.

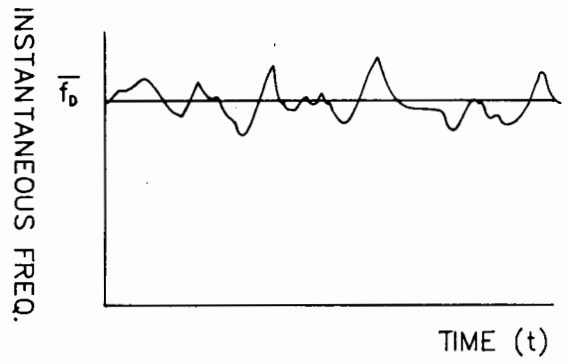

Fig. 5.9 Instantaneous frequency fluctuating about a mean value

(i) The PDF of the instantaneous Doppler frequency has approximately the same width as the width of the power spectrum. In particular, the standard deviation of instantaneous frequency equals half the 3 dB bandwidth of the signal as in Eqn. 5.34 (see Fig. 5.9)

$$\sigma_D = \delta f_D/2 \qquad (5.34)$$

where σ_D is the standard deviation of f_D and δf_D is the 3dB bandwidth of the Doppler PSD.

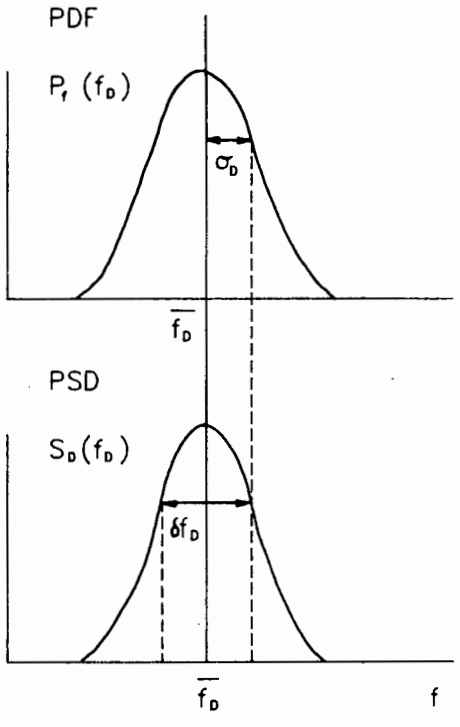

Fig. 5.10 Graphical representation of the relationship between a Doppler PDF and PSD

(ii) Measurements of instantaneous frequency are statistically independant if seperated in time by the reciprocal of half the 3 dB bandwidth.

The significance of these two statements can be appreciated after the Doppler bandwidth [δf_D] due to all the broadening effects of the Doppler signal has been derived.

These two results are applied in Section 6.5.5.2 to derive and improve the accuracy of determining the mean Doppler frequency.

5.7 ULTRASONIC DESIGN CONSIDERATIONS

5.7.1 Introduction

The transducer of the system consists of two PZT piezoelectric crystals, one the transmitter (Tx.), the other the receiver (Rx.). The crystals convert electrical energy into mechanical vibrational (ultrasonic) energy and vica versa, depending on its application.

The Tx. converts electrical energy into an ultrasonic beam which travels through the transmission path (see Section 6.3.2), is backscattered by the bed-load particles, travels back through the transmission path and is detected by the Rx. crystal which converts the ultrasonic beam into electrical energy.

In this section, the ultrasonic principles relevant to the optimization of the transducer design are discussed. Their relevance will become clear in the Chapter 6 on the System Design.

For purposes of illustration two examples of a set of transducer parameters are used. The parameters within the set are the operating frequency [f_T], the crystal radius [r] and the ultrasonic velocity within the transducer window transmission medium [c_{TW}]. The operating frequency is 1MHz and the crystal radius is 5mm as is the case in the final design. Two examples of typical transducer window materials are Epoxy resin (with c_{TW} = 2400m/s) and steel (with c_{TW} = 5600m/s).

The ultrasonic principles that must be presented in the following sections include the axial and the directivity intensity beam patterns, the propagation losses within the slurry and the backscattering strength from a layer of slurry particles. These principles are applied in Chapter 6 on the system design.

5.7.2 Axial Intensity Distribution

For the case of a circular disc crystal (as is the case in the final design) operating in thickness mode vibrations (ie. as a piston source with CW stimulation), in a homogenous medium, the axial intensity distribution varies as a function of the distance from the crystal face. The relative intensity is given by a(z) as in Eqn. 5.35 [for example, Ref. 41, p188]:

$$a(z) = I_z/I_0 = \sin^2 [\sqrt{(r^2 + z^2)} - z]\cdot\pi / \lambda \qquad (5.35)$$

where I_z is the intensity at distance z from the crystal

I_0 is the maximum intensity

r is the crystal radius

λ is the wavelength in the transmission medium

Expressed in dB it is referred to as the Axial Index [AI] and is expressed as a function of z as follows:

$$AI(z) = 10 \text{ Log } [a(z)] \qquad (5.36)$$

The axial intensity ratio $[I_z/I_0]$ is plotted against z in the two examples of Fig. 5.10 for f_T = 1MHz and r = 5mm.

The first graph is for c_{TW} = 2400m/s and the second is for c_{TW} = 5600m/s. Two distinct zones for each case can be seen. In the region near the surface of the crystal, known as the near field, the intensity undergoes large variations. With increasing distance the intensity runs through a series of maxima (equal to one) of constant amplitude, with nulls (equal to zero) inbetween.

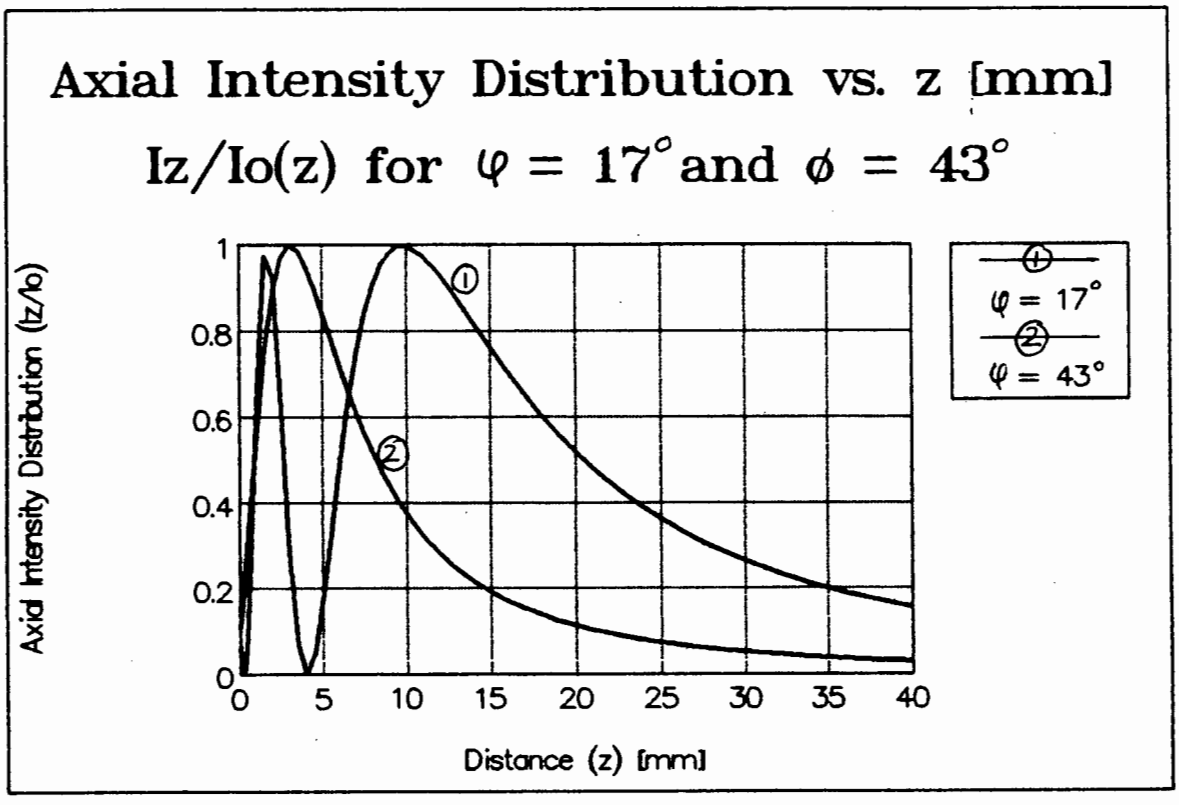

Fig. 5.11 Axial intensity distribution for a circular crystal

The distance (z_{MAX}) from the crystal to the last axial maximum intensity is given by the following relation [Ref. 41, p188]:

$$z_{MAX} = (4r^2 - \lambda^2)/4\lambda \qquad (5.37)$$

The region beyond z_{MAX} is generally referred to as the far field. In this region the intensity falls off with distance as illustrated in Fig. 5.10.

5.7.3 Directivity Intensity Pattern

The radiation pattern of a beam in the far-field of a piston source oscillating in an infinite baffle is given by the directivity function [b(θ)]. The directivity function defines the ultrasonic beam pressure intensity [I_θ] at an angle θ from the normal axis of the crystal face. Along the axis the directivity function, defined by I_0, is a maximum value of one.

The directivity function for an ultrasonic beam can be expressed by Eqn. 5.38 [Ref. 20, p177]:

$$b(\theta) = I_\theta/I_0 = \left[\frac{2\ J_1\ (kr \cdot \sin\ \theta)}{kr\ \sin\ \theta} \right]^2 \qquad (5.38)$$

where J_1 is the Bessel function of the first kind

θ is the crystal beamwidth measured from the normal

k is the wave number = $2\pi/\lambda$

r is the crystal radius as defined in Section 5.7.2

It is seen that the directivity is simply a function of θ for any given crystal and medium (ie. r and λ fixed). The directivity function can also be expressed in dB as a function of θ and is referred to here as a Directivity Index as follows:

$$DI(\theta) = 10\ Log\ [b(\theta)] \qquad (5.39)$$

Fig. 5.12 shows two polar plots illustrating the manner in which the directivity pattern of the crystals of the system vary with wavelength [λ] (with r = 5mm, f = 1MHz). The polar plot on the left in Fig. 5.11 is for c_{TW} = 5600m/s eg. for radiation into steel and the polar plot on the right is for c_{TW} = 2400m/s eg. for radiation into resin.

The first zero occurs at an angle defined by φ:

$$2 J_1 (kr \cdot \sin \varphi) = 0$$
$$kr \cdot \sin \varphi = 3.83$$

solve for φ:

$$\varphi = \sin^{-1} (0.61 \lambda / r) \qquad (5.40)$$

Therefore the far field main-lobe of a crystal source is theoretically confined within a cone of half-angle φ, the beamwidth as determined by the above equation.

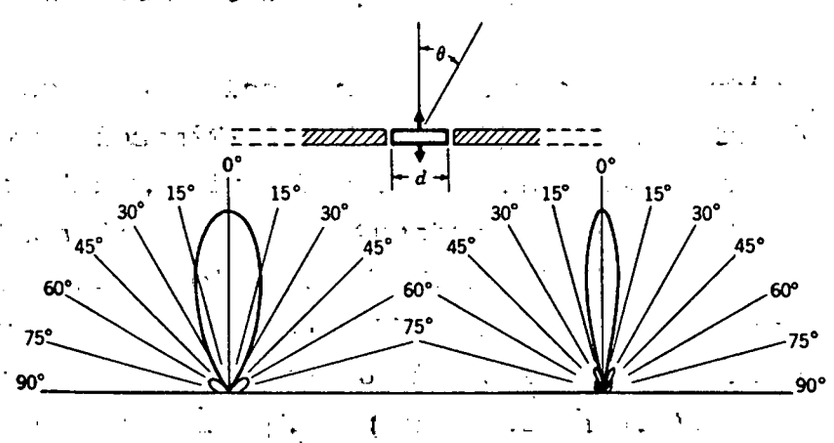

Fig. 5.12 Two polar directivity patterns

The directivity function can also be expressed in terms of φ by substituting sin φ into Eqn. 5.38. If x is set according to Eqn. 5.41, then the directivity function can be expressed by Eqn. 5.42 for angles, θ within the beamwidth.

beam may impinge upon another particle and be returned to its original path.

b) The mobility of the particles will be altered since the probability of collision is increased at high concentrations."

Generally the attenuation of an ultrasonic beam propagating through a slurry increases with frequency and depends on fluid properties such as viscosity, thermal conductivity, density and molecular structure; on particle properties such as size, shape, density and elasticity and the slurry properties such as density and concentration [Ref. 26, p60] give both experimental and theoretical results in which the above loss mechanisms are investigated. Attenuation through a medium is expressed in dB per distance travelled in the medium.

Due to the complex dependance of the ultrasonic attenuation on the fluid, particle and the slurry properties, no attempt will be made to summarize these results.

However Busby [Ref. 6] for example has measured experimentally the attenuation constant [α] per meter [α/m] in high concentration saturated slurry composed of marine sand in the frequency range 500kHz to 2MHz. Data is obtained for three grades of sand with particle diameters as follows, (mean particle diameter in given in brackets):

(i) course: 350-650μm [450μm]
(ii) medium: 70-300μm [180μm]
(iii) fine: 60-180μm [120μm]

These three grades of sand are typical of the type of solid particle that constitutes the slurry that is transported hydraulically in pipelines. The attenuation constants for

these saturated sands are presented here in tabular form in dB/mm to be used in later sections. For a particular penetration depth within the slurry [h], the Intensity Loss due to attenuation [AT, expressed in dB] is calculated by multiplying the attenuation constant by the penetration depth as follows:

$$AT = \alpha \cdot h \qquad (5.43)$$

PARTICLE SIZE (μm) [mean]	F R E Q U E N C Y (kHz)		
	500kHz	1MHz	2MHz
60-180 [120]	0.21	0.24	0.40
70-300 [180]	0.12	0.26	1.70
350-650 [450]	0.35	1.10	10.0

Table. 5. 2 Data of Attenuation constants [α] in saturated marine sands expressed in dB/mm

5.7.5 Backscattering Strength from a Slurry Surface

It is important to calculate the relative backscattering power from the bed-load layer compared with the backscattering power from the suspended-load so that a value for the Penetration constant, k_p can be derived. The Penetration constant is dicsussed in detail in Section 6.4.2 and in Section 6.4.10.

To derive values for the Penetration constant we only need to determine the relative backscattering power from the defined suspended-load compared with that from the bed-load layer. The absolute backscattering strengths from these layers need not be determined.

The backscattering strength from a layer of slurry particles can be assumed to be similar to the backscattering from the sea bottom since they both usually consist of saturated sediment. According to Urick [Ref. 43], the sea bottom acts as a reflecting and scattering boundary. If the boundary is perfectly plane, then only reflection occurs. As the boundary becomes more rough, so the scattering effect dominates the reflection effect.

In the present case, the reflection effect can be ignored and only the scattering effect considered. This is because of the arrangement of the Tx. and Rx. crystals. For reflected energy to be received, the beamwidth of the Rx. crystal must lie within the specular direction, as defined by the Tx. beamwidth, which is not the case in the present system as in Fig. 5.13.

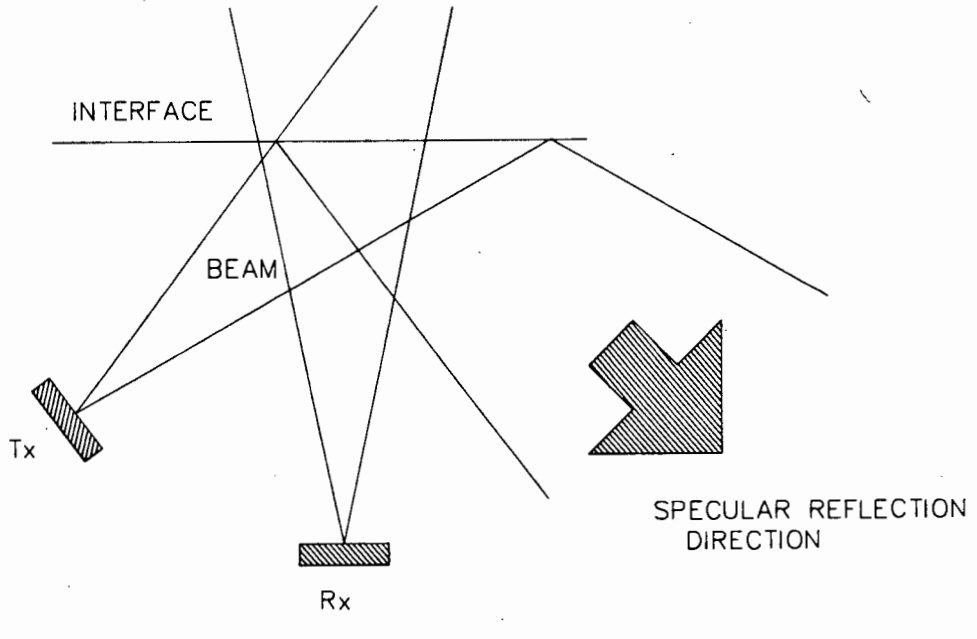

Fig. 5.13 Illustration of specular reflection

Scattering effects are complicated to analyse and are beyond the scope of this thesis. It suffices to mention that scattering is measured in terms of an intensity loss ,ie. as a ratio of the scattered to the incident intensity of the ultrasonic beam. This scattering loss from (sand slurry) particles depends on the particle size and roughness, the grazing angle and the operating frequency [Ref. 43, p243-251].

In the context of backscattering from the sea bottom, variations from one place to another in the size and packing of the particles lead to differences in backward scattering [Ref. 31]. This implies that the backscattering strength from layers of particles within the slurry will not be constant but rather fluctuate about a mean value. The backscattering strength can therefore be expressed statistically by a mean and a standard deviation.

Since the backscattering parameters are common to both the bed-load particles and the suspended-load particles, the mean and standard deviation of the scattering strength from these two layers can be assumed to be equal.

CHAPTER 6

6. SYSTEM DESIGN OF THE UDBV

6.1 INTRODUCTION

The Ultrasonic Doppler Bed-load Velocimeter (UDBV) system is based on the principle of operation of a fluid flowmeter as discussed in Section. 5.1. It consists of two integral parts, namely the transducer (comprising the transmitter (Tx.) and the receiver (Rx.) and the electronic system.

The transducer function is to perform the conversion between electrical and ultrasonic energy and vica versa. Ultrasonic energy, represented by an ultrasonic beam travels from the Tx. crystal through the transducer window material, through the pipe-wall, and penetrates into the pipe transporting slurry in the form of saturated solid particles (usually quartz) in solution. It is arranged, by means of focusing, that the particles that are travelling on the bed of the pipeline as bed-load backscatter the beam. Part of the backscattered beam is received by the Rx. crystal.

Movement of the bed-load particles cause the Rx. signal to possess a Doppler shifted frequency content. Demodulation of the received signal is performed to extract this Doppler shift signal, which is then processed and converted to a current to provide an indication of the bed-load particle velocity.

The system must be designed to satisfy all the requirements presented in Chapter 3.

6.2 DOPPLER DEMODULATION

6.2.1 Introduction

Demodulation is the detection and extraction (or recovery) of a usually smaller amplitude, lower frequency, wanted signal which is modulating a usually known, larger signal (usually called the carrier). In the case of the Doppler Velocimeter, it is the moving particles which modulates part of the transmitted ultrasound by changing its frequency content. If we recall from Eqns. 5.17 to 5.20 presented here below, it can be seen that the received signal can be regarded as a carrier signal, being the breakthrough signal $[R_B \cdot \cos w_T t]$, which is both amplitude and phase modulated by the small Doppler signal.

$$R(t) = [R_B + R_D(t)] \cos \Phi(t) \qquad (5.17)$$

with $R_D(t) = R_D \cos (w_D t + \theta_D)$ (5.18)

and $\Phi(t) = w_T t + \varphi(t)$ (5.19)

where $\varphi(t) = - \frac{R_D}{R_B} \sin (w_D t + \theta_D)$ (5.20)

Amplitude modulation of the received signal is apparent from the $R_D(t)$ term, with the frequency of the amplitude (envelope) being equal to the Doppler frequency. Phase modulation is apparent from the $\varphi(t)$ term, where the phase is clearly seen to be a function of w_D.

The purpose of the demodulator is to extract the Doppler frequency as accurately and as reliably as possible.

6.2.2 Possible Demodulation Techniques and Choice

Since the received signal is both amplitude and phase modulated by the Doppler signal, either amplitude or phase demodulation may be used to extract the Doppler signal. Amplitude demodulation techniques may be either non-synchronous (such as envelope detection, square law demodulation etc) or synchronous.

Synchronous amplitude demodulation as apposed to a non-synchronous or phase demodulation technique was chosen for the following reasons:

(i) Firstly, amplitude demodulation techniques are easier to implement than phase demodulation techniques.

(ii) Secondly, phase demodulation will yield a demodulated signal with an amplitude proportional to R_D/R_B (see $\varphi(t)$ term of Eqn. 5.20) while synchronous amplitude demodulation will yield an amplitude proportional to R_D. Because $R_D >> R_D/R_B$, the S/N ratio for synchronous amplitude demodulation is superior to that of phase demodulation.

(iii) Thirdly, synchronous as apposed to non-synchronous amplitude demodulation was chosen because of its superior S/N ratio performance for the case when a large noise is present in the received signal. In Fig. 6.1, the output S/N ratio is plotted against the input S/N ratio, expressed as [γ] from Lathi [Ref. 22, p265]]. From Fig. 6.1, it is clear that synchronous detection is superior to other forms of demodulation (such as envelope detection) when the input S/N ratio is low.

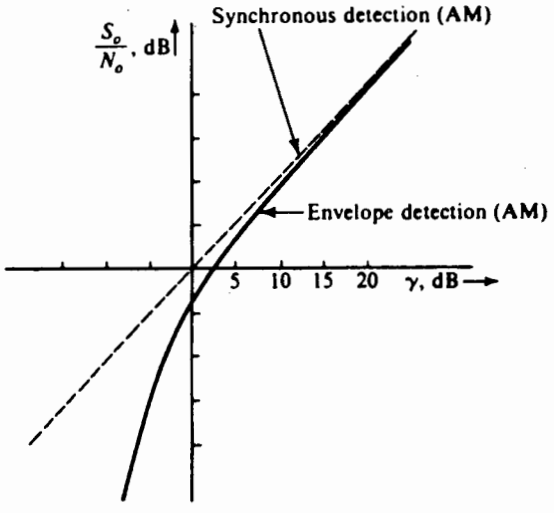

Fig. 6.1 Performance of synchronous as apposed to non-synchronous (envelope detection) demodulation

(iv) Lastly, synchronous detection is easier to implement then phase demodulation techniques when the carrier signal is available for use in the demodulation, as is the case here, since it is directly available from the transmitter.

6.2.3 Synchronous Demodulation

Synchronous demodulation is a technique whereby the received signal to be demodulated is compared with the carrier signal, to yield the wanted modulating signal (ie. the Doppler signal). The process is as follows: the received signal [R(t)] is multiplied by a fraction [k_C] of the carrier signal [$k_C T(t)$] (which is obtained from the

transmitted signal, since it is identical to the carrier, except for the fixed phase relation [θ_B] existing between the two signals and a lower amplitude). The multiplication will yield sum and difference frequency terms as well as a DC term due to θ_B. The DC term and the high frequency sum term (with a center frequency of $2w_T$) are then filtered out with a band-pass filter, leaving the difference frequency term, being the modulating Doppler signal. The demodulation by multiplication can be expressed by $D_M(t)$ as in Eqn. 6.1 below. The expression for R(t) in Eqn. 5.15 is substituted into Eqn. 6.1.

$$D_M(t) = R(t) \cdot k_C T(t) \tag{6.1}$$

$$D_M(t) = \{R_B \cos(w_T t + \theta_B) + R_D \cos(w_T t + w_D + \theta_D)\}\ k_C T \cos w_T t$$

$$= k_C T \cdot R_B/2 \{\cos (2w_T t + \theta_B) + \cos \theta_B\}$$
$$+k_C T \cdot R_D/2 \{\cos (2w_T t + w_D t + \theta_D) + \cos (w_D t + \theta_D)\}$$

The DC term, $k_C T \cdot R_B/2 \cos \theta_B$ and the high frequency terms in the region $2w_T$ are then removed by band pass filtering. Let $D=k_C T \cdot R_D/2$, leaving the filtered, demodulated Doppler signal, expressed as D(t):

$$D(t) = D \cos (w_D t + \theta_D) \tag{6.2}$$

synchronous demodulation has thus eliminated the carrier (ie. the breakthrough) and shifted the wanted Doppler signal into the base-band of the frequency spectrum for further analysis.

6.3 TRANSDUCER DESIGN TERMS, PARAMETERS AND SIMPLIFICATIONS

6.3.1 Introduction

The transducer is defined as that part of the system consisting of the Tx. and Rx. crystals to convert ultrasonic energy into an electrical signal, (or vica versa) and the window material which provides efficient ultrasonic coupling between the crystals and the pipe-wall (see Fig. 5.1).

The system parameters describing the transducer will be discussed in the following sections. Limits imposed on these parameters if applicable are to be discussed.

6.3.2 Transmission Path

The transmission path is the path that the ultrasonic beam travels along from the Tx. to the backscattering particles and back to the Rx. Along this path, the beam travels through three, four or five media before being backscattered.

The beam travels from the Tx. within the transducer, through the transducer window material (within the transducer housing or the wedge), through the pipe-wall (typically steel or 'perspex'), through the pipe-lining material (polyurethane) if present and then enters the slurry. A part of the beam is backscattered at the bottom of the bed-load layer by the bed-load particles while a part penetrates through the bed-load layer slurry to be backscattered by the suspended-load layer particles. (see Fig. 6.2)

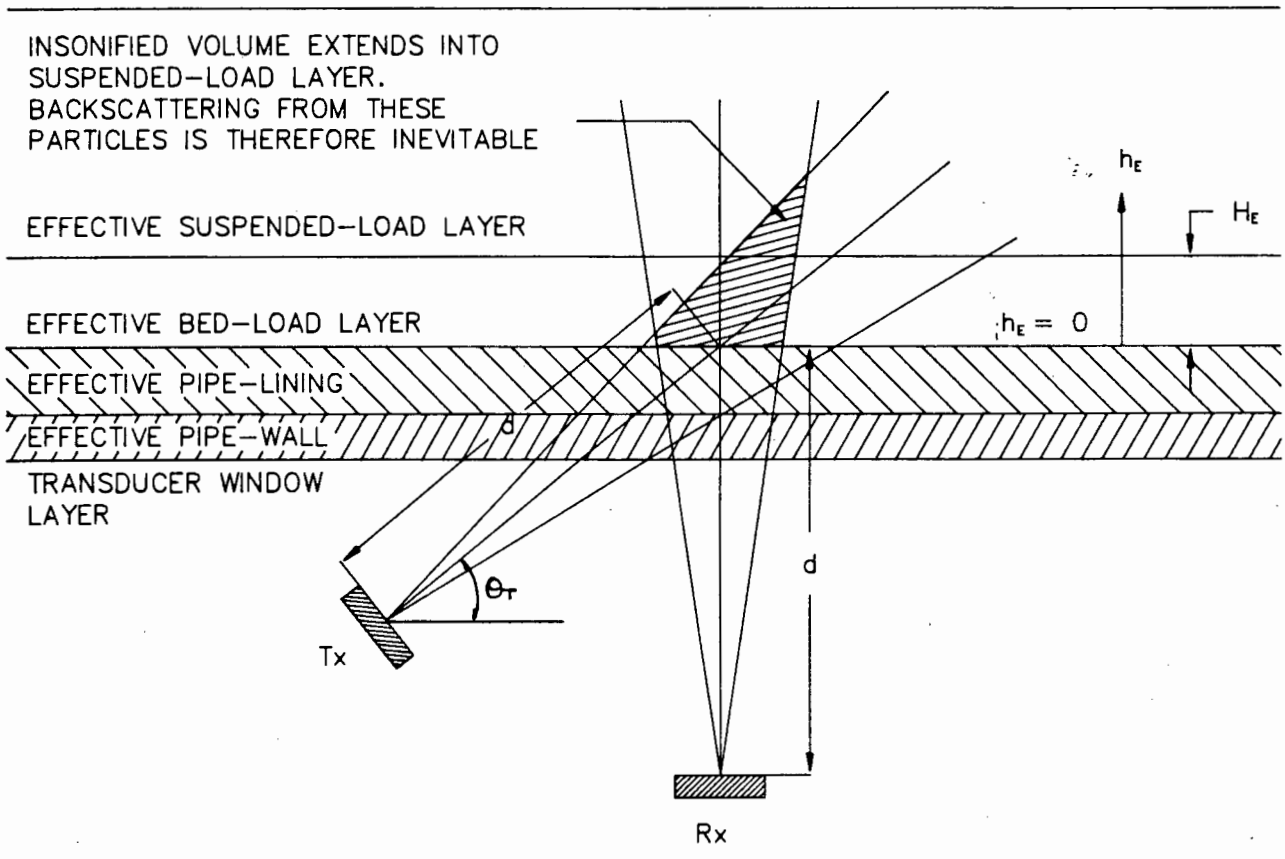

Fig. 6.2 Transmission Mediums

In the sections that follow, the relative backscattering power from the suspended-load layer is compared with the backscattering power from the bed-load layer. The transmission path is different for both cases. In determining the bed-load backscattering power, the transmission path is through the transducer window and the pipe-wall (and the pipe-lining material if present). However, for the case of determining the backscattering power from the suspended-load particles, the transmission path includes the bed-load slurry layer since the beam will

penetrate through this layer too in detecting suspended-load particles.

6.3.3 Transducer System Constant Parameters

The transducer system variables must be defined so that the transducer design parameters can be optimized. These variables are listed, with their corresponding units in (brackets):

(i) The transmitter operating frequency [f_T] (kHz)

(ii) The ultrasonic velocity in the transducer window transmission medium [c_{TW}] (m/s).

(iii) The crystal radii [r] (mm)

(iv) The effective transmission path length [d] (mm) (see Fig. 6.2).

(v) The crystal orientation angles [θ_T and θ_R] (as discussed in Section 6.3.7 (i), $\theta_R = 90^\circ$)

In the final design, circular crystals with an operating resonant frequency [f_T] of approximately 1MHz and with a radius [r] of 5mm were used. These crystals were chosen since they were easily available and also because they satisfy the optimized design parameter choice discussed in Section 6.6.

Two examples of transducer window materials are used in the system design analyses which follow to illustrate the effect of the ultrasonic velocity on various aspects of the system operation. These materials are Epoxy Resin with

c_{TW} = 2400m/s (which is the case in the final design) and steel, with c_{TW} = 5600m/s.

A set of three system parameters, f_T, r and c_{TW} together describe the value of the beamwidth in the transmission medium [φ] according to Eqn. 5.40. Each parameter will seperately influence the beamwidth which influences various system design analyses. The beamwidth alone can be used as a system parameter for the system design analyses. In this way the three system parameters [f_T, r and c_{TW}] are defined in terms of one parameter, the beamwidth [φ].

Two sets of system parameters were used in the system design analyses that follow in later sections. Both sets had f_T = 1MHz and r = 5mm. However the first had c_{TW} = 2400m/s (Epoxy Resin) and the second set had c_{TW} = 5600 (steel). The value of the beamwidth for the first and second set is calculated from Eqn. 5.40: $\varphi = 17^\circ$ (for propagation in resin) and $\varphi = 43^\circ$ (for propagation in steel). These two values of φ are used in later sections for the two sets of system parameters. Other sets of system parameters could abviously also yield the same value for φ.

6.3.4 Transducer System Assumptions

Transducer design assumptions are presented and verified. These assumptions are implied in the transducer system design that is discussed in later sections.

(i) Total internal reflection at the transducer window/pipe-wall does not occur

If an ultrasonic beam propagates from one medium [medium 1] into another medium [medium 2] which has a different

ultrasonic velocity from the first medium, then the beam will refract (bend) at the interface of the two mediums if the incident angle is greater than zero (ie. incidence is not perpindicular to the interface).

If the second medium velocity [c_2] is greater than the first beam velocity [c_1] (as is the case for propagation from a Resin transducer window into a steel pipe-wall) and if the second medium were infinitely thick then total internal reflection would take place within it at incident angles below the critical angle [θ_c]. The incident angle is defined as a grazing angle (ie. an angle between the incident beam and the interface, such as the angle θ_1 of Fig. 6.5), to be consistent with the notation of the Tx. and Rx. orientation (grazing) angles defined by the Doppler equation.

The critical angle [θ_c] is defined by equation 6.3:

$$\theta_c = \cos^{-1} (c_1/c_2) \qquad (6.3)$$

For incidence in the Epoxy Resin transducer window (ie. c_1 = 2400m/s) and transmission into a steel pipe-wall (ie. c_2 = 5600m/s), the critical angle can be derived as follows:

$$\theta_c = \cos^{-1} (c_1/c_2)$$
$$\approx 65^\circ$$

This implies that incident angles below 65° measured from the interface will not propagate from the resin transducer window into the steel pipe-wall, if the steel pipe-wall were infinitely thick. However, in the case of finite transmission medium [medium 2] thickness (ie. for a steel pipe-wall of finite thickness), total reflection will not occur, and partial penetration through the layer will take place. [Ref. 4, p22]. Generally, as the layer becomes

thicker, and as the incident angle as defined in this section decreases , so the reflection at the interface becomes larger.

It is verified in practice that total internal reflection does not occur even when the incident angle of the Tx. exceeds the critical angle. In the final design, the Tx. orientation angle [θ_T] equals approximately 30°, which is in fact below the critical angle. At this angle, Doppler signals are detected from particles travelling within the pipeline, implying that propagation through the steel pipe-wall exists. The steel pipe-wall should be as thin as possible to increase the transmission of the ultrasound through it. The Tx. orientation angle [θ_T] should not be too small since this will increase unwanted reflections from the transmission path interfaces and degrade the S/N ratio of the Doppler signals.

(ii) Only longitudinal wave propagation is considered.

Only longitudinal waves are supported by both liquid and solid materials. Other types of ultrasonic waves are supported by solids alone, such as shear waves. Since the slurry is composed of liquid it is assumed that the backscattered ultrasonic beam from the slurry is only in the form of a longitudinal wave. In practice, the Doppler frequencies are close to the frequency predicted by the Doppler equation. If the shear wave velocity within the transmission medium is assumed and used by the Doppler equation to predict the Doppler frequency, then it is seen that the predictions are false. It is therefore assumed that the ultrasonic energy of the beams due to backscattering from the slurry is in the form of longitudinal waves.

(iii) The surface scattering strength from the bed-load equals that from the suspended-load.

As discussed in Section 5.7.5, the scattering strength statistics from the bed-load layer equals that from the suspended-load.

6.3.5 Requirements that the Transducer must Satisfy

The following requirements must be satisfied by the transducer for improving the operating performance of the Velocimeter:

(i) The signal to noise ratio (S/N) of the Doppler shifted received signal from the bed-load slurry particles should be as high as possible to maximise the probability of detecting bed-load Doppler signals compared with the unavoidable detection of noise signals. Care must therefore be taken to ensure that the attenuation through the transmission path is as low as possible.

(ii) The probability of detecting bed-load particle velocities should be high compared with the probability of detecting suspended particles. ie. detecting Doppler shift signals from the bed-load particles must be high compared with detecting Doppler shift signals from suspended-load particles.

(iii) Reflections at the interfaces in the transmission path must be minimized. The S/N ratio stated above in

point (i) will be maximised if the reflections are minimised and the transmission energy is maximised.

(iv) The Doppler spectrum must be as narrow as possible ie. the broadening effects must be minimized so that the accuracy in determining the mean Doppler frequency is increased.

6.3.6 Construction Details

As already mentioned, the transducer consists of a Tx. and Rx. Piezoelectric (PZT) ceramic crystal mounted on the transducer window. The transducer window can consist of a material that supports ultrasonic transmission at the chosen operating frequency of 1MHz with a suitably low attenuation. Its ultrasonic velocity is important since it determines the beamwidth of the Tx. and Rx. beams. This is discussed more fully in later sections. It must be a hard, stiff material to withstand normal mechanical stresses and strains encountered by mounting the transducer on a pipe-line.

Two types of transducers were constructed and experimented with as follows:

(i) Wedge

A mounting structure, often referred to in the literature as a 'wedge' (from its shape), shaped so that its front face is attached to the pipe-line as in Fig. 6.3.

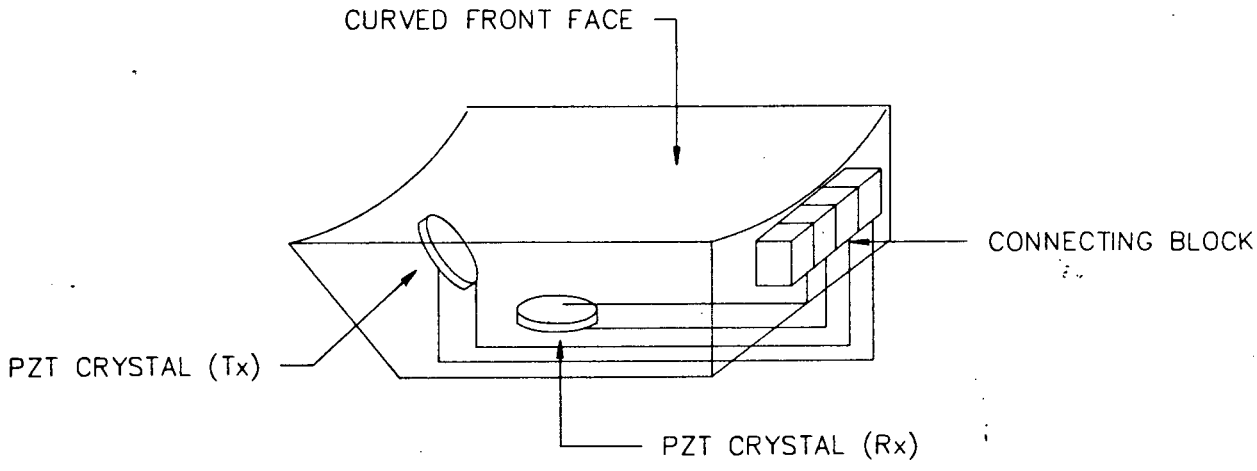

Fig. 6.3 Construction of the wedge-type transducer

The Tx. and Rx. crystals are glued onto seperate faces so that the intersection of the Tx. and Rx. beams is at the point of velocity detection.

Two thin wires are soldered onto each of the silvered faces of the crystals and lead to a connecting block on the wedge.

Various wedges were constructed of different shapes and materials. Three materials experimented with were PVC, 'Perspex' and Steel.

(ii) Metal Housing

A closed-cell rigid PVC foam block was shaped as in Fig. 6.4 to effectively provide an air backing for the crystals. The surfaces were shaped to provide the correct orientation of the crystals relative to the bed-load. (ie. the angles θ_T and θ_R).

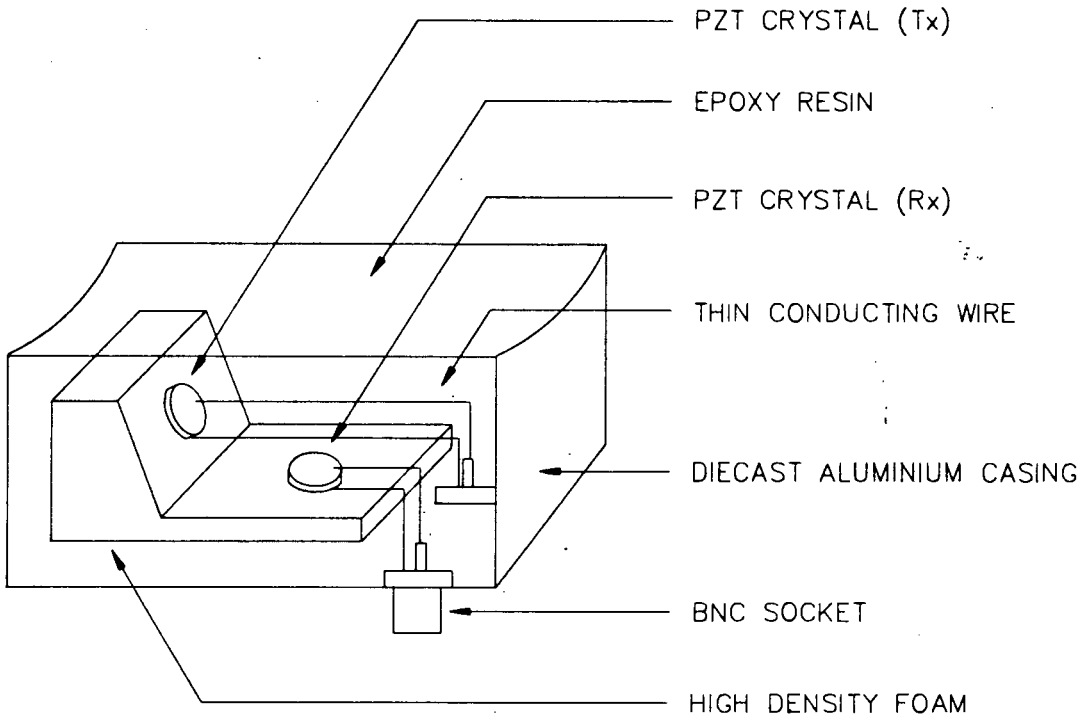

Fig. 6.4 Construction of the metal-housing type-transducer

A thin wire conductor was soldered to each of the silvered faces of the transducers and led to the edge of the foam where they were connected to co-axial sockets. (The crystals were similarly orientated with respect to their polarity).

The foam block was placed in an open-topped metal housing. The ground terminals of the co-axial sockets were commoned together via the metal housing. The housing was then filled with a low viscosity Ciba Geiga epoxy resin until the level of the resin approached the rim of the housing. The resin was poured with care to ensure that no air-bubbles formed, which would retard the ultrasonic transmission.

The advantages of this type of construction is that the entire transducer is sealed, which is ideal for harsh, external environmental conditions.

6.3.7 Transducer Crystal Geometry

(i) The Orientation angles [θ_T and θ_R] (deg)

The orientation angles of the Tx. and Rx. crystals (defined by θ_T and θ_R) are the angles between their normals and the pipe wall. The normal of the Rx. crystal face is perpindicular to the pipe wall (ie. $\theta_R = 90^\circ$). In this way, the Rx. is focused on the bed-load directly above it. This orientation is suitable since it simplifies the transducer window construction. It also facilitates focusing on the bed-load particles. The Tx. crystal orientation angle is a focusing design parameter. Focusing analysis is carried out for θ_T between 10° and 50° in Section 6.4.12.

(ii) Effective Axial Path Length [d] (mm)

The effective axial path length [d] is the effective straight line that the ultrasonic beam travels along the transmission path from the Rx. crystal to the focused point on the bottom of the bed-load layer. This dimension also describes the effective straight line path length from the Tx. crystal to the focused point on the bottom of the bed-load layer.

Along the transmission path the beam will refract at the interfaces (assuming no pipe lining material is present then refraction will occur at the transducer window/pipe-wall

interface and at the pipe-wall/slurry interface). The refraction depends on the ultrasonic velocity ratio of the two layers and the incident angle at the interface of the layers and can be described by Snell's Law as follows:

$$\frac{c_1}{\cos \theta_1} = \frac{c_2}{\cos \theta_2} \qquad (6.4)$$

where c1 and c2 are the velocities in the two mediums and θ1 and θ2 are the beam angles in the two mediums (between the beams and the interface of the mediums) as in Fig. 6.5.

To simplify the system design analysis that follows (axial intensity, beam patterns etc.) the second medium can be assumed to have an identical velocity to the first medium. If this is the case then refraction effects at the interface between the two mediums can be ignored, so that the beam travels in a straight line. For this assumption to hold without errors being introduced requires the beam path length to be defined in terms of an effective path length.

This effective path length is defined as follows:

$$d_{2(E)} = d_2 \cdot c_2/c_1 \qquad (6.5)$$

where c_2 is the ultrasonic velocity in the second medium (in which refraction occurs), c_1 is the velocity in the (first) transmission medium, d_2 is the actual transmission path length in medium 2 and $d_{2(E)}$ is the effective transmission path length within the second medium with straight line beam propagation referred to the first medium as in Fig. 6.5.

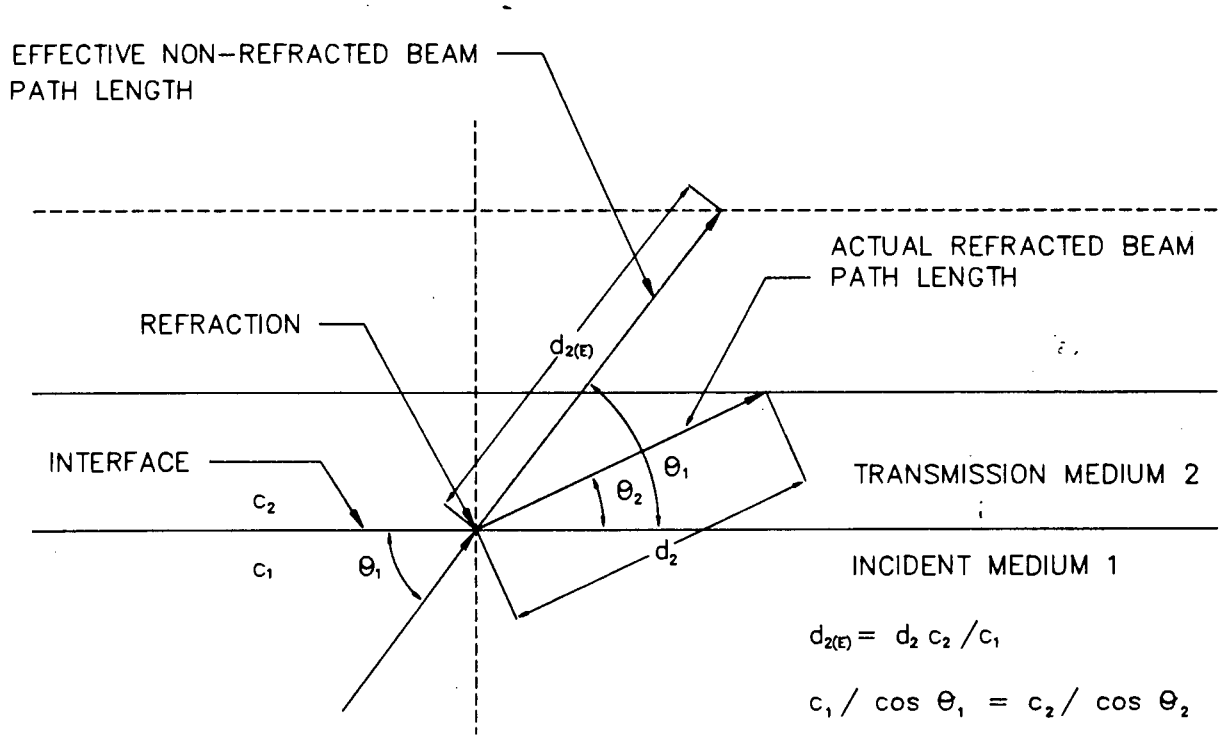

Fig. 6.5 Snell's Law of refraction in terms of effective path lengths

Equation 6.5 can be applied to the pipe-wall, which has an ultrasonic velocity defined by c_{PW} and an actual thickness dimension defined by d_{PW}. This effective dimension [$d_{PW(E)}$] (see Fig. 6.6) can be referred to the transducer window material, which has an ultrasonic velocity defined by c_{TW}, as follows:

$$d_{PW(E)} = d_{PW} \cdot c_{PW}/c_{TW} \qquad (6.6)$$

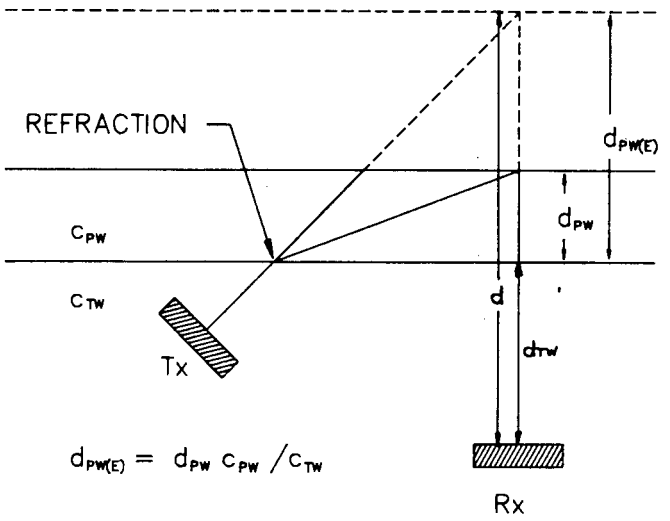

Fig. 6.6 Actual and effective pipe-wall thickness

For example, the effective transmission path length can be calculated for a steel pipe-wall (c_{PW} = 5600m/s) of 4mm and a transducer window material of Epoxy Resin (c_{TW} = 2400m/s) as follows:

$$d_{PW(E)} = 5600/2400 \cdot 4$$
$$= 9.33\text{mm}$$

The effective transmission path length [d] can now be determined by adding the path length within the transducer window [d_{TW}] to the effective path length of the pipe-wall [$d_{PW(E)}$]. If a pipe-lining material is present, then its effective thickness [defined by $d_{PL(E)}$] should be calculated according to the procedure for the pipe-wall. Assume for the system analysis that follows that no pipe-lining is present so that the effective path length can be expressed as follows:

$$d = d_{TW} + d_{PW(E)} \qquad (6.7)$$

6.3.8 Pipe-wall Thickness

The pipe-wall thickness influences the ultrasonic reflection at the transducer-window/pipe-wall interface within the transmission path. If the pipe-wall material has an ultrasonic velocity which differs markedly from the ultrasonic velocity of the transducer window, then the pipe-wall thickness should be minimized. This is necessary so that the requirement above (Section 6.3.5 (iii)), of minimising the ultrasonic reflections at the interfaces within the transmission path is minimized. Most of the reflection within the transmission path occurs at the transducer window/pipe-wall interface, especially if their ultrasonic velocities are markedly different.

If the pipe-wall material has an ultrasonic velocity similar to the ultrasonic velocity of the transducer window material (eg. Perspex, PVC pipe-wall for an Epoxy Resin transducer window) then the reflection is small and of little consequence.

However, with a steel pipe-line, the reflection coefficient is large. A derivation of the actual reflection coefficent for the particular system parameters (the ultrasonic velocities within the mediums, the operating frequency, the dimensions of the mediums and the angles of incidence etc.) is beyond the scope of this thesis. Suffice is to state (from Section 6.3.4 (i)) that as the material (pipe-wall) thickness is reduced, so the reflection coefficient is reduced and correspondingly, the S/N ratio of the ultrasonic transmitted signal is improved. It is therefore desirable to have as thin a pipe-wall as possible (for the case of Steel and other pipe materials that have ultrasonic

velocities considerably greater than the velocity within the transducer window).

A lower limit on the pipe-wall thickness [d_{PW}] is determined from the lower limit of the pressure that the pipeline must withstand. The minimum thickness for most applications of the UDBV is 4mm. A steel pipeline that has a wall thickness that exceeds 4mm can usually be milled down to 4mm while still being able to support the hydraulic pressures. For purposes of analysis, this dimension is assumed in later calculations.

6.3.9 Lower Limit on the Effective Path Length

The lower limit of the effective transmission path length [d] depends on the lower limit of the dimensions of the transducer window path length [d_{TW}] and the lower limit on the effective pipe-wall thickness [$d_{PW(E)}$] according to Eqn. 6.6 above. For a steel pipe-wall it was stated above that the minimum wall thickness, d_{PW} = 4mm, which corresponds to an effective value calculated from the example above in Section 6.3.7 (ii) of 9.33mm

The lower limit of the transducer window path length is equal to z_{MAX}, where z_{MAX} is calculated according to Eqn. 5.37 for a particular set of transducer parameters (see Section 6.3.3). For example, with the set of parameters such that f_T = 1MHz, r = 5mm and c_{TW} = 2400m/s, z_{MAX} = 9.82mm as verified by the value of z at the peak of the $\varphi = 17^{\circ}$ graph in Fig. 5.10 (this graph is for the same set of system parameters). The lower limit on d for these system parameters is calculated by adding $d_{PW(E)}$ and d_{TW} as in Eqn. 6.7, to yield d = 9.33 + 9.82 = 19.15mm (for a 4mm pipe-wall).

It is arranged so that d_{TW} exceeds z_{MAX} so that ultrasonic far-field beam equations can be applied to the focusing analysis that follows in Section 6.4. It is desirable that $d_{TW} > z_{MAX}$ for two reasons:

(1) Axial intensity from bed-load particles is a maximum

The backscattering power from the bed-load particles depends on the ultrasonic beam intensity at the focused point. It is desirable to maximize the backscattering power to increase the probability of detecting bed-load particle velocities as apposed to the detection of suspended-load particle velocities.

The region close the crystal at a distance < z_{MAX} is known as the near-field. Within this region the axial beam intensity undergoes large relative amplitude variations (I_z/I_0 ranges between 0 and 1, see Fig. 5.10.) within short axial distances from the crystal. It is therefore difficult in practice to ensure that the beam intensity is large at the focused point on the bed. Slight variations in the focusing system parameters (see Section 6.4.2) will have a marked effect on the axial beam intensity.

In the far-field, the axial intensity falls off with distance gradually. The relative intensity, I_z/I_0 will be a maximum at the beginning of the far-field compared with distances further away from the crystal. Operation in the far field will ensure that the axial intensity from bed-load particles exceeds the intensity from suspended-load particles (since they are further from the crystal).

(2) The λ is defined by the transducer window.

The ultrasonic wavelength [λ] in a medium determines the beam intensity characteristics within the medium. The focusing efficiency (defined in Section 6.4.2) depends on the beam intensity characteristics. The focusing efficiency can be optimized by suitably chosing a transducer window material which has a desirable ultrasonic wavelength.

The λ is accurately defined in terms of the transducer window material only if the dimensions are large relative to the λ within it ie. if $d_{TW} > z_{MAX}$. If $d_{TW} < z_{MAX}$ then the pipe wall material would influence the value of λ and the focusing efficiency would be dependant on the pipe-wall material, which is undesirable.

6.3.10 Lower Limit on Transmitter Orientation Angle

As mentioned in Section 6.3.5 (iii) above, the ultrasonic reflection at the transducer window/pipe-wall interface should be minimized. The reflection coefficient at this interface is dependent on the incident angle of the ultrasonic beam (ie. on θ_T). As θ_T approaches zero so the reflection coefficient increases. The exact relationship between θ_T and the reflection coefficient is complicated to predict in theory for the following two reasons:

(i) the pipe-wall thickness is usually thin (within the vacinity of one or a few wavelengths) and

(ii) if the pipe-wall material is steel then θ_T exceeds the critical angle (as defined above by θ_C), which implies

that the angle of the ultrasonic beam in the pipe-wall is a complex angle.

Calculating the reflection coefficent for these conditions is complex and beyond the scope of this dissitation. Experimentation however proved that the minimum value of θ_T for an acceptable Doppler S/N ratio is 30°.

6.3.11 Upper Limit on Frequency Choice

The ultrasonic attenuation through materials is dependent on the operating frequency. In certain practical situations pipe-lines are lined with rubber to reduce the wear rate of the pipeline. Attenuation will occur in this lining material. The lining material is typically 6mm. Results of tests carried out on the ultrasonic transmission through this rubber at the chosen operating frequency of 1MHz demonstarted that the S/N ratio of a beam propagating through this material was too low to be acceptable for detecting Doppler signals. For this reason tests on polyurethane materials having as low or lower wear rates than typical rubber were carried out. Also, tests on the attenuation through these polyurethane materials was carried out and it was demonstrated that the attenuation was considerably lower than for the rubber.

A polyurethane that possessed both low wear rates and relatively low attenuation was chosen: a Polyether Polyurethane. The attenuation through the polyurethane was considerable lower than through the rubber at 1MHz. The improvement in the propagation strength could not accurately be compared with rubber since the attenuation through the rubber was too low to be measured accurately. At frequencies of 1MHz and below, the S/N ratio through this

polyurethane is acceptable, imposing an upper limit of 1MHz on the operating frequency.

A low operating frequency is unacceptable since the beamwidth [φ] will increase. In Section 6.6 on the transducer design parameter optimization, it will be shown that a wide beamwidth is unacceptable. Therefore as a compromise between lowering the transmission S/N ratio and reducing the beamwidth, an operating frequency of 1MHz is chosen for the design.

6.4 ULTRASONIC FOCUSING ON THE BED-LOAD

6.4.1 Introduction

Focusing involves directing the Tx. and Rx. crystals at the bed-load layer particles. The necessity and main objective of focusing is to receive backscattered Doppler signals due to the velocity of the bed-load particles as accurately as possible within a specified response time. However, because the Tx. and Rx. have a finite beamwidth, the intersection of the beams, known as the insonified volume, extends into layers of particles above the bed-load (see Fig. 6.2).

The two main problems inherent in a system of this kind is that firstly the detected Doppler frequency is not discrete but rather has a spectral content which is spread about its mean value over a finite width and secondly unwanted Doppler shift signals are detected from particles travelling above the bed-load particles as suspended-load particles. These two problems reduces the accuracy of determining bed-load velocities accurately.

Focusing of the Tx. and Rx. crystal on a specific point can be achieved so that the intensity of reflections from this point can be maximised. The following two conditions must be satisfied:

(i) The crystals are directed at the point

(ii) The transmission path length exceeds z_{MAX}.

The maximum intensity of the crystals lie on a line extending from the normal of the center of the face of the crystal. If these lines intersect at a point on the bottom of the bed-load particles above the transducer then the reflection strength from these particles is a maximum.

The analysis of focusing is carried out on a "Quatro" Spreadsheet for a particular set of focusing parameters. All the aspects of focusing and its implementation on the Spreadsheet is discussed in the relevant sections that follow.

6.4.2 Focusing Efficiency and Focusing Parameters

The efficiency of a focused system can be defined as a measure of:

(i) The probability of detecting bed-load particle velocities relative to the detection of suspended-load particle velocities.

(ii) The Doppler spectral width. The focusing efficiency is increased if the Doppler spectral width due to the broadening causes (see Section 6.5) is reduced.

The focusing efficiency is dependant on four system parameters, referred to as the focusing parameters. These parameters are:

(i) The beamwidth within the transmission path [φ].

(ii) The transmission path length [d].

(iii) The Tx. crystal orientation angle [θ_T]

(iv) The suspended-load particle height [H]

For a particular set of focusing parameters, the ultrasonic beam pattern in terms of its intensity, power and effective insonified surface area are derived at the bed-load and at the suspended-load particles. From this information, a focusing efficiency analysis can be carried out.

In Section 6.7.7 the focusing efficiency in terms of detecting bed-load particle velocities is defined by a bed-load particle detection probability function. This probability function depends on a constant referred to as the Penetration constant [k_p], which in turn is a function of the focusing parameters.

The focusing efficiency in terms of the Doppler spectral broadening effects is also dependant on the focusing parameters. Specifically, transit time broadening is a function of φ, d and θ_T and is discussed in detail in Section 6.5.2. Beamwidth broadening is derived from one of the ultrasonic beam pattern intensity terms, namely the Directivity Index which is expressed in terms of φ.

6.4.3 Penetration Constant Defined

If we recall from Section 5.2.2, the bed-load particles travel in a layer that extends up to H within the pipeline. The bottom layer of the bed-load layer is defined by h = 0, ie. the layer of particles that travel on the pipe soffit. The particles travelling above H are defined as the suspended-load particles. If these particles are located within the insonified volume then the incident beam from the Tx. penetrates through the bed-load layer and is backscattered by the suspended-load particles. In this case the bed-load layer forms part of the transmission path as in Fig. 6.2.

When the flow regime is defined by $v_{M1} < v_M < v_{M2}$, the bed-load layer is stationary and the suspended-load particles are in motion. In this regime, part of the backscattering beam will possess Doppler shifted frequencies due to suspended-load particle motion, and falsely indicate a moving bed.

A Penetration constant [k_p] is defined and evaluated to describe the relative maximum backscattered power from a surface layer of the suspended-load layer particles compared with the maximum backscattering power from a surface layer of the bed-load layer of particles. It is expressed as a ratio of these two backscattering powers as follows:

$$k_p(H) = \text{Max } \{P_{SUS}(h)\} \; / \; \text{Max } \{P_{BED}(h)\} \qquad (6.8)$$

and in dB, k_p is expressed as follows:

$$k_p(H)\{dB\} = 10 \text{ Log } [\text{Max } \{P_{SUS}(h)\} \; / \; \text{Max } \{P_{BED}(h)\}]$$

The value of this constant is a function of the focusing parameters. If the two focusing criteria above (Section 6.4.1) are satisfied then k_p is a maximum at h = 0 and is inversely related to h for all sets of focusing parameters. This means that the maximum backscattering power from the bed-load is due to backscattering from the lowest layer of particles, ie. from the particles travelling at h = 0 (when $v_{BED} > 0$) and is defined by P(0). Similarly, the maximum backscattering power from the suspended-load is due to backscattering from the lowest layer of particles, ie. from the particles travelling at h = H (when $v_{SUS} > 0$) and is defined by P(H):

$$\text{Max } \{P_{SUS}(h)\} = P(H) \quad \text{where } h \geq H \tag{6.9}$$

$$\text{Max } \{P_{BED}(h)\} = P(0) \quad \text{where } 0 \leq h < H \tag{6.10}$$

The Penetration constant can therefore defined as follows:

$$k_p(H) = P(H)/P(0) \tag{6.11}$$

The Penetration Constant [k_p] is defined in this Section and evaluated in Section 6.4.11 after the relevant constants required to evaluate k_p are derived.

Focusing parameters determine the value of k_p. The probability function of detecting bed-load particle velocities is expressed in Section 6.7.7 in terms of k_p. Simply, a lower value of k_p leads to a higher probability of detecting bed-load particle velocities relative to detecting suspended-load particle velocities. It is therefore desirable to minimize the value of k_p with a suitable choice of focusing parameters.

6.4.4 Intensity and Power of a Focused Ultrasonic Beam

The relative intensity of a focused Tx. and Rx. system must be analysed and derived so that the relative backscattering power from the bed-load layer and from the suspended-load layer within the slurry can be derived, since this information is necessary to derive k_p.

Generally, the power of an ultrasonic beam at a distance z eminating from a source is defined as the intensity times the area of the beam at z. If a surface target is insonified by a Tx. beam, then the backscattering power [P] strength from the target at a Rx. is related to the intensity [I] times the insonified surface area of the target [A] times the surface backscattering strength [S] of the target as in Eqn. 6.12.

$$P = I \cdot A \cdot S \qquad (6.12)$$

If the intensity is not constant over the insonified area of the target, then the intensity must be integrated over the area to yield the backscattering power. The integration process can be simplified by using the peak value of the intensity over the surface of the target and by defining the effective area as the area over which the intensity does not deviate by more than a pre-determined amount (eg. 3dB) from the maximum intensity at the target.

The simple relation above is applied in calculating P(H) and P(0) so that k_p can be calculated.

The peak intensity from a layer of particles travelling at a height of h up from the pipe soffit is defined by I(h). At the bed-load bottom surface (at h = 0) the peak intensity is expressed by I(0) and at a layer of particles at the

suspended-load bottom surface (at h = H) the peak intensity is referred to as the suspended-load intensity and is expressed by I(H).

The effective areas as defined above of the insonified bed-load layer is expressed by A(0) and the effective insonified surface area of the suspended-load layer is defined by A(H). These areas are determined by evaluating the intensity beam pattern and is explained in detail in Section 6.4.10.

Since the backscattering strengths for each surface layer are equal (as discussed in Section 5.7.5), the ratio of the backscattering power can be defined independently of the surface backscattering strength. Also, since it is a relative backscattering power that must be determined, the transmitter power and the receiver sensitivity can be ignored since these factors are common to both calculations. The attenuation loss along the common transmission path can be ignored (ie. along d). The attenuation that occurs along the extra transmission path ie. within the bed-load layers for backscattering from the suspended-load surface must be included in the I(H) intensity term. The ratio of the backscattering powers is defined by Eqn. 6.13 as follows:

$$k_p(H) = P(H)/P(0) = I(H)\cdot A(H)/I(0)\cdot A(0) \qquad (6.13)$$

6.4.5 Focused Total Intensity Index and Peak Total Intensity Index

The peak intensity expressed in dB is referred to as a Peak Total Intensity Index [$TL_p(h)$] as follows:

$$TL_p(h) = 10 \text{ Log } [I(h)] \qquad (6.14)$$

$TL_p(h)$ must be evaluated for h = 0 and for h = H from which I(0) and I(H) can be determined and Eqn. 6.13 can be solved. $TL_p(h)$ is determined from the peak of a Focused Total Intensity Index term defined for the layer of particles at h. This Focused Total Intensity Index term describes the intensity index at a defined particle location within the slurry.

The particle location is defined by a coordinate system $[h,\delta\varphi_R]$ in terms of the particle height [h] up from the pipe soffit and a particle angle $[\delta\varphi_R]$. The particle angle specifies the direction that a beam ray travels relative to the Rx. normal within the transmission medium (ie. the transducer window) so that the ray passes through the specific particle. The angle lies within the beamwidth so that $-\varphi < \delta\varphi_R < \varphi$. This definition of the angle includes the effects of refraction at the slurry interface, as illustrated in Fig. 6.6, which also illustrates other transducer geometry variables, which will be discussed where appropriate. The actual and effective particle heights of the slurry as illustrated in Fig. 6.6 will be discussed in the following section.

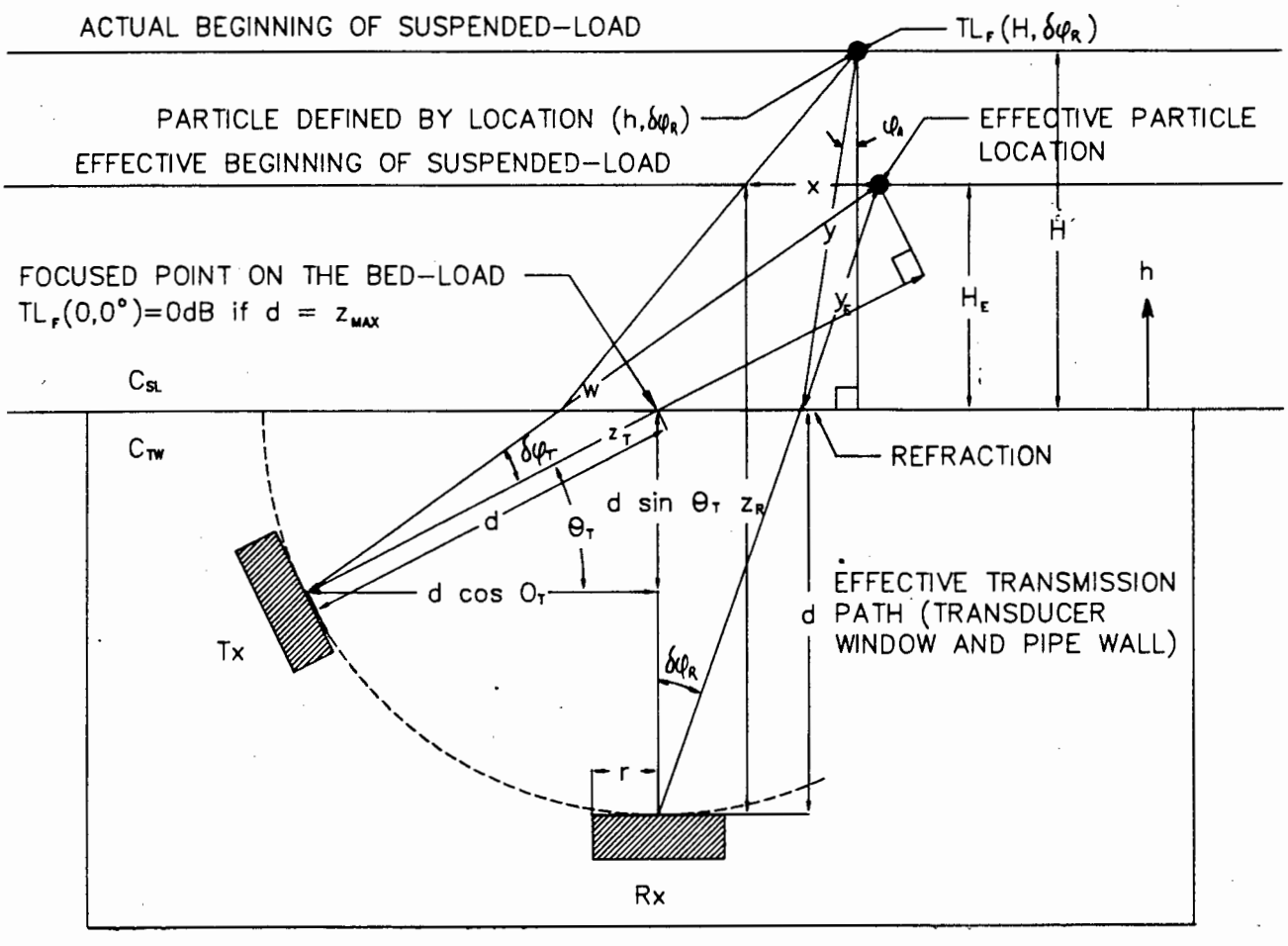

Fig. 6.7 Actual and Effective particle locations within the slurry

The Focused Total Intensity Index [$TL_F(h,\delta\varphi_R)$] is calculated by adding the three beam intensity loss terms defined for the location $(h,\delta\varphi_R)$. These three loss terms are the Focused Directivity Index [$DI_F(h,\delta\varphi_R)$] the Focused Axial Index [$AI_F(h,\delta\varphi_R)$] and the Attenuation Index [AT(h)].

The Focused Directivity Index is the sum of the Directivity Index of the Tx. and the Rx. These Directivity Indexes are

the relative ultrasonic beam intensities calculated from the directivity function equation (Eqns. 5.38 and 5.39) at the location within the slurry defined by the coordinates $h,\delta\varphi_R$. The intensities are relative to the maximum intensity which will occur for the focused point (ie. $h = 0$ and $\delta\varphi_R = 0^\circ$).

The Focused Axial Index is the sum of the Axial Index of the Tx. and the Rx. These Axial Indexes are the relative ultrasonic beam intensities calculated from the axial intensity equation (Eqn. 5.35 and 5.36) at the location within the slurry defined by the coordinated $h,\delta\varphi_R$. The intensities are relative to the maximum intensity which will occur for the focused point (ie. $h = 0$ and $\delta\varphi_R = 0^\circ$).

The Attenuation Index is the sum of the attenuation losses of the Tx. and Rx. beams as they penetrate into the slurry to the location defined by $h,\delta\varphi_R$.

Both the Focused Directivity Index and the Focused Axial Index are functions of h and $\delta\varphi_R$. The Attenuation Index is a function of h only and is independant of $\delta\varphi_R$. $TL_F(h,\delta\varphi_R)$ is expressed as follows:

$$TL_F(h,\delta\varphi_R) = DI_F(h,\delta\varphi_R) + AI_F(h,\delta\varphi_R) + AT(h) \qquad (6.15)$$

The peak value of $TL_F(h,\delta\varphi_R)$ for the bed-load layer (ie. within $0 \leq h < H$ and $-\varphi \leq \delta\varphi_R \leq \varphi$) will exist for h=0 (since the axial intensity is a maximum at a focused point on the bottom of the bed-load layer) and at a particle angle defined by $\delta\varphi_R'(0)$ which lies within the beamwidth. If it is arranged so that the $d = z_{MAX}$ then the peak value of the intensity index will be at the focused point directly above the Rx. crystal ie. at $\delta\varphi_R = 0^\circ$. This Total Peak Intensity Index is defined by $TL_p(0)$ for the bed-load layer as follows:

$$TL_p(0) = \text{Max } \{TL_F(h,\delta\varphi_R) \qquad \text{for } 0 \leq h < H \text{ and } -\varphi \leq \delta\varphi_R \leq \varphi \qquad (6.16)$$

$$= TL_F(0,\delta\varphi_R'(0)) \qquad \text{where } \delta\varphi_R'(0)=0^\circ \text{ if } d=z_{MAX}$$

The peak value of $TL_F(h,\delta\varphi_R)$ for detection of the suspended-load particles (ie. for $h \geq H$ and $-\varphi \leq \delta\varphi_R \leq \varphi$) will occur at $h = H$ and at a particle angle defined by $\delta\varphi_R'(H)$ which lies within the beamwidth. The peak total intensity index for detection of suspended-load particles is expressed by $TL_p(H)$ as follows:

$$TL_p(H) = \text{Max } (TL_F(H,\delta\varphi_R) \qquad \text{for } h \geq H \text{ and } -\varphi \leq \delta\varphi_R \leq \varphi \qquad (6.17)$$

$$= TL_F(H,\delta\varphi_R'(H))$$

The relationship between $TL_p(0)$ and $I(0)$ and $TL_p(H)$ and $I(H)$ is given as follows:

$$TL_p(0) = 10 \text{ Log } [I(0)] \qquad (6.18)$$

$$TL_p(H) = 10 \text{ Log } [I(H)] \qquad (6.19)$$

A discussion and derivation of each intensity index term follows so that $I(0)$, $I(H)$, $A(0)$ and $A(H)$ can be derived from which a value for $k_p(H)$ can be derived. Generally, it is desirable for the ratio of the Peak Total Intensity Index at $h = H$ compared with the Peak Total Intensity Index at $h = 0$ to be as small as possible at a particular height since this will generally lead to a lower value of $k_p(H)$. This will become clear later in the discussion of the probability function of detecting bed-load particle velocities in Section 6.7.7

6.4.6 Effective Slurry Particle Location

Refraction effects will occur as the ultrasonic beam penetrates into the slurry layers. This is because the propagation velocity within the slurry layers [c_{SL}] differs from the propagation velocity which is defined by the transducer window material [c_{TW}]. The refraction will cause the actual insonified volume to extend into layers of particles deeper than if no refraction occured (see Fig. 6.8.). The effective insonified volume is labelled on Fig. 6.8 which represents the insonified volume for the case of no refraction.

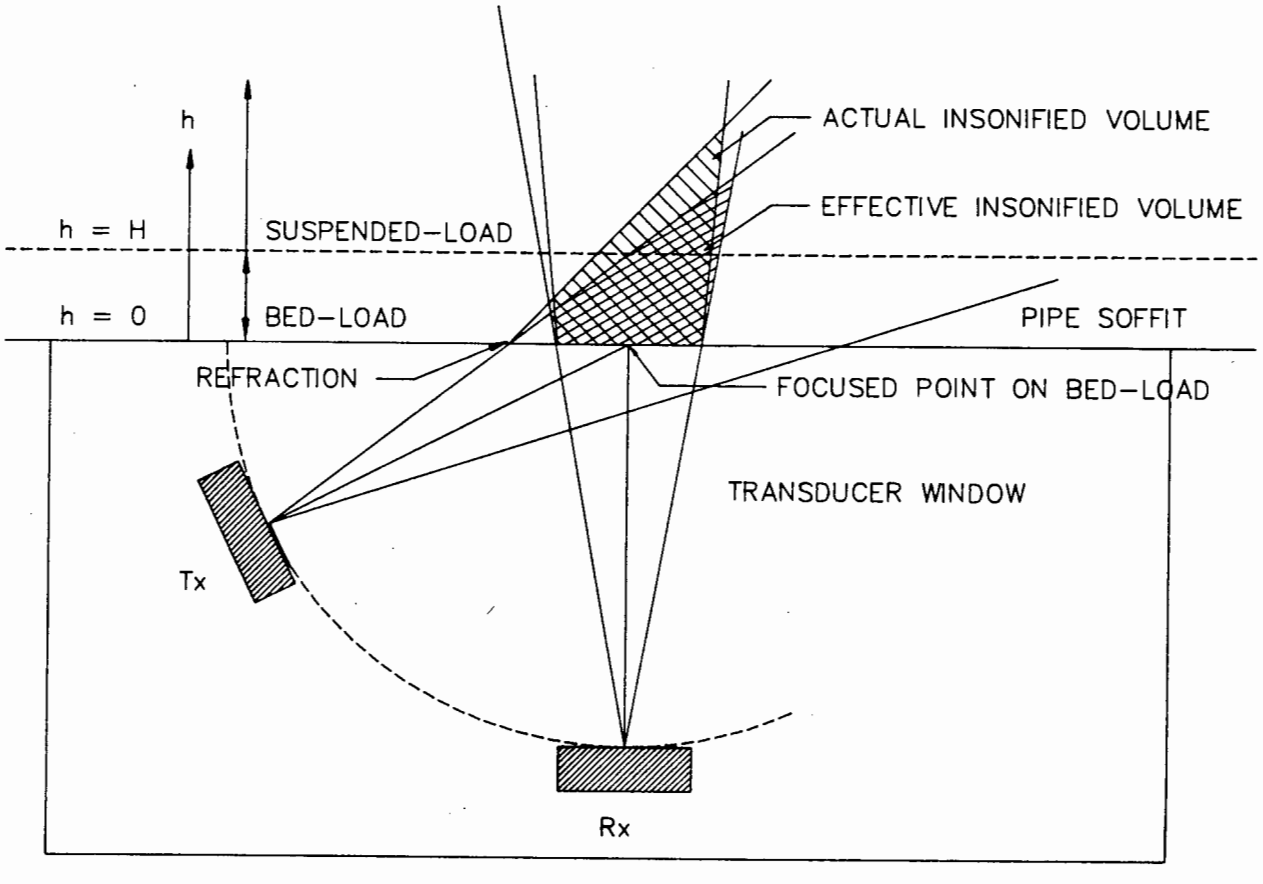

Fig. 6.8 Actual refracted insonified volume and effective insonified volume without refraction

A specific particle location within the slurry layer defined by the coordinated $h,\delta\varphi_R$ will have a Focused Total Intensity Index associated with it $[TL_F(h,\delta\varphi_R)]$. It is difficult to calculate this TL_F term since the beams refract and also because the slurry medium has a different ultrasonic propagation velocity to that of the transducer window.

To account for the refraction effects and to simplify the calculations of the intensity loss terms making up the TL_F term, an effective slurry particle layer height $[h_E]$ is defined. At this height defined below, it can be shown that the intensity terms can be calculated with three simplifying assumptions applying without any errors being introduced (these simplifications relate to each other). They are:

(i) The beams from the Tx. and Rx. travel in straight lines.

(ii) The ultrasonic velocity within the slurry equals that of the transducer window (ie. the transmission medium).

(iii) The axial intensity and the directivity intensity are defined in terms of the transducer window velocity (beamwidth).

The effective slurry height is determined for a particular slurry height so that the axial and directivity intensity terms can be evaluated by treating the slurry layer as an extension of the transmission medium (ie. the transducer window layer). The slurry can then be assumed to have an ultrasonic velocity equal to that of the transducer window so that refraction effects can be ignored (ie. the beams travel in a straight line).

The effective slurry height can be calculated by applying Snell's Law of refraction. Let the ultrasonic velocity in the transducer window be defined by c_{TW} and that of the slurry be defined by c_{SL}. According to Hamilton [Ref. 18], the ultrasonic propagation through saturated marine quartz sand can be related to the particle size as is presented in Table 6.1 below. The saturated concentration for which the measurements were made are also tabulated in Table 6.1. These saturated sands are typical of the type of particles making up the bed-load slurry in hydraulic transportation systems. They are presented here so that a value for c_{SL} can be chosen depending on the mean bed-load particle size for a particular hydraulic system.

Particle Type	Mean Particle size	Volumetric Concent-ration	Particle Density	Ultrasonic Velocity
	(μm)	(%)	(g/cm)	(m/s)
Course sand	530	61	2.71	1836
Fine sand	160	54	2.70	1749
Silt	24	43	2.66	1615

Table 6.1 Saturated sand ultrasonic velocity for different types of solid particles

In system design analyses in later sections, a typical value of c_{SL} of 1800m/s is used, corresponding approximately to the ultrasonic velocity in a course grain saturated as in Table 6.1 above.

For a particular particle location defined by $(h,\delta\varphi_R)$, the effective particle height $[h_E]$ can now be defined by Eqn. 6.20 (see Appendix. B, Part 1 (Eqn. B6) for a

derivation in terms of Snell's Law and the geometry of the transducer):

$$h_E = \frac{c_{SL}\, h \cos \delta\varphi_R}{c_{TW} \cos [\sin^{-1} (c_{SL}/c_{TW}) \sin \delta\varphi_R]} \qquad (6.20)$$

For h = H, the effective suspended-load height is defined in terms of H_E as in Eqn. 6.21:

$$H_E = \frac{c_{SL}\, H \cos \delta\varphi_R}{c_{TW} \cos [\sin^{-1} (c_{SL}/c_{TW}) \sin \delta\varphi_R]} \qquad (6.21)$$

Eqns. 6.20 and 6.21 can be simplified to Eqns. 6.22 and 6.23 with minimal error being introduced.

$$h_E = h \cdot c_{SL}/c_{TW} \qquad (6.22)$$

$$H_E = H \cdot c_{SL}/c_{TW} \qquad (6.23)$$

The errors introduced in these approximations are slight. For example, with c_{SL}/c_{TW} = 0.75 (such as propagation in a Resin transducer window, where c_{TW} = 2400m/s for a typical sand-water slurry with c_{SL} = 1800m/s) then the error will be <2% for $-17^\circ < \delta\varphi_R < 17^\circ$.

6.4.7 Directivity Intensity Pattern (Index)

To derive values for $TL_p(0)$ and $TL_p(H)$ for the particular set of focusing parameters, first the Focused Directivity Index term is derived since this is a loss term that is part of the derivation of the Focused Total Intensity Index term used in the expression for the Penetration Constant.

The Focused Directivity Index is defined by $DI_F(h,\delta\varphi_R)$ for a particle at the location defined by the coordinates

$(h,\delta\varphi_R)$. It is evaluated by determining the sum of the Directivity Index of the Tx. and the Rx. for the effective particle height $[h_E]$ and at the particle angle $\delta\varphi_R$. The sum of these two Directivity Indexes equals the focused Directivity Index for the particle location at $h,\delta\varphi_R$ as in Eqn. 6.24 that follows:

$$DI_F(h,\delta\varphi_R) = DI_T(h_E,\delta\varphi_R) + DI_R(h_E,\delta\varphi_R) \qquad (6.24)$$

A discrete number [n] of particle angles $[\delta\varphi_R]$ in the range $-\varphi_R$ to φ_R are evaluated on a Spreadsheet, where φ_R is the Rx. crystal's beamwidth as defined by Eqn. 5.40:

$$\delta\varphi_R = -\varphi_R \text{ to } \varphi_R \quad \text{in steps of } 2\varphi_R/n$$

The Directivity Index of the Rx. $[DI_R(\delta\varphi_R)]$ is now evaluated for each particle location within the Rx. beamwidth at the particle height [h] using Eqn. 5.38. $DI_R(\delta\varphi_R)$ is independent of particle height:

$$DI_R(\delta\varphi_R) = 10 \text{ Log } [b(\delta\varphi_R)] \qquad (6.25)$$

The Directivity Index of the Tx. $[DI_T(h_E,\delta\varphi_R)]$ is evaluated for the same particle locations as calculated for the Rx. This Directivity Index term is a function of the particle angle $[\delta\varphi_R]$ and of the effective particle height $[h_E]$.

The particle angle of the Tx. $[\delta\varphi_T]$ is calculated according to Eqn. 6.26. It is a function of the effective particle height, the particle angle and other focusing parameters. The effective particle height $[h_E]$ is first calculated according to Eqn. 6.20 for the particular particle height [h]. Once h_E is determined then $\delta\varphi_T$ can be calculated. A derivation of the expression for $\delta\varphi_T$ can be found in Appendix B.

$$\delta\varphi_T = \theta_T - \tan^{-1}\left[\frac{-(d \sin \theta_T + h_E)}{d \cos \theta_T + (d + h_E) \tan \delta\varphi_R}\right] \quad (6.26)$$

Now the Directivity Index of the Tx. can be calculated:

$$DI_T(\delta\varphi_T, h_E) = 10 \text{ Log } [b(\delta\varphi_T)] \quad (6.27)$$

To define the overall focused Directivity Index $[DI_F(h,\delta\varphi_R]$ at the defined particle location $(h,\delta\varphi_R)$, we add the Directivity Index of the Tx. and Rx.as in Eqn. 6.28.:

$$DI_F(h,\delta\varphi_R) = DI_R(\delta\varphi_R) + DI_T(\delta\varphi_T, h_E) \quad (6.28)$$

The $DI_F(h,\delta\varphi_R)$ function is evaluated vs. the particle angle $[\delta\varphi_R]$ on a "Quatro" Spreedsheet for various transducer system geometries. The data is evaluated for the system constants as follows: f_T = 1MHz and r = 5mm as in the final system design as follows.

(i) DI_F vs. $\delta\varphi_R$ for h=0mm for $\theta_T = 10^\circ, 30^\circ, 50^\circ$

Fig. 6.9 is a graph of the Focused Directivity Index due to backscattering from the bottom bed-load particles ie. for h = 0 for ultrasonic transmission in a medium with a 17° beamwidth (such as within the resin window at 1MHz with r = 5mm and c_{TW} = 2400m/s) for three Tx. orientation angles $[\theta_T]$

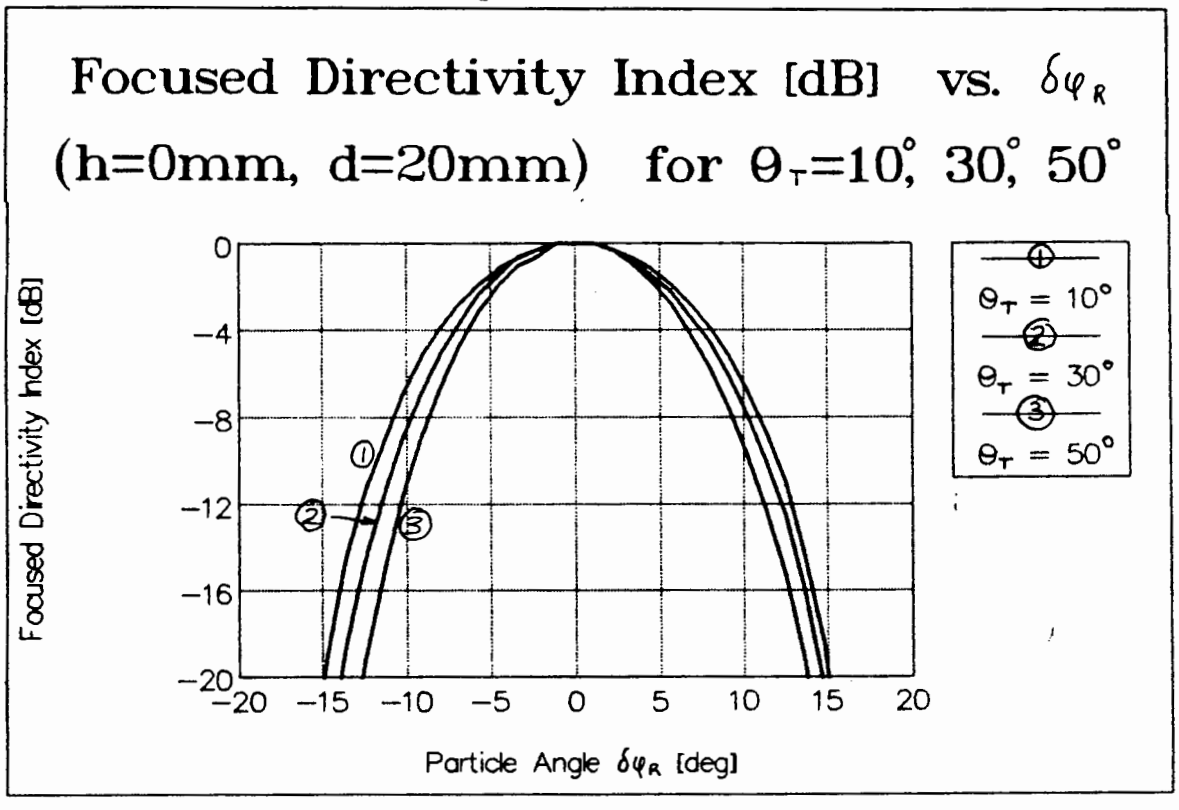

Fig. 6.9 Focused Directivity Index for three Tx. angles

At the point defined by h = 0 and $\delta\varphi_R = 0^\circ$, the value of DI_F is a maximum of 0dB since the Tx. and Rx. beams are focused directly at this point.

From Fig. 6.9 it can be seen that for lower Θ_T angles, the value of DI_F is lower for a particular particle angle.

(ii) DI_F vs. $\delta\varphi_R$ for $\Theta_T = 30^\circ$ for h = 0, 5 and 10mm

Fig. 6.10 is a graph of the Focused Directivity Index due to backscattering from layers of particles at three different

particle layer heights: h = 0, 5 and 10mm for the same set of focusing parameters as (i) above.

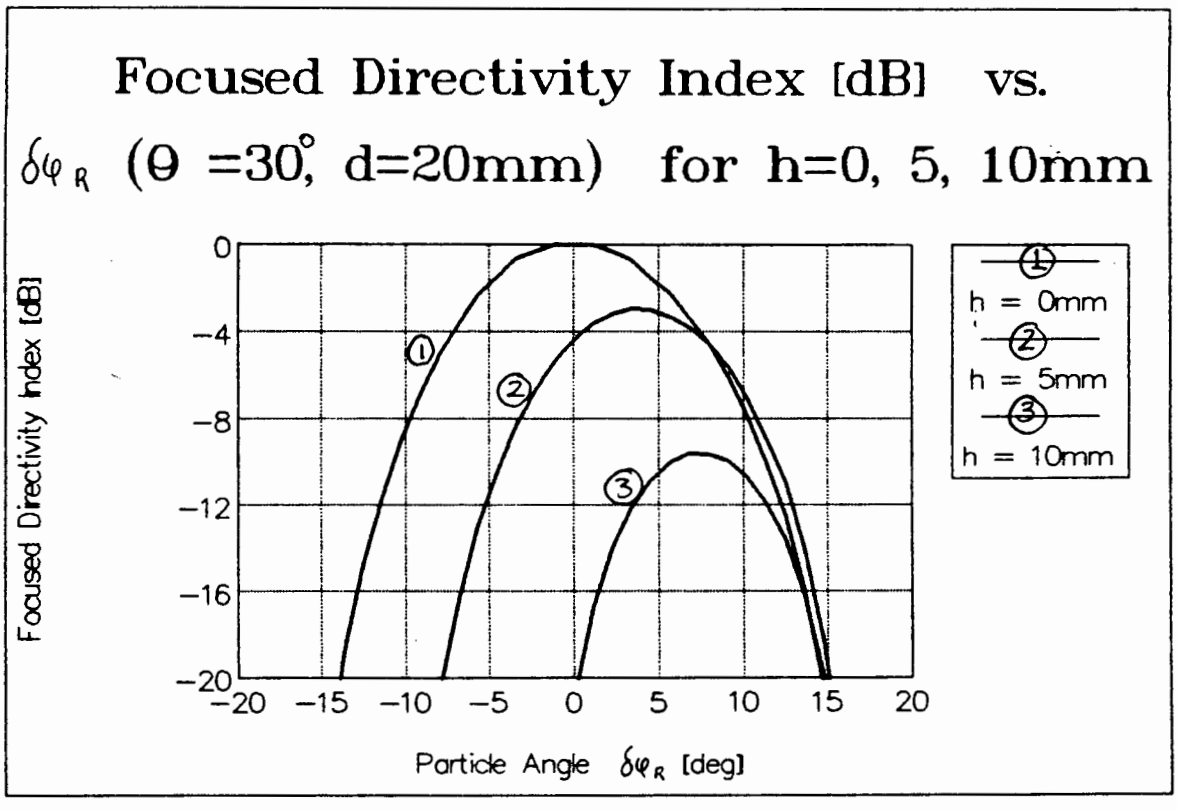

Fig. 6.10 Focused Directivity Index for three slurry layer heights

DI_F is seen to decrease for larger values of h, which is to be expected since the beams are focused on the bed-load bottom. The assymetry in the graphs for h > 0 is clear. This is because the insonified volume is assymmetric (see for example Fig. 6.8)

(iii) DI_F vs. $\delta\varphi_R$ for h = 0mm and $\theta_T = 30^\circ$ for $\varphi=17^\circ$ (Resin) and $\varphi = 43^\circ$ (Steel)

Fig. 6.11 illustrates the effect of beamwidth on the Focused Directivity Index by plotting DI_F for h = 0 for ultrasonic transmission in a medium with a 17° beamwidth and for transmission in a 43° beamwidth for the same set of focusing parameters as (i) above.

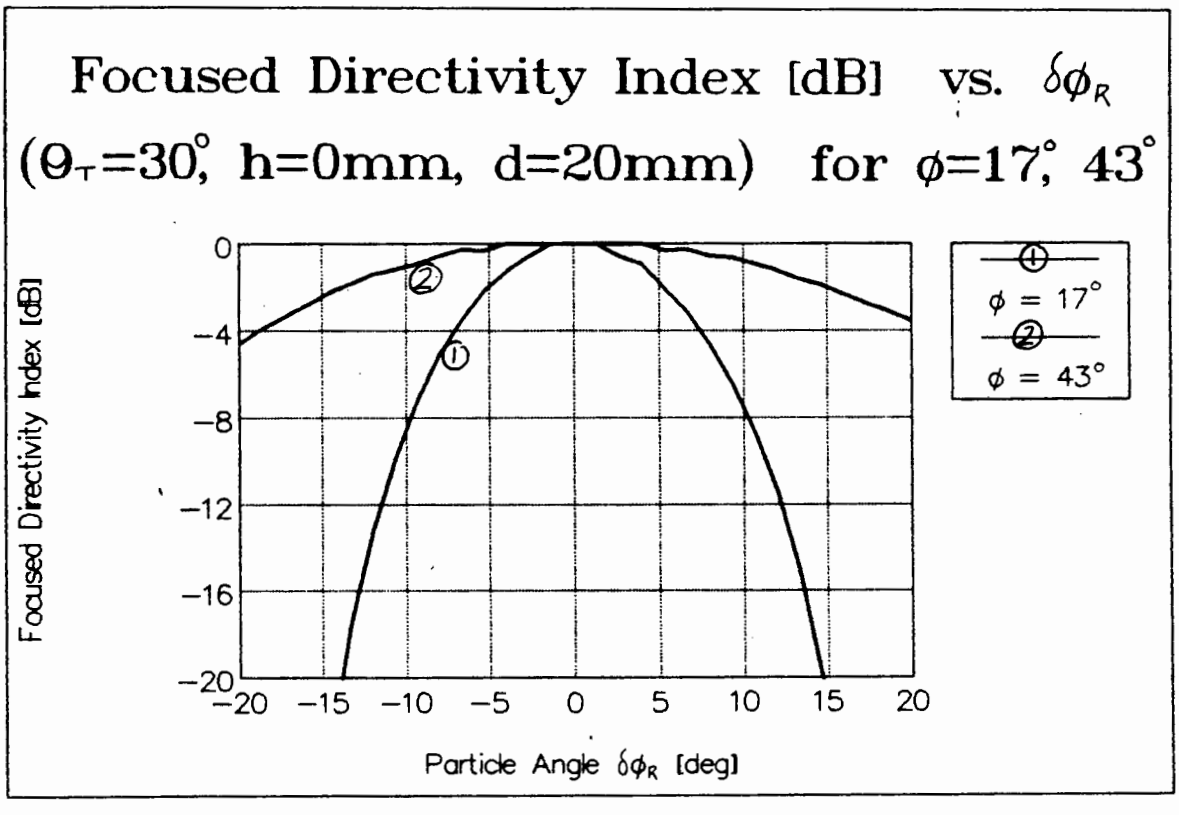

Fig. 6.11 Focused Directivity Index for two different beamwidths

Clearly the graphs show that the focused Directivity Index is directly related to the beamwidth. The DI_F is wider for wider beamwidths as expected, so that focusing will not be as directional.

Data from these graphs is used in deriving a value for the Pentration constant [k_p] in Section 6.4.11.

In addition to this Intensity Index term is the Axial Intensity Index, as follows.

6.4.8 Axial Intensity Distribution (Index)

The Axial Intensity distribution of the crystals (see Section 6.4.8.) is derived for the set of focusing parameters since this is an intensity term that is part of the derivation of the Total Intensity Index term used in the expression for the Penetration Constant.

The value of the axial intensity at a particular particle location defined by ($h, \delta\varphi_R$) is dependant only on the axial distance of the normal of each crystal face to the point of measurement of the particle within the slurry.

For each particle location, values for the effective height [h_E] is evaluated according to Eqn. 6.20.

The axial distance of the normal from the face of the Rx. crystal to the effective particle location [z_R] is calculated according to the geometry of the focusing system and equals the sum of the effective particle height [h_E] and the transmission path length [d] (see Fig. 6.7).

$$z_R = d+h_E \tag{6.29}$$

z_R can be expressed simply in terms of h by applying the simplification of Eqn. 6.22 and is valid for all particle angles, $\delta\varphi_R$, within the beamwidth $-\varphi$ to φ with minimal error as follows:

$$z_R = d + h \cdot c_{SL}/c_{TW} \quad (6.30)$$

The Axial Intensity index at $(h,\delta\varphi_R)$ for the Rx. $[AI_R(z_R)]$ can be calculated with Eqn. 5.35 and 5.36 for z set to z_R.

$$AI_R(z_R) = 10 \text{ Log } [a(z_R)] \quad (6.31)$$

To calculate the Axial Intensity index of the Tx. $[AI_T(z_T)$ at $(h,\delta\varphi_R)$, first the axial distance of the normal from the face of the Tx. crystal to the effective particle location $[z_T]$ is calculated according to Eqn. 6.32. A derivation of this equation which depends on the geometry of the focusing system and on Snell's Law is relegated to Appendix B, Part 3 (Eqn. B.10). It is a function of h and $\delta\varphi_T$ as follows:

$$z_T = \frac{(d \sin \Theta_T + h_E) \cos \delta\varphi_T}{\sin (\Theta_T - \delta\varphi_T)} \quad (6.32)$$

The expression for the axial Axial Intensity of the Tx. for this axial path length is as follows:

$$AI_T(z_T) = 10 \text{ Log } [a(z_T)] \quad (6.33)$$

The focused Axial Intensity Index $[AI_F(h,\delta\varphi_R]$ at the particle location $(h,\delta\varphi_R)$ is calculated by summing the Axial Intensities of the Tx. and Rx. as follows:

$$AI_F(h,\delta\varphi_R) = AI_R(z_R) + AI_T(z_T) \quad (6.34)$$

At the point defined by $z_R = z_T = z_{MAX}$ (see Eqn. 5.37), the value of $AI_F(h,\delta\varphi_R)$ is a maximum of 0dB according to the definition of Eqn. 5.37.

6.4.9 Focusing Effect on the Doppler Spectrum

Ignoring the transit time broadening effects (discussed later in Section 6.5.2), the Doppler PSD due to backscattering from the bed-load particles will resemble the $TL_F(0,\delta\varphi_R)$ vs. $\delta\varphi_R$ graph. The frequency-axis must however be altered. The Doppler frequencies can be derived from the orientation angles of the Tx. and Rx. beams on the bottom of the bed-load layer (h = 0mm) using the Doppler equation.

The mean Doppler frequency as defined by the Doppler equation corresponds to the detection of bed-load particles travelling at the location defined by h = 0mm and $\delta\varphi_R = 0^\circ$. The actual mean Doppler frequency, derived from the peak of the $TL_F(0,\delta\varphi_R)$ vs. $\delta\varphi_R$ graph will be due to the detection of particles defined by h = 0 and $\delta\varphi_R = \delta\varphi_R'(0)$ (as defined by Section 6.4.5). Only when $d = z_{MAX}$ will $\delta\varphi_R'(0)$ equal 0° (then the Axial Index and the Beamwidth Index will both be a maximum at h = 0 and $\delta\varphi_R = 0^\circ$ so that $\delta\varphi_R' = 0^\circ$). However, for the values of d investigated in the following examples, it may be assuemed, with slight error, that $\delta\varphi_R' = 0^\circ$, so that the mean Doppler frequency as defined by the Doppler equation holds.

The 3dB width of the Doppler PSD due to the finite ultrasonic beamwidth can be derived by calculating the Doppler frequencies (using the Doppler equation) that correspond to the detection of particles travelling at the location defined by the particle angles $\delta\varphi_R = \delta\varphi_R^-(0)$ and $\delta\varphi_R^+(0)$. This is because at these angles, the value of $TL_F(0,\delta\varphi_R)$ is -3dB down from the peak of the $TL_F(0,\delta\varphi_R)$ vs. $\delta\varphi_R$ graph. This 3dB width is defined as the Doppler beamwidth broadening and is derived later in Section 6.5.3. The other Doppler spectral broadening effects are also dicussed in Section 6.5.

6.4.10 Effective Surface Area of Insonified Particles

From Eqn. 6.13 to determine the Penetration constant we must first derive values for the effective target surface areas, A(0) and A(H). The bed-load and suspended-load surfaces can be approximated to be insonified by two cone-shaped beam-patterns with a surface area depending on the dimension of the cone in the x-direction as in Fig. 6.12

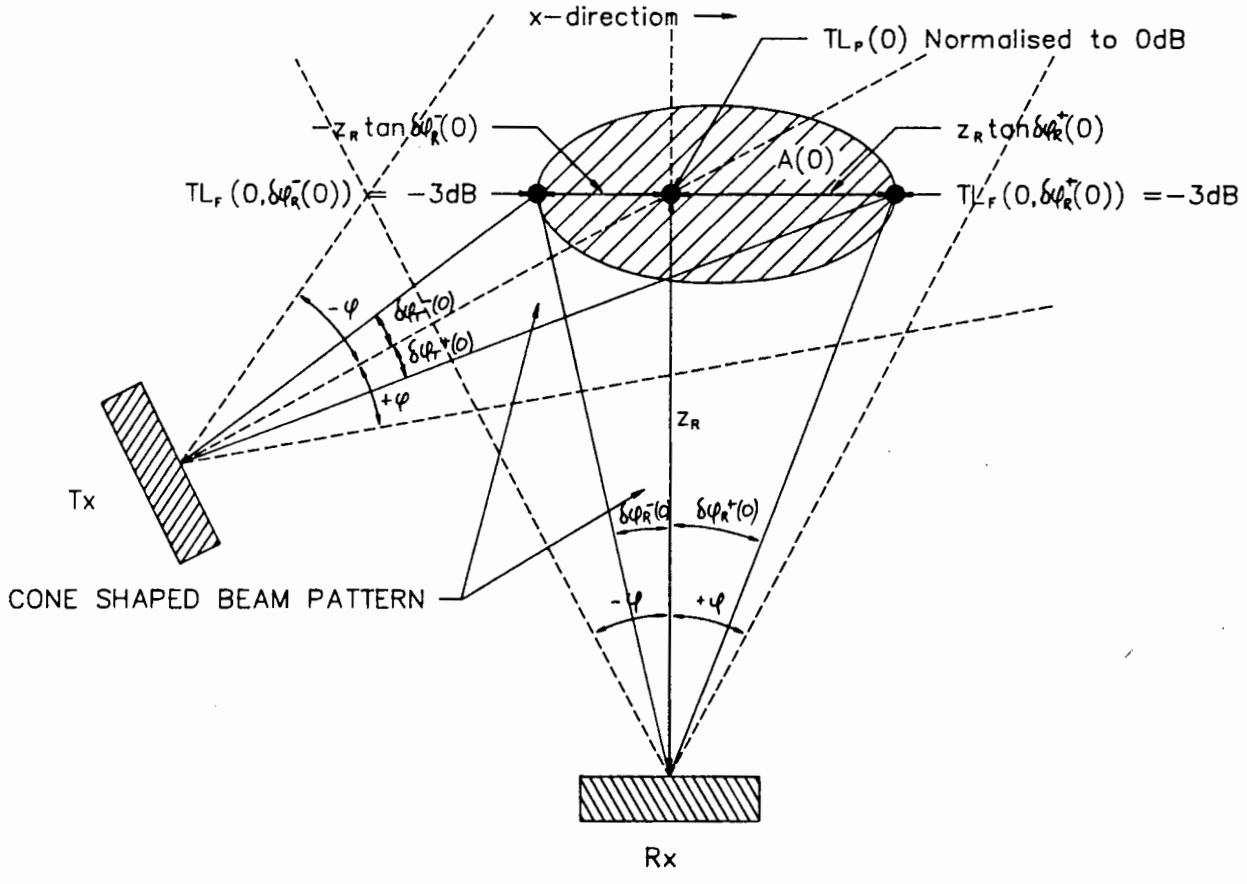

Fig. 6.12 Cone-shaped beam pattern geometry for calculating effective surface-area of bed-load and suspended-load

$$A(H) = \pi \left[z_R \left(\tan \delta\varphi_R^{+}(H) - \tan \delta\varphi_R^{-}(H) \right) \right]^2 \qquad (6.40)$$

The relative backscattering power ratio, or the Penetration constant [k_p] can now be determined from Eqn. 6.13.

$$k_p(H) = I(H) \cdot A(H) / I(0) \cdot A(0) \qquad (6.13)$$

where $I(H) = 10^{\wedge}(TL_p(H)/10)$

$I(0) = 10^{\wedge}(TL_p(0)/10)$

6.4.11 Focusing Analysis: Procedure for Calculating k_p from Focusing Parameters

This section describes the procedure for evaluating $k_p(H)$ from the set of focusing parameters by way of example.

The focusing parameters for this example are: $\Theta_T = 30^{\circ}$, d = 20mm and $\varphi = 17^{\circ}$. The ultrasonic velocity within the slurry layer [c_{SL}] is set equal to 1800m/s. The attenuation loss term with α = 0.26dB/mm is used. This value is chosen from Table 5. 2 for an operating frequency of 1MHz and for a slurry having a mean particle size of 180µm. k_p is evaluated for H = 10.

First, the $TL_F(H, \delta\varphi_R)$ term as a function of the particle angle $\delta\varphi_R$ is evaluated and graphed in Fig. 6.13. Two $TL_F(H, \delta\varphi_R)$ graphs are plotted on the same set of axis. The first graph is for H = 0mm, the second for H = 10mm.

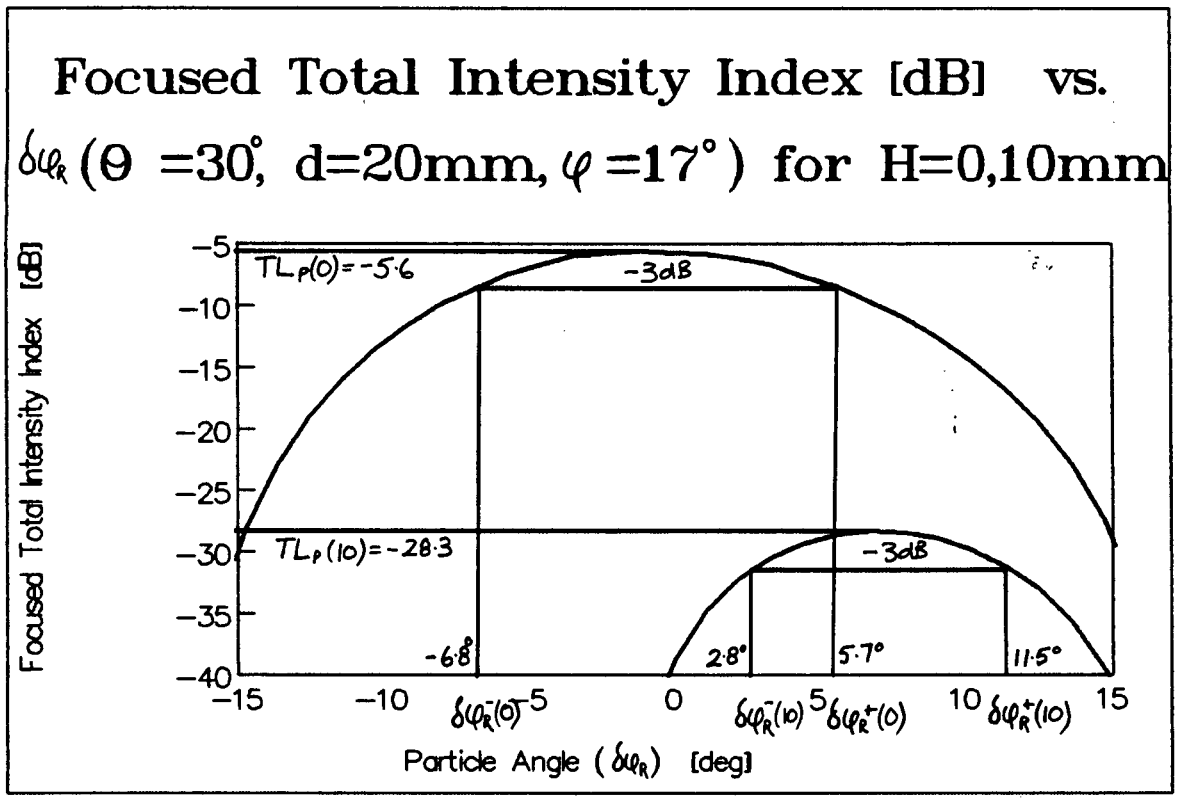

Fig. 6.13 Focused Total Intensity vs. Particle angle for the bed-load (H = 0) and for the suspended-load (H = 10)

The graphs of this figure clearly resemble the Directivity Index graph with h as a parameter in Fig. 6.10 except that in this case the losses are greater due to the Axial Intensity Index and the Attenuation Loss terms being added. As the value of H increases so the value of $TL_p(H)$ decreases as expected.

The procedure for determining $k_p(H)$ is as follows:

(1) Determine $TL_p(0)$ and $TL_p(H)$ (see Fig. 6.13.)

From the peak of these graphs, the Peak Focused Total Intensity Index for H = 0 and for H = 10 can be obtained:

$TL_p(0) = -5.6dB$
$TL_p(10) = -28.3dB.$

(2) The effective surface area A(0) is evaluated from the graph of Fig. 6.13.

- The particle angles $\delta\varphi_R^-(0)$ and $\delta\varphi_R^+(0)$ are determined.

These angles are determined from Fig. 6.13 according to the procedure discussed above in Section 6.4.10. In this example, $\delta\varphi_R^-(0) = -6.8^\circ$ and $\delta\varphi_R^+(0) = 5.7^\circ$ (see Fig. 6.14).

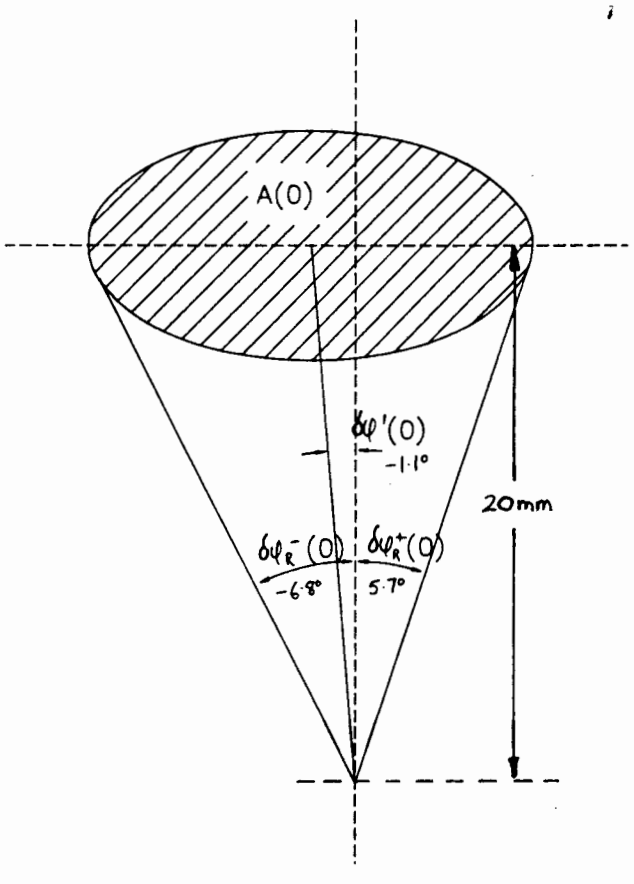

Fig. 6. 14 Cone shaped beam pattern for determining the surface area, A(0)

- The circular surface area of the cone is evaluated

Using Eqn. 6.37, A(0) can be calculated as follows:

$$A(0) = \pi \, [z_R \, (\tan \delta\varphi_R^+(0) - \tan \delta\varphi_R^-(0))]^2$$

with $z_R = d = 20mm$:

$$A(0) = \pi \, [20 \, (\tan (5.7^\circ) - \tan (-6.8^\circ)]^2$$
$$= 60.3mm^2$$

(3) The effective surface area, A(H), is evaluated from the graph of Fig. 6.13 with H = 10mm

- The particle angles $\delta\varphi_R^-(10)$ and $\delta\varphi_R^+(10)$ for H = 10 are determined.

From Fig. 6.13, $\delta\varphi_R^-(10) = 2.8^\circ$ and $\delta\varphi_R^+(10) = 11.5^\circ$.

- The circular surface area of the cone is evaluated

The area A(H) is calculated form Eqn. 6.40:

$$A(H) = \pi \, [z_R \, (\tan \delta\varphi_R^+(H) - \tan \delta\varphi_R^-(H))]^2$$

where $z_R = d + H_E$. Applying the simplification of Eqn. 6.23, $z_R = d + H \cdot c_{SL}/c_{TW}$. For H = 10mm, $H_E \approx 7.50$

$$A(10) = \pi \, [27.5 \tan (11.5^\circ) - \tan (2.8^\circ))]^2$$
$$= 56.7mm^2$$

(4) Calculate k_p from A(0), A(H), $TL_p(0)$ and $TL_p(H)$

For the above parameters, $k_p(H)$ with H = 10 can be calculated with Eqn. 6.13 as follows:

$$k_p(10) = P(10)/P(0)$$
$$= I(10)\cdot A(10)/I(0)\cdot A(0)$$

where $I(10) = 10^{(TL_p(10)/10)}$
$= 10^{(-28.3/10)}$
$= 0.0015$

and $I(0) = 10^{(TL_p(0)/10)}$
$= 10^{(-5.6/10)}$
$= 0.275$

$A(10) = 56.7mm^2$
$A(0) = 60.3mm^2$

$k_p(10) \approx 0.0051$

Expressed in dB, $k_p(10)\{dB\} = 10 \text{ Log } [k_p(10)] \approx -23dB$

6.4.12 Focusing Results and Conclusions: Relationship Between k_p and Focusing Parameters

Values for $k_p\{dB\}$ are evaluated on a Spreadsheet according to the procedure explained above and represented graphically below in Figs. 6.15, 6.16 and 6.17. These graphs are presented to illustrate the way in which k_p depends on the focusing parameters. From these graphs, the focusing parameters can be optimized by chosing those parameters which cause k_p to be a minimum. The graphs of Figs. 6.15 and 6.17 illustrates the relationship between k_p and the suspended-load height [H]. These two graphs are used in conjuction with the graphs of Section 6.7.8 to predict the probability of detecting particle velocities of those

particles that travel above the bed-load as suspended-load particles and are discussed further in Section 6.7.10 where they are applied.

(i) Penetration constant as a function of the suspended-load hight [H] for three Tx. angles of 10°, 30° and 50°. The transmission path length is set to 20mm and the beamwidth is 17° (see Fig. 6.15)

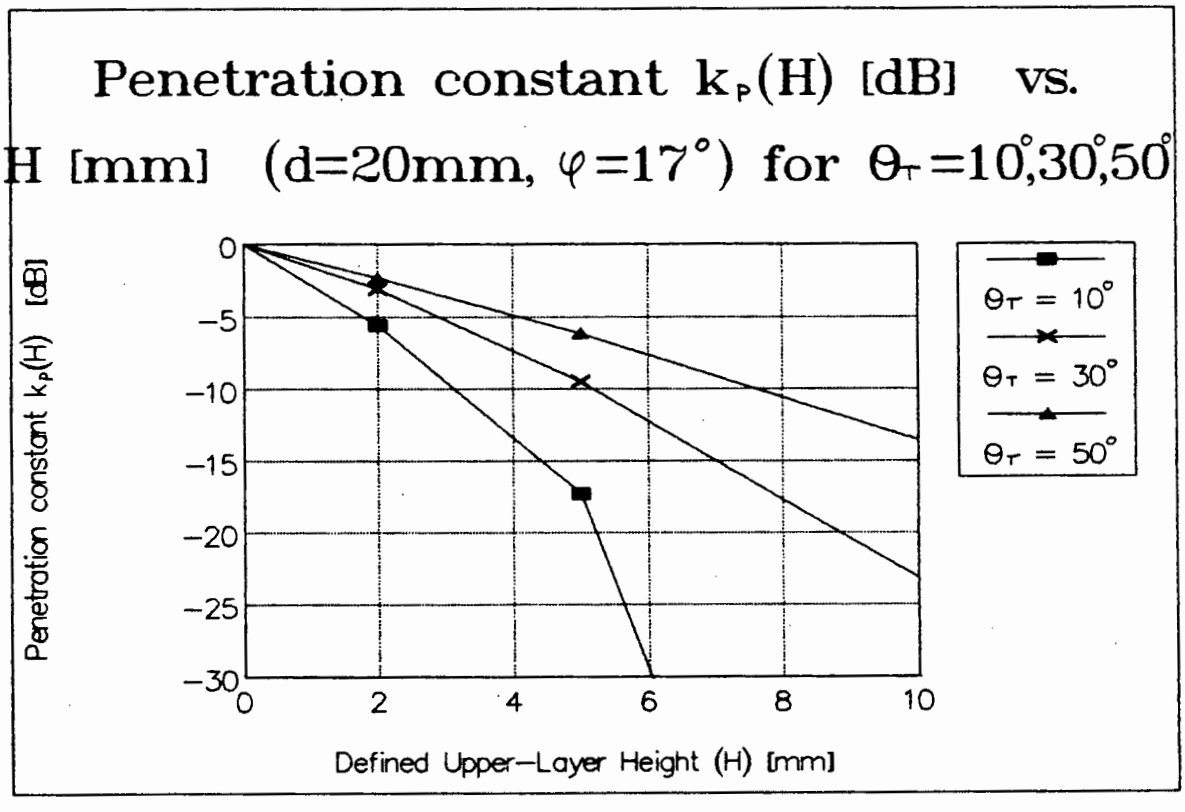

Fig. 6.15 Penetration constant vs. H for three Tx. angles

As expected, from Fig. 6.15, k_p decreases as H increases. This is to be expected for a focused system, since the maximum backscattered power is arranged to be from the bed-load layer bottom. k_p is seen to be smaller for smaller Tx. angles. For example, the value of $k_p(6)$ for this set of focusing parameters is as follows: $\theta_T = 50^\circ$, $k_p(6) = -7.5$dB; $\theta_T = 30^\circ$, $k_p(6) = -12.5$dB; $\theta_T = 10^\circ$, $k_p = -30$dB. Ideally, to minimize k_p, the smallest Tx. angle should be chosen.

(ii) Penetration constant as a function of the transmission path length for two different beamwidths of 17° and 43° (see Fig. 6.16).

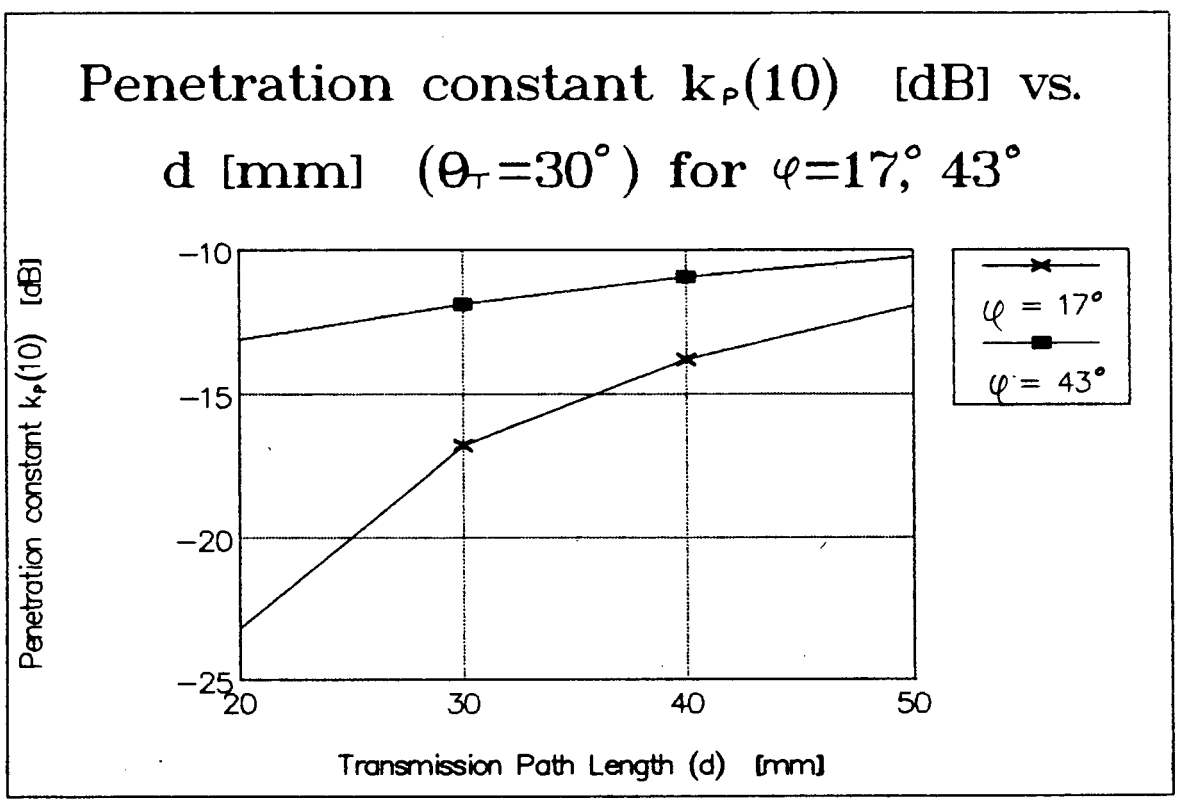

Fig. 6.16 Penetration constant vs. transmission path length for two beamwidths

From Fig. 6.16, for both cases of beamwidth, the value of k_p is seen to decrease with smaller values of d. It is therefore desirable to design the transducer window with the minimum possible transmission path dimensions. The lower restriction on the transmission path length and the transducer window path length is discussed in Sections 6.3.7, 6.3.8 and 6.3.9.

From this graph it is also clear that a larger beamwidth contributes to a larger value for k_p. It is therefore preferable to employ a transducer material so that the beamwidth is minimized.

(iii) Penetration constant as a function of the suspended-load height [H] for two different beamwidths of 17° and 43° (see Fig. 6.17)

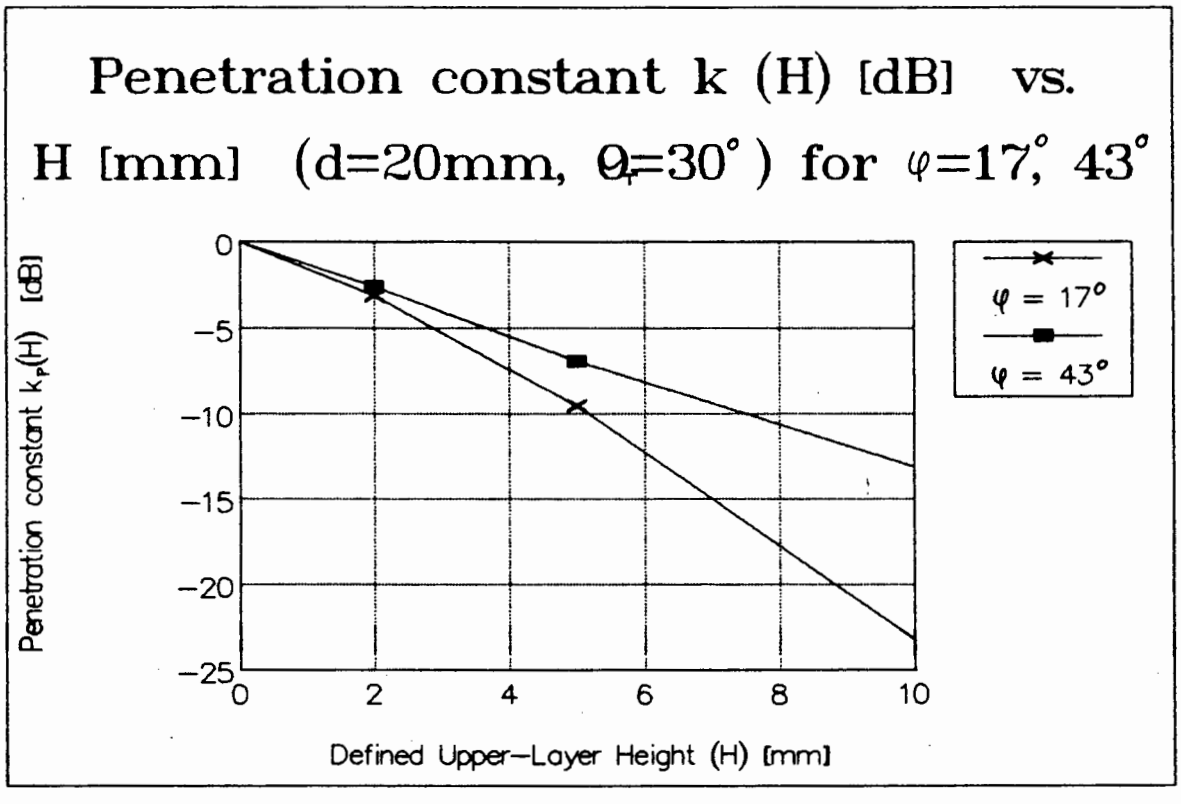

Fig. 6.17 Penetration constant vs. H for two beamwidths

k_p is seen to be smaller for the narrower beamwidth. A norrow beamwidth is therefore preferable to minimize k_p. For both beamwidth cases, k_p is seen to be inversely related to the height, H as expected.

Information presented in the graphs of Figs. 6.15, 6.16 and 6.16 is referred to in section 6.6 in optimizing the transducer parameters. Fig. 6.5 is referred to in Section 6.7.8 to investigate the probability of detecting bed-load particle velocities.

6.5 DOPPLER SPECTRAL BROADENING

6.5.1 Introduction

As discussed in Section 5.5.3, various causes contribute to the broadening of the Doppler spectrum. It should be bourne in mind that only the broadening of the bed-load Doppler signal is considered since it is assumed that appropriate design methods (as discussed in Section 6.7) are implemeted to prevent suspended-load Doppler signals from being processed. Therefore h = 0 can be assumed in the sections on broadening that follow. The mean Doppler frequency [f_D] therefore pertains the the detection of bed-load particle velocities.

In Section 5.5 it was determined that the two main causes of the broadening are finite transit time effects and finite beamwidth effects. These two broadening effects as they pertain to the present design are discussed and derived

below for a particular set of focusing parameters. Section 6.5.5 follows by discussing the way in which the Doppler broadening effects the processing of the mean Doppler signal, with specific reference to the accuracy in determining the mean Doppler frequency [f_D].

6.5.2 Transit Time Broadening

6.5.2.1 Transit Time Broadening Derived

Refering to the theory presented in Section. 5.5.5, the Doppler spectrum due to transit time broadening is Gaussian if the insonified volume is defined by two focused intersecting beams, which is the case in the present design. The 3dB transit time broadening bandwidth [f_{TT}] is expressed by Eqn. 5.27 as follows:

$$f_{TT} = 2 \,/\, (\sqrt{2}\, \tau_{TT}) \qquad (5.27)$$

where τ_{TT} is the transit time of the particle scatterers in the insonified volume.

From Eqn. 5.28, f_{TT} can be expressed in terms of the insonified volume dimension [δx] in the direction of the velocity of the moving particles (x-direction) (see Fig. 6.18):

$$f_{TT} = 2v \,/\, (\sqrt{2}\, \delta x) \qquad (5.28)$$

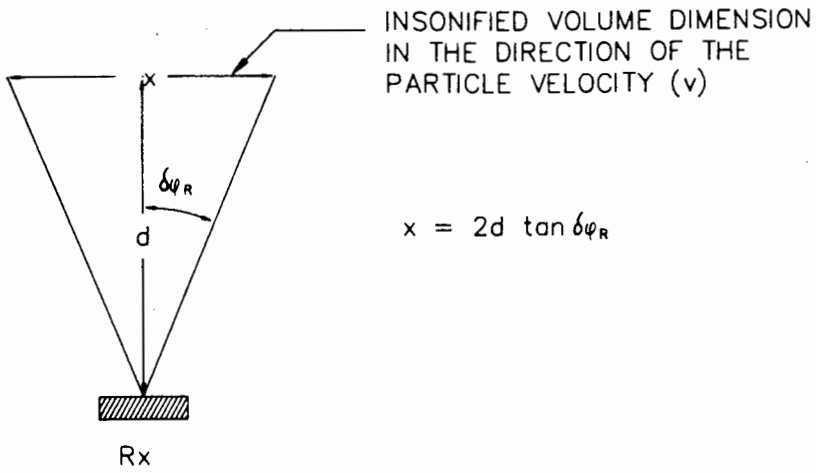

Fig. 6.18 Insonified volume dimension (x-direction)

From the geometry of the insonified volume (see Fig. 6.18), δx can be expressed as follows:

$$\delta x = 2 \cdot d \cdot \tan \varphi \qquad (6.41)$$

where d is the transmission path length and φ is the Rx. crystal's beamwidth.

To calculate the ratio of the transit time spectral broadening width as a ratio of the mean Doppler frequency [β_{TT}], substitute Eqn. 6.41 into Eqn. 5.28 and divide Eqn. 5.28 by the mean Doppler frequency as expressed by the Doppler equation (Eqn. 5.9):

$$\beta_{TT} = f_{TT}/f_D = \frac{2 \cdot v \cdot c}{2 \cdot \sqrt{2} \cdot d \cdot \tan \varphi_T \cdot f_T \cdot v \cdot \cos \theta_T} \qquad (6.42)$$

Making the substitution: $\lambda = c/f_T = r \cdot \sin \varphi / 0.61$, from Eqn. 5.40 and putting r = 5mm (as in the final design), we can derive the following expression for the ratio:

$$\beta_{TT} = 5.8 \cdot \cos \varphi / d \cdot \cos\theta_T \quad \text{(where d is in mm)} \qquad (6.43)$$

6.5.2.2 Analysis with Focusing Parameters

To investigate the manner in which the transit time broadening is dependent on the focusing parameters, β_{TT} is evaluated for various focusing parameters on a Spreadsheet and presented in graphical form in the following two examples.

(i) β_{TT} is evaluated in Fig. 6.19 for transmission in resin ($\varphi = 17^\circ$) as a function of the Tx. angle [θ_T] for three different transmission path lengths [d] equal to 20, 30 and 40mm.

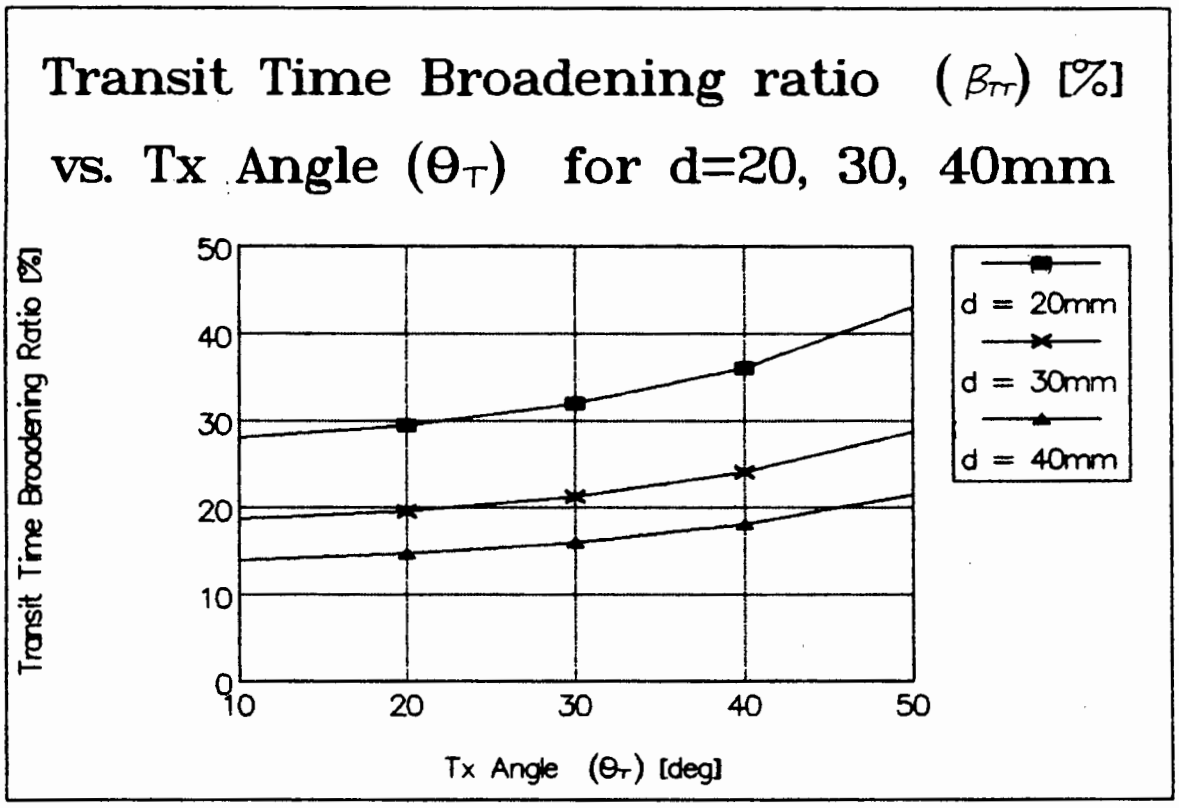

Fig. 6.19 Finite transit time broadening ratio as a function of Tx. angle for three transmission path lengths

It is evident that β_{TT} is reduced as the Tx. angle is reduced. For example, with d = 20mm, β_{TT} = 43% for $\theta_T = 50^\circ$ and β_{TT} = 28% for $\theta_T = 10^\circ$. Also clear is that β_{TT} is inversely proportional to d. For example, with $\theta_T = 30^\circ$ and d = 20mm, β_{TT} = 32% but with d = 40mm, β_{TT} = 16%

(ii) Fig. 6.20 is a graph of β_{TT} as a function of the transmssion path length [d] for two different beamwidths: φ = 17° (eg. resin transducer window) and φ = 43° (eg. steel transducer window material) for Θ_T = 30°.

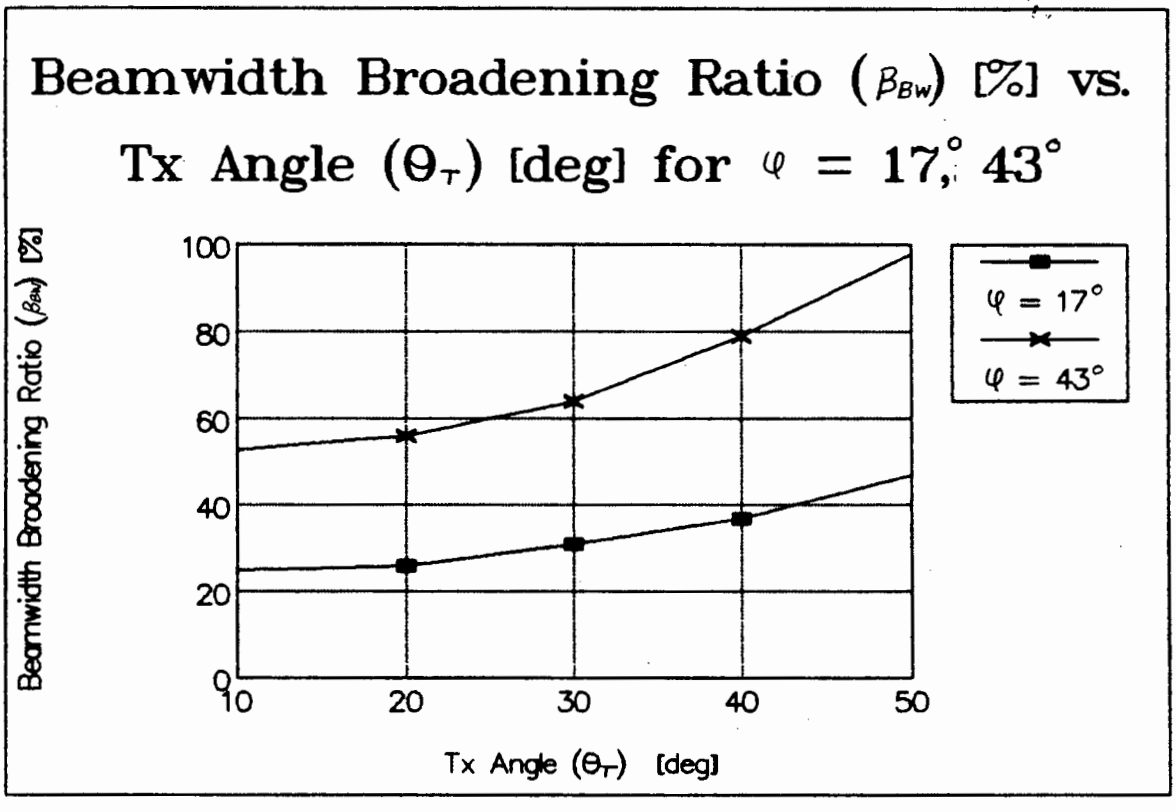

Fig. 6.20 Transit time broadening ratio as a function of transmission path length for two different beamwidths

From the graph of Fig. 6.20, the transit time broadening is seen to be reduced for the larger beamwidth case. For example, for d = 20mm and φ = 17° , β_{TT} = 32% and for φ = 43°, β_{TT} = 25%. Also, β_{TT} is seen to be inversely proportional to d as in the previous example of Fig. 6.19.

In Section 6.6, following this section, the focusing parameters are optimised. Referrence is made to the two previous examples.

6.5.3 Beamwidth Broadening

6.5.3.1 Beamwidth Broadening Derived Using Directivity Index

Note: In this Section, for shorthand of notation, the particle angles defined in Section 6.4.5: $\delta\varphi_R'(0)$, $\delta\varphi_R-(0)$ and $\delta\varphi_R+(0)$ are written as $\delta\varphi_R'$, $\delta\varphi_R-$ and $\delta\varphi_R+$ respectively.

Refering to the theory presented in Section 5.5.6, the finite beamwidth of the crystals cause a spread of Doppler frequencies. This is because θ_T and θ_R as defined by the Doppler equation are spread by an amount related to the beamwidth of the crystals. Reflections and hence Doppler shift signals are received from particles lying within the intersection of the Tx. and Rx. finite beamwidths (φ) and not only from particles lying specifically at the focused point of intersection of the beams defined by θ_T and θ_R. ie. the insonified volume is finite. This spreading effect is dependent on the geometry of the intersection of the beams.

The Power Spectral Density (PSD) of the Doppler spectrum due to beamwidth broadening can be determined from the Focused Total Intensity Index expression $[TL_F(h,\delta\varphi_R)]$ for a focused beam. Since it is the broadening of the bed-load Doppler signal that is to be determined, h is set to zero. The expression is used to evaluate values for the intensity index at the points defined by $(0,\delta\varphi_R)$ as in Section 6.4.5 for $\delta\varphi_R$ lying within the angle defined by the beamwidth of the Rx. beam ie. $-\varphi < \delta\varphi_R < \varphi$.

As mentioned in Section 6.4.9, the 3dB Doppler PSD width due to the beamwidth broadening effect can be derived by evaluating the Doppler frequency at the particle angles defined by $\delta\varphi_R^-$ and $\delta\varphi_R^+$. Recall from Section 6.4.10, the Focused Total Intensity Index expression (and therefore the Doppler PSD) is -3dB down from the Peak Total Intensity Index at these angles. The difference in the Doppler frequency from these angles equals the 3dB beamwidth broadening width.

Generally, the Doppler frequency from the point $(0,\delta\varphi_R)$ is given in terms of the beam angles at this point, as in Fig. 6.7 and is expressed as follows:

$$f_D(0,\delta\varphi_R) = f_T \cdot v \,[\cos(\theta_R+\delta\varphi_R) + \cos(\theta_T+\delta\varphi_T)] \qquad (6.44)$$

The Doppler frequency at the -3dB power points are defined by $f_D(\delta\varphi_R^-)$ and $f_D(\delta\varphi_R^+)$ and can be derived using the Doppler equation for these particle angles, as follows:

$$f_D(\delta\varphi_R^-) = \frac{f_T \cdot v \cdot (\cos(\theta_R+\delta\varphi_R^-)+\cos(\theta_T+\delta\varphi_T^-)}{c} \qquad (6.45)$$

$$f_D(\delta\varphi_R^+) = \frac{f_T \cdot v \cdot (\cos(\theta_R+\delta\varphi_R^+)+\cos(\theta_T+\delta\varphi_T^+)}{c} \qquad (6.46)$$

As mentioned above, the beamwidth broadening can be determined by calculating the difference between $f_D(\delta\varphi_R^+)$ and $f_D(\delta\varphi_R^+)$ as follows:

$$f_{BW} = f_D(\delta\varphi_R^-) - f_D(\delta\varphi_R^+) \qquad (6.47)$$

and dividing by the mean Doppler frequency $[f_D]$, β_{BW} is expressed as follows:

$$\beta_{BW} = f_{BW}/f_D = \frac{f_D(\delta\varphi_R^-) - f_D(\delta\varphi_R^+)}{f_D} \qquad (6.47)$$

By susbstituting Eqns. 6.45 and 6.46 into Eqn. 6.47 an expression for β_{BW} can be derived as follows:

$$\beta_{BW} = \frac{[\cos(\Theta_R+\delta\varphi_R^-)+\cos(\Theta_T+\delta\varphi_T^-)] - [\cos(\Theta_R+\delta\varphi_R^+)+\cos(\Theta_T+\delta\varphi_T^+)]}{\cos(\Theta_R) + \cos(\Theta_T)} \qquad (6.48)$$

6.5.3.2 Analysis with Focusing Parameters

An analysis of this beamwidth broadening as a ratio of the mean Doppler frequency is analysed using the same spreadsheet as in Section 6.4 (See Apendix D) by deriving values for Eqn. 6.48 with the focusing parameters as variables.

To derive the beamwidth broadening ratio [β_{BW}] as a function of the two focusing parameters [Θ_T, φ] that affect this ratio, the following four steps are taken. An example for $\Theta_T = 30^\circ$ and $\varphi = 17^\circ$ (recall that $\Theta_R = 90^\circ$) follows (note that the value of d has no effect on this broadening effect).

(1) Focused Total Intensity Index expression [$TL_F(h,\delta\varphi_R)$] with h = 0 is derived for $-\varphi < \delta\varphi_R < \varphi$. This expression is plotted in Fig. 6.13 for a Tx. angles [Θ_T] = 30°.

(2) The -3dB Rx. particle angles [$\delta\varphi_R^-$ and $\delta\varphi_R^+$] are obtained from the graph. From the graph of Fig. 6.13, $\delta\varphi_R^- = -6.8^\circ$ and $\delta\varphi_R^+ = 5.7^\circ$.

(3) The -3dB Tx. particle angles [$\delta\varphi_T^-$ and $\delta\varphi_T^+$] are derived using Eqn. 6.26 (with h_E=0). For this example, $\delta\varphi_T^- = -3.8^\circ$ and $\delta\varphi_T^+ = 2.7$

(4) The beamwidth broadening ratio, β_{BW}, can now be evaluated by using Eqn. 6.48 above. For example, with $\theta_T = 30^\circ$ and $\varphi = 17^\circ$, $\beta_{BW} = 30\%$.

β_{BW} is plotted as a function of the Tx. angle in Fig. 6.21 for two values of the beamwidth [φ] by following the above four steps. The calculations are carried out on a Spreadsheet as in Appendix D. The first graph is for $\varphi = 17^\circ$ and the second graph is for $\varphi = 43^\circ$.

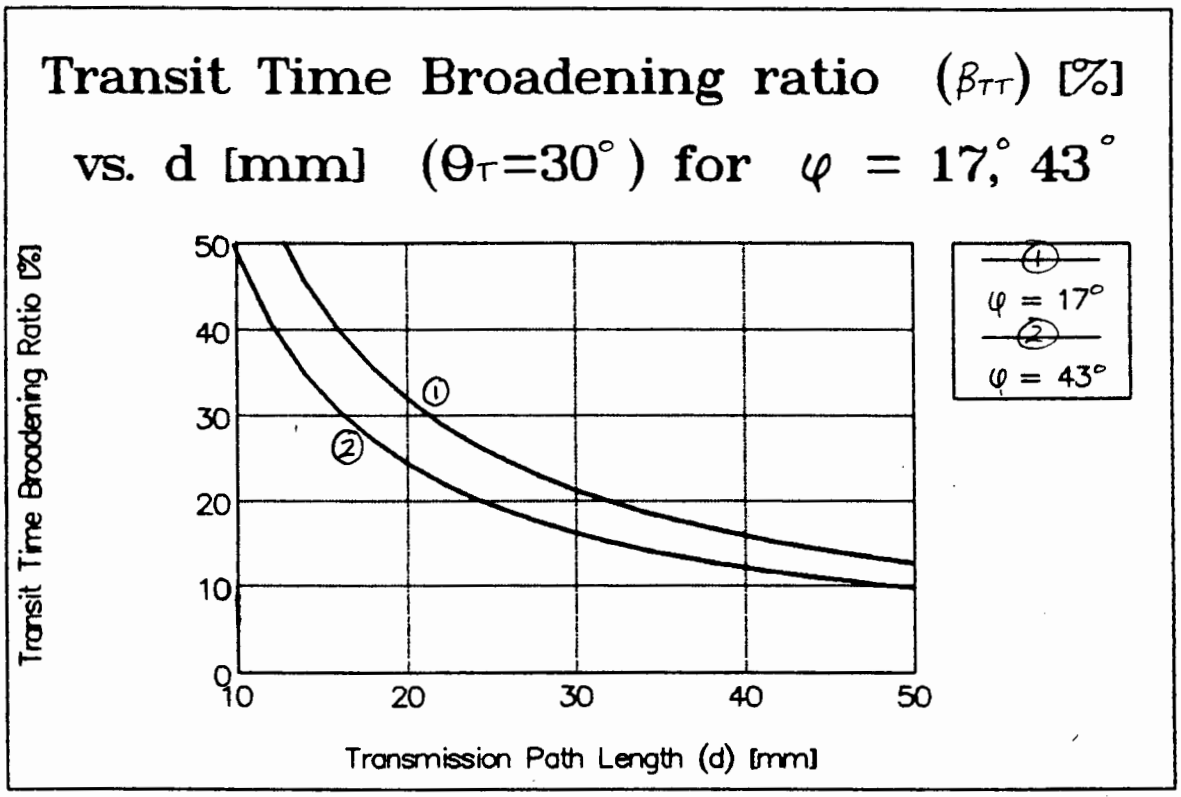

Fig. 6.21 Beamwidth broadening as a function of Tx. angle for two different beamwidths

It can be seen that as θ_T increases, the broadening ratio increases. Also, as φ increases, so the broadening ratio increases. For example for $\theta_T = 30^\circ$, with $\varphi = 17^\circ$ the Doppler power spectral width is 30% of the mean Doppler frequency and if $\varphi = 43^\circ$ then the Doppler spectral width is is 64% of the mean Doppler frequency.

6.5.4 Total Bandwidth due to Broadening

The 3dB Doppler bandwidth due to the two causes of broadening discussed above is defined by Eqn. 5.30 of Section 5.5.9:

$$f_{DB}^2 = f_{TT}^2 + f_{BW}^2 \qquad (5.30)$$

From Eqn. 5.29, the total 3dB bandwidth $[\delta f_D]$ due to the broadening effects and due to the detection of a fluctuating particle velocity is given as follows:

$$\delta f_D^2 = f_{DV}^2 + f_{DB}^2 \qquad (5.29)$$

The ratio of this total 3dB bandwidth to the mean Doppler frequency is expressed by the constant β as in Eqn. 5.31 as follows:

$$\beta = \delta f_D / f_D \qquad (5.31)$$

Using the result from Section 5.6.5 that the standard deviation of a single measurement of instantaneous frequency equals half the 3dB bandwidth, the standard deviation of the instantaneous Doppler frequency can be expressed as follows:

$$\sigma_D = \delta f/2 \qquad (6.49)$$

This result is used in the following section to analyse the accuracy in determining f_D in a finite measurement time.

6.5.5 Doppler Broadening Effect on the Doppler Processing

The Doppler PSD is represented as a broadened spectrum with its mean value defined by the Doppler equation [f_D] with a 3dB power bandwidth defined by δf_D, where δf_D is the total 3dB width of the Doppler PSD due to both broadening effects as well as from the detection of a particle velocity which fluctautes about a mean value [v] (see Section. 5.5.9)

The Doppler signal is processed (ie. its mean frequency is converted to a voltage) by means of a ZCC which is realized with a F-V converter circuit (discussed in Section 6.8.10). The influence of the broadening of the Doppler spectrum on the output voltage of the F-V converter [V_{FV}] is analysed below with reference to Section 5.5 on the Doppler Spectral broadening.

6.5.5.1 Deviation of Measurement from Mean Doppler Frequency

The Doppler signal is the input to the ZCC and the expected instantaneous frequency provided by the ZCC [expressed by f_Z] is defined by Eqn. 5.33 in terms of the mean Doppler frequency. This expression equals the RMS value of the Doppler frequency as follows:

$$f_Z = \overline{(f_D^2)}^{1/2} = f_{D(RMS)} \qquad (5.33)$$

We can evaluate Expression 5.33 for two cases to see the way f_Z and f_D are related. The first case is for the flat broadened Doppler PSD as given in Fig. 6.22 with f1 and f2

and the mean Doppler frequency, f_D as illustrated. The Doppler spectral width [δf_D] is the difference between f2 and f1:

$$\delta f_D = f2 - f1 \qquad (6.50)$$

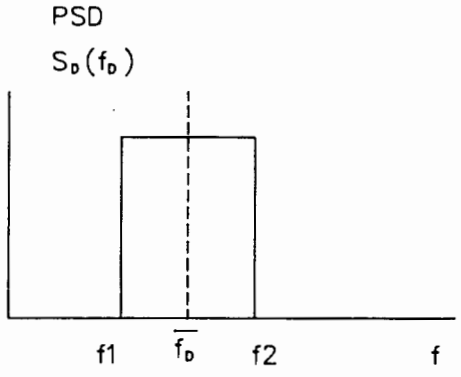

Fig. 6.22 Flat Doppler spectrum for case (i)

The second case [case (ii)] is for a Gaussian shaped Doppler PSD (see Fig. 6.23) with the constant β defined as above by Eqn. 5.31. The Gaussian shaped Doppler PSD is a good approximation of the actual Doppler PSD of the system.

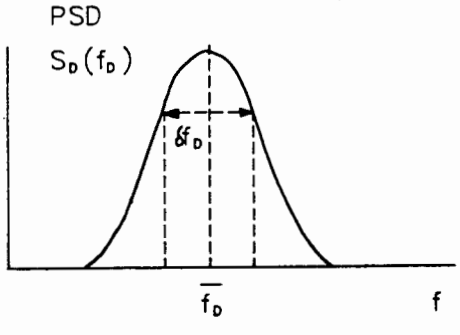

Fig. 6.23 Gaussian Doppler spectral shape for case (ii)

Case (i):

The Doppler frequency is the mean of f1 and f2:

$$f_D = (f1+f2)/2 \tag{6.51}$$

The RMS Doppler frequency from the ZCC is given by the expression from Brody et al. [Ref. 5]:

$$f_Z = \left[\frac{f2^3 - f1^3}{3\,(f2-f1)} \right]^{1/2} \tag{6.52}$$

The ratio of f_Z to f_D is given by Eqn. 6.53 from Ref. 5.

$$f_Z/f_D = \left[\frac{4}{3} \frac{f2^3 - f1^3}{(f2-f1)\,(f2+f1)^2} \right]^{1/2} \tag{6.53}$$

Now, for a broad spectrum, let f1 = 0. Then the ratio will be:

$$f_Z/f_D = \left[\frac{4}{3} \right]^{1/2} \approx 1.15 \tag{6.54}$$

Hence, for estimation of broad spectra, the ZCC produces a deviation of 15% from f_D, asuming a flat spectrum.

Case (ii):

For the case of a Gaussian shaped Doppler PSD, the result is adapted from Peronneau et al [Ref. 33]. A graph of f_Z/f_D vs. β is in Fig. 6.24.

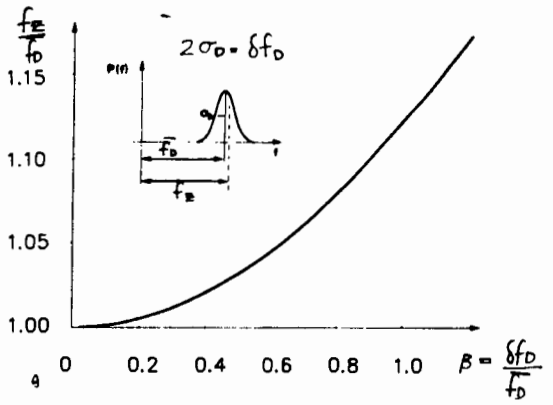

Fig. 6.24 Influence of the Doppler spectral width on determining the mean Doppler frequency

Clearly, it can be seen that as the Spectral width is reduced ie. as β approaches zero, so the ratio of f_{ℓ}/f_D approaches unity.

This case closely approximates the actual Doppler PSD. For a particular system, the value of β depends on all the broadening causes discussed above. Its value will be constant for a particular system. Its effect can therefore be eliminated if necessary by scaling the output voltage of the F-V converter by $k_{FV} \cdot f_D/f_{\ell}$, where k_{FV} is the F-V converter constant (see Section 6.8.10). This scaling operation is not actually performed in practice since the entire system is calibrated as discussed in Chapter 7, Section 7.2.

6.5.5.2 Accuracy of Mean Doppler Frequency Measurement

An expression for the accuracy of determining the mean Doppler frequency from the instantaneous Doppler frequency by means of a ZCC can be derived.

The expression for the accuracy is derived with reference to the two results from Schultheis in Section 5.6.5. Techniques to reduce this error will also be discussed. According to Denbigh [Ref. 10], the standard deviation of the instantaneous Doppler frequency [σ_D] equals the accuracy as a fraction of mean Doppler frequency [f_D] in determining the mean Doppler frequency from the instantaneous frequency. For example, if $\sigma_D/f_D = 0.3$ say, then the accuracy [defined by an error term, ϵ] in determining f_D is 30% of its mean value. The general expression for determining ϵ is given by Eqn. 6.55.

$$\epsilon = \sigma f_D/f_D \tag{6.55}$$

To improve the accuracy (ie. to reduce the error), the following two results from Denbigh [Ref. 10] are applied. Result (i): the accuracy of an estimate improves in proportion to the square root of the number of independant samples that are averaged. Result (ii): measurements of instantaneous frequency are statistically independant if seperated in time by the reciprocal of half the 3dB bandwidth.

If the output of the instantaneous Doppler frequency measuring device ie. the ZCC is smoothed or averaged over a time τ (the response time of the system), the resultant error will be reduced by $1/\sqrt{N}$ from result (i) above, where N is the number of statistically independant samples of f_D in τ seconds. From result (ii) above, the time between independant samples equals $1/2\delta f_D$. The number of independant samples is therefore expressed by Eqn. 6.56.

$$N = 2\tau \cdot \delta f_D \tag{6.56}$$

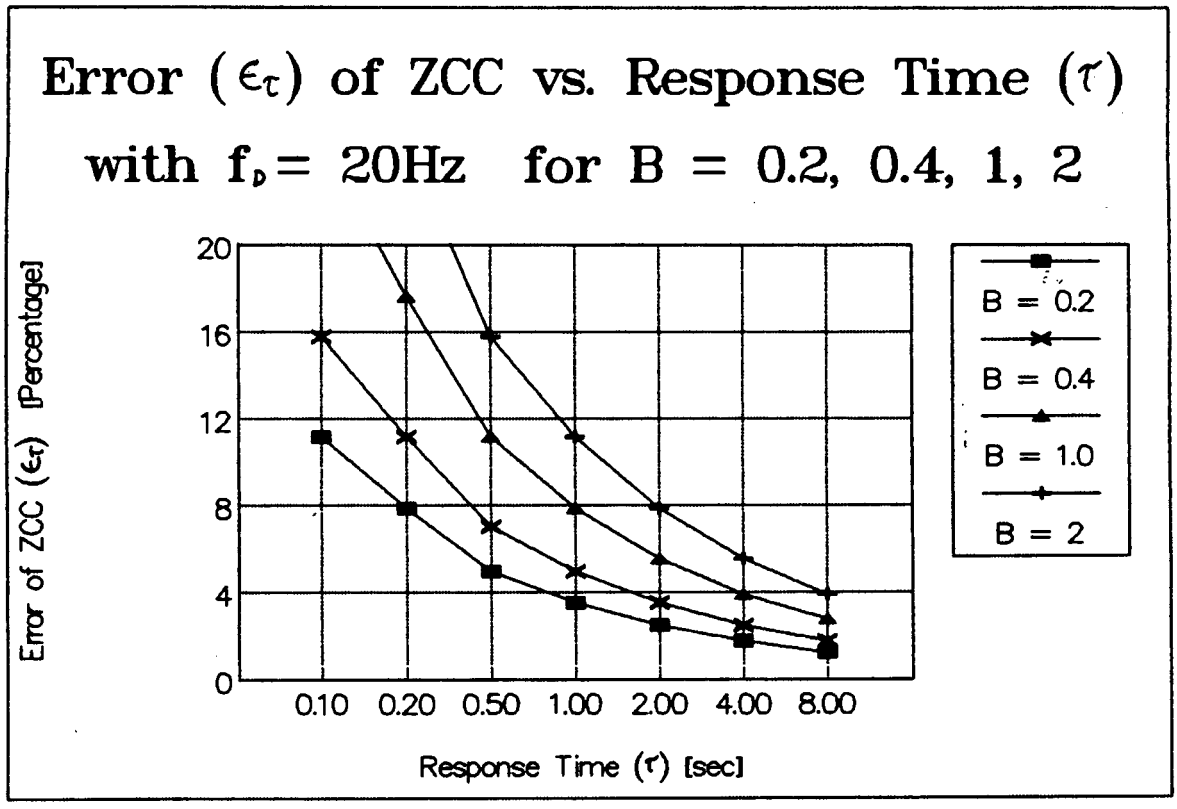

Fig. 6.25 ZCC Error function as a function of the response time for f_D = 20Hz for four different values of β

The error function is seen to reduce for larger response times as expected. The error function is also seen to be reduced for narrower Doppler spectrums (ie. β is smaller).

In Fig. 6.26 ϵ_τ is plottted as a function of the Doppler frequency with the response time set to 4s for four different values of β.

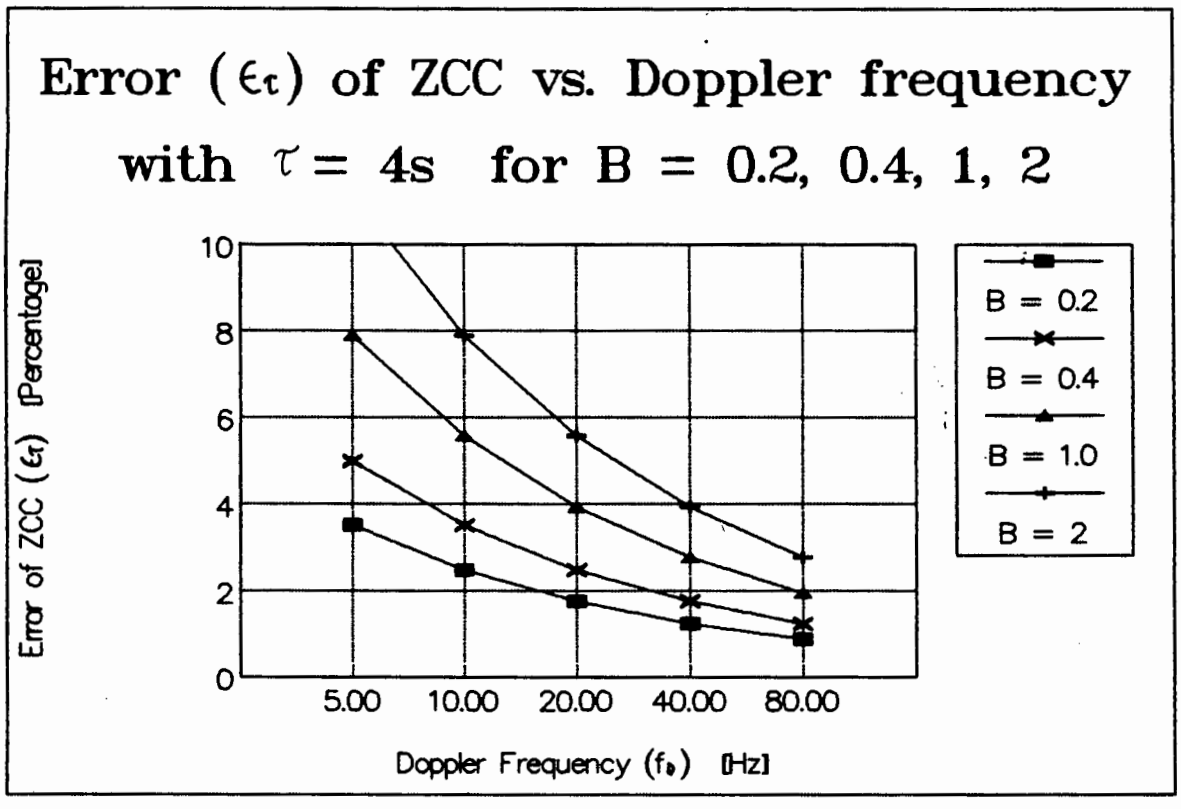

Fig.6.26 Error function as a function of the Doppler frequency with τ = 4s for four different values of β

The error function is seen to reduce for larger Doppler frequencies as expected. The error function is also seen to be reduced for narrower Doppler spectrums (ie. β is smaller) as above.

6.5.6 Conclusions

The two causes of Doppler spectral broadening, namely finite transit time broadening and beamwidth broadening have been derived for various sets of focusing parameters. The 3dB

Doppler spectral width due to transit time broadening is expressed as a ratio of the mean Doppler frequency by β_{TT}. It is seen that β_{TT} is reduced if the Tx. angle is reduced or if the transmission path is increased or if the beamwidth is wider.

The 3dB Doppler spectral width due to beamwidth broadening is expressed as a ratio of the mean Doppler frequency by β_{BW}. It is seen that β_{BW} is reduced if the Tx. angle is reduced or if the beamwidth is reduced.

The overall spectral width in terms of the two broadening effects has been expressed by a 3dB broadedning constant as a ratio of the mean Doppler frequency [β].

Processing the Doppler signal to determine the mean Doppler frequency using a zero-crossing counter [ZCC] has been discussed. It has been shown that a ZCC does not give a true mean value of a spectrum but rather gives an indication of the RMS value of the signal. The relationship between the mean Doppler frequency [f_D] and the output of the ZCC [f_Z] for a flat and a Gausssian Doppler PSD has been presented.

The accuracy in determining the mean Doppler frequency has been expressed by a Doppler error term [ϵ] and is dependent on the standard deviation of the Doppler PDF or on the spectral width of the Doppler PSD [β]. By definition, the accuracy is increased if the Doppler error is reduced. This error term can be reduced if a larger response time in determining the mean Doppler frequency is employed or if a larger minimum mean Doppler frequency is to be determined.

6.6 TRANSDUCER DESIGN PARAMETER OPTIMIZATION

6.6.1 Introduction

The three focusing parameters, namely the Tx angle (θ_T), the beamwidth (φ) and the transmission path length (d) determine: (i) the Doppler Spectral broadening effects and (ii) the probability of detecting bed-load particle velocities compared with the probability of detecting suspended-load particle velocities.

The two predominant Doppler spectral broadening components are the finite transit time broadening [β_{TT}] and the beamwidth broadening [β_{BW}] effects. They are both expressed as a percentage of the mean Doppler frequency and influence the accuracy of determining the mean Doppler frequency in a finite time (the system response time).

Extracting that part of the Doppler signal that is due to the detection of bed-load particle velocities will be expressed as a probability function which will be seen to be dependant on a Penetration constant [k_p] (see Section 6.7.7), which has been defined and evaluated in terms of the focusing parameters.

It has been stated that the efficiency of the transducer system is increased if (i) the Doppler Spectral broadening effects are minimized and (ii) if the probability of detecting bed-load particle velocities is maximized (which is identical if restated as: the Penetration constant [k_p] is minimized).

6.6.2 Transducer System Parameters

The descriptions in Table 6.2 is a summary of the optimum choice for the transducer focusing parameters so that k_p, β_{TT} and β_{BW} are all minimized, for example the beamwidth should be small to minimize k_p, while the beamwidth should be large to minimize β_{TT}.

Focusing Parameter	Penetration constant [k_p]	Transit Time Broadening [β_{TT}]	Beamwidth Broadening [β_{BW}]
(i) Tx Angle [θ_T]	1. small	2. small	3. small
(ii) Beamwidth [φ]	4. small	5. large	6. small
(iii) Transmission Path length [d]	7. small	8. large	9. No effect

Table 6.2 Optimum choice for focusing parameters to minimize k_p, β_{TT} and β_{BW}

The effect of each focusing parameter on the three terms: k_p, β_{TT} and β_{BW} is discussed below. (The numbering below corrsponds to the numbering in the table).

(i) Tx Angle [θ_T]

(1) Tx. Angle effect on the Penetration constant

Referring to Fig. 6.17 of Section 6.4.12, the graph of k_p vs. suspended-load height [H] with φ=17° and d=20mm for three Tx. angles of 10°, 30° and 50°. The optimum choice for θ_T is as small as possible, since the value of k_p is a minimum at the lowest Tx. angle. For example from the graph for H equal to say 4mm, $k_p(4)$=-5dB for θ_T=50° and $k_p(4)$=-13dB for θ_T=10°.

(2) Tx. Angle effect on the transit time broadening

Referring to Fig. 6.19 of Section 6.5.2.2., the graph of β_{TT} vs. θ_T, it is evident that the transit time broadening effects are minimized as θ_T is minimized.

(3) Tx. angle effect on the beamwidth broadening

Referring to Fig. 6.21 of Section 6.5.2.2, the graph of β_{BW} vs. θ_T, it is evident that the beamwidth broadening effects are minimized as θ_T is minimized.

The final choice for θ_T should therefore be as small as possible to reduce k_p, β_{TT} and β_{BW}. A lower limit on θ_T of 30° is however imposed as discussed in Section 6.3.10. This lower limit is therefore the chosen value for θ_T.

(ii) Beamwidth

(4) Beamwidth effect on the Penetration constant

Referring to Fig. 6.16 of Section 6.4.12, the graph of k_p vs. d for $\varphi=17^\circ$ and $\varphi=43^\circ$, the optimum choice for the beamwidth is the smaller of the two. Generally, as φ is reduced, so k_p is reduced, therefore a smaller beamwidth is desirable.

Referring to Fig. 6.17, the graph of k_p vs. H, it can be seen that a narrower beamwidth has a more marked effect on k_p when the suspended-load is high (ie. H is high).

(5) Beamwidth effect on the transit time broadening

Referring to Fig. 6.20 of Section 6.5.2.2, the graph of β_{TT} vs. d for φ=17° and φ=43°, the optimum choice for φ is the larger of the two. For example, referring to the figure, with d=20mm, β_{TT}=32% for the narrower beamwidth case (φ=17°) while β_{TT} is reduced to 25% for the wider beamwidth (φ=43°).

(6) Beamwidth effect on the beamwidth broadening

Referring to Fig. 6.21 of Section 6.5.3.2, the graph of β_{BW} vs. Θ_T for φ=17° and φ=43°, the beamwidth broadening effects can be minimized with a narrower beamwidth choice. This graph illustrates the marked effect that the beamwidth has on β_{BW}. With Θ_T=30° for the narrow beamwidth (φ=17°) , β_{BW}=32% and for the wider beamwidth (φ=43°), β_{BW}=64%.

In terms of minimizing the overall Doppler spectral width due to both broadening effects, φ should be chosen as 17°. Ignoring the Doppler broadening due to the fluctuation of the detectable particle velocities, then the Doppler spectrum will be broadened by the combination of both broadening effects and can be expressed by β (see Eqn. 5.31). At the chosen focusing parameters of Θ_T=30° (see (i) above) and d=20mm (see (iii) below), the overall spectral width is minimized when β_{BW} and β_{TT} are equal which occurs when φ=17°. The optimum beamwidth is therefore 17°.

This beamwidth is realized in practice with an operating frequency of 1MHz, r=5mm and with an Epoxy Resin transducer window with c_{TW}=2400m/s.

(iii) Transmission Path Length

The minimum transmission path length [d] is discussed in Section 6.3.8 and 6.3.9. For a steel pipe-wall, 4mm thick, the minimum value of d is approximately 20mm for φ=17° and r=5mm. This is therefore the minimum transmission path length used in the analysis of Figs. 6.16 and Fig. 6.20.

(7) Transmission path length effect on the Penetration constant

Referring to Fig. 6.16, the graph of k_p vs. d, it is clearly seen that a minimum value of d is desirable to reduce k_p.

(8) Transmission path length effect on the transit time broadening

Referring to Fig. 6.20, the graph of β_{TT} vs. d, the value of β_{TT} is inversely proportional to d. To reduce transit time broadening effects requires a larger transmission path length. However, with d set to its minimum value of 20mm and with φ=17° then β_{TT}=32%. This error is acceptable as discussed above in (ii).

(9) Transmission path length effect on the beamwidth broadening

The beamwidth broadening is independant of the value of d, so the value of d is chosen as a compromise between effect (7) and (8) above only.

The final choice for d is its minimum value of 20mm so that k_p is reduced, and so that β_{TT} does not exceed β_{BW} thereby

ensuring that the overall Doppler spectral width is a minimum.

6.6.3 Conclusion

The influence of the three focusing parameters: Tx. angle [Θ_T], beamwidth [φ] and transmission path length [d] on the efficiency of the focusing system has been analysed. The efficiency is increased by reducing the Penetration constant [k_p], and reducing the two spectral broadening causes: transit time broadening [β_{TT}] and beamwidth broadening [β_{BW}].

It was shown that the Tx. angle should be set to its minimum value of 30° to reduce k_p, β_{TT} and β_{BW}.

The narrower beamwidth was shown to reduce k_p and β_{BW} while it increased β_{TT}. As a compromise φ was set to 17° so that $\beta_{BW} = \beta_{TT}$ thereby reducing the overall Doppler spectral width [β] while still ensuring that k_p is minimized.

Lastly, a shorter transmission path length [d] was seen to reduce k_p while increasing β_{TT}. To reduce k_p, d was chosen to be its minimum value of 20mm (for a 4mm steel pipe-wall). For this low value of d, β_{TT} equals 32% (for Θ_T=30° and with φ=17°). This was stated as an acceptable error since it equals β_{BW} thereby ensuring that β is still a minimum.

6.7 BED-LOAD PARTICLE VELOCITY MEASUREMENT

6.7.1 Introduction

Eqn. 6.2 for the Doppler signal [D(t)] is an inaccurate over-simplification. Firstly, it ignores the fact that Doppler signals may be detected from slurry particles travelling above the bed-load as suspended-load particles. Detection of suspended-load Doppler signals will cause erroneous indications of bed-load velocities. This will be most evident when the bed-load is stationary and the suspended-load particles are in motion (ie. for the regime $v_{M2} < v_M < v_{M1}$). In this case, the bed-load layer acts as an extension of the transducer window with ultrasonic propagation existing within it. The suspended-load particles in motion above this layer will cause backscattering of the beam, containing Doppler shifted signals. These Doppler shifted signals will cause erroneous indications of a moving bed-load.

Secondly, the Doppler broadening effects have been neglected in the equation. Thirdly, the Doppler power is inversely proportional to height [h] and lastly, the Doppler power is not constant in time.

To investigate these effects on the Doppler signal, we must examine the physical features of the ultrasonic and hydraulic system in more detail. Once the Doppler signal is expressed more accurately then steps can be taken to maximise the probability of detecting bed-load particle velocities more accurately.

6.7.2 Accurate Representation of the Doppler Signal

The Doppler signal can be represented more accurately by taking the following four considerations that follow into account:

(1) Particles travelling anywhere within the insonified volume are detected.

Particles travelling within the insonified volume (ie. bed-load or suspended-load particles) could cause backscattering of the transmitted signal, producing Doppler signals to be received and demodulated. Suspended-load particles which are in motion while the bed-load particles are stationary (as in the flow regime $v_{M1} < v_M < v_{M2}$), will falsely indicate the presence of a moving bed unless design action is taken to prevent this.

The Doppler signal can be represented as the sum of the bed-load and the suspended-load signals as in Eqn. 6.60.

$$D(t) = D_{BED}(t) + D_{SUS}(t) \qquad (6.60)$$

At each height h, of infinitesimal thickness (δh), a layer of particles are present, and depending on the flow regime may or may not be moving at a velocity defined by v(h). Recall that the bed-load Doppler signals extend from a height [h] from the pipe soffit (h = 0) to the beginning of the bed-load/suspended-load interface (h = H) and the suspended-load particles travel above these particles (ie h > H). The bed-load and the suspended-load velocities are therefore defined in terms of h. Refer to Figs. 5.3, 5.4, 5.5 in Section 5.2.2 for examples of $v_{BED}(h)$ and $v_{SUS}(h)$ for different flow regimes.

The signal has a peak amplitude [D] at its mean frequency [f]. The signal is broadened with a (say 3dB) width defined by δf according to Eqn. 6.65.

$$\delta f = \beta \cdot f \tag{6.65}$$

P can be expressed as the product of the amplitude and the width as in Eqn. 6.66.

$$P = D \cdot \delta f \tag{6.66}$$

Solving Eqn. 6.66 for δf and substituting δf into Eqn. 6.65 and setting $A = P/\beta$ yields an expression for D as in Eqn. 6.67.

$$D = A/f \tag{6.67}$$

This general expression for D in terms of A and f can be applied to the bed-load and suspended-load Doppler amplitudes. $D_{BED}(h)$ and $D_{SUS}(h)$ are therefore functions of $A_{BED}(h)$ and $f_{D(BED)}(h)$ and $A_{SUS}(h)$ and $f_{D(SUS)}(h)$ respectively and are represented as follows:

$$D_{BED}(h) = A_{BED}(h) \;/\; f_{D(BED)}(h) \tag{6.68}$$

$$D_{SUS}(h) = A_{SUS}(h) \;/\; f_{D(SUS)}(h) \tag{6.69}$$

where $A_{BED}(h) = P_{BED}(h) \;/\; \beta$ (6.70)

and $A_{SUS}(h) = P_{SUS}(h) \;/\; \beta$ (6.71)

The broadening constant, β is identical for both bed-load and suspended-load Doppler frequencies since the same causes of the broadening apply to both frequencies.

The Doppler amplitude [$D_{BED}(h)$] from the detection of bed-load particles travelling at a particular bed-load height h, is zero when the bed-load is stationary ($v_M < v_{M2}$) and has a

maximum value, $Max\{D_{BED}(h)\}$, at the minimum detectable Doppler frequency, $[f_D(min)]$, corresponding to the lowest detectable value of v_{BED} at $v_M \geq v_{M2}$:

$$Max\ \{D_{BED}(h)\} = A_{BED}(h)\ /\ f_D(min) \qquad (6.72)$$

The minimum bed-load Doppler amplitude occurs when the maximum Doppler frequency is detected as follows:

$$Min\ \{D_{BED}(h)\} = A_{BED}(h)\ /\ f_D(max) \qquad (6.73)$$

Similarly, at a particular suspended-load height h, $D_{SUS}(h)$ is zero for $v_M < v_{M1}$ and is a maximum value, $Max\{D_{SUS}(h)\}$, at the minimum detectable Doppler frequency $[f_D(min)]$, corresponding to the lowest detectable value of v_{SUS} at $v_M \geq v_{M1}$:

$$Max\ \{D_{SUS}(h)\} = A_{SUS}(h)\ /\ f_D(min) \qquad (6.74)$$

(3) The power of the Doppler signals are inversely proportional to h.

In Section 6.4.3 a Penetration constant $[k_P]$ was defined and evaluated to describe the relative backscattered power from particles travelling at a height h = 0 (the bed-load bottom) and for h = H (the bottom of the suspended-load layer). The value of this constant is a function of the focusing parameters. If the two focusing criteria of Section 6.4.1 are satisfied then k_P is a maximum at h = 0 and is inversely related to h for all sets of focusing parameters.

This means that the maximum backscattering power from the bed-load is due to backscattering from the lowest layer of particles, ie. from the particles travelling at h = 0 (when $v_{BED} > 0$). Similarly, the maximum backscattering power from

the suspended-load is due to backscattering from the lowest layer of particles, ie. from the particles travelling at h = H (when $v_{SUS} > 0$). The Penetration constant therefore describes the ratio of the maximum suspended-load backscattering power to the maximum bed-load Doppler power as expressed by Eqn. 6.8:

$$k_p(H) = \text{Max } \{P_{SUS}(h)\} \; / \; \text{Max } \{P_{BED}(h)\} = P(H)/P(0) \qquad (6.8)$$

From Eqns. 6.70 and 6.71 above, the Penetration constant can also be expressed as follows:

$$k_p(H) = \text{Max } \{A_{SUS}(h)\} \; / \; \text{Max } \{A_{BED}(h)\} = A_{SUS}(H)/A_{BED}(0) \qquad (6.75)$$

The maximum bed-load Doppler amplitude at height h is given by Eqn. 6.72., Within the entire bed-load layer, the maximum Doppler amplitude occurs when $A_{BED}(h)$ is a maximum ie. at h = 0 and is expressed by Max $\{D_{BED}(0)\}$ as in Eqn. 6.76.

$$\text{Max } \{D_{BED}(0)\} = \text{Max } \{A_{BED}(h)\}/f_D(\text{min}) = A_{BED}(0)/f_D(\text{min}) \qquad (6.76)$$

Similarly, the maximum suspended-load Doppler amplitude within the entire suspended-load, occurs when $A_{SUS}(h)$ is a maximum ie. at h = H and is expressed by Max $\{D_{SUS}(H)\}$ as in Eqn. 6.77.

$$\text{Max } \{D_{SUS}(H)\} = \text{Max } \{A_{SUS}(h)\}/f_D(\text{min}) = A_{SUS}(H)/f_D(\text{min}) \qquad (6.77)$$

Eqn. 6.77 can be written in terms of $A_{BED}(0)$ and $k_p(H)$ from Eqn. 6.75 as follows:

$$\text{Max } \{D_{SUS}(H)\} = A_{SUS}(H)/f_D(\text{min}) = k_p(H) \cdot A_{BED}(0)/f_D(\text{min}) \quad (6.78)$$

The minimum bed-load Doppler amplitude from particles travelling at h = 0 occurs when the maximum Doppler frequency is detected and is given by Eqn. 6.79 with h = 0 as follows:

$$\text{Min } \{D_{BED}(0)\} = A_{BED}(0)/f_D(\text{max}) \quad (6.79)$$

(4) The power of the Doppler signals are not constant in time

The power of the bed-load and suspended-load Doppler signals [$P_{BED}(h)$ and $[P_{SUS}(h)]$ are not constant at all times but fluctuate in time depending on the ultrasonic backscattering strengths which in turn mainly depends on the orientation of the 'faces' of the solid particles relative to the Tx. and Rx. beams at the time of detection. The variable backscattering strength phenomenon can be represented by a Gaussian PDF.

This implies that $P_{BED}(h)$ and $P_{SUS}(h)$ should rather be represented by mean values [$\overline{P_{BED}(h)}$ and $\overline{P_{SUS}(h)}$] with standard deviations [$\sigma_{P(BED)}(h)$ and $\sigma_{P(SUS)}(h)$].

The actual values of $\sigma_{P(BED)}$ and $\sigma_{P(SUS)}$ are dependent on the fluctuation of the backscattering strength of the bed-load and suspended-load particles. $\sigma_{P(BED)}(h)$ and $\sigma_{P(SUS)}(h)$ can be expressed as linear functions of $\overline{P_{BED}(h)}$ and $\overline{P_{SUS}(h)}$. This linear relationship was verified in practice by connecting the demodulated Doppler signal from the Velocimeter to a

spectrum analyser and observing the standard deviation of the power of the Doppler signal due to reflections from moving particles. By increasing the power of the returned Doppler signal (eg. by increasing the Tx. power), the standard deviation of the Doppler power increased proportionately. A 'standard deviation constant' [k_σ] can be defined as the ratio of $\sigma_{P(BED)}(h)$ to $\overline{P_{BED}(h)}$ as follows:

$$k_\sigma = \sigma_{P(BED)}(h) \;/\; \overline{P_{BED}(h)} \qquad (6.80)$$

Since statistically, the backscattering nature of the slurry particles in the bed-load is much the same as that of the suspended-load particles as discussed in Section 5.75, the term k_σ is applied to the suspended-load power too:

$$k_\sigma = \sigma_{P(SUS)}(h) \;/\; \overline{P_{SUS}(h)} \qquad (6.81)$$

Since the Doppler amplitudes, $\overline{D_{BED}(h)}$ and $\overline{D_{SUS}(h)}$ are linearly related to $\overline{P_{BED}(h)}$ and $\overline{P_{SUS}(h)}$ (by $1/(f_{D(BED)}(h)\cdot k_B)$ and $1/(f_{D(SUS)}(h)\cdot k_B)$ respectively), the standard deviation constant can be applied to $\overline{D_{BED}(h)}$ and $\overline{D_{SUS}(h)}$ and is applicable for all Doppler frequencies as follows:

$$k_\sigma = \sigma_{D(BED)}(h) \;/\; \overline{D_{BED}(h)} \qquad (6.82)$$

$$k_\sigma = \sigma_{D(SUS)}(h) \;/\; \overline{D_{SUS}(h)} \qquad (6.83)$$

The above information is presented in summary in tabular form in Table 6.3:

v_M:	$\geq v_{M1}$	$\geq v_{M2}$	$> v_{M2}$
D_{BED}:	0	$\text{Max}\{D_{BED}(0)\} = \frac{A_{BED}(0)}{f_D(\text{min})}$	$\text{Min}\{D_{BED}(0)\} = \frac{A_{BED}(0)}{f_D(\text{max})}$
D_{SUS}:	$\text{Max}\{D_{SUS}(H)\} = \frac{A_{SUS}(H)}{f_D(\text{min})}$		
$f_{D(BED)}$ detected:	0	$f_D(\text{min})$	$f_D(\text{max})$
$f_{D(SUS)}$ detected:	$f_D(\text{min})$		
v_{BED} detected:	0	minimum	maximum
v_{SUS} detected:	minimum		

Table 6.3 Summary of the bed-load and the suspended-load Doppler amplitude, frequency and detectable velocities

The bed-load Doppler amplitude $[D_{BED}(0)]$ for the layer of particles at h = 0 is plotted as a function of $f_{D(BED)}(0)$ on the graph in Fig. 6.27 (i). The suspended-load Doppler amplitude $[D_{SUS}(H)]$ for the layer of particles travelling at h = H is plotted as a function of $f_{D(SUS)}(H)$ on the graph in Fig. 6.27 (ii). The value of Max $\{D_{BED}(0)\}$ is normalised to one (0dB) at $f_D(\text{min})$.

Values on the graph are derived for the following example as follows: If we assume that v_{BED} (at h = 0) ranges between 0.1 to 5m/s and the Doppler constant $[k_D]$ = 200 where the Doppler equation applied to the bed-load Doppler frequency, $f_{D(BED)}(0) = k_D \cdot v_{BED}$ holds, then the minimum and maximum values of the Doppler frequency $[f_D(\text{min})$ and $f_D(\text{max})]$ are calculated from the Doppler equation:

$f_D(min) = 200 \cdot 0.1 = 20Hz$

$f_D(max) = 200 \cdot 5 = 1kHz$

The value of $\overline{A_{BED}(0)}$ can be derived using Eqn. 6.79 and normalising Max $\{\overline{D_{BED}(0)}\}$ to 1 at $f_{D(BED)}(0) = f_D(min) = 20Hz$, to give $\overline{A_{BED}(0)} = 20$. Since $\overline{D_{BED}(0)}$ is inversely proportional to $f_{D(BED)}(0)$, $\overline{D_{BED}(0)}$ expressed in dB falls off at 6dB/octave from 0dB at $f_D(min) = 20Hz$ (ie. $v_M \geq v_{M2}$) to -34dB at $f_D(max) = 1kHz$.

If we assume $k_p(H) = -20dB$ (or 0.1), then Eqn. 6.75 can be used to calculate a value for $\overline{A_{SUS}(H)}$ equal to $0.1 \cdot 20 = 2$. The maximum of $\overline{D_{SUS}(H)}$ occurs at the minimum detectable suspended-load velocity (ie. $v_M \geq v_{M1}$), corresponding to $f_D(min)$ being detected, as follows:

$$\begin{aligned} Max\{\overline{D_{SUS}(H)}\} &= \overline{A_{SUS}(H)} \;/\; f_D(min) \\ &= 2/20 \\ &= 0.1 \;[=-20dB] \end{aligned} \qquad (6.78)$$

$\overline{D_{SUS}(H)}$ falls off at 6dB/octave from -20dB as in Fig. 6.27.

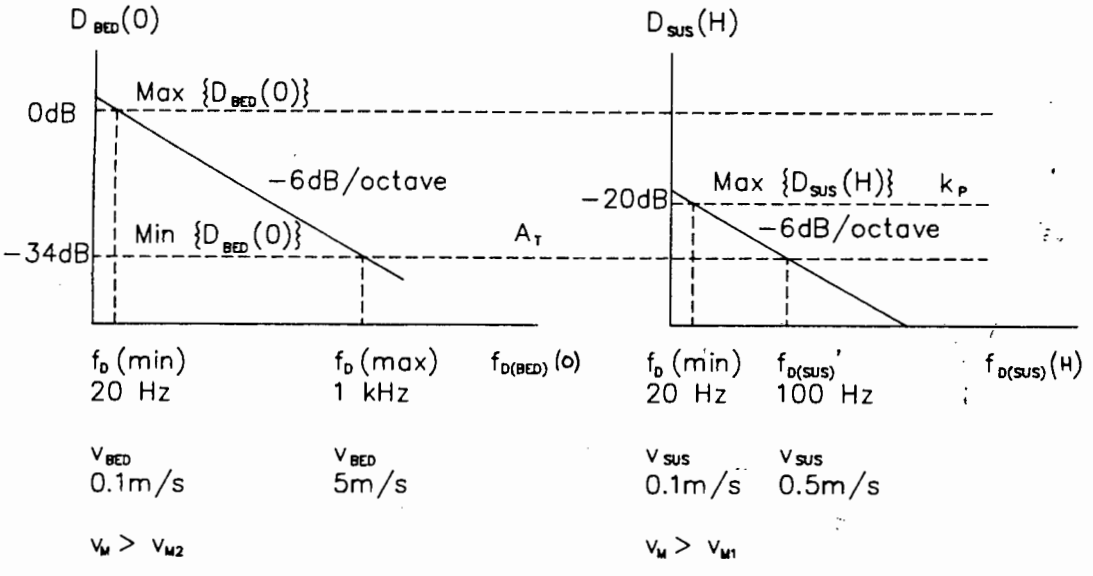

Fig. 6.27 Graph of $D_{BED}(0)$ as a function of $f_{D(BED)}$ and $D_{SUS}(H)$ as a function of $f_{D(SUS)}$

6.7.3 Comparator Stage: Errors of Suspended-load Detection

The method of detecting the bed-load velocity entails converting the detected Doppler frequency into a voltage by passing the demodulated Doppler signal into a F-V converter. Before passing into the F-V converter, the demodulated Doppler signal is squared by passing it through a comparator stage with an effective adjustable amplitude threshold (A_T) for triggering (see Section 6.8.9). All Doppler amplitude signals (due to bed-load or suspended-load) that exceed the value of A_T will cause the comparator to trigger and contribute to the F-V convertion.

In order that all bed-load Doppler frequencies at h = 0 [$f_{D(BED)}(0)$] have a high probability of being detected and

$\overline{D_{SUS}(H)} > 0$. The condition that $\overline{D_{SUS}(H)} > A_T$ is most likely to exist when the minimum suspended-load Doppler velocities are detected (ie. $f_{D(SUS)}(H) = f_D(min)$) since $\overline{D_{SUS}(H)}$ will be a maximum at this velocity defined by Eqn. 6.77. Max $\{\overline{D_{SUS}(H)}\}$ can be calculated for the values given in the example as follows:

$$\text{Max } \{\overline{D_{SUS}(H)}\} = \overline{A_{SUS}(H)}/f_D(min) = 2/20 = 0.1 = -20dB$$

Since Max $\{\overline{D_{SUS}(H)}\}$ is shown to exceed A_T, then a particular suspended-load Doppler frequency exists, called say $f_{D(SUS)}'$, such that $\overline{D_{SUS}(H)}$ equals A_T. All suspended-load Doppler signals having Doppler frequencies below $f_{D(SUS)}'$ will have a probability of being detected which exceeds the probability of detecting the bed-load Doppler signal having a minimum amplitude (ie. at $f_D(max)$). This is because suspended-load Doppler amplitudes will exceed the minimum bed-load Doppler amplitude when the Doppler frequency is below $f_{D(SUS)}'$. We can determine $f_{D(SUS)}'$ by solving Eqn. 6.85.

$$\overline{D_{SUS}(H)} = \overline{A_{SUS}(H)} \;/\; f_{D(SUS)}' = A_T \qquad (6.85)$$

Now solve for $f_{D(SUS)}'$ as follows:

$$f_{D(SUS)}' = \overline{A_{D(SUS)}(H)} \;/\; A_T = 2 \;/\; 0.02 = 100Hz$$

From the Doppler equation, 100Hz corresponds to $v_{SUS} = 0.5m/s$.

This means that when the bed-load is stationary and $v_{SUS} > 0$ (ie. when $v_{M1} < v_M < v_{M2}$) then all suspended-load Doppler frequencies $[f_{D(SUS)}(H)]$ between $f_D(min)$ and 100Hz will be detected, corresponding to false indications of bed-load velocities from 0.1m/s to 0.5m/s (see Fig. 6.27).

6.7.4 Doppler Dynamic Range Defined

A term defined as the Doppler Dynamic range [DR] indicates the ratio of the maximum suspended-load Doppler amplitude at h = H to the minimum bed-load Doppler amplitude at h = 0 over the entire range of detectable Doppler frequencies as in Eqn. 6.86.

$$DR(H) = \text{Max } \{\overline{D_{SUS}(H)}\} \; / \; \text{Min } \{\overline{D_{BED}(0)}\} \qquad (6.86)$$

and expressed in dB:

$$DR(H)\{dB\} = 20 \text{ Log } [DR(H)] \qquad (6.87)$$

If DR(H) > 1 then the probability of detecting suspended-load Doppler signals (at the lowest Doppler frequency) exceeds the probability of detecting bed-load Doppler signals (at high Doppler frequencies). This effect is most noticeable in the real situation where a flow regime of $v_{M1} < v_M < v_{M2}$ exists ie. the bed-load particles are stationary and the suspended-load particles are in motion. If the suspended-load Doppler amplitude ever exceeds the threshold voltage [A_T] of the comparator stage (see Section 6.7.3) then the probability of detecting suspended-load Doppler frequencies exceeds 50% and a false indication of a moving bed-load could occur.

Techniques are presented (Doppler Dynamic Range Reduction Filter, Comparator with an adjustable threshold voltage) in the following sections to eliminate the above effect.

6.7.5 Design Strategy to Ensure Only Bed-load Velocity is Detected

To eliminate the process of falsely detecting suspended-load particle motion, the following design strategy is implemented:

(i) The Doppler Penetration constant [k_p] is minimized so that the amplitude of the suspended-load Doppler signals relative to the bed-load Doppler signals are minimized.

(ii) A Dynamic Range Reduction Filter is implemented which adjusts the Dynamic Range of the bed-load Doppler amplitude.

(iii) A comparator with an adjustable trigger level (A_T) is implemented. The trigger level is adjusted so that bed-load Doppler amplitudes have a high probability of being detected to cause triggering while suspended-load Doppler amplitudes have a low probabilty of causing triggering.

6.7.6 Doppler Dynamic Range Reduction (DDRR) Filter

Note: In the following Section, the designation of the bed-load and the suspended-load particles as being due to particles travelling at h = 0 and h = H respectively is dropped for shorthand notation. The mean bed-load and suspended-load Doppler amplitudes are written without the notation designating that a mean value is referred to. It is however assumed that these amplitudes are mean values.

Also $k_p(H)$ is written as k_p for shorthand. The bed-load particles are defined as those particles travelling at h = 0 and similarly, the suspended-load particles are those particles travelling at h = H.

The Doppler Dynamic Range [DR] as defined above can be expressed in shorthand as follows:

$$DR = \text{Max } \{D_{SUS}\} \;/\; \text{Min } \{D_{BED}\} \tag{6.86}$$

Substituting Eqn. 6.77 and using Eqn. 6.75, DR can be expressed by Eqn. 6.88 as follows:

$$DR = \frac{A_{SUS}/f_D(\min)}{A_{BED}/f_D(\max)} = \frac{k_p \cdot f_D(\max)}{f_D(\min)} \tag{6.88}$$

For the above example, DR = 0.1·1000/20 = 5 = 14dB. If the detected Doppler signals are transformed by passing them through a network with a transfer function [F(f)] which is linearly related to the input frequency [f] as follows:

$$F(f) = 2\pi \cdot \tau_F \cdot f \tag{6.89}$$

where $2\pi \cdot \tau_F$ is chosen as follows:

$$2\pi \cdot \tau_F = 1/f_D(\max) \tag{6.90}$$

then the transformation of the bed-load and suspended-load Doppler signals can be expressed by DF_{BED} and DF_{SUS}. The transformation is determined from the product of the Doppler signal and the network transfer function at any Doppler frequency [f_D]:

$$\begin{aligned} DF_{BED}(f_D) &= D_{BED}(f_D) \cdot F(f_D) \\ &= A_{BED}/f_D \cdot 2\pi \cdot \tau_F \cdot f_D \\ &= 2\pi \cdot \tau_F \cdot A_{BED} \end{aligned} \tag{6.91}$$

In this way, the previously defined maximum bed-load Doppler amplitude [at $f_D = f_D(min)$] and minimum bed-load Doppler amplitude [at $f_D = f_D(max)$] and all the bed-load Doppler signals for all Doppler frequencies are transformed into signals which are independant of their Doppler frequency and is expressed as follows:

$$\text{Max } \{DF_{BED}\} = \text{Min } \{DF_{BED}\} = DF_{BED} = 2\pi \cdot \tau_F \cdot A_{BED} \qquad (6.92)$$

Substituting Eqn. 6.90, into Eqn. 6.92, yields an expression for DF_{BED} as follows:

$$DF_{BED} = A_{BED} \; / \; f_D(max) \qquad (6.93)$$

In the same way, the network also affects the suspended-load Doppler signals so that D_{SUS} at all Doppler frequencies [f_D] at the output of the network is expressed by Eqn. 6.94.

$$\begin{aligned} DF_{SUS}(f_D) &= D_{SUS}(f_D) \cdot F(f_D) \\ &= A_{SUS}/f_D \cdot 2\pi \cdot \tau_F \cdot f_D \\ &= 2\pi \cdot \tau_F \cdot A_{SUS} \end{aligned} \qquad (6.94)$$

and similarly, all the suspended-load Doppler amplitudes including the maximum and minimum are transformed too and expressed by DF_{SUS} as follows:

$$\text{Max } \{DF_{SUS}\} = \text{Min } \{DF_{SUS}\} = DF_{SUS} = 2\pi \cdot \tau_F \cdot A_{SUS} \qquad (6.95)$$

Substituting Eqn. 6.90 into Eqn. 6.95, yields an expression for DF_{SUS} as follows:

$$DF_{SUS} = A_{SUS} \; / \; f_D(max) \qquad (6.96)$$

In order that all $f_{D(BED)}$ frequencies are detected, the value of A_T must be set to the transformed minimum possible bed-

load Doppler amplitude. The value of A_T is therefore set to:

$$A_T = \text{Min } \{DF_{BED}\} = 2\pi \cdot \tau_F \cdot A_{BED} \tag{6.97}$$

The maximum transformed suspended-load Doppler amplitude is given as follows:

$$\text{Max } \{DF_{SUS}\} = 2\pi \cdot \tau_F \cdot A_{SUS} = 2\pi \cdot \tau_F \cdot k_p \cdot A_{BED} \tag{6.98}$$

The Dynamic Range is transformed by the network and expressed by DR'. It can be shown that DR' = k_p, by expressing DR' as the ratio of Max $\{DF_{SUS}\}$ to Min $\{DF_{BED}\}$, which according to Eqns. 6.92 and 6.94 can be written as follows (and is valid over the entire range of Doppler frequencies):

$$DR' = \frac{\text{Max } \{DF_{SUS}\}}{\text{Min } \{DF_{BED}\}} = \frac{DF_{SUS}}{DF_{BED}}$$

$$= \frac{2\pi \cdot \tau_F \cdot k_p \cdot A_{BED}}{2\pi \cdot \tau_F \cdot A_{BED}} = k_p \tag{6.99}$$

For the values given above, DR has been reduced considerably from 14dB to -20dB (a 34dB improvement)

As long as $k_p < 1$, which in practice it always is, then the maximum suspended-load Doppler amplitude will never exceed A_T. This implies that the probability of ever detecting suspended-load Doppler signals is always less than the probability of detecting bed-load Doppler signals.

The network has successfully reduced the probability of detecting suspended-load particle velocities. In practice, the network is realized by a RC high pass filter. The

design and parameters of the high pass Dynamic Range Reduction filter is discusses in Section 6.8.8.

6.7.7 Probability Functions of Detecting Bed-load and Suspended-load Particles

The probability of detecting the DDRR filtered bed-load and suspended-load Doppler amplitudes [DF_{BED} and DF_{SUS}] is expressed by probability functions. One of the main objectives of the system design is to detect bed-load Doppler signals. There is however, a probability of detecting suspended-load Doppler signals. This probability has been greatly reduced by the DDRR filter, but the probability is still greater than zero. It is important to calculate the probabilities of detecting bed-load (at h = 0, defined by P{bed}) and suspended-load (at h = H, defined by P{sus}) Doppler signals so that design steps can be taken to increase P{bed} and decrease P{sus}.

The probability functions are shown to be functions of the penetration constant [k_p], the standard deviation constant [k_σ], and a newly defined constant, the threshold voltage constant [k_T]. The threshold voltage constant defines the setting of the comparator threshold voltage (see Section 6.8.9) following the DDRR filter.

Before probability functions can be derived, the above constants must first be defined. The Penetration constant is defined above in Eqn. 6.96. The threshold voltage constant simply expresses the comparator threshold voltage [A_T] in terms of DF_{BED} as follows:

$$A_T = k_T \cdot DF_{BED} \qquad (6.100)$$

Next, the standard deviation constant [k_σ as defined above in Eqns. 6.80, 6.81, 6.82 and 6.83], is defined.

Since the Doppler amplitudes, DF_{BED} and DF_{SUS} are linearly related to A_{BED} and A_{SUS} (both are related by $1/(f_D(max))$, k_σ also expresses the ratio of the standard deviation of DF_{BED} and DF_{SUS}, namely $\sigma_{DF(BED)}$ and $\sigma_{DF(SUS)}$ to DF_{BED} and DF_{SUS} respectively.

$$k_\sigma = \sigma_{DF(BED)}/DF_{BED} \tag{6.101}$$

$$k_\sigma = \sigma_{DF(SUS)}/DF_{SUS} \tag{6.102}$$

In terms of A_{BED} and A_{SUS}, the standard deviations [$\sigma_{DF(BED)}$ and $\sigma_{DF(SUS)}$] can be expressed by Eqns. 6.103 and 6.104 by substituting Eqns. 6.93 and 6.96 into Eqns. 6.101 and 6.102:

$$\sigma_{DF(BED)} = k_\sigma \cdot A_{BED}/f_D(max) \tag{6.103}$$

$$\sigma_{DF(SUS)} = k_\sigma \cdot A_{SUS}/f_D(max) \tag{6.104}$$

The probability of detecting bed-load Doppler frequencies equals the probability that $DF_{BED} > A_T$. It is expressed as follows:

$$P\{bed\} = P\{DF_{BED} > A_T\} = 1 - Q\left[\frac{DF_{BED} - A_T}{\sigma_{DF(BED)}}\right] \tag{6.105}$$

where Q(x) is defined as in Lathi [Ref. 22, p377].

Similarly, the probability of detecting suspended-load Doppler frequencies equals the probability that $DF_{SUS} > A_T$.

It is expressed as follows:

$$P\{sus\} = P\{DF_{SUS} > A_T\} = Q\left[\frac{A_T - DF_{SUS}}{\sigma_{DF(SUS)}}\right] \qquad (6.106)$$

Making substitutions from Eqns. 6.100 and 6.101 we obtain the following expressions:

$$P\{bed\} = 1 - Q\left[\frac{DF_{BED} - k_T \cdot DF_{BED}}{k_\sigma \cdot DF_{BED}}\right] \qquad (6.107)$$

$$P\{bed\} = 1 - Q\left[\frac{1 - k_T}{k_\sigma}\right] \qquad (6.108)$$

From Eqn. 6.106, P{sus} can be expressed by the following expression by susbstituting Eqns. 6.100 and 6.102 into Eqn. 6.106:

$$P\{sus\} = Q\left[\frac{k_T \cdot DF_{BED} - DF_{SUS}}{k_\sigma \cdot DF_{SUS}}\right] \qquad (6.109)$$

Make the substitution from Eqn. 6.99 for k_p, P{sus} can be expressed as follows:

$$P\{sus\} = Q\left[\frac{k_T/k_p - 1}{k_\sigma}\right] \qquad (6.110)$$

6.7.8 Analysis of Probability Functions

To analyse the effects of k_T, k_p and k_σ on P{bed} and P{sus}, an analysis was carried out on a "Quatro" Spreadsheet.

Values for P{bed} were calculated on the spreadsheet for P{sus} = 0.1 (case 1) and P{sus} = 0.01 (case 2) and plotted as a function of k_p in Fig. 6.29 for P{sus} set to 0.1 and in Fig. 6.30 for P{sus} set to 0.01.

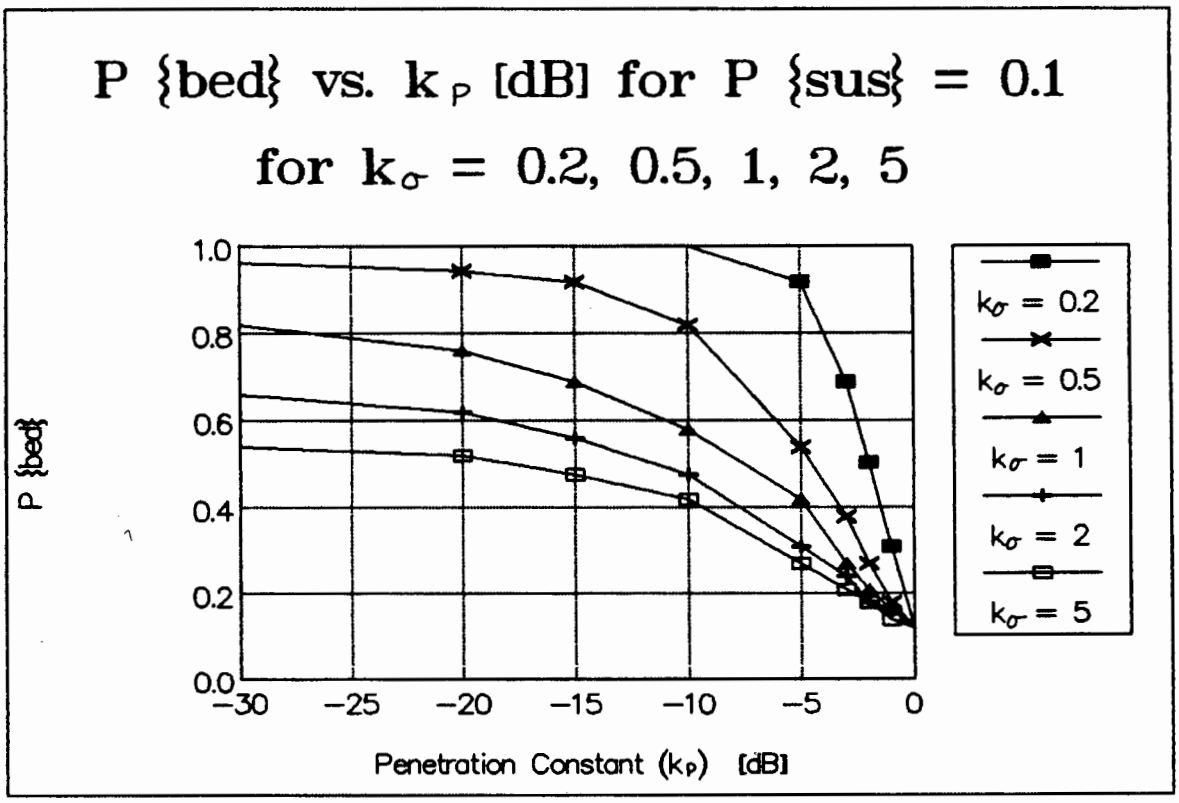

Fig. 6.29 Probability of bed-load particle detection as a function of the Penetration constant with P{sus}=0.1 for five different standard deviation constants

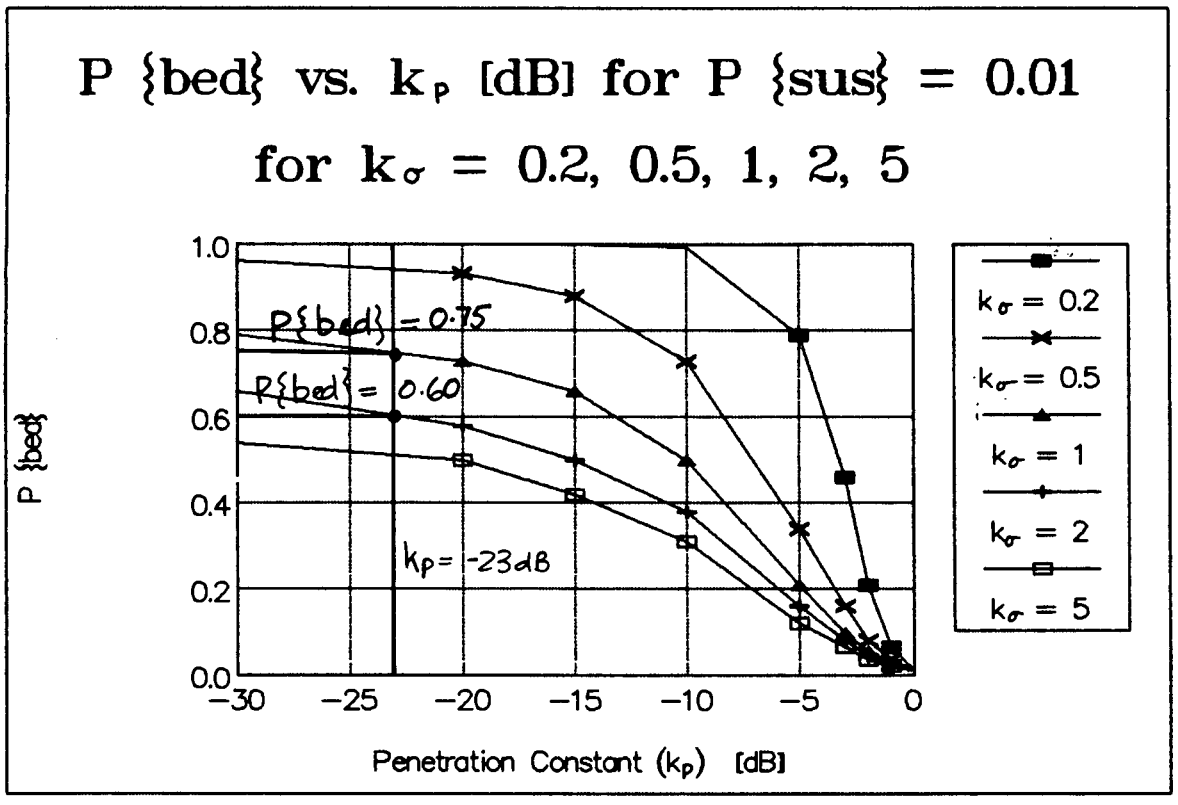

Fig. 6.30 Probability of bed-load particle detection as a function of the Penetration constant with P{sus}=0.01 for five different standard deviation constants

For the two cases above, the values in Figs. 6.29 and 6.30 are obtained by first solving for k_T in Eqn. 6.110 for P{sus} = 0.1 (case (i)) and for P{sus} = 0.01 (case (ii)) for the range of k_p and k_σ values. The values derived for k_T and k_σ are then substituted into Eqn. 6.108 to solve for P{bed}.

from Figs. 6.29 and 6.30 the following general conclusions can be drawn:

(i) P{bed} is larger for lower k_p values.

(ii) P{bed} is larger for smaller k_σ values.

(iii) P{bed} approached a maximum value as k_p is reduced irrespective of the value of k_σ or P{sus}.

(iv) At $k_p = 1$, the value for P{bed} equals P{sus} as expected since $DF_{SUS} = DF_{BED}$ at $k_p = 1$.

(v) At lower values of k_p, P{bed} is lower for the case of a lower P{sus} value.

The value of k_σ is entirely dependent on the slurry make-up. No design strategy can be implemented to decrease its value to increase the probability of correctly detecting bed-load velocities (P{bed}).

However, the value of the penetration constant (k_p) is dependent on design parameters. The most important design parameter that affects the value of k_p is the extent of the focusing of the ultrasonic crystals on the bed-load particles, which is a function of the focusing parameters and the height of the beginning of the suspended-load layer [H] as discussed in detail in Section 6.4.12.

The ultrasonic attenuation through the slurry also influences the value of k_p. Generally, the higher the atenuation, the lower is the value of k_p.

In summary, to increase P{bed} for a fixed value of P{sus} we must:

(i) Decrease k_σ
(ii) Decrease k_p

However, k_σ is dependent on the characteristics of the detectable particles and is determined from the standard deviation of the backscattering strength of the detectable particles. It is therefore independent of system design.

The value of k_p however is dependant on system design. Specifically, the efficiency of the focusing technique has a direct affect on k_p.

With the focusing parameters as chosen in Section 6.6: (Θ_T=30°, φ=17° and d=20mm), a value for k_p can be derived using either Fig. 6.15 or Fig. 6.17, depending on the suspended-load height [H]. For example, if the suspended-load height begins at 10mm up from the pipe soffit then k_p = -23dB.

To ensure that the probability of detecting suspended-load particles from this height is very low (say 1% or 0.01 as in case (ii) of Fig. 6.30.) then the comparator threshold voltage (see Section 6.8.9) can be set according to Eqn. 6.110.

Now Fig. 6.30 can be used to provide a prediction of the probability of detecting bed-load particle velocities. First, a value for k_σ must be known. This constant is dependant on the slurry particle properties that influence the fluctuation of the ultrasonic backscattering strength. Experimentation on typical sand-water slurries demonstrated that the backscattering strength fluctuated about a mean value with k_σ between approximately 1 and 2.

From Fig. 6.30 with k_σ between 1 and 2 and with k_p = -23dB, P{bed} ranges between 0.60 to 0.75. (60% to 75%), which is at least 60 times greater (P{bed}/P{sus} = 0.6/0.01 = 60) than the probability of detecting suspended-load particle

velocities, demonstrating that the UDBV has successfully been designed to measure bed-load particle velocities.

6.7.9 Implication of the Probability Function on the Doppler Equation

The implication of the P(bed) function on relating the peak Doppler frequency to the bed-load velocity is discussed. Simply, the output voltage of the F-V converter will be related to the bed-load particle velocity according to the Doppler equation if P(bed) = 1. If P(bed) < 1, which is usually the case in practice, then by definition of the probability function, the bed-load Doppler frequency will on average be converted to a voltage only P(bed) of the time within a unit time. This implies that the relationship between the Doppler frequency and the detectable particle velocity according to the Doppler constant [k_D] is more accurately expressed by Eqn. 6.111 as follows:

$$f_{D(BED)} = P(bed) \cdot k_D \cdot v_{BED} \qquad (6.111)$$

6.7.10 Conclusion

The demodulated Doppler signal as expressed by Eqn. 6.2 has been expressed more accurately by taking into account three factors that are ignored by the Doppler equation. These three factors are: (i) suspended-load particles travelling within the insonified volume will be detected (ii) the Doppler frequency is broadened (iii) the power of the Doppler signals are inversely proportional to the height of the particles detected and (iv) the Doppler power is not constant in time.

The implication of the above factors is that suspended-load Doppler signals are detected, falsely indicating a bed-load velocity. This effect is especially apparent in practice in the flow regime $v_{M1} < v_M < v_{M2}$, ie. when $v_{BED} = 0$ and $v_{SUS} > 0$, since the Velocimeter will indicate a moving bed when it is actually stationary.

To reduce the probability of falsely detecting suspended-load velocities a Doppler Dynamic Range Reduction Filter (DDRR Filter) was implemented to ensure that the Doppler amplitude is independent of the Doppler frequency. The probability of detecting bed-load and suspended-load particle velocities has been described by probability functions.

It has been shown that the probability functions are functions of the Penetration constant [k_p], the standard deviation constant [k_σ] and a comparator threshold voltage constant [k_T]. The probability functions provide information so that the comparator threshold voltage can be correctly set and provide predictions of the probability of detecting bed-load and suspended-load particle velocities. It has been shown that with appropriate design methods, the Velocimeter will detect bed-load particle velocities with a far higher probability compared with detecting suspended-load particle velocities.

6.8 ELECTRONIC CIRCUITRY DESIGN

6.8.1 Introduction

Note: For shorthand in this Section, the mean bed-load Doppler frequency [$f_{D(BED)}$] is referred to as f_D unless a distinction between the bed-load and suspended-load Doppler frequencies needs to be drawn for the discussion.

Each circuit module is first briefly discussed in the following section in the order in which the block diagram of Fig. 6.31 is layed out. Following this discussion, details of important modules are investigated in individual sections. In these sections component values are referred to as labelled in the circuit diagrams of Appendix C.

6.8.2 Block Diagram Description

A list of the electronic circuitry modules of the UDBV and their functions follows. The labelling is with reference to the block diagram of Fig. 6.31.

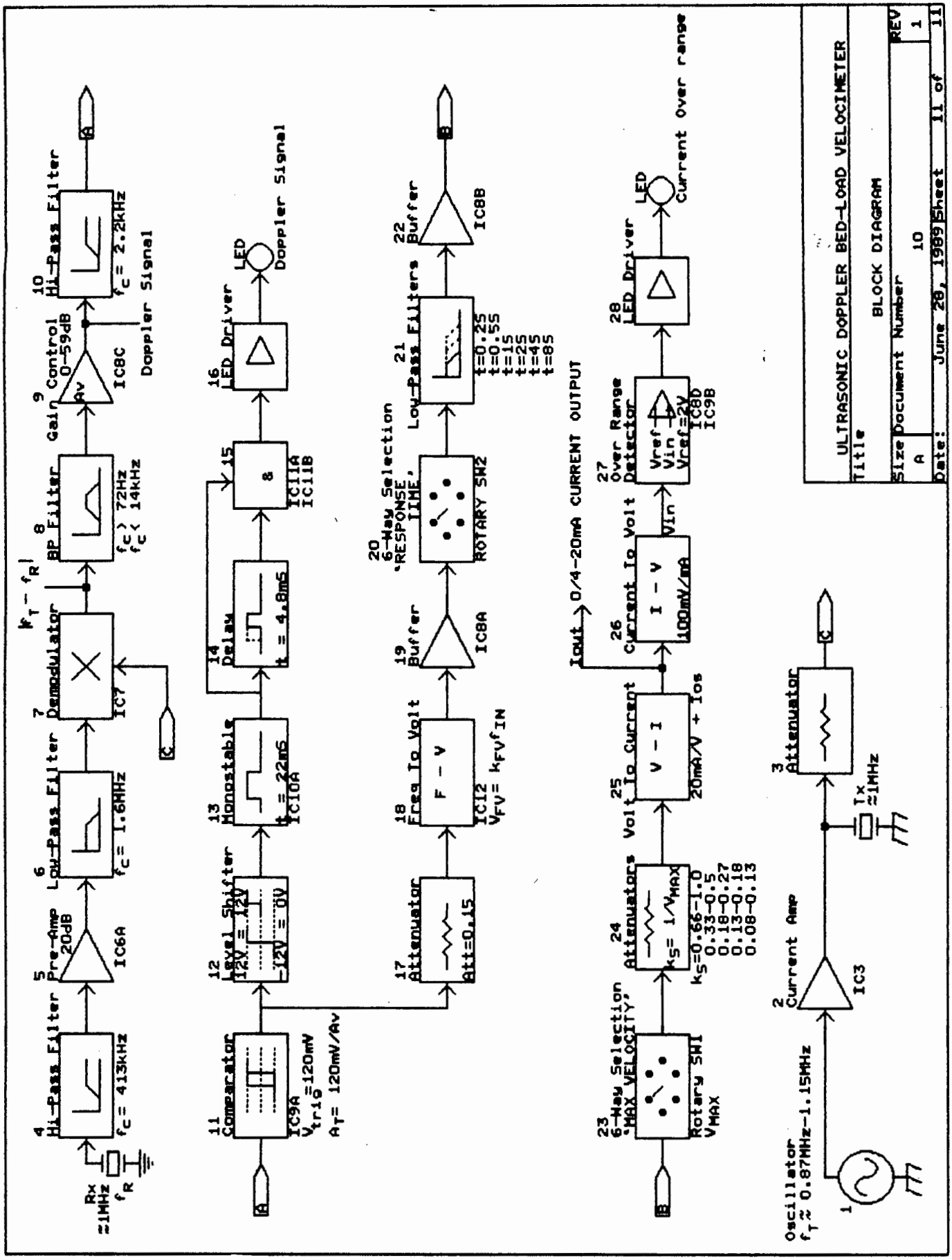

Fig. 6.31 UDBV Block Diagram

(1) Oscillator

A tuneable 1MHz oscillator, to drive the Tx. crystal in CW operation. The tuneable bandwidth is approximately 200kHz (see Section 6.8.4)

(2) Current Amplifier

To provide sufficient current to drive the Tx. crystal via a 20m coaxial cable and to provide isolation between the oscillator and the Tx., a unity gain, current amplifier is used capable of delivering 200mA. (see Section 6.8.5)

(3) Attenuator

A small part of the oscillator current is tapped off to supply the demodulator with a reference frequency. The oscillator voltage to the demodulator is attenuated to 300mV rms as this is the optimum voltage for the demodulator (block no. 7)

(4) Band Pass Filter

The Rx. signal is bandlimited by a bandpass filter to cut out unnecessary noise signal from being amplified and demodulated. The filter consists of a single pole RC hi-pass filter at the input of the pre-amp (Block no. 5) with a high pass cut off frequency, f_{HC} = 413kHz and a low-pass single pole RC filter constituting the feedback impedance of the pre-amp with f_{LC} = 1.6MHz.

(5) Pre-Amp

The Rx. signal is amplified by a pre-amp by 20dB. The pre-amp also serves as a buffer stage between the Rx. signal (after filtering) and the demodulator. (see Section 6.8.6)

(6) Low-Pass Filter

High frequency noise received by the pre-amp is filtered by a RC filter with f_C = 1.6MHz.

(7) Demodulator

The Rx. signal is demodulated to extract any Doppler shifted terms by multiplying the Rx. signal with a reference Tx. signal tapped off from the transmitter oscillator. (see Section 6.8.7)

(8) Band-Pass Filter

Since the demodulation process (7) involves multiplying as described in Section 6.2, the product will contain DC terms and terms at a frequency of $2f_T$. These terms are filtered out by a bandpass filter stage following the demodulator stage. The high [f_{HC}] and lower [f_{LC}] cut-off frequencies are: f_{HC} = 14kHz and f_{LC} = 72Hz. All Doppler signals for all practical particle velocities will fall well below f_{HC}. Doppler frequencies below f_{LC} will probablly still be detected, depending on their amplitudes.

(9) Adjustable Doppler Gain Control

The demodulated Doppler signal is amplified by a variable gain amplifier. The voltage gain (A_V) can be set between 0dB to 59dB. The setting of the gain is dependant on the strength of the Doppler signal for a particular system. The Doppler signal strength depends on many factors such as the backscattering strength from the slurry particle scatterers, the ultrasonic transmission strength through the transmission layer, the oscillator frequency, the coaxial cable length etc.

It is set so that the amplified bed-load Doppler signal is large enough to be processed by the proceeding modules but not too large so that noise is detected by the following modules. Suspended-load Doppler signals are considered to be noise too. Its setting effectively influences the comparator threshold voltage [A_T] (see block no. 11 below).

(10) Doppler Dynamic Range Reduction (DDRR) High-Pass Filter

To reduce the dynamic range of the Doppler signal as discussed in Sections 6.7.4 and 6.7.6. It consists of a RC single pole high pass filter with f_{HC} = 2.2kHz (the maximum Doppler frequency)

(11) Comparator

The function and necessity of a comparator stage with an adjustable threshold voltage [A_T] is discussed in Sections 6.7.5, 6.7.6 and 6.7.7. Briefly, its function is to only pass bed-load Doppler signals and not the suspended-load Doppler signals. (see Section 6.8.9)

This comparator stage is not adjustable but rather has a fixed threshold voltage equal to 120mV. The adjustable threshold voltage is realized with the combination of the adjustable Doppler gain stage (block no. 9) and the fixed threshold voltage of this comparator. The effective value of A_T is therefore the 120mV multiplied by the reciprocal of the Doppler gain:

$$A_T = 120mV/A_V \qquad (6.112)$$

The output of the comparator stage will under correct operating conditions, be a square wave with its fundamental frequency equal to f_D. (see Section 6.8.8)

(12) Level Shifter

A voltage level shifter module follows the comparator stage so that the voltage is compatible with the required input voltage of the monostable of block no. 13.

(13) Monostable

A monostable forms the first module of a set of modules (block nos. 13,14,15 and 16) to drive the Doppler Signal (Bed-Condition) Indicator LED as decribed in Section 6.8.14.

The monostable produces a 22mS pulse when the Doppler signal causes the comparator stage (block no. 11) to trigger. The output of the monostable will be continuously high for $f_D > 1/22mS > 45Hz$, indicating a Doppler signal of $f_D > 45Hz$ is being detected. If however $f_D < 45Hz$ then the output of the monostable will not be continuously high but will be a string of pulses occuring every $1/f_D$ second with a width of

22mS. If the bed-load velocity is zero then no Doppler signal will be present so the output will remain low.

(14) Delay

A delay stage of 4.8ms follows the monostable stage. This stage prevents noise pulses that are either < 12V in amplitude and/or < 4.8ms in duration from being detected to falslely indicate a moving bed-load velocity.

(15) Nand-Gate Pair

The Nand gate following the delay stage operates as a Schmidt trigger to 'clean-up' the transition voltage from low to high of the delay stage. The second Nand-gate of the pair acts as a voltage inverter.

(16) LED Driver and "Doppler Signal (Bed Condition)" LED

The output of the Nand-gate pair must be indicated by the "Doppler-Signal" indicator LED. To provide sufficient drive of 20mA for the LED, a LED current amplifier Driver is implemented.

(17) Attenuator

The output square wave of the comparator (Block no. 11) is attenuated by 0.15 (-16dB) so that the F-V converter following it is driven within the specified volatge.

(18) Frequency to Voltage Converter (ZCC)

A frequency to volatge converter (a zero-crossing-counter) is provided to process the demodulated Doppler frequency and convert it to a voltage for further processing. The relationship between the bed-load velocity [v_{BED}] and the output voltage of the F-V converter [V_{FV}] is as follows:

$$V_{FV} = 2 \cdot v_{BED} \qquad (6.113)$$

so that if and when v_{BED} is a maximum of 5m/s then V_{FV} reaches its maximum of 10V.

The analysis of the F-V converter used as a ZCC has been discussed in Section 6.5.5. The circuitry implementation is discussed in detail in Section 6.8.10.

(19) Buffer

A unity gain buffer stage follows the F-V converter to provide current amplification and isolation between the F-V converter stage and the following stages.

(20) 6-Way "Response Time" Selector Rotary Switch

A 6-way rotary switch is used to set the desired value for the response time of the system. The switch provides a choice of the 3dB cut-off of the low-pass filter stage that follows.

(21) Low-Pass Filter Bank

A bank of RC single pole low-pass filters with the response time [τ] set according to the position of the Selector rotary switch (Block no. 20). The six response time settings are: 0.2, 0.5, 1, 2, 4 and 8 seconds. (see Section 6.8.11)

(22) Buffer

Another unity gain buffer stage follows the Low-Pass Filter bank.

(23) 6-Way "Maximum Velocity" Selector Rotary Switch

Another 6-way rotary switch is used to set the desired value for the maximum detectable bed-load velocity [v_{MAX}] of the system. v_{MAX} may be set to one of six discrete settings: 0.5, 1, 2, 3, 4 or 5m/s. The switch provides a choice for the scaling settings that follow.

(24) Adjustable Scaling

Depending on the v_{MAX} setting (block no. 23), the output DC voltage from the F-V converter must be scaled according to a scaling constant [k_S] so that it has a maximum of 1V when $v_{BED}=v_{MAX}$. The scaling constant satisfies Eqn. 6.114.

$$k_S = 1/v_{MAX} \tag{6.114}$$

The voltage at the output of the scaling module is defined by V_{VI} (the subscript $_{VI}$ refers to the fact that this voltage

is the input voltage to the voltage to current converter module, which follows). V_{VI} can be expressed by Eqn. 6.115.

$$V_{VI} = k_S \cdot V_{FV} \qquad (6.115)$$

(25) Voltage to Current Converter

The voltage to current converter (V-I) converts the scaled DC voltage between 0 to 1V (from block no. 24) to a current between 0 to 20mA [Iout]. An optional manually adjustable offset current [Ios] between 0 to 6mA is provided as in Eqn. 6.116.

$$Iout = V_{VI}/50 + Ios \qquad (6.116)$$

(26) Current to Voltage Converter

The output current is converted to a voltage [V_{IV}] according to Eqn. 6.117).

$$V_{IV} = 100\ Iout \qquad (6.117)$$

so that it produces an output voltage of 2V when Iout = 20mA. This voltage is used in the next module, the "Over Range Detector" comparator (block no. 27).

(27) "Over Range Detector" Comparator

This module determines whether the output current exceeds 20mA and if so the output goes high to drive a "Current Over range" LED indicator via a current LED driver (block no. 28). The voltage V_{IV} is compared with a reference voltage adjusted so that the output of this comparator triggers high

when Iout exceeds 20mA. If V_{IV} is exactly equal to Eqn. 6.117 then the reference voltage is set to exactly 2V.

(28) LED Driver and "Current Over range" Indicator LED

The output of the "Over Range Detector" Comparator must be indicated by the "Current Over range" Indicator LED. To provide sufficient drive of 20mA for the LED, a current amplifier LED Driver is implemented.

6.8.3 Transducer Matching Circuitry

6.8.3.1 Crystal Electrical Parameters

The parameters of the piezoelectric ceramic PZT (lead zirconate titanate) crystals used in the transducer of the Velocimeter can be defined in terms of electrical parameters. It is important to determine the values of these parameters so that efficient operating conditions can be established (eg. operation at resonance). It is also important so that electrical matching circuitry between the transducer and the circuitry can be designed to increase efficiency.

A Piezoelectric crystal operating near resonance in a vacuum (air is almost an identical approximation and data for operation in a vacuum is obtained from measurements in air) can be modelled by an equivalent circuit as in Fig. 6.32.

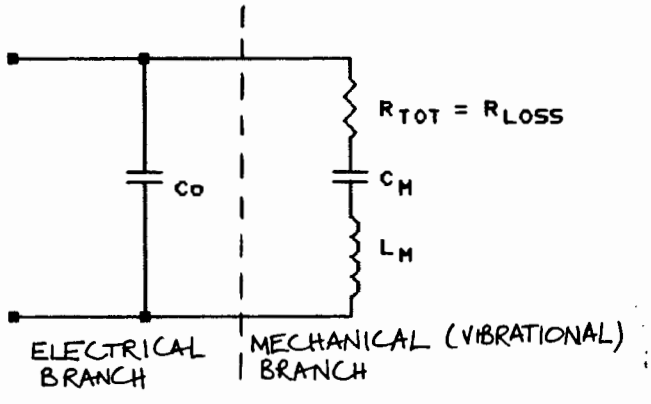

Fig. 6.32 Equivalent circuit for a crystal radiating into air

In this model the mechanical (or vibrational) resonance is defined by the series branch R_{LOSS}, L_M, C_M. R_{LOSS} is the component which defines the energy dissipation both internally (R_{LOSS}) and as ultrasonic radiation (R_{RAD}). Since no the ultrasonic radiation occurs in air, R_{TOT} is due solely to internal losses within the crystal so that:

$$R_{TOT} = R_{LOSS} \qquad \text{(in air)} \qquad (6.118)$$

L_M represents the equivalent mass of the vibrating system and C_M the stiffness responsible for the restoring force. C_O is the electrical capacitance of the crystal due to its parrallel metal contacts on the two faces.

A circle diagram, which is effectively an admittance locus [Y = G + jB] where G is real (conductance) represented by the x-axis and jB is imaginary (susceptance) represented by the y-axis, can be used to determine the crystals

parameters. The admittance is calculated (by means of a network analyser) for a range of frequencies near mechanical resonance.

From the equivalent circuit of Fig. 6.32 it is evident that two resonant circuits exist. Mechanical resonance is determined by C_M and L_M and is responsible for a minimum impedance equal to R_M at the series resonant frequency, as follows:

$$f_S = 1/2\pi\sqrt{L_M \cdot C_M} \qquad (6.119)$$

At f_S, the only susceptance [jB] is due to C_0 and is represented by a shift of the entire circle diagram up the susceptance axis to a value $jB = C_0$ at the series resonant frequency.

The Velocimeters crystals were 1 MHz, 10mm diameter piezoelectric crystals. The circle diagram for the crystal unmounted and propagating in air (which approximates a vacuum) is given by Fig. 6. 33.

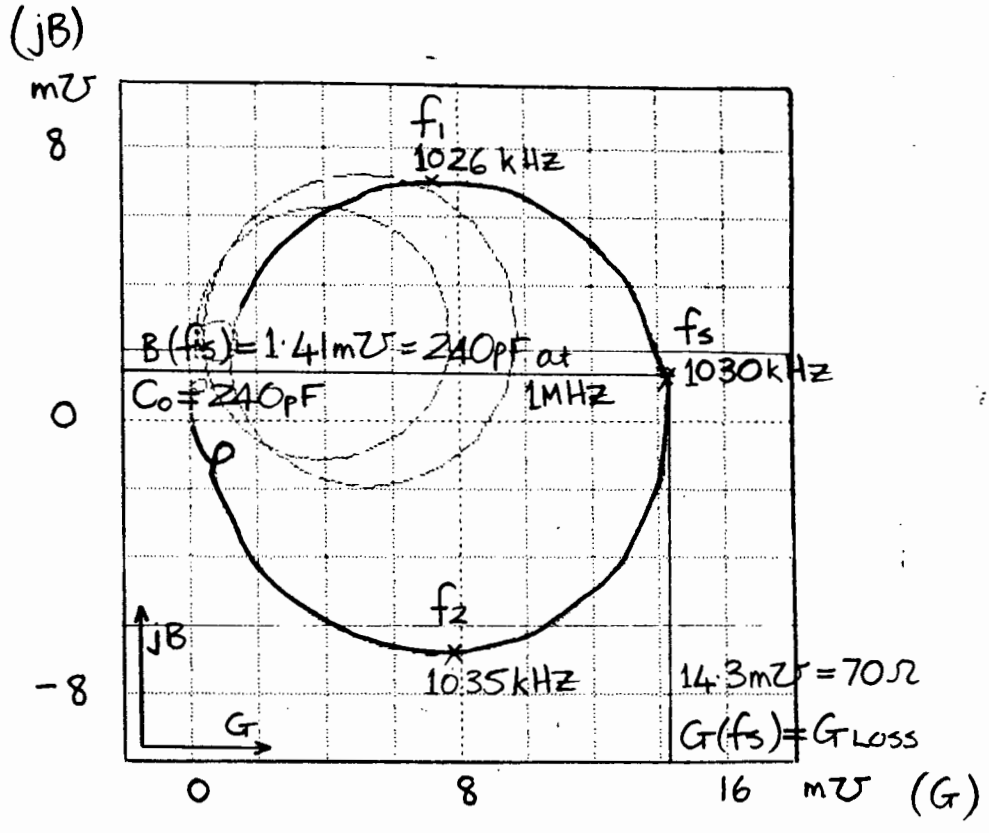

Fig. 6.33 Circle Diagram for crystals radiating into air

From this circle diagram, the series mechanical resonant frequency [f_S], the natural 3dB unmatched bandwidth [f_{3dB}], the value of C_0, L_M, C_M and R_{LOSS} can all be determined.

f_S occurs at the point of maximum admittance. f_{3dB} is given by Eqn. 6.120, where f_1 and f_2 are the top and bottom points of the circle diagram [Ref. 20]:

$$f_{3dB} = f_2 - f_1 = 1035\text{kHz} - 1026\text{kHz} = 9\text{kHz} \qquad (6.120)$$

At a frequency equal to f_S, the value of the conductance [$G(f_S)$] is solely due to internal losses so that $G(f_S) = G_{LOSS} = 1/R_{LOSS}$ (see Fig. 6.33) as given by Eqn. 6.121

$$R_{LOSS} = 1/G_{LOSS} = 1/\ G(f_S) \qquad (6.121)$$
$$= 1/14.3m = 70\Omega$$

The value of L_M is determined as follows, for a series resonant circuit:

$$L_M = R_{LOSS} \ / \ 2\pi \cdot (f_{3dB}) \qquad (6.122)$$
$$= 70/2\pi \cdot 9k = 1.24mH$$

The value of C_M is determined from L_M and the series resonant frequency as follows:

$$f_S = 1 \ / \ 2\pi \ \sqrt{L_M \cdot C_M} \qquad (6.123)$$

where f_S = 1030kHz, solve for C_M:

$$C_M = 1 \ / \ (2\pi \cdot f_S)^2 \cdot L_M$$
$$= 19pF$$

When the crystal is mechanically loaded by mounting it on the pipe-line by means of a a transducer window (eg. resin), then radiation from the crytal into the contact medium occurs. The equivalent electrical model is modified as shown in Fig. 6.34.

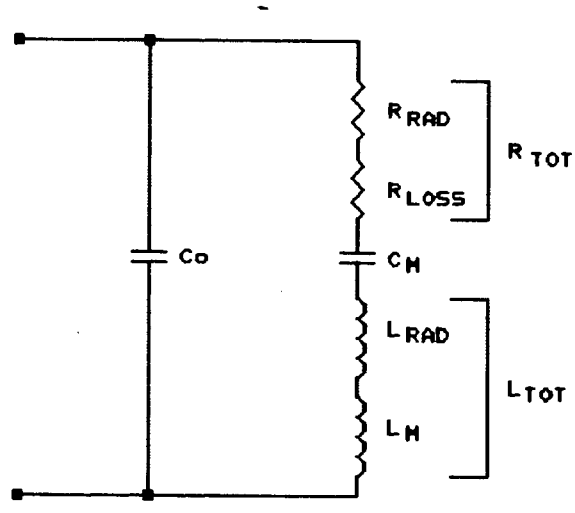

Fig. 6.34 Equivalent circuit for a crystal radiating into a load

The resistive and mass loading of the transducer window and pipeline, R_{RAD} and L_{RAD}, appear in the series RLC branch to produce a combined resistance R_{TOT} and inductance L_{TOT} as follows:

$$R_{TOT} = R_{RAD} + R_{LOSS} \tag{6.124}$$

$$L_{TOT} = L_{RAD} + L_M \tag{6.125}$$

The mechanical loading does not contribute any stiffness loading and thus C_M remains unchanged.

The circle diagram will exhibit a lower conductance value (G_{TOT}) due to loading then when radiating into air (G_{LOSS}) and will therefore by smaller. From the circle diagram of Fig. 6.35, G_{TOT} can be determined from which R_{TOT} is obtained.

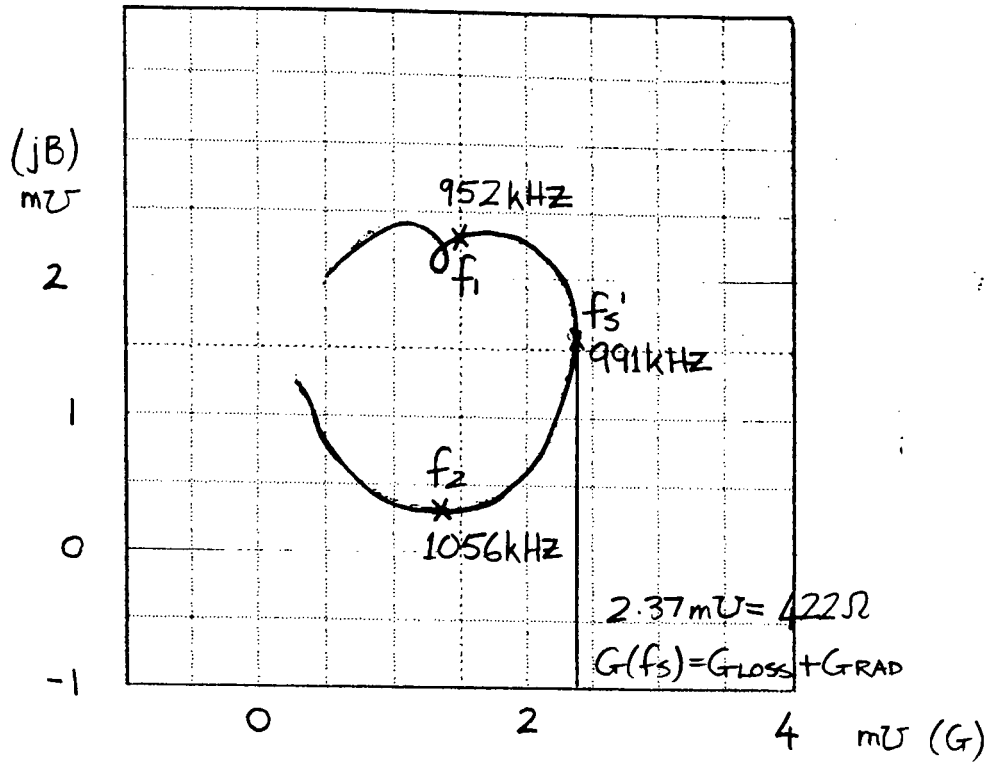

Fig. 6.35 Circle Diagram for the Rx. crystal loaded with the transducer window and the pipe-line

For the Rx. crystal:

$$R_{TOT} = 1/G_{TOT} = 1/2.37m = 422\Omega \qquad (6.126)$$

and for the Tx.:

$$R_{TOT} = 1/G_{TOT} = 1/2.77m = 361\Omega \qquad (6.127)$$

The value of R_{RAD} for the loaded Rx. crystal can be determined using Eqn. 6.124 and with R_{LOSS} as calculated for the case above with the crystal radiating into air:

$$R_{RAD} = R_{TOT} - R_{LOSS}$$

$$R_{RAD} = 422 - 70 = 352\Omega$$

and for the Tx.:

$$R_{RAD} = 361 - 70 = 291\Omega$$

Mechanical loading also causes the bandwidth and series resonant frequency to be altered. From the circle diagrams of Fig. 6.35, the bandwidth of the Rx. mounted is as follows:

$$f_{3dB} = 1056 - 952 = 104kHz$$

and for the Tx.:

$$f_{3dB} = 1055 - 955 = 100kHz$$

The value of L_{TOT} for the Rx. can be determined from the series resonant frequency [f_S'] of the Rx. when loaded (see Fig. 6.35) with C_M as determined above, as follows:

$$f_S' = 1/2\pi \sqrt{L_{TOT} \cdot C_M} \qquad (6.128)$$

$$991kHz = 1/2\pi \sqrt{L_{TOT} \cdot 19pF}$$

solve for L_{TOT}:

$$L_{TOT} = 1.36mH$$

Similarly, for the Tx, with $f_S' = 1034kHz$:

$$L_{TOT} = 1.25mH.$$

The value of L_{RAD} for the Rx. and Tx. respectively can be derived from Eqn. 6.125 using the values of L_{TOT} given above.

First, the Tx.:

L_{RAD} = 9uH

and for the Rx:

L_{RAD} = 119uH

6.8.3.2 Receiver Matching and Sensitivity Improvement

This section discusses the receiver matching technique and the improvement in the sensitivity due to the matching.

Since the transducer is placed on the pipeline some distance away from the circuitry housing, the signal is interfaced between the circuitry and the transducer via a pair of co-axial cables. The equivalent circuit of a Rx crystal driving a co-axial cable and a pre-amp stage is shown in Fig. 6.36.

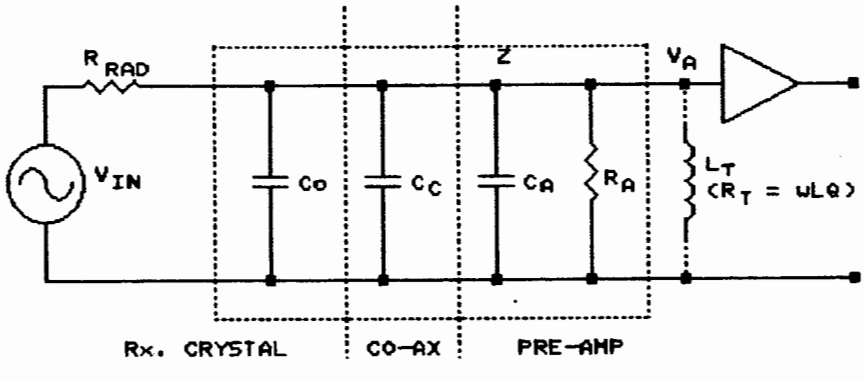

Fig. 6.36 Rx. crystal driving a coaxial cable and a pre-amp stage

At mechanical series resonance the Rx. is characterized by a real impedance, R_{RAD} being driven by a voltage v_{IN}. An internal impedance determined by the un-clamped electrical capacitance C_O is in parralel. The co-axial cable can be represented by a lumped shunt capacitance C_C. The input impedance of the pre-amp is represented by a shunt capacitor C_A and a shunt resistor R_A. The voltage at the amplifier input resulting from the Rx. signal is v_A.

For a sinusoidal input signal, as is the case in this design, the ratio of v_A/v_{IN} is the sensitivity of the crystal.

$$\text{Sensitivity} = v_A/v_{IN} = |Z/(R_{RAD} + Z)| \qquad (6.129)$$

where $Z = 1/Y$

with $Y = 1/R_A + jw(C_O + C_C + C_A)$ (6.130)

Consider first the case when no inductive tuning exists. The operating frequency is 1MHz, so $w = 2\pi \cdot 1MHz$. The pre-amp (see Section 6.8.6) has a real resistive input impedance [R_A] equal to 1K2. The maximum co-axial cable length is 20m. C_C can be determined from the specification of 50Ω co-axial cable which has a capacitance typically of 86pF/m. At 20m, C_C = 1n7. Typically the capacitance of the pre-amp stage is below 20pF, so it can be ignored relative to C_C. The value of C_O is obtained from Section 6.8.3.1 above and has a value of 240pF. From the equivalent circuit of Fig. 6.34, the value of R_{RAD} is 352Ω.

For these parameters, Y at 1 MHz is:

$$Y = 1/1K2 + j2\pi \cdot 1MHz\ (240pF+1n7)$$
$$= 0.83 \times 10^{-3} + j12.19 \times 10^{-3}$$

from which Z can be determined:

$$Z = 1/Y = 5.6 - j81.7$$

The sensitivity for these conditions is as follows:

$$\text{Sensitivity} = v_A/v_{IN} = |Z / (R_{RAD}+Z)|$$
$$= |5.6-j81.7 / (352+5.6-j81.7)|$$
$$= 0.22 \quad [=-13dB]$$

The sensitivity can be increased by adding a parallel inductor [L_T] tuned to resonate with the combination of $C_O+C_C+C_A$ at the mechanical series resonance of 1MHz. The value of the inductor is:

$$L_T = 1/w^2 \cdot C \qquad (6.131)$$

where $C = C_O+C_C+C_A$

For the above parameters, the value of $L_T = 13\mu H$. The new value of Z with inductive tuning is expressed by Z_T and depends on the Q of the LC tuned circuit. An inductor with a Q of 50 at 1MHz was used. Z_T equals the parallel combination of the effective resistance at resonance [R_T] and the input impedance of the pre-amp as in Eqn. 6.132.

$$Z_T = R_T \cdot R_A/(R_T+R_A) \qquad (6.132)$$

where $R_T = wLQ = 4K1$ (6.133)

therefore $Z_T = 928\Omega$

The new sensitivity is now equal to:

$$\text{Sensistivity} = v_A/v_{IN} = |Z_T/(R_{RAD}+Z_T)| = 0.73 \quad [-2.8\text{dB}]$$

The sensitivity of the Rx. has been improved by 10.2dB by appropriate matching techniques.

6.8.3.3 Transmitter

For maximum sensitivity of the Tx. crystal, the output impedance of the driver circuit must be as low as possible. This is one reason for the necessity of a current buffer following the oscillator stage. (see Section 6.8.5) The output impedance of the buffer is low at the operating frequency. It is specified as 6Ω at 1KHz. At the operating frequency of 1MHz, the output impedance was measured and equals 10Ω which is suitably low for driving the Tx. crystal with high sensitivity.

If a current buffer is employed to drive the Tx., then a matching network is not required.

6.8.4 Transmitter Oscillator (block no. 1)

6.8.4.1 Requirements

To drive the Tx. crystal in constant wave (CW) operation a suitable designed oscillator is required which must satisfy the following criteria:

(i) Center frequency of 1MHz

This is the approximately the series resonant frequency of the Tx. and Rx. crystal.

(ii) Tuneable in the range (bandwidth) of approximately 200kHz

The oscillator must be tuneable for the following two reasons: All PZT crystals are slightly different, thay have slightly different resonant frequencies. Maximum efficiency in terms of ultrasonic sensitivity and in terms of minimizing the required driving current is achieved by operating the crystals at series resonance.

Also, the maximum efficiency of transmission of the ultrasound at the interface of the transducer window material (eg. resin) and the pipe-wall (eg. steel), and at the interface of the pipe-wall and the pipe-lining material (eg. polyurethane) will probablly occur at a frequency away from the series resonance of the crystal.

The optimum operating frequency is the frequency for which the S/N ratio of the demodulated signal is a maximum. This frequency is best determined in practice by tuning the transmitter oscillator until the Doppler signal is a maximum (this frequency set up is achieved when the bed-load velocity is greater than zero and the demodulated Doppler signal is observed on an oscilloscope or spectrum analyser).

The oscillator tuneable bandwidth is approximately 200kHz so that any operating frequency within the bandwidth of the Tx. and Rx. crystals (which have a bandwidth $\approx$ 100kHz) can be chosen for optimum operating conditions.

6.8.4.2 Circuit Design

The circuit consists of a transistor differential pair, with a parallel resonant tuned circuit in the collector load of the non-inverting differential pair. Positive feedback is provided from the resonant load to the inverting input of the differential pair to maintain oscillations. The tuned circuit consists of a fixed inductor (L1) and fixed capacitor (C9) and two trimmer capacitors (fine tuning: CT1) and (course tuning: CT2) all in parallel. Stray capacitance (C_{STRAY}) is also present in the tuned circuit with a value ≈ 50pF. The desired tuneable bandwidth is approximately 200kHz with a ceneter frequency of 1 MHz. L1 is a chosen to be a wire wound ferrite coil former with an inductance of 100uH and a rated Q of 65 at 1.5 MHz. To determine values for C9, CT1 and CT2, the following equations are used to describe the minimum and the maximum oscillating frequency:

$$f_{MIN} \approx 900kHz \approx 1/2\pi\sqrt{L \cdot C_{MAX}} \quad (6.134)$$

$$f_{MAX} \approx 1100kHz \approx 1/2\pi\sqrt{L \cdot C_{MIN}} \quad (6.135)$$

where L = L1 = 100uH, solve for c_{MAX} and c_{MIN}:

$$C_{MAX} = C9 + C_{STRAY} + CT1_{MAX} + CT2_{MAX} \quad (6.136)$$

$$C_{MIN} = C9 + C_{STRAY} + CT1_{MIN} + CT1_{MIN} \quad (6.137)$$

With the following component values used in the final design, the actual values of f_{MIN} and f_{MAX} can be calculated:

C9 = 150pF, CT1 = 1.8-22pF, CT2 = 7-100pF

f_{MIN} = 887kHz
f_{MAX} = 1101kHz

Which is validated in practice to be very closely equal to theory.

6.8.5 Current Amplifier Buffer (block no. 2)

6.8.5.1 Requirements

(i) Provide current gain

The current buffer is the stage that follows the transmitter oscillator. Its function is to provide current gain and isolation between the oscillator and the transducers crystals with minimal distortion.

The Tx. crystal within the transducer is connected via a 20m co-axial cable having a capacitance [C_C] of 1n7 for a 20m length. This is equivalent to a real resistive load with a magnitude of 94Ω at 1MHz. Current amplification is therefore necessary to prevent the transmitted signal from being distorted at the Tx.

6.8.5.2 Circuit Design

A commercially available current IC amplifier, namely the National LH0002 is suitable for this application. Its wide bandwidth (30MHz), its low harmonic distortion and its steady state output current capability of 100mA make it suitable for this application. Also, it has a reasonably high input impedance (30kΩ at 1 MHz) which will not load the oscillator significantly, it has a low output impedance (6Ω) suitable for driving a low impedance load. The output current that the buffer should be capable of delivering [I_B] can be expressed as follows:

$$I_B = V_{RMS} / Z_L \qquad (6.138)$$

where V_{RMS} is the RMS volatge of the oscillator and Z_L is the combination of the impedance of the co-axial cable and the Tx. crystal as follows:

$$Z_L = 1/(2\pi \cdot f \cdot (C_0+C_C) \qquad (6.139)$$

with C_0 = 240pF (see Section 6.8.3.1) and C_C = 1n7 (see Section 6.8.5.1).

At 1MHz, Z_L = 82Ω and with a peak to peak voltage from the oscillator [V_{PP}] of 12V, I_B should be at least:

$$I_B = (V_{PP} / 2\sqrt{2}) / 82 \qquad (6.140)$$
$$I_B = 52mA$$

The 100mA rated output current of the buffer is therefore acceptable to drive the Tx. crystal via a 20m co-axial cable.

6.8.6 Pre-Amp and Filters (block nos. 5 and 6)

The signal from the Rx. crystal is relayed along a coaxial cable to the circuitry housing. This received signal is filtered, amplified and buffered by means of a National LM359 Norton (current) amplifier and associated passive components. The LM359 is chosen because it has a high gain bandwidth product (specified gain of up to 100 at 400MHz) and a low spot noise figure specified at 6 nV/$\sqrt{Hz}$ for frequencies above 1kHz. Spot noise = 6uV at 1 MHz.

The LM359 is configured with a gain = 20dB, and a -3dB bandwidth ≈ 450kHz to 1.6MHz. The input signal comes from the coaxial cable and matching network discussed in

Section 6.8.3.2. The interfacing between the Rx. crystal and co-axial cable to the pre-amp has been discussed in Section 6.8.3.2. The circuit configuration of the pre-amp is based on an inverting video amplifier design example presented in the National Linear Data book [Ref. 29,p3-234].

The output impedance at 1 MHz is approximately 4Ω which is an effective buffer for interfacing to the low pass filter stage following its output.

6.8.7 Demodulator: Multiplier (block no. 7)

A demodualtor as described in Section 6.2 above can be realized with a commercially available balanced modulator/ demodulator such as the LM1496. It produces an output voltage proportional to the product of an input (signal) voltage and a switching (carrier) signal.

The LM1496 was chosen as it has a sufficiently wide specified frequency response (100MHz); has an adjustable gain, has fully balanced inputs and outputs and has low offset and drift. The external components are chosen based on a typical application circuit in the National Linear Data book [Ref. 29, p10-109] which operates as a single sideband suppressed carrier demodulator (or product detector). The voltage supply is 0 to +12V DC.

A small portion of the transmitter oscillator signal is a.c coupled to the carrier input pin (pins 8 (+ve) and 10 (-ve). A value of 300mV is tapped off the transmitter oscillator with a potential divider voltage attenuator (block no. 3) to satisfy the suggested optimum operating condition. The pre-amplified Doppler received signal is a.c coupled to the signal pin (pin 1). The gain is set with resistors R13 and

R22 and is approximately equal to R22/R13 = 2K7/100 ≈ 29dB which prevents any distortion of the Doppler signal.

The ouput of the demodulator (pin 12) is passed through a band-pass filter (block no. 4). The band pass (BP) filter attenuates the high frequency carrier breakthrough, the multiplied sum frequency ($2 \cdot f_T$) and the DC term $R_B/2 \cos \Theta_B$ (see Section 6.2.3). The BP filter consists of a RC low pass filter ($f_{LC} \approx 14kHz$), which exceeds the highest expected demodulated Doppler frequency, coupled directly to a RC high pass filter ($f_{HC} \approx 72Hz$) to cut out the unwanted DC signal.

The output of the B.P filter will be the Doppler shift signal devoid of DC or high frequencies.

6.8.8 Doppler Dynamic Range Reduction (DDRR) Filter (block no. 10)

The dynamic range reduction filter network discussed in Section 6.7.6 should have a transfer function as follows:

$$F(f) = 2\pi \cdot \tau_F \cdot f \qquad (6.89)$$

where $2\pi \cdot \tau_F = 1/f_D(max)$ (6.90)

This transfer function can be realized with a RC hi-pass filter circuit having a transfer function as follows:

$$F(f) = 2\pi \cdot f \cdot \tau_F \; / \; \sqrt{(1 + (2\pi \cdot f \cdot \tau_F)^2} \qquad (6.141)$$

with τ_F = RC chosen according to eqn. 6.90.

From Eqn. 6.141, Eqn. 6.89 will be accurately satisfied for all frequencies [f] such that $f << f_D(max)$. At $f = f_D(max)$, Eqn. 6.89 will be have a maximum error of 3dB, which can be ignored.

6.8.9 Comparator (block no. 11)

The function and necessity of a comparator stage with an adjustable threshold voltage [A_T] is discussed in Section 6.7.3. Briefly, its function is to only pass bed-load Doppler signals and not the suspended-load Doppler signals.

In Section 6.7.3 the analysis is in terms of an adjustable comparator threshold voltage and no mention is made of the Doppler gain stage. In practice however, a comparator with an adjustable threshold voltage is not implemented as problems such as unwanted oscillations in the comparator stage could exist, especially for the wide dynamic range required by the threshold voltage. More preferable is a comparator stage with a fixed threshold voltage (120mV) which is preceeded by an adjustable Doppler Gain control amplifier (block no. 9). The effective value of A_T as defined in Section 6.7.3 can be redefined in terms of the fixed comparator threshold voltage of 120mV, and the adjustable Doppler Gain [A_V] as in Eqn. 6.112.

$$A_T = 120mV/A_V \qquad (6.112)$$

Once the Doppler Gain has been correctly set (see Chapter 7, Section 7.2), the output of the comparator stage will be a square wave with its fundamental frequency equal to f_D.

6.8.10 Doppler Processing (F-V converter or ZCC)

6.8.10.1 Introduction

Note: The input frequency to the frequency to voltage converter [f_{IN}] is the mean bed-load Doppler frequency [$f_{D(BED)}$] or expressed simply as f_D

Processing the Doppler frequency involves linearly converting its frequency to a voltage. As has been discussed in Section 5.6 and Section 6.5.5, a recognized technique for processing the demodulated Doppler signal [f_D] is to count the average number of zero crossings of the signal over a period of time by means of a ZCC. The expected number of zero crossings [N] is related to the PSD of the input Doppler signal, where N is given by Eqn. 5.33:

$$f_Z = N/2 = (\overline{f_D^2})^{1/2} = f_{D(RMS)} \qquad (5.33)$$

where f_D is the mean bed-load Doppler frequency [$f_{D(BED)}$].

The expected instantaneous frequency provided by a ZCC is expressed by f_Z according to Eqn. 5.33 and equals the RMS (bed-load) Doppler frequency. This method of converting a frequency to a voltage can be realized with a commercially available frequency to voltage converter (F-V) IC, the National LM2907. The input frequency and output voltage of the F-V converter are defined by f_{IN} and V_{FV} respectively. The output voltage of the F-V converter will then be linearly related to f_Z, according to the F-V constant [k_{FV}] as in Eqn. 6.142.

$$V_{FV} = k_{FV} \cdot f_Z \qquad (6.142)$$

The relationship between V_{FV} and f_D can be derived by expressing f_Z in terms of f_D according to the data presented in Fig. 6.24, which relates the ratio $[f_Z/f_D]$ to the Doppler spectral width ratio $[\beta]$ for a Gaussian Doppler PSD.

If the Doppler PSD is narrow then $f_Z = f_D$ and Eqn. 6.142 can be expressed as:

$$V_{FV} = k_{FV} \cdot f_D \qquad \text{(for a narrow Doppler PSD)} \qquad (6.143)$$

A broadened Doppler spectral width will cause V_{FV} to be higher than defined by Eqn. 6.143, as follows:

$$V_{FV} > k_{FV} \cdot f_D \quad \text{(for a wide Doppler PSD)} \qquad (6.144)$$

The percentage increase in V_{FV} can be derived using the data presented in the graph of Fig. 6.24. In practice, the Doppler broadening ratio $[\beta = \delta f_D/f_D]$ ranges between 0.3 to 0.6, which according to Fig. 6.24 constitues a ratio of f_Z/f_D of below 1.05, so that the assumption that $f_Z = f_D$ (defined by f_{IN} in this section) can be made. Eqn. 6.143 therefore holds with minimal error.

6.8.10.2 Requirements

The following four requirements must be satisfied by a well designed F-V conerter circuit so that the Doppler signal is suitably processed.

(i) High F-V linearity oyer entire Doppler frequency range.

For all values of v_{BED} up to a maximum of 5m/s, the output voltage [V_{FV}] must be linearly related to the input frequency [f_{IN}] with a linearity error < say 0.5%.

(ii) Calibration Facility

In practice, the Doppler constant [k_D] can vary at most between 160 (defined as $k_D(min)$) to 430 (defined as $k_D(max)$) depending on the type of pipe-line, the value of P{bed} and other factors that influence the Doppler equation. This implies that for identical maximum bed-load velocities equal to 5m/s (as specified in the requirements of Chapter 3), the maximum Doppler frequency [$f_D(max)$] can range between 800Hz to 2150Hz, depending on the value of k_D for the system.

A calibration trimmer potentiometer [RT2] is provided to adjust the relationship between the input frequency [f_{IN}] and V_{FV} of the F-V converter. RT2 is adjusted so that the output voltage equals the maximum value of V_{FV} (defined by v_{MAX} and equal to 10V) when v_{BED} equals 5m/s, for any particular value of k_D so that Eqn. 6.113 is satisified:

$$V_{FV} = 2 \cdot v_{BED} \qquad (6.113)$$

(iii) Fast Response Time

The response time [τ_{FV}], or the time it takes V_{FV} to stabilize at a new voltage must be adjustable between 0.2s to 8s according to the specification of Chapter 3, Section 3.7.

(iv) Low ripple

The ripple on V_{FV} is measured in terms of a maximum peak to peak voltage over the entire input frequency range. The ripple on V_{FV} should be minimized as it could be misinterpreted as a fluctuating bed-load velocity.

6.8.10.3 Circuit Design

To satisfy the above four requirements, the following circuit design is implemented and discussed as follows in the same order in which the requirements are discussed.

(i) High linearity

The typical linearity error of the LM2907 is specified as 0.3%. The linearity is dependant on the resistance R_l. When R_l exceeds 50kΩ, then the linearity error < 0.5% over a temperature range from -35°C to 85°C.

R_l is the sum of a fixed resistance (R39) and a variable resistance (RT2) as follows:

$$R_l = R39 + RT2 \qquad (6.145)$$

where RT2 is a trimmer potentiometer with a resistance that ranges between 0Ω to the value of RT2. The minimum value of the combination of RT2 and R39 equals R39 when RT2 = 0Ω. R39 has a chosen value of 56kΩ to satisfy the requirement of exceeding 50kΩ.

(ii) Calibration Facility for different Doppler constants

The relationship between f_{IN} and V_{FV} is given as follows (from Eqn. 6.143 with $f_{IN} = f_D$):

$$V_{FV} = k_{FV} \cdot f_{IN} \tag{6.146}$$

where k_{FV} is the F-V constant.

The value of the F-V constant is specified in the National Data Book [Ref. 29, p9-140) as being equal to the following expression:

$$k_{FV} = Vcc \cdot C33 \cdot R_Z \tag{6.147}$$

where Vcc is the 12V DC supply voltage. k_{FV} has a minimum value [defined by $k_{FV}(min)$] when R_Z is a minimum value equal to the value of R39. k_{FV} has a maximum value [defined by $k_{FV}(max)$] when R_Z is a maximum value equal to the value of R39+RT2. The following two equations describe the relationship between $k_{FV}(min)$ and $k_{FV}(max)$ and the component values:

$$k_{FV}(min) = Vcc \cdot C33 \cdot R39 \tag{6.148}$$

$$k_{FV}(max) = Vcc \cdot C33 \cdot (R39+RT2) \tag{6.149}$$

From the Doppler equation (Eqn. 5.10), $f_D = k_D \cdot v_{BED}$, where v is written as v_{BED} to signify that the particle velocity is the bed-load particle velocity in this case. Substitute this into Eqn. 6.143 to get:

$$V_{FV} = k_{FV} \cdot k_D \cdot v_{BED} \tag{6.150}$$

constants may be determined from the calibration procedure discussed in Section 7.2.

The values for C33 can be chosen using Eqn. 6.153 with R39 = 56K:

$$k_{FV}(min) = Vcc \cdot C33 \cdot R39 \qquad (6.153)$$

$$0.00465 = 12V \cdot C33 \cdot 56K$$

Solve for C33:

$$C33 = 6n9$$

Let C33 = 6n8 since this value capacitor is readily available. Now, to calculate the value of RT2, use Eqn. 6.154:

$$k_{FV}(max) = Vcc \cdot C33 \cdot (R39+RT2) \qquad (6.154)$$

$$0.0125 = 12V \cdot 6n8 \cdot (56K+RT2)$$

Solve for RT2:

$$RT2 = 97K$$

A 100kΩ 20 turn potentiometer is chosen for RT2.

The calibration technique described above was validated to operate correctly in practice by measuring the output voltage of the F-V converter for a range of input frequencies with different settings for RT2.

(iii) Fast Response Time and Low Ripple Voltage

The size of C34 is dependant only on the amount of ripple voltage allowable and the required response time. Its choice is therefore a compromise decision between these two effects. The maximum response time of the F-V converter [τ_{FV}] is expressed by (RT2 + R39)·C34 and occurs when RT2 is a maximum of 100K. To ensure that the response time is less then 0.2 seconds (as specified by the requirement of Section 6.8.10.2 (iii)) for all settings of RT2, we set τ_{FV} = 0.2s and solve for C34 to get C34 = 1.28uF. Chose C34 to be 1uF with τ_{FV} = 0.16s

An expression for the ripple voltage [V_{RIP}] of V_{FV} is expressed by Eqn. 6.155 with Vcc = 12V [Ref. 29, p9-140]:

$$V_{RIP} = 6 \cdot C33/C34 \cdot (1-f_{IN}/f_{MAX}) \quad \text{pk-pk} \qquad (6.155)$$

where f_{IN} is the input Doppler frequency and f_{MAX} = 785 to 2188Hz, depending on the desired calibration setting ie. potentiometer RT2. The ripple voltage is a maximum when f_{IN} = 0Hz. From Eqn. 6.155, V_{RIP} is a maximum of 40.8mV pp at f_{IN} = 0Hz with C33 and C34 as chosen.

From Eqns. 6.146 and 6.147 with $f_{IN} = f_{MAX}$ so that $V_{FV} = V_{MAX}$ = 10V, f_{MAX} is expressed as follows:

$$f_{MAX} = 10/(12 \cdot C33 \cdot R_Z) \qquad (6.156)$$

An expression for V_{RIP}/V_{FV} can be derived, in terms of f_{IN} by dividing Eqn. 6.155 by Eqn. 6.146 after Eqn. 6.147 has been substituted into Eqn. 6.146. Now use Eqn. 6.156 to solve for R_Z and substitute this into the expression for V_{FV} to get:

$$V_{RIP}/V_{FV} = 3 \cdot C33/5 \cdot C34 \ (f_{MAX}/f_{IN} - 1) \qquad (6.157)$$

The ratio f_{MAX}/f_{IN} equals $5/v_{BED}$ from Eqn. 6.151 above so that Eqn. 6.157 can be rewritten as:

$$V_{RIP}/V_{FV} = 3 \cdot C33/5 \cdot C34 \ (5/v_{BED} - 1) \qquad (6.158)$$

This ripple voltage is inversely proportional to v_{BED} and C34. Eqn. 6.158 is solved for C33 = 6n8 and C34 = 1uF (as above) for v_{BED} ranging between 0 to 0.5m/s and plotted in Fig. 6.37. The graph labelled no.1 is the relevant graph for this section.

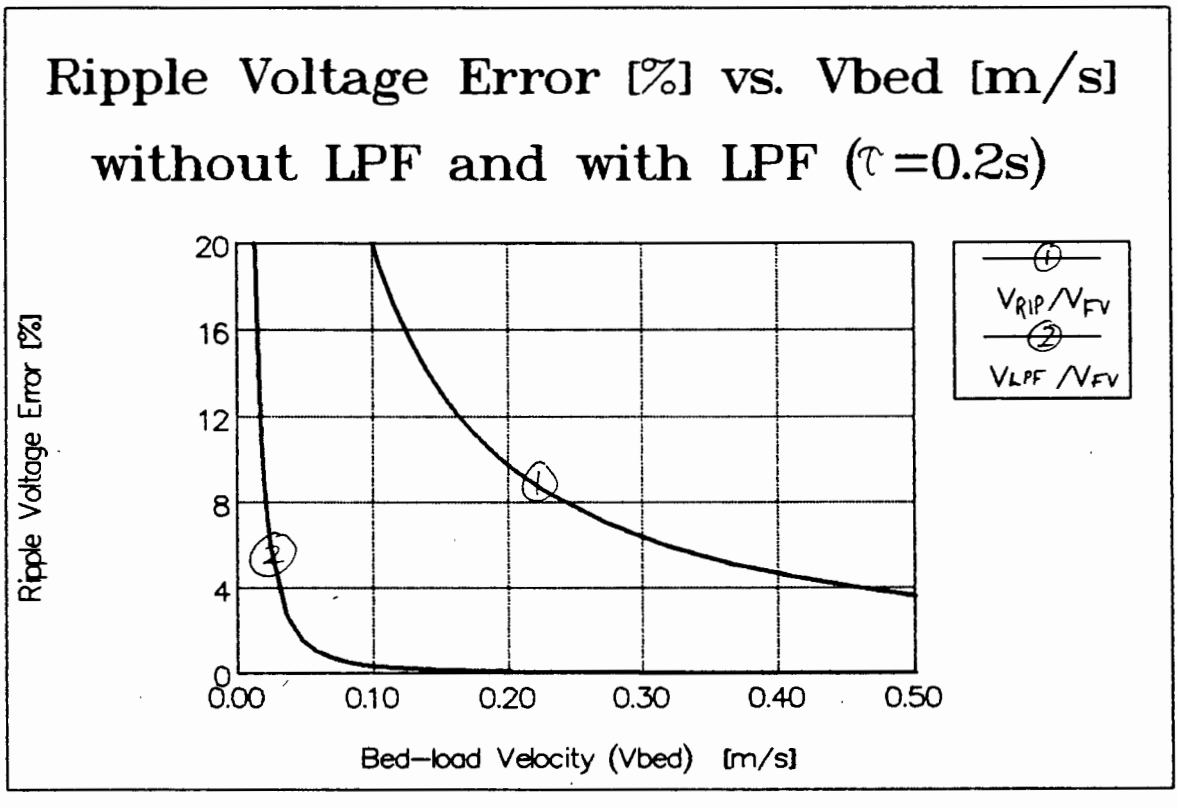

Fig. 6.37 Ripple voltage Error as a function of bed-load velocity without and with a LPF

From Fig. 6.37 the ripple voltage error has a value of 10% when v_{BED} = 0.2m/s for the component values chosen and with RT2 = 100K. This error can be considerably reduced by using a longer system response time. The response time settings and their effect on the ripple voltage is discussed in the following section.

6.8.11 Response Time

6.8.11.1 Introduction

The response time of the UDBV system is is the time it takes for the output (output current) to stabilize at a new value for a unit step change in the input bed-load velocity. The minimum response time of the system is set to 0.2s by the F-V converter. The response time can be increased with an adjustable "Response Time" rotary switch (see Section 6.8.2 block no. 20) setting on the UDBVs front panel. The position of the rotary switch sets the response time to either its minimum of 0.2s or 0.5s, 1s, 2s, 4s or 8s by switching one of the low pass RC filters from the bank of six filters (block no. 21). The time constants [τ] of the filters are equal to the response times above. The response time is set so that a compromise between system accuracy and system response time can be achieved. Increasing the system response time (defined by τ), has the following effects:

(i) Accuracy in determining f_D is increased

(ii) Ripple voltage is reduced

(iii) Response time is slower.

6.8.11.2 Response Time, Accuracy and Ripple Voltage

The analysis of the effect of the response time on the accuracy in determining f_D is carried out in Section 6.5.5.2. The graph of Fig. 6.25 demonstrates the decrease in error [ϵ] (which corresponds to an increase in accuracy) in determing the mean Doppler frequency [f_D] for larger response times.

The effect of the low pass response time filters is to considerably reduce the ripple voltage present at the output of the F-V converter so that the ripple voltage error can be ignored. The DC voltage out of the F-V converter [V_{FV}] is unaffected. The effect on the ripple voltage error ratio [V_{RIP}/V_{FV}] follows. For example, from Fig. 6.37, without response-time filtering the ripple voltage error is 20% when v_{BED} = 0.1m/s.

The reduction of this ripple voltage error can be calculated from the amplitude transfer function of the particular filter chosen from the filter bank of low-pass filters. If for example the filter with the lowest response time is chosen ie. τ = 0.2s, then this will have the least effect on the ripple voltage error. The amplitude transfer function for the low pass RC filter is given as:

$$V_{LPF} = \frac{Vi}{\sqrt{(2\pi f\tau)^2+1}} \qquad (6.159)$$

where V_{LPF} is the peak to peak amplitude of the output voltage of the response time filter, Vi is the peak to peak amplitude of the input voltage which in this case equals the ripple voltage [V_{RIP}] from the F-V converter (as defined by Eqn. 6.157 as a ratio of V_{FV}). The frequency of Vi is defined by f and equals the frequency of the ripple voltage,

which is the frequency of the input Doppler frequency to the F-V converter [f_{IN}].

The ratio V_{LPF}/V_{FV} is calculated by substituting Eqn. 6.157 into Eqn. 6.159 as follows:

$$V_{LPF}/V_{FV} = \frac{3 \cdot C33/5 \cdot C34 \ (f_{MAX}/f_{IN} - 1)}{\sqrt{(2\pi f_{IN}\tau)^2+1}} \qquad (6.160)$$

This ratio is calculated for the worst case when f_{MAX} = 2188Hz and τ is the minimum value of 0.2s. The ratio is calculated in terms of v_{BED} by substituting $f_{MAX} \cdot v_{BED}/5$ into f_{IN} from Eqn. 6.151. Fig. 6.37 is a graph of the original ripple voltage error ratio [V_{RIP}/V_{FV}] and the filtered ripple voltage error ratio [V_{LPF}/V_{FV}] on the same set of axix as a function of v_{BED}. At v_{BED} = 0.1m/s, V_{RIP}/V_{FV} = 20% but at the same bed-load velocity, V_{LPF}/V_{FV} = 0.36%, which is a substantial reduction. The effective ripple voltage error can therefore be ignored for all practical bed-load velocities (>0.1m/s say).

6.8.12 Maximum Velocity Scaling

6.8.12.1 Introduction

The output of the UDBV is either in the form of a 0 to 20mA or a 4 to 20mA output current. Assume for the time being that the range is 0 to 20mA. In the practical situation when the UDBV is to be used as a control sensor, the output current is usually converted to a voltage and digitized to be read by a computer. Maximum resolution of the digital conversion can be achieved by ensuring that the output fills the entire span of 0 to 20mA. Since the maximum bed-load velocity may be considerably lower than the specified

maximum of 5m/s, a facility for adjusting the maximum bed-load velocity range must be provided. This is necessary so that the 0 to 20mA range corresponds closely to the full range of bed-load velocities measured in a particular application.

6.8.12.2 Circuit Design

The DC output voltage from the F-V converter will satisfy the relationship of Eqn. 6.113 ie:

$$V_{FV} = 2 \cdot v_{BED} \quad \text{where } V_{FV} \leq 10V \text{ so that } v_{BED} \leq 5m/s \tag{6.113}$$

After being passed through a buffer and low pass filter for response time adjustment, the DC output voltage is still defined by V_{FV}. This voltage is then scaled (block no. 24) so that its range will lie between 0 to 1V depending on the "Maximum Velocity" rotary switch (block no. 23) setting. This scaled voltage is defined by V_{VI}, signifying that it is an input voltage to the voltage-to-current converter module (block no. 25)

The "Maximum Velocity" rotary switch [v_{MAX}] may be set to one of six settings: 0.5m/s, 1m/s, 2m/s, 3m/s, 4m/s and 5m/s. From Eqn. 6.113 above, it is clear that $V_{FV} = 1V$ when $v_{BED} = 0.5m/s$. When v_{MAX} is set to the 0.5m/s position then no scaling is required. When v_{MAX} is set to the 1m/s setting then V_{FV} must be scaled so that it is 1V when $v_{BED} = 1m/s$. Similarly, when the v_{MAX} setting is adjusted to 2,3,4 and 5m/s respectively, then V_{FV} must be scaled accordingly so that its voltage is 1V.

There are five scaling constants [k_S] each corresponding to the v_{MAX} rotary switch setting. The scaling constant is related to v_{MAX} according to Eqn. 6.114.

$$k_S = 1/2v_{MAX} \tag{6.114}$$

When v_{MAX} is set to 0.5m/s then $k_S = 1$ and no scaling is required as discussed above. When, for example, v_{MAX} is set to 4m/s then $k_S = 1/8$. The output voltage from the scaling module [V_{VI}] can be expressed as follows:

$$V_{VI} = k_S \cdot V_{FV} \tag{6.161}$$

With k_S chosen according to Eqn. 6.114, V_{VI} of Eqn. 6.161 will range between 0 to 1V for all bed-load velocities (between 0 to 5m/s) as required.

Ths scaling is realized with a bank of potential dividers (R60-R64 and R70) set according to Eqn. 6.114. Trimmer potentiometers (RT5-RT10) are included in each potential divider to provide approximately 30% scaling range adjustment to allow for deviations in the potential divider resistor values.

6.8.13 Voltage to Current Conversion (block no. 25)

6.8.13.1 Introduction

Since the UDBV is to be used as a control sensor in a feedback control loop usually on a mining plant, the output signal from the system (voltage or current) must be such so that it can be remotely sensed away from the instrument. An output in the form of a current is provided by the instrument which can then be sent along a shielded twisted pair of wires to be converted to a voltage at the remote

sensing destination. An output current rather than an output voltage is desirable for the following four reasons:

(i) noise is less likely to be picked up with current sensing

(ii) voltage drops (voltage divider effect) does not exist with current sensing

(iii) the voltage can be 'programmed' at the sensing location by measuring the voltage across any small fixed resistor.

(iv) an output current is an industry standard technique so that the instrument will be compatible with data logging devices etc.

6.8.13.2 Requirements

The following four requirements must be satisfied by the V-I converter:

(i) The voltage from Vmax scaling module must be linearly converted to a current source of between 0 to 20mA [Iout].

(ii) An adjustable current offset [Ios] must be provided. Iout equals Ios when the input voltage is zero (usually set to 4mA). The purpose of Ios is to indicate that the UDBV is on and operational when the current output is being remotely sensed (by, for example, a computer). Also, it prevents the output from being negative which could more likely occur if Ios=0 and perhaps cause a malfunction in the remote sensing computers.

(iii) Voltage output sensing by means of a resistor must provide up to 8V (ie the V-I converter must provide 20mA into a load of up to 400Ω).

(iv) Current sensing must be referred to ground

6.8.13.3 Circuit Design

The voltage from the scaling module will be between 0 to 1V depending on v_{BED} and v_{MAX} and can be defined by V_{VI}, the voltage into the V-I converter as discussed in Section 6.8.12 above. The output current of the V-I converter [Iout] must satisfy Eqn. 6.116 to fulfill requirements one and two above.

$$Iout = V_{VI}/50 + Ios \qquad (6.116)$$

with Ios adjustable between 0 to say 6mA

To satisfy the four requirements listed above, a circuit was designed (see Appendix C) consisting of an op-amp (IC13,LF151H) configured in the inverting mode driving a PNP transistor (Q5,2N2907) to provide the current gain. The input voltage [V_{VI}] enters the inverting input. An offset voltage [V+] obtained from a potential divider with RT3 providing an adjustable small voltage variation, enters the non-inverting input.

The circuit configured provides an output current [Iout] expressed as follows:

$$Iout = V_{VI}/R48 + (6-V^{+})/R48 \qquad (6.162)$$

The offset current [Ios] is defined by $(6-V^{+})/R48$. For the case with Ios=0mA, V^{+} is set to 6V from a potential divider.

Since the setting of V^+ is critical, the potential divider and the op-amp are powered from the same voltage regulator which is placed physically close to both the potential divider and the op-amp circuitry to reduce the effects of noise. R48 is chosen to be as close to 50Ω as possible so that Iout = 20mA when V_{VI} = 1V.

In order that Ios is set to 4mA, the voltage, V^+ must be set equal to 5.8mV. The setting of V^+ is by means of a potentiometer, RT3.

6.8.14 Bed-load Particle Condition Indicator

6.8.14.1 Requirements and Description

To indicate whether a Doppler-shift signal is being detected, a Doppler Signal LED indicator (or Bed Condition Indicator) is provided. When the LED is on it means either noise is being picked up and being demodulated or else a Doppler shift signal has been demodulated due to the bed-load particle velocity.

This LED indicator therefore serves two purposes:

(i) Provides information used for set-up of Doppler gain

The Doppler gain setting (potentiometer RT1) is important and must be correctly set. If it is set too low then the demodulated Doppler signal cannot be processed to be converted to an output current. If however, the Doppler gain setting is set too high then demodulated noise will be processed to falsely indicate the bed-load velocity.

The Doppler gain setting comprises a part of the set-up procedure and is discussed in detail in Chapter 7, Section 7.2.

(ii) Provides information about the bed-load velocity status

If the Doppler gain is correctly set then the LED must indicate whether the bed-load velocity is stationary, approaching incipient deposition or is moving.

Three seperate 'states' of this indicator are possible: on, off or flashing. When the bed-load velocity is moving then the LED must indicate movement by turning on. When the bed-load settles and is stationary then the LED must turn off.

When the bed-load is either on the verge of settling or is moving slowly then the LED must flash. The flashing rate also gives a visual indication of the bed-load condition at low velocities. If the flashing rate is steady and continuous then the bed is moving slowly but steadily and no deposition is occuring: slower flashing corresponding to lower bed-load velocities and vica versa.

When the LED flashes sporadically then the time that the LED is off indicates slurry particles are stationary within the ultrasonic insonified volume above the transducer and the time that the LED is on (or flashing) indicates that bed-load particles are in motion above the transducer. This condition will exist when the bed-load is begining to settle or else when 'dunes' are present within the bed-load and are creeping along the bed. A dune moves by particles on the top of the dune 'peeling off' the dune structure. The particles on the bottom of the dune will be stationary and indicated by the LED being off. Once the top of the dune has been peeled off and eventually moves past above the

transducer then this will be indicated by either flashing of the LED (if moving slowly), or a continuously on LED (for quicker moving dunes).

If the flashing rate decreases then it indicates that the bed-load is probablly beginning to settle. Once off then the bed-load has settled.

6.8.14.2 Cicuit Design

The circuit to satisfy the above requirements are implemented with circuit modules consisting of a level shifter (block no. 12), a monostable (13), a delay (14), a nand-gate pair (15) and a LED driver (16). Each block and their funcions and operation are discussed seperately as follows.

In brief, the operation of this circuit is as follows: the presence of a Doppler signal (detected from the output of the comparator stage so that the Doppler signal will be a square wave with its fundamental frequency equal to f_D) will cause a monostable to trigger. The monostable, after passing through another module, a delay stage, to reduce the effect of detecting noise, drives the "Bed-load condition" LED indicator. If $f_D > 1/(t_M-t_D)$, where t_M is the pulse width of the monostable and t_D is the delay time of the delay module, then the LED will be continuously on. If f_D is zero then the LED will be continuously off since the monostable is not triggered.

If $0 < f_D < 1/(t_M-t_D)$, then the LED indicator will flash at a frequency of $1/f_D$, indicating that the bed-load velocity

is causing low Doppler frequencies to be detected, implying that the bed-load is on the verge of deposition. The flashing rate is decribed above in Section 6.8.14.1.

(i) Level shifter (12)

A level shifter forms the first module of a set of modules (12,13,14,15 and 16) to drive the Doppler Signal (Bed-Condition) Indicator LED. The level shifter shifts the DC voltage levels from the preceeding comparator stage (block no. 11) from -12V,+12 to 0V,12V so that the voltage levels are compatible for driving the monostable stage.

(ii) Monostable (13)

The Doppler frequency [f_D], after passing through the comparator module (block no. 11) and the level shifter (block no. 12) will be a square wave between 0 to 12V with its fundamental frequency equal to f_D. This square wave is input to the monostable. The monostable will produce a pulse of width tm when the input voltage is a transition from low (0V) to high (12V). If the input receives a transition voltage from low to high at a rate exceeding $1/t_M$ per second (ie for $f_D \geq 1/t_M$) then the output of the monostable will be continuously high, indicating a Doppler signal of $f_D \geq 1/t_M$ is being detected. If however $f_D < 1/t_M$ then the output of the monostable will not be continuously high but will be a string of pulses occuring every t_M second with a width of t_M. The pulse width, t_M is chosen to be 22ms.

(iii) Delay (14)

A delay stage of t_D seconds follows the monostable stage. All signals that are present at the output of the monostable which are high (12V DC) for a duration that exceeds t_M in duration are delayed by t_D. The value of t_D is 4.8ms. However, if a signal is present at the output of the monostable which is not high for a duration that exceeds tm, then this delay module output will remain low. In this way most noise signals that are present at the output of the monostable are eliminated. For example, if a Doppler signal causes the monostable to trigger then the output pulse of the monostable will be high for 22mS. The delay will reduce this width by 4.8mS from 22mS to 22-4.8=17.2mS ie the output will be continuously high for $f_D > 1/17.2mS > 58Hz$. However, if a noise spike is present at the output of the monostable and the spike width < 4.8mS, or the spike amplitude < 12V, then the output of the delay will remain low, preventing the noise signal from being detected by the proceeding module (no. 15)

(iv) Nand-Schmitt Trigger pair (15)

The pair of Nand-gate triggers following the delay stage 'cleans-up' the transition voltage from low to high of the delay stage. The voltage at the output of the delay stage will climb from a low (0V DC) to a high (12V DC) in the delay time of 4.8mS. The output of the monostable and the output of the delay are 'Nanded' together so that the output of the Nand-gate is resting high until the output of the delay exceeds the positive-going threshold voltage of the Nand-gate (≈7V) at which point the output of the Nand-gate will trigger low. The voltage 'climbing' effect of the delay stage is illiminated in this way. The second Nand-gate acts as a voltage inverter.

If the Doppler gain stage is set correctly then the output of the Nand-gate pair will be continously high for Doppler frequencies of $f_D > 58Hz$. For Doppler signals where $f_D < 58Hz$, the output of the Nand-gate pair will be a string of pulses occuring at a rate of $1/f_D$ a second, with a pulse width of 17.2mS.

(v) LED Driver and "Bed Condition" LED

A transistor current amplifier following the Nand-gate stage provides the 20mA drive requirement for the "Bed Condition" LED.

For Doppler signals satisfying $f_D > 58Hz$, the "Bed Condition" LED will be continuously on indicating a moving bed. The bed-load velocity [v_{BED}] corresponding to these Doppler frequencies depends on the Doppler constant [k_D]. For the two possible extreme cases of $k_D = 160$ and 430 respectively, v_{BED} must exceed 0.36m/s and 0.13m/s respectively for the LED to be continuously on. When v_{BED} is below these values then the LED will flash at a rate of $1/f_D$ and indicate the bed-load conditions as described above in Section 6.8.14.1. When $v_{BED} = 0$ then the LED will be off.

6.9 CROSS-CORRELATION TECHNIQUE OF MEASURING BED-LOAD VELOCITIES

6.9.1 Introduction

The motivation for employing the cross-correlation technique is discussed. The description of the implemetation in terms of the hardware interface circuitry is presented. The description of the software is described in detail by Elliott [Ref. 13]. The application of the cross-correlator is explained. In Chapter 7, the method of calibrating the UDBV is detailed and presented graphically.

6.9.2 Motivation for Employing a Cross-Correlation Technique

If all the system parameters are known then the demodulated Doppler frequency can be related to the bed-load particle velocity. If the operating frequency [f_T], the ultrasonic velocity in the transmission path [c] and the orientation angles of the Tx. and Rx. (Θ_T and Θ_R) are known, then the Doppler equation relates the peak Doppler frequency to the detectable (bed-load) particle velocity. However, in Section 5.3.2, and in detail in Section 6.7, details of the limitations of directly applying the Doppler equation for predicting the bed-load velocity from the mean Doppler frequency is discussed.

Specifically, the probability term [P(bed)] of Section 6.7.9 influences the relationship between the Doppler frequency and the bed-load velocity. Expressions have been derived to determine the value of P(bed), however it can not be determined accurately with certainty, which implies that the Doppler frequency cannot simply be related to the bed-load particle velocity. For this reason and for the reason of

validating the correct operation of the Velocimeter under various flow conditions, an alternative method of measuring bed-load particle velocities was developed which was independant of all unknown variable parameters such as the slurry particle backscattering strength etc.

6.9.3 Description

This alternative method of measuring the bed-load velocity is based on a Cross-Correlation principle. This principle is employed because it is a technique which will yield the bed-load velocity without any need for calibration.

Two sensors, one placed a known, short distance upstream of the other, measure some property of the particle flow at the bed. This may be its temperature, absorption of ultrasonic energy, its local concentration or density or its electrical conductivity etc. This system measures the conductivity.

If the two sensors are placed a short enough, known distance apart, then one would expect the signal appearing at the downstream sensor to be simply a delayed replica of the upstream signal. A cross-correlator is used to compare the two signals and to give an indication of the match for a range of time delays. The period of time by which the upstream signal must be delayed to achieve the best match, is the time taken for the signal to travel from the upstream to the downstream sensor.

Since the signal is the result of local turbalences in the bed-load particles while they are in motion, one will expect this time delay to be the time taken for the bed to travel the distance between the sensors. As this distance is known it is possible to compute the bed-load velocity using the time delay measured by the cross-correlator.

A dedicated cross-correlator was developed on a Spectrum microcomputer with a Z80 CPU. The cross-correlator algorithm, written in Z80 machine code was implemented on the microprocessor. Croos-correlation graphs could be calculated and then displayed on the monitor. The graphs presented the cross-correlation function as a function of the time delay. The time delay at which the two signals most closely resemble each other, is represented by a peak on the graph. The option existed within the software for either manual or automatic operation. With manual operation, a user could observe the graph to determine the validity and position of the peak. With automatic operation, algorithms would decide on whether the peak is valid or not. If not then either the sample correlation length of the signals would be automatically adjusted using existing data from the two sensors or else new data would be read from the sensors to determine a new cross-correlation function. If however the peak is valid and satisifies validity criteria, then the location of the peak is determined in terms of the delay time, which is then divided by the known sensor spacing to provide an indication of the bed-load velocity.

For further details of the cross-correlation technique see S.Elliot's BSc. Thesis [Ref. 13]. The interface electronic hardware between the conductivity sensor and the microprocessor of the cross-correlator described by Elliott differs from the hardware developed for this thesis. The hardware consists primarily of three stages to convert the sensor signal into a string of 1 bit data compatibile with the microprocessor. Briefly it consists of a high impedance, low noise buffer, followed by an adjustable gain pre-amp with six discrete gain settings, a variable low pass filter with six discrete cut off frequencies and a comparator stage with an adjustable threshold to convert the signal to a 1 bit string of data being either low (0V DC) or high (+5V DC). (See Fig. 6.38 for a block diagram)

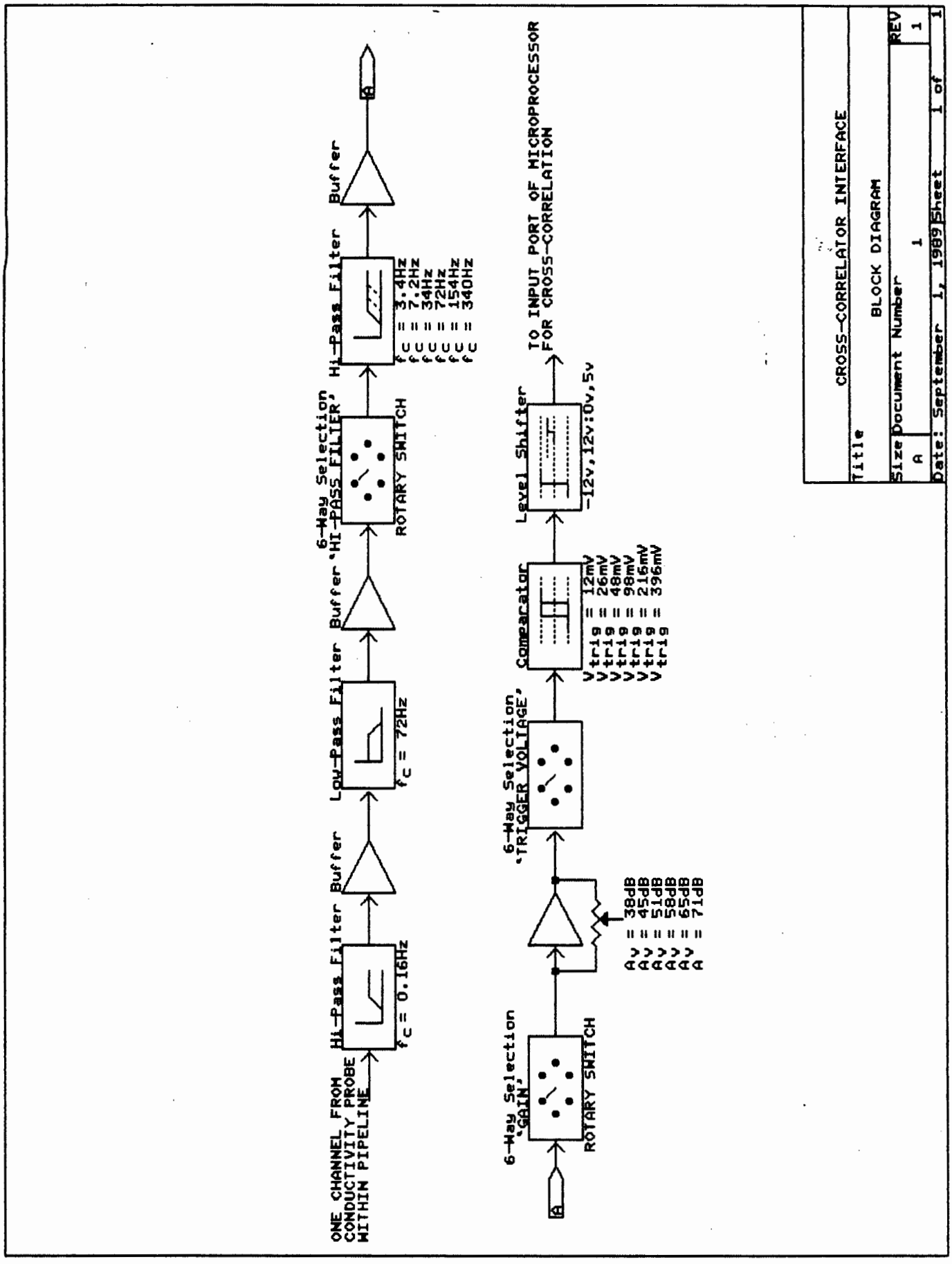

Fig. 6.38 Cross-correlator Interface Block Diagram

The hardware is straight forward and the circuit diagrams are in Appendix E. The pre-amp gain, cut off frequency of the low pass filter and the comparator threshold voltage were all adjusted to provide optimum performance by maximising the wanted correlated peak and minimizing the correlation peaks due to noise.

Typical cross-correlation graphs are presented in Chapter 7.

6.9.4 Calibration of the UDBV Using the Cross-Correlator

As discussed above, the purpose of the Cross-correlator is to provide a means of calibrating the UDBV. The UDBV provides an output current [Iout] in the range 0 (or 4) to 20mA corresponding to the range of bed-load velocities detected. If the UDBV is calibrated correctly then the maximum output current of 20mA must corresponds to a bed-load velocity equal to the "maximum velocity" setting. In Chapter 7, bed-load particle velocity readings are taken with both the UDBV and with the cross-correlator. These readings are then used to adjust the UDBV by means of the calibration setting [RT2, see Section 7.3.3].

CHAPTER 7

RESULTS, CALIBRATION AND DISCUSSION

7.1 INTRODUCTION

Three test-rigs were utilised to test various aspects of the operation of the Velocimeter. A simulation test-rig was constructed to test the linearity between the output current of the Velocimeter and a detectable sand particle velocity. This simulation test-rig also verified characteristics of the Doppler spectral shapes.

A hydraulic test-loop in the Hydro-Transport Research of the Civil Engineering Department was used to perform calibration tests on the Velocimeter using the cross-correlation technique for a range of flow regimes. Two industrial tests were also carried out. These tests were performed at Rossing Uranium, Namibia and at the East Rand Gold and Uranium Mine (ERGO) in the Transvaal.

7.2 SIMULATION TEST RIG-ROTATING DISC

7.2.1 Test-Rig Description and Objective

A simulation of a moving bed load travelling at a fixed, known velocity was created using a simulation test rig as shown in Fig. 7.1. The simulation consisted of a 330mm diameter PVC disc driven by a variable speed D.C. motor. The lower quarter of the disc was submerged in a perspex tank of water. The rim of the disc was coated in sand to model the bed-load and to act as a good reflector of the ultrasonic beam. The velocity of the disc could be varied from 0.45m/s to 1.42m/s and could be accurately determined.

The transducer was bonded to the outside of the tank directly under the lowest point of the disc with a layer of silicone sealant acting as an ultrasonic bond.

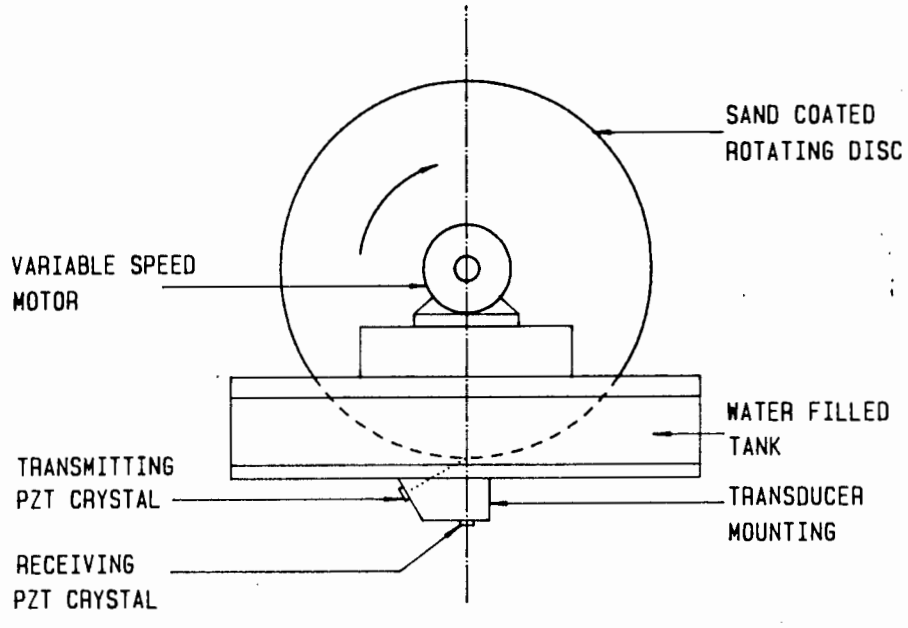

Fig. 7.1 Simulation test-rig: rotating disc

The objective of this simulation test rig is to investigate the linearity of the Velocimeter and to investigate the Doppler spectral shapes.

7.2.2 Test-Rig Results

(i) Doppler Frequency Spectrum

The demodulated Doppler shift frequencies are plotted in Figs. 7.2(i) to 7.2 (vi) for various disc velocities. The span of the spectrums extend from DC to 2kHz. The peak of the spectrum is the point marked with a (x) and is assumed to also be the mean Doppler frequency [f_D].

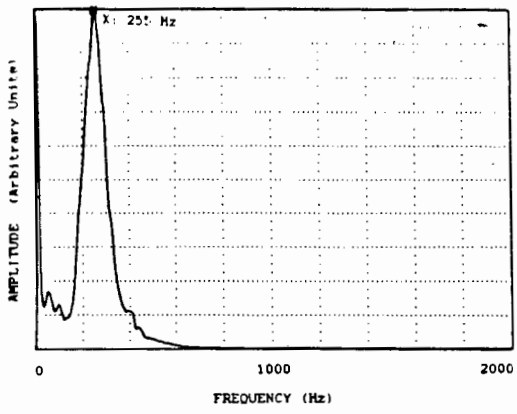

(i) f_D = 255Hz
v_D = 0.45m/s

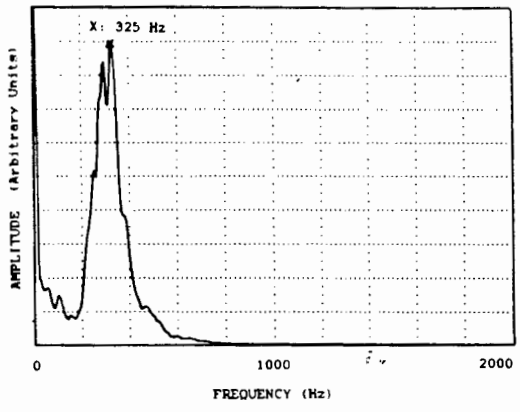

(ii) f_D = 325Hz
v_D =0.53m/s

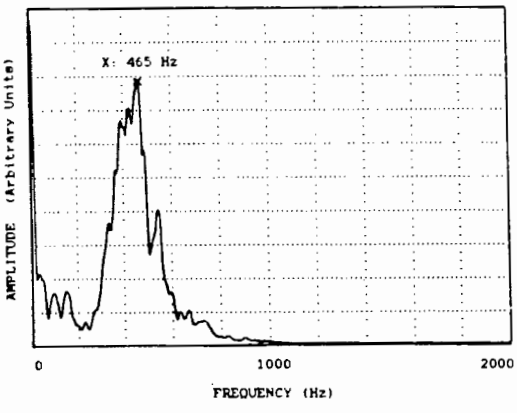

(iii) f_D = 465Hz
v_D = 0.71m/s

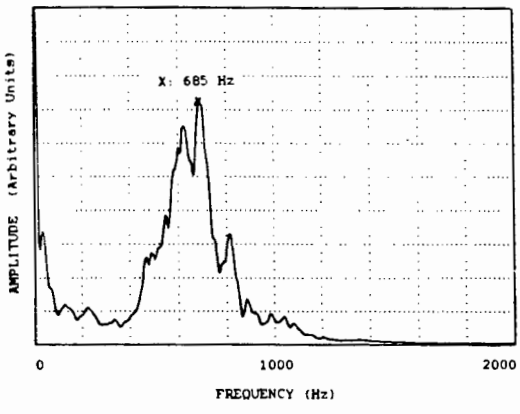

(iv) f_D = 685Hz
v_D = 1.02m/s

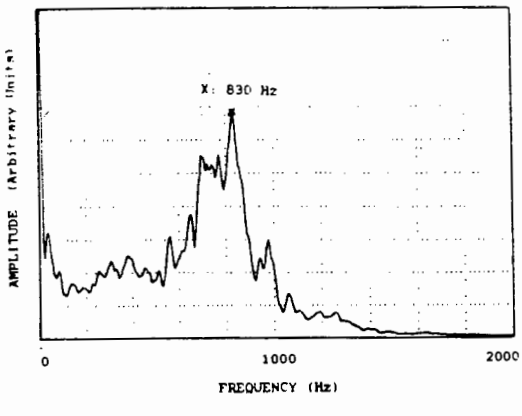

(v) f_D = 830Hz
v_D = 1.22m/s

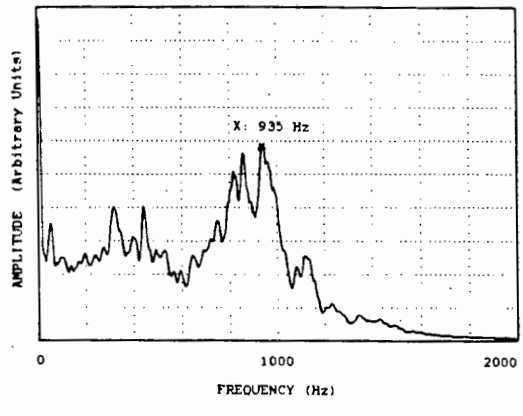

(vi) f_D = 935Hz
v_D = 1.42m/s

Fig. 7.2 Doppler spectrums for various disc velocities

If the Doppler spectral shapes are imagined to be smoothed then the amplitude of the Doppler signal can be seen to be inversely related to the Doppler frequency as was presented in Section 6.7.2 (No DDRR Filter is present for these spectrums).

At higher disc velocities as in Figs. 7.2 (v) and (vi), the spectra start exhibiting relatively large amplitude frequencies below the expected Doppler frequency. This is due to bubbles occuring under the disc when the disc velocity increases. These bubbles travel slower than the sand particles on the rim of the disc and so present lower frequency peaks due to their velocity.

Also evident from Fig. 7.2 is that the 3dB Doppler spectral width $[\delta f_D]$ is linearly related to f_D as proposed in Section 5.5.9, Eqn. 5.31.

A table listing the disc velocities, the peak of the Doppler spectrum and the output current of the Velocimeter is tabulated in Table 7.1. The Velocimeter 'Maximum Velocity' range is set to 2m/s. The output current is in the range of 0 to 20mA with 20mA corresponding to 2m/s.

Disc Velocity	Peak Doppler Frequency	Output Current
(m/s)	(Hz)	(mA)
0.00	0	0.0
0.45	255	4.5
0.53	325	5.3
0.71	465	7.2
0.82	555	8.2
1.02	685	10.1
1.22	830	11.6
1.42	935	13.0

Table 7.1 Results from rotating disc simulation test-rig

The peak Doppler amplitude frequency [f_D] as a function of the disc velocity [v_D] is plotted in Fig. 7.3.

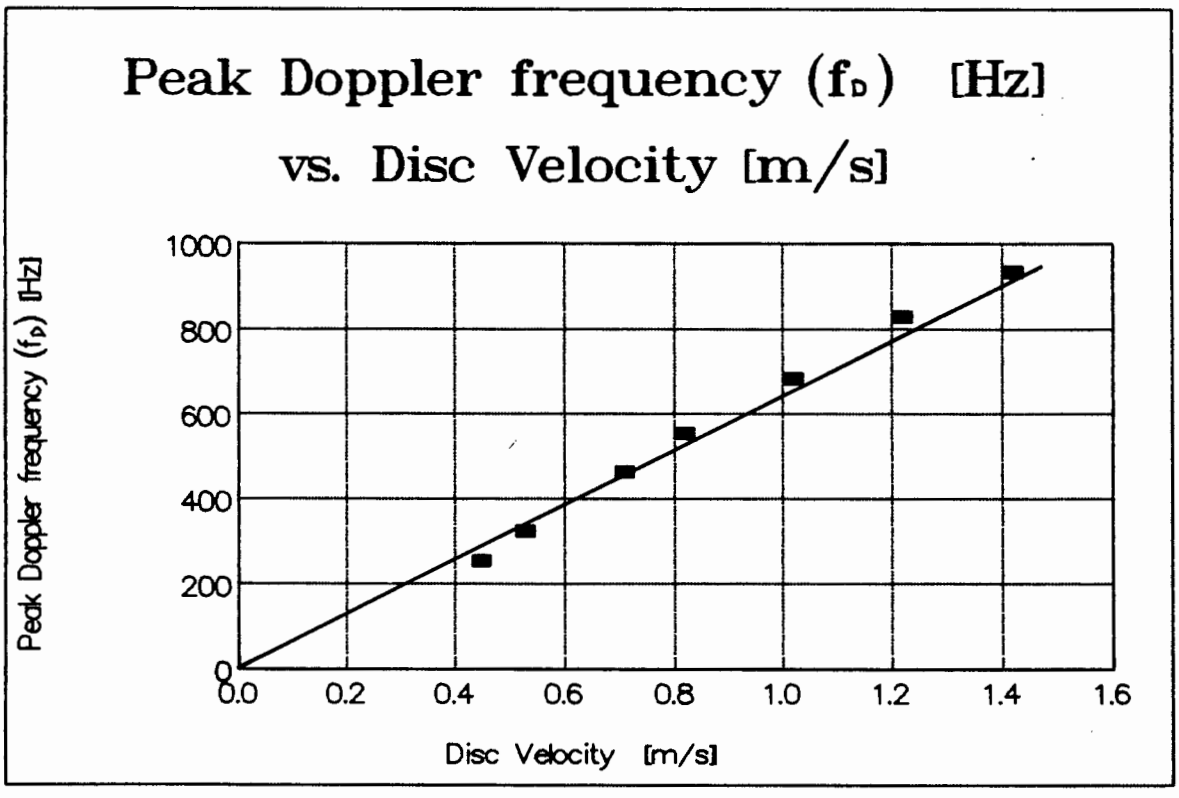

Fig. 7.3 Peak Doppler frequency as a function of v_D

The graph is seen to be linear as expected.

(ii) Voltage output

Readings were taken from the output current [Iout] of the Velocimeter. This current is tabulated in Table 7.1 above and is presented on a graph in Fig. 7.4 as a function of the disc velocity.

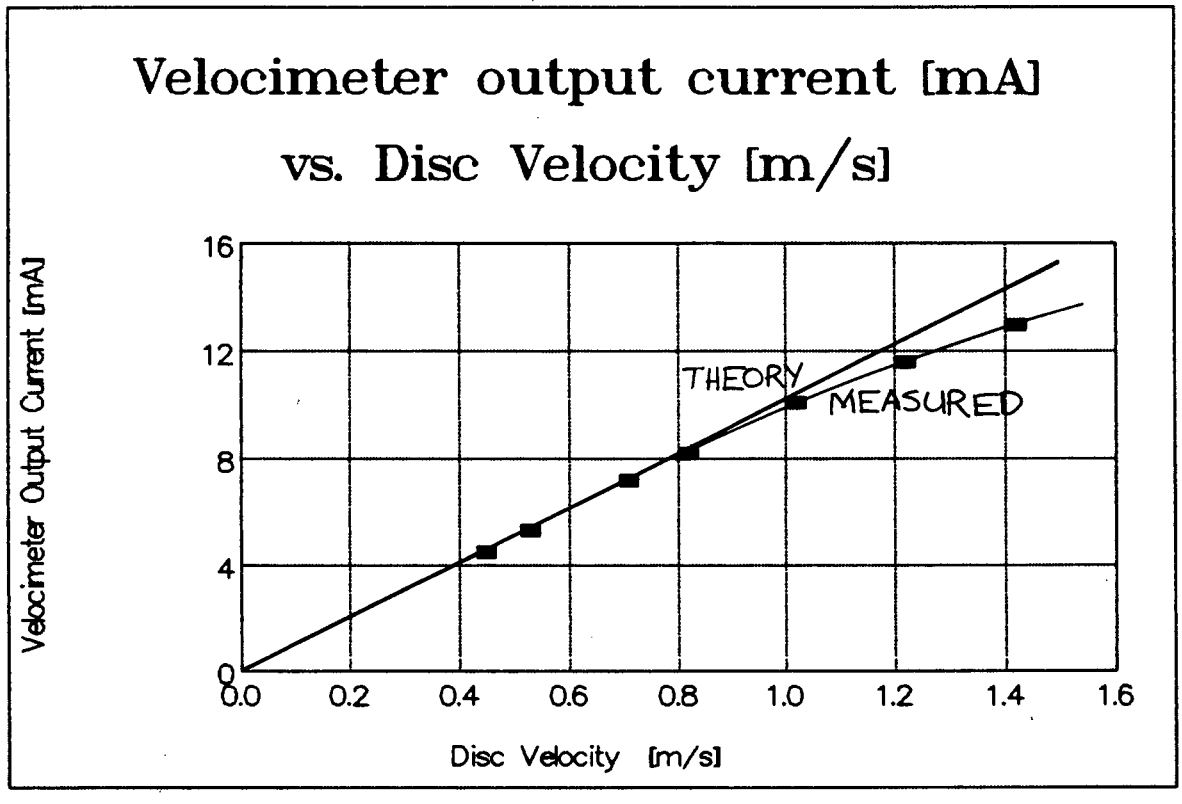

Fig. 7.4 Velocimeter output current as a function of the disc velocity

The graph of Fig. 7.4 is seen to be linear at disc velocities below approximately 1m/s. At higher disc velocities the graph losses linearity because of the presence of the slower moving bubbles causing a spread of frequencies at low frequencies relative to f_D. According to Eqn. 5.32, a spectum containing frequency components below the frequency of the peak will cause the output of the F-V converter to read low. This effect is not expected to occur in the measurement of the bed-load velocity in a slurry filled pipeline as there are no slower moving bubbles present below the bed-load.

7.2.3 Conclusions

The simulation test rig provided useful information confirming various aspects of the operation of the Velocimeter:

(i) Linearity between the detected particle velocity of a rotating disc [v_D] and the Peak Doppler Amplitude frequency [f_D] is confirmed.

(ii) Linearity between the Peak Doppler Amplitude frequency and the output current [Iout] of the Velocimeter is confirmed.

(iii) The Doppler amplitude proved to be related to the inverse of the demodulated Doppler frequency as presented in Section 6.7.2.

(iv) The Doppler spectral width [δf_D] is shown to be related to the Doppler frequency [f_D].

(v) The output current [Iout] is related to the 'shape' of the Doppler spectrum. ie. when the shape was such that low frequency terms were present (the case with air bubbles), then Iout was reduced. Eqn. 5.33 of Section 5.6.3 desribes the relationship between the output of the F-V converter for a particular Doppler spectrum. Iout is directly related to the output of the F-V converter voltage.

7.3 HYDRAULIC TEST LOOPS

7.3.1 Test-Rig Description

A 140mm diameter PVC and perspex section of pipeline containing a sand water slurry was also used for testing the Velocimeter. This pipeline is one of the test loops in the Hydrotransport Research of the Civil Engineering Department, U.C.T.

The sliding bed-load contained a transport volumetric concentration of about 50%. The slurry rate was controlled with a variable speed pump so that a flow regime could be achieved with the bed load remaining stationary and the suspended-load particles being in motion. The speed of the pump could be increased so that bed-load velocities in the range of 0m/s to 3.8m/s could be achieved.

The pipeline has a transparent perspex viewing sections with mirrors placed underneath to aid with the inspection of the bed-load conditions. A flow regime could be set up with, for example, a stationary bed and suspended-load particle

motion, by visual inspection and corresponding adjustment of the pump rate.

The transducer was attached to the bottom of a steel section of pipeline placed within the line. A flat rectangular section, slightly larger than the transducer front face (Epoxy Resin face) dimensions, was millied onto the pipe-bottom. The pipe-wall thickness at this section was arranged to be 4mm. The transducer was atttached to the flat section by tapping it with a layer of silicone sealant acting as an ultrasonic bond.

The cross-correlator probes were inserted into the same pipeline in a perspex situated close to the ultrasonic transducer. The cross-correlation probe head was flush with the pipe soffit. A range of flow regimes were set up by adjusting the pump speed and allowing the flow regime to reach steady state conditions. This was done at each new pump setting before data on the flow rate was read. A Khronhe Magnetic Flowmeter was used to indicate the mean mixture flow rate. To give a true indication of the mean flow rate, the Magnetic Flowmeter was attached to a vertical section of the pipeline.

7.3.2 Doppler Gain Set-Up Procedure

Before the UDBV can be used to indicate bed-load particle velocities with accuracy, the Doppler gain (expressed by A_V in Section 6.8.9 and adjusted with RT1) must be adjusted. This gain setting effectively adjusts the comparator threshold voltage [A_T] as discussed in Sections 6.7.5, 6.7.6, 6.7.7 and 6.8.9. The adjustement of A_V affects A_T according to Eqn. 6.112. Recall that the setting of A_T is accomplished so that the probability of detecting suspended-load particle velocities is low compared with the

probability of detecting bed-load particle velocities. If it is set correctly then only the bed-load Doppler signals have an amplitude large enough to cause the comparator stage (block no. 11) to trigger, thereby converting the bed-load Doppler signal frequency into a square wave for further processing to be converted to an output current.

The set-up procedure is as follows:

(i) Adjust the mean flow velocity so that the incipient stationary bed-load condition exists.

First, a flow condition is set up so that a stationary bed exists and suspended-load particles above the bed can be seen to be in motion. The flow rate is increased from zero until v_M just approaches v_{M2}. In this regime, the bed-load layer will be stationary but on the verge of sliding. The bed-load height [h_{BED}] will extend up to the height defined by H. Since the bed-load is stationary, no bed-load Doppler signals are detected.

This regime is suitable for set-up purposes for two reasons:

(1) The bed-load is stationary while the suspended-load is moving.

This regime is suitable since it provides a clear indication of whether the set-up is correct or not. If set-up is correct, then the Velocimeter should simply indicate a zero reading.

(2) The bed-load height [h_{BED}] is equal to its minimum value and defined by H.

The set-up procedure should be performed in the regime for which the bed-load layer has a minimum height [H] since the

probability of falsely detecting suspended-load particle velocities [P{sus}] (see Section 6.7.8) will be a maximum (this is clear from the Penetration constant [k_p], which is a function of H, which influences P{sus}). The bed-load layer has a minimum height [H] defined for all flow regimes such that $v_M > v_{M2}$.

Correct operation when the bed-load layer is a minimum height will therefore guarantee that the Velocimeter will operate correctly at lower mean velocities since the bed-load height will then be greater and the backscattered power from the suspended-load will be less (ie. k_p will be less).

(ii) The Doppler gain is set to a minimum

The Doppler gain setting (potentiometer RT1) is turned fully anti-clockwise to its minimum value. The Doppler Signal LED (LD2) will now be extinguished since no Doppler signal has an amplitude large enough to cause the comparator stage (block no. 11) to trigger.

(iii) Doppler Gain is increased

The Doppler gain is now increased by turning RT1 clock-wise until the Doppler Signal LED just begins to turn on, signifying the comparator is beginning to trigger.

(iv) Doppler Gain is reduced slightly

With the present gain setting, the Doppler signal due to the suspended-load particle motion directly above the bed-load is causing the comparator to trigger. However, since the bed is stationary, the gain should now be slightly reduced

until the comparator just ceases to trigger as indicated by the Doppler Signal LED turning off. The output of the comparator will now 'rest' at either its positive or negative trigger voltage ie. the frequency of the output will be zero, indicating a correct reading of a stationary bed-load. The Doppler gain is now correctly set up so that only bed-load motion will be detected.

(v) Increase flow regime so that $v_M > v_{M2}$ and the bed is moving

If the flow condition is now slightly increased to cause the bed to creep slowly, then the mean Doppler signal amplitude will be slightly larger than for the previous flow condition. Theoretically this can be shown to be true by referring to Fig. 6.15 the graph of the Penetration constant [k_p] vs. particle height. In this flow regime, the particles at h = 0 are moving as apposed to case of (i) above where the moving particles are moving directly above the bed-load at h = H. The value of k_p is a maximum of 0dB in this case, indicating maximum Doppler power is received (with a corresponding maximum mean Doppler amplitude). This increase in the mean Doppler amplitude will now cause the comparator to trigger, so that the output of the comparator (which resembles the bed-load Doppler frequency only) can be converted to an output current indicating the bed-load velocity.

In practice the above operation performed well, so that the UDBV after adjustment correctly indicated the presence of a moving or stationary bed-load.

7.3.3 Calibration Using Cross-Correlator

The UDBV must be calibrated to relate the output current [Iout] to the bed-load velocity [v_{BED}] according to the setting of v_{MAX}, where Iout must be 20mA when $v_{BED} = v_{MAX}$.

The motivation for employing the cross-correlation technique has been discussed in Section 6.9. Briefly, it provides a method of calibrating the UDBV in situ. For a particular bed-load velocity determined by the cross-correlator, the UDBV calibration setting (potentiometer RT2) can be adjusted so that v_{BED} as determined from Iout of the UDBV corresponds to the actual v_{BED} as determined form the cross-correlator. This process need only be performed for one reading since the UDBV provides an output linearly related to v_{BED}. The zero readings when the bed-load just begins to settle can be used as another data point. The process of comparing the readings from the UDBV with the readings from the cross-correlator is verified in practice for a range of bed-load velocities.

In Figs. 7.5 (i) to (iv), four typical cross-correlation graphs illustrate the cross-correlation function plotted as a function of the delay time. The peak of the cross-correlation function corresponds to the delay time for the bed-load particles to travel from the upstream to the downstream probes. The distance between the probed divided by this delay time provides an absolute accurate means of determining the bed-load particle velocity.

In Figs. 7.5 (i) to (iv), the label on the graphs referred to as 'PEAK' indicates the position of the peak [p] of the cross-correlation graph in unit delay times [τ_D]. The bed-load particle velocity [v_{BED}] can be determined by dividing the sensor spacing [d_S] by the delay time corresponding to the position of the peak. The delay time is determined by

multiplying the position of the peak by the unit delay time, as follows:

$$v_{BED} = d_S \; / \; (p \cdot \tau_D) \qquad (7.1)$$

In practice, the sensor spacing [d_S] is 20mm and the unit delay time, set by the microprocessor algorithm is 535μs for the data illustrated, so that Eqn. 7.1 can be simplified to:

$$v_{BED} = 37.38/p \qquad (7.2)$$

The 'PEAK' position is determined automatically by a peak searching algorithm. A manually controlled marker may also be used to validate the peak searching algorithm. This peak value (printed in brackets in the following graphs) sometimes differs slightly from the automatic prediction of the peak, especially if the cross-correlation function has a peak which resembles a plateau. This is the peak value used to evaluate Eqn. 7.2 The height of the peak and of the second highest peak are also determined by algorithms, so that a peak may be validated according to its height.

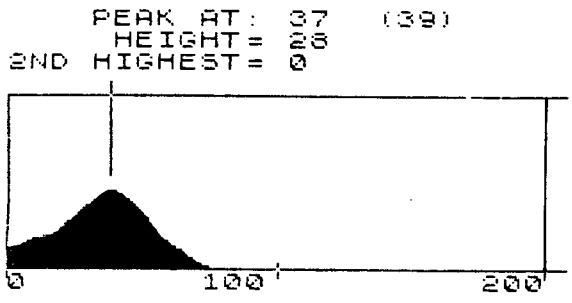

(i) v_M = 2.22m/s
Peak: 39
v_{BED} = 0.96m/s

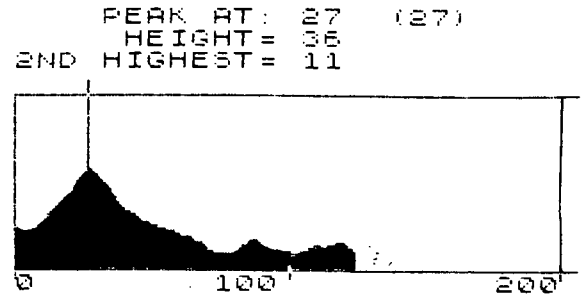

(ii) v_M = 2.59m/s
Peak: 27
v_{BED} = 1.38m/s

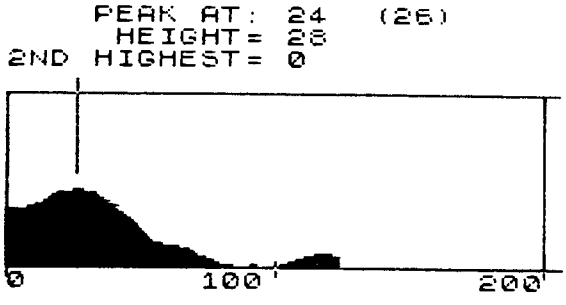

(iii) v_M = 2.74m/s
Peak: 26
v_{BED} = 1.44m/s

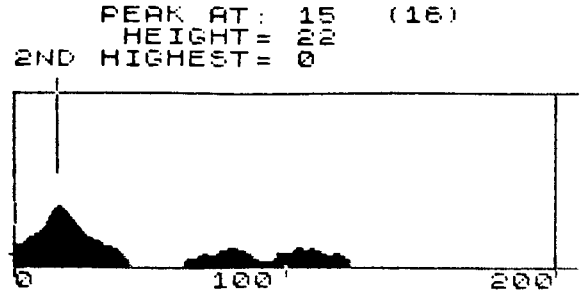

(iv) v_M = 3.36m/s
Peak: 16
v_{BED} = 2.34m/s

Fig. 7.5 Three typical cross-correlation functions demonstrating the position of the peak for different flow rates.

7.3.4 Results to Verify Calibration Process

Results from the cross-correlation technique and from the UDBV after calibration has been implemeted were obtained. The response time [τ] setting of the UDBV was adjusted to its maximum of 8s to maximize the accuracy of determining the bed-load velocity.

A range of mean mixture velocities [v_M] between 0m/s to 3.8m/s were obtainable with the flow rig as measured with a Mag-meter. Data of v_{BED} from the Cross-correlator and from the UDBV are tabulated in Appendix E. The readings from the UDBV are uncalibrated in the column labelled v_{BED}. The readings in the column labelled v_{BED}' are readings taken with the UDBV after calibration. These calibrated readings appear in Fig. 7.6 plotted as a function of the mean mixture velocity [v_M]. The readings taken from the cross-correlator are also plotted for comparison with the UDBV readings.

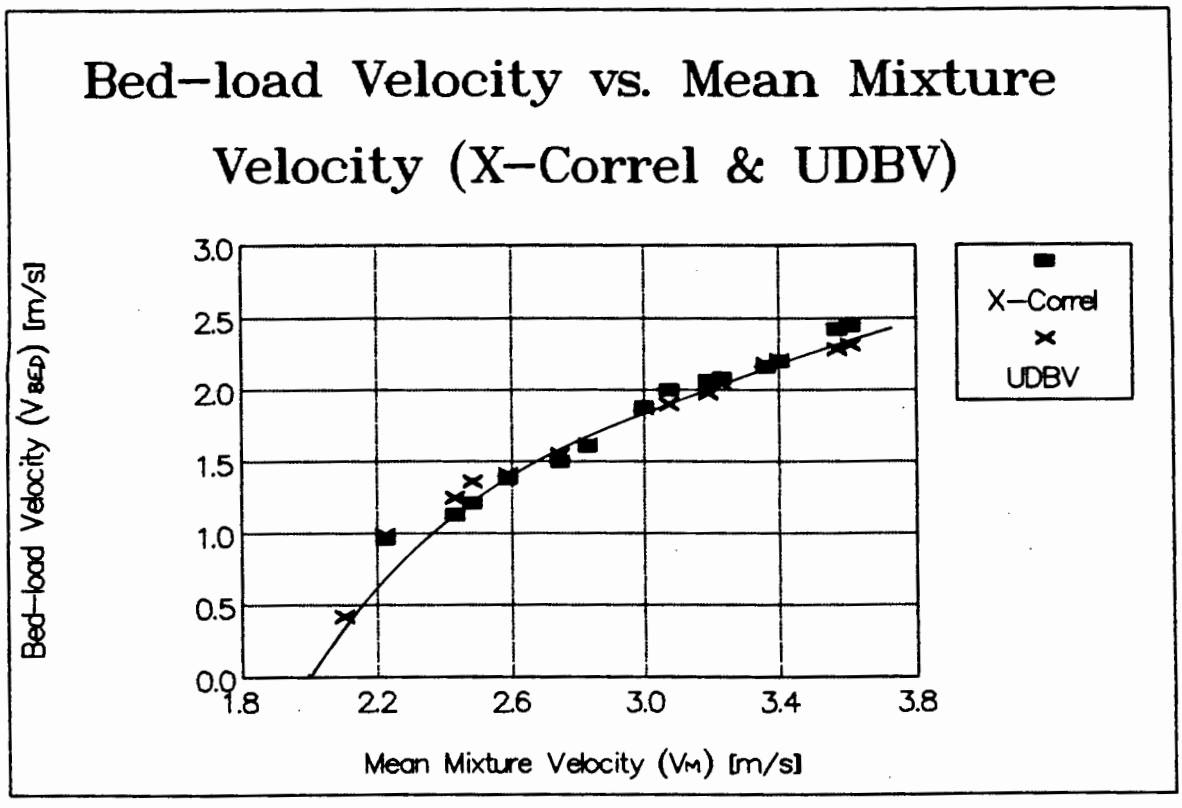

Fig. 7.6 Test-loop bed-load particle velocities measured with the cross-correlator and with the calibrated UDBV

From the graph it is evident that the data obtained by each method resemble each other closely as expected.

7.4 INDUSTRIAL APPLICATIONS: ROSSING URANIUM AND ERGO

The UDBV was tested in an industrial mining application at Rossing Uranium Mine, Namibia and at the East Rand Gold and Uranium Mine (ERGO), Transvaal. Fig. 7.7 shows Rossing Uranium Tailings in a section of a polyurethane lined steel pipeline.

Fig. 7.7 Rossing Uranium Tailings material within a Polyurethane-lined steel pipeline

Three transducers were mounted onto a pipe-section at different locations around the wall of the pipeline as in Fig. 7.8. Each transducer monitors the particle velocity at the wall of the pipeline at the location of the transducers.

Fig. 7.8 Placement of three transducers radially around a pipeline

7.4.1 ERGO Tailings Line Description

The ERGO line on which the UDBV was tested, is a tailings line transporting disused Gold slimes to a tailings dam. The volumetric concentration of the slimes is approximately 35%. The pipeline is steel with a flat section milled onto the bottom for attachment of the transducer. The transducer

was attached by tapping it in place with a layer of silicone sealant placed on the transducer resin face to acts as an ultrasonic transmission medium between the transducer and the pipe-wall. The wall thickness at this location was arranged to be 4mm, the minimum acceptable dimension. The mean mixture flow rate [v_M] could be adjusted by means of a diversion valve. The value of v_M was determined from a Magnetic-meter placed within the line.

7.4.2 Calibration Test-Rig

The calibration and the adjustment of the Doppler gain control were set up for the ERGO pipe-section as described above in Sections 7.3.2 and 7.3.3. A rectangular window was cut in the bottom of the Hydrotransport Research 140mm diameter PVC pipeline. The ERGO 350mm diameter test section was clamped around the 140mm diameter pipeline. The bed-load thus passed through the bottom of the ERGO test section at the window.

The cross-correlator probes in the 140mm test-loop could as before provide an alternative method of measuring the bed-load velocity independently of unknown system parameters. In this way the 140mm diameter test-loop could be used to calibrate the ERGO pipe-section. The UDBV is calibrated for the ERGO pipe-section which is then removed from the test-rig to be used in the ERGO plant.

7.4.3 Results-Bed-load Velocity vs. Mean Mixture Velocity

Output results taken from the UDBV at the ERGO plant are plotted in Fig. 7.9 as a function of the mean mixture velocity.

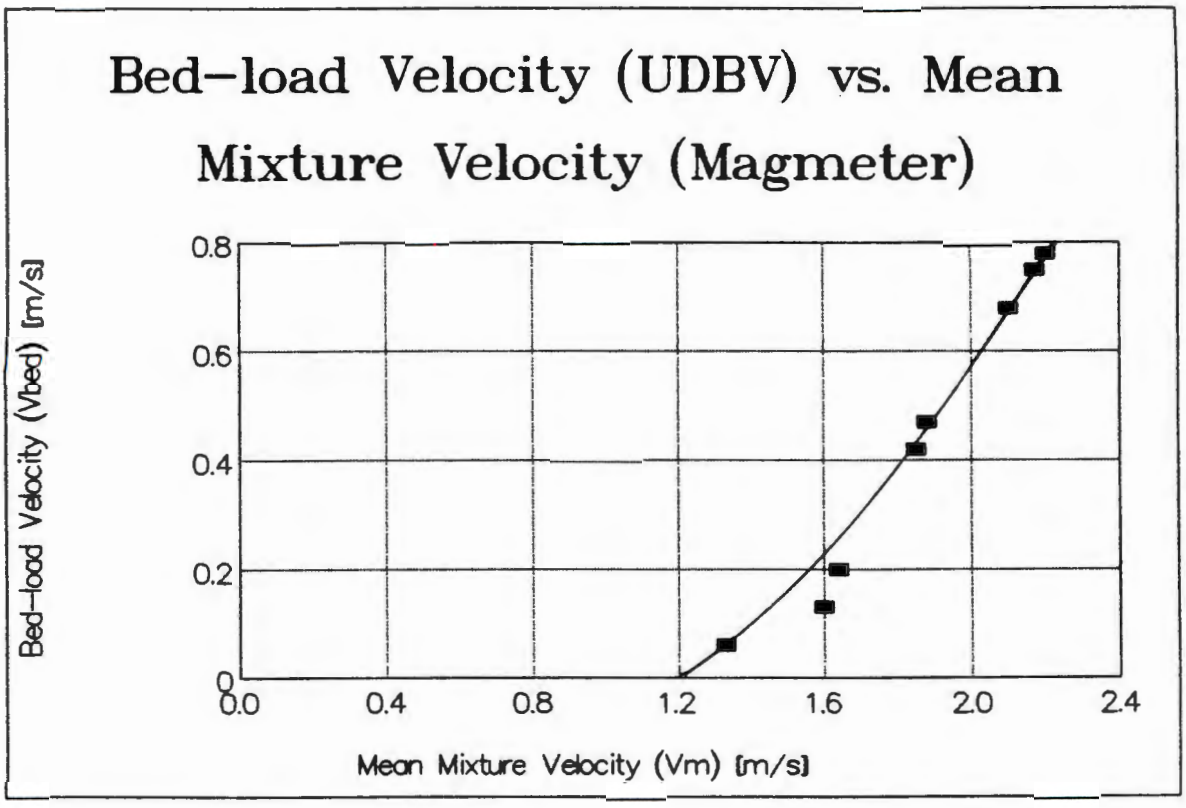

Fig. 7.9 Output of UDBV as a function of the mean mixture velocity taken at ERGO plant

It is clear from Fig. 7.9 that when $v_M < 1.2$m/s then v_{BED} is zero. The bed-load velocity reached a maximum value of 0.8m/s when v_M was 2.2m/s

7.5 CONCLUSIONS

Three seperate types of experimental tests were performed to validate various aspects of the operation of the UDBV. The first test, namely the simulation test consisting of a disc rotating at a fixed, known velocity, validated the linearity of the UDBV and confirmed the properties of the Doppler spectrum which are used in Chapter 6.

The second set of tests, performed on the Hydrotransport Research hydraulic test-loops enabled the UDBV to be calibrated in situ using a cross-correlator.

The final set of results were obtained on actual waste (tailings) lines at ERGO and at Rossing Uranium mines. The results obtained from ERGO have been presented as a function of the mean mixture velocity of the tailings slurry. Results of this nature indicate that the UDBV may be used to provide information about the slurry bed-load velocity. It is envisaged that this type of information about the bed-load velocity may be used as a novel and superior way of controlling high concentration slurry pipelines.

CHAPTER 8

CONCLUSIONS

1. An instrument, referred to as an Ultrasonic Doppler Bed-load Velocimeter (UDBV) has been developed which successfully measures the velocity of those particles which constitute the bed-load adjacent to the pipe-wall in a solid-liquid slurry.

2. A cross-correlation technique was implemented to measure the bed-load velocity by accurately determining the time taken for a group of representative bed-load particles to travel between two sensors, one downstream of the other.

3. Tests were carried out in the Laboratory in pipelines to calibrate the UDBV using the cross-correlation technique and to verify that design methods successfully ensured that only the velocity of bed-load particles was measured.

4. A rotating test-rig was constructed to test the linearity of the UDBV and to confirm that the Doppler spectral width and amplitude are related to the mean Doppler frequency.

5. Tests were carried out on full scale industrial pipelines (at Rossing Uranium and ERGO) to verify the operation under a harsh industrial environment.

6. The focusing efficiency has been defined in terms of:

   (i) the probability of detecting bed-load particle velocities relative to suspended-load particle velocities and

   (ii) the bed-load Doppler spectral broadening width

7. The focusing efficiency is shown to be dependent on four system parameters: beamwidth, transmission path length, transmitter orientation angle and the bed-load layer height.

8. A Penetration constant [k_p] has been defined and evaluated to describe the ultrasonic backscattered beam power from a defined suspended-load layer of particles relative to the backscattered power from the bed-load particles. The value of k_p depends on the focusing parameters and is used in the evaluation of the bed-load probability function (see 6(i) above).

9. The Doppler spectral broadening effects are shown to influence the accuracy and response time of determining the mean bed-load Doppler frequency. The spectral broadening effects are analysed and minimized using a suitable focusing parameter choice.

10. The focusing parameters have been optimized by suitable chosing parameters that will maximize the focusing efficiency. The optimum focusing parameters chosen for a 1MHz, 5mm radius crystal are: Tx. orientation angle [θ_T] equal to 30°, a transmission path length [d] equal to 20mm and a 17° beamwidth accomplished by using a resin transducer window.

11. The Doppler signal was accurately described by taking factors into consideration that are not included in the description of the Doppler Equation as it appears in the literature. Once the Doppler signal was accurately described then techniques could be discussed and implemented to increase the probability of detecting bed-load Doppler signals.

12. The electronic system design included Doppler demodulation techniques, with synchronous demodulation being chosen as the best technique.

13. Circuit techniques were implemented to increase the probability of detecting bed-load particle velocities accurately, such as a Doppler Dynamic Range Reduction [DDRR] filter, and an adjustable threshold voltage comparator circuit.

14. A "bed-load condition / Doppler signal indicator" circuit was designed and implemented which functioned to provide a visual indication of the Doppler signal which is used in setting-up the UDBV and for indicating the status of the bed-load velocity.

15. The UDBV has been shown to operate successfully and should provide a new method for monitoring and controlling slurry pipeline operations.

REFERENCES

1. Atkinson, P. and Woodcock, J.P., "Doppler Ultrasound and its Use in Clinical Measurement", Medical Physics Series, Academic Press (1982)

2. Bagnold, R.A., "The Flow of Cohensionless Grains in Fluids", Phil. Trans. Roy. Soc. London, Ser.A. **249**, 235-297 (1956)

3. Berger, F.B., "The Nature of Doppler Velocity Measurement", IRE Trans., **ANE-4**, 103-112 (1957)

4. Brekhovskikh, L.M., "Waves in Layered Media", 2nd Ed., Applied Mathematics and Mechanics, Academic Press, New York (1980)

5. Brody, W.R. and Meindl, J.D., "Theoretical Analysis of the CW Doppler Ultrasonic Flowmeter", IEEE Trans. on Biomed. Eng., **BME-21**, (3), 183-192 (1974).

6. Busby, J., Richardson, E.G., "The Absorption of Sound in Sediments", Geophysics, **22**, 821-828 (1957)

7. Chalupnik, J.D. and Green, P.S., "A Doppler-Shift Ocean-Current Meter", Marine Sciences Instrumentation, **1**, 194-199 (1962)

8. Chilowsky, C. and Langevin, P., U.S. Patent 1,471,547 (1923)

9. Chilowsky, C., U.S. Patent 1,864,638 (1932)

10. Denbigh, P.N., "Ship Velocity Determination by Doppler and Correlation Techniques", IEE Proceedings, **131**, Part F,(3), 315-326 (1984)

11. Di Pietro, D.M., Meindl, J.D., "Optimal System Design for an Implantable CW Doppler Ultrasonic Flowmeter" IEEE Trans. on Biomed. Eng., **BME-25**, (3), 255-266 (1978).

12. Durst, F., Melling, A., Whitelaw, J.H., "Principles and Practice of Laser-Doppler Anemometry", 2nd Ed., Academic Press Inc. London (1981)

13. Elliott, S.D.H., "A Microprocessor Based Cross-Correlator for Determining Slurry Flow Velocities", BSc Thesis, University of Cape Town (1987)

14. Flax, S.W., Webster, J.G. and Updike, S.J., "Statistical Evaluation of the Doppler Ultrasonic Blood Flowmeter", ISA Trans., **10** (1), 1-20 (1971)

15. Franklin, D.L., Schlegel, W.A. and Rushmer, R.F., Science, **134**, 564-565, (1961)

16. Green, P.S., "Spectral Broadening of Acoustic Reverberation in Doppler-Shift Fluif Flowmeters" J. Acoust. Soc. Am., **36** (7), 1383-1390 (1964)

17. Hamilton, E.L., "Compressional-Wave Attenuation in Marine Sediments", Geophysics, **37** (4), 620-646 (1972)

18. Hamilton, E.L., "Geoacoustic modelling of the sea floor", J. Acoust. Soc. Am., **68** (5), 1313-1339 (1980)

19. Jervis, B.W. "Microwave Doppler-effect particle flow measurement", IEEE Trans. Indust. Electron. Control Instrum. **IECI-24**, 322-327 (1977)

20. Kinsler, L.E., Frey, A.R., "Fundamentals of Acoustics", John Wiley & Sons, Inc. (1950)

21. Koczy, F.F., Kronengold, M. and Loewenstein, J.M., "A Doppler Current meter", Marine Sciences Instrumentation, **2**, 127-134 (1963)

22. Lathi, B.P., "Modern Digital and Analog Communication Systems", Holt-Saunders International Editions (1983)

23. Lazarus, J.H., "Introduction To Hydraulic Transport of Solids in Pipelines", Course notes CIV515F, U.C.T

24. Lazarus, J.H., "Classification of Flow Regimes", Course notes CIV515F, U.C.T

25. Lazarus, M.D., Lazarus, J.H., "Development of an Ultrasonic Doppler Bed Load Velocimeter", In Proc. 11th International Conference on the Hydraulic Transport of Solids in Pipes, U.K, BHRA, Paper C4, 173-181, October, (1988)

26. Leitner, J.R., "Slurry Flowmetering Using Correlation Techniques", PhD Thesis, University of Cape Town (1979)

27. Lynnworth, L.C., "Ultrasonic Flowmeters" in Mason, W.P., Thurston, R.N., editors "Physical Acoustics-Principles and Methods", Academic Press (1979)

28. McShane, J.L., "Ultrasonic Flowmeters" In Dowdell, R.B, Editor-in-Chief "Flow-Its Measurement and Control in Science and Industry", Vol. 1, Part 2: Flow Measurement Devices, Wendt Jr., R.E.,editor, Instrument Society of America, Pittsburgh (1974)

29. National Semiconductor Corporation, Linear Data Book (1982)

30. Newhouse, V.L., Bendick, P.J., Varner, L.W, "Analysis of Transit Time Effects on Doppler Flow Measurement", IEEE Trans. on Biomed. Eng., **BME-23**, (5), 183-192 (1976).

31. Nolle, A.W., Hoyer, W.A., Mifsud, J.F., Runyan, W.R., Ward, M.B., "Acoustical Properties of Water-Filled Sands", J. Acoust. Soc. Am., **35**, (9), 1394-1404 (1964)

32. Ormrod, G.T.W., "The Suitability of Doppler Flowmeters For Use in the Minerals-Processing Industry", Mintek Report No. M68, January (1983)

33. Peronneau, P.A., Bournat, J.P., Bugnon, A., Barbet, A., Xhaard, M., "Theoretical and Practical aspects of pulsed Doppler flowmetry:real-time application to the measure of instantaneous velocity profiles in vitro and in vivo" in Reneman, R.S., editor, "Cardiovascular Applications of Ultrasound", Proceedings of an International Symposium, Belgium (1973), North-Holland Publishing Company, Amsterdam (1974)

34. Rice, S.O., "Mathematical analysis of random noise", Bell Syst. Tech. J., **23**, 282 and **24**, 46, (1944)

35. Roevros, J.M.J.G., "Analogue processing of C.W. Doppler flowmeter signals to determine average frequency shift momentaneously without the use of a wave analyser", in Reneman, R.S., editor, "Cardiovascular Applications of Ultrasound", Proceedings of an International Symposium, Belgium (1973), North-Holland Publishing Company, Amsterdam (1974)

36. Sanderson, M.L., Hemp, J., "Ultrasonic Flowmeters-A review of the State of the Art", International Conference on Advances in Flow Measurement Techniques, Warwick, U.K.,Sept, BHRA Fluid Engineering (1981)

37. Satomura, J. Acoust. Soc. Am., **29**, 1181-1185 (1957)

38. Schultheiss, P.M., Wogrin, C.A., Zweig, F., "Short-Time Frequency Measurement of Narrow-Band Random Signals in the Presence of Wide-Band Noise", J. Appl. Phys., **25**, (8), 1025-1036 (1954)

39. Scott, M.J., "Doppler ultrasonic flowmeters", CME, 51-54, October (1978)

40. Sive, A.W. "An Analytical and Experimental Investigation of the Hydraulic Transport of High Concentration Mixed Regime Slurries", PhD. Thesis, University of Cape Town (1988)

41. Stewart, H.F., Repacholi, M.H., Benwell, D.A., "Ultrasound Therapy", in Repacholi, M.H., Benwell, D.A., editors, "Essentials of Medical Ultrasound", The HUMANA Press Inc. (1982)

42. Thorn, R., Beck, M.S., Green, R.G., "Non-intrusive methods of velocity measurement in pneumatic conveying", J. Phys. E:Sci Instrum, **15**, 1131-1138 (1982)

43. Urick, R.J., "Principles of Underwater Sound", McGraw-Hill Book Company, U.S.A (1975)

APPENDIX A

Research paper presented at the
11th International Conference on the
Hydraulic Transport of Solids in Pipes

HYDROTRANSPORT 11

Stratford-upon-Avon, U.K: 19-21 October 1988

"Development of an Ultrasonic Doppler Bed Load Velocimeter"

M.D. Lazarus
J.H. Lazarus

11th International Conference on the
Hydraulic Transport of Solids in Pipes

HYDROTRANSPORT 11

Stratford-upon-Avon, UK: 19-21 October 1988

PAPER C4

DEVELOPMENT OF AN ULTRASONIC DOPPLER BED LOAD VELOCIMETER

M.D. Lazarus
Department of Electrical Engineering. University of Cape Town, South Africa

J.H. Lazarus
Hydrotransport Research Unit, Department of Civil Engineering. University of Cape Town. South Africa.

Summary

An Ultrasonic Doppler Velocimeter (UDV) for measuring the bed load velocity of high concentration slurries is being developed for increasing hydraulic efficiency by minimizing head loss gradient. Head loss gradient may be minimized using an accurate indication of the bed load velocity. A further application of the instrument is as a control sensor to provide feedback to the system pumps causing them to speed up when the bed load particle velocity becomes too low thereby preventing possible pipe blockage. Transporting the material at or near the limit deposit velocity also substantially reduces the wear rate in systems transporting abrasive materials. An added function of the instrument is its application to the theoretical and analytical study of pipe blockage.

The instrument is based on the Ultrasonic Doppler shift technique and satisfies various requirements, namely the measurement of bed load velocity only, non-intrusiveness, linear, accurate and repeatable readings, independence of the properties of the transporting slurry, short response time, reliable and low maintenance. The results of from two experimental test rigs, indicates that the instrument appears to satisfy the requirements.

1. Introduction

In high concentration slurries of the stabilised and dense phase type a bed load invariably exists. This bed load may even occupy the entire pipe cross section. The bed load may be stationary and this could lead to pipe blockage. An instrument for measuring the bed load velocity of high concentration slurries is being developed for increasing hydraulic efficiency. Head loss gradient may be minimised using an accurate indication of the bed load velocity. Doppler ultrasonic flowmeters are presently commercially available for measuring the average velocity of low concentration slurries. However, the present bed load Velocimeter only measures

Held in Stratford-upon-Avon, UK. Organised and sponsored by BHRA, The Fluid Engineering Centre

the velocity of those particles close to the pipe wall and is thus applicable to high concentration, dense phase of stabilised flow slurries.

It is advantageous to monitor the bed load velocity rather than the mean mixture flow velocity as pipe blockage is usually initiated at the bed (see Fig. 1). Also the bed load velocity can be detected without penetration into the pipe. The instrument may also be used for determining the extent of a stationary bed by positioning the transducer at various points around the pipe.

The bed load velocity is dependent on pipe variables, particle variables and slurry variables. The mass flow throughput may not be constant and usually varies with time in an industrial application. It is for this reason that the bed load velocity should be monitored. Transporting the material at or near the limit deposit velocity also substantially reduces the wear rate in systems transporting abrasive materials.

An important function of the instrument is its application to the theoretical and analytical study of pipe blockage. A further application of the instrument is as a control sensor to provide feedback to the system pumps causing them to speed up when the bed load particle velocity becomes too low thereby preventing possible pipe blockage.

The paper presents a list of requirements which the Velocimeter should possess. To find a solution to satisfy the requirements, recognised techniques for measuring particle velocities were investigated. These techniques fall into two main groups, Doppler shift methods and the cross correlation method. Doppler shift instruments may be constructed using either light (laser), microwaves, or ultrasound as an energy source. Based on the list of requirements of the system, the Ultrasonic Doppler technique was chosen and the system was designed around this recognised technique.

The Ultrasonic Doppler Velocimeter (UDV) employs two piezoelectric (PZT) ceramic crystals mounted outside the pipe wall by means of a mounting structure or wedge, set at a defined angle to the flow. One crystal acts as the transmitter and is excited by a constant sinusoidal signal from an oscillator, thereby sending out an ultrasonic beam into the fluid. Targets (the bed load particles) within this beam travelling in the fluid, reflect and backscatter the beam, some of which return to the receiving transducer. The velocity of the bed load particles cause part of the received signal to be Doppler shifted from the transmitted signal. The amount by which the received signal is Doppler shifted is proportional to the velocity of the particles.

The Doppler shifted received signal is pre-amplified and then demodulated so that any Doppler shifted component can be extracted. The frequency of the Doppler shift signal is then electronically analysed and converted to a voltage to give an indication of the bed load velocity.

2. Requirements of the system

The instrument should satisfy a number of requirements, namely:

2.1 The instantaneous bed load velocity is measured rather than the mean mixture flow velocity.

2.2 The transducer is non-intrusive. The pipe wall requires minimal or no modifications so that installation is quick and simple and maintenance costs are kept low. Also, the absence of an obstruction to the flowing medium avoids pressure loss, possible pipe blockage and transducer wear.

2.3 Linearity and repeatability for bed load velocities ranging from stationary bed load to velocities of about 4 m/s, is desirable.

2.4 It is important to achieve high accuracy at low particle velocities (near deposition) so that effective control of the pumps can be implemented to prevent pipe blockage.

reasons for the great interest shown in this measurement technique is that it is capable of achieving non-intrusive point velocity measurements in the range 0.1 m/s to 100 m/s with an extremely high accuracy, claimed to be better than ±0.5% of measured value. Furthermore, no calibration is required (Thorn, Beck and Green, 1982).

Disadvantages of the LDV are: (i) the LDV requires an optically transparent pipeline; (ii) it is too expensive, fragile and difficult to set up for routine velocity measurements in an industrial situation.

3.1.2 Microwave methods

Microwaves are another suitable source for the Doppler particle velocimeter, and possess advantages over the LDV of being low cost, compact and suitable for use in hostile environments. In addition the pipeline does not need to be optically transparent. However, a disadvantage is that even if calibrated, a Microwave Doppler Velocimeter (MDV) can only be used for reliable particle flow measurements in situations where both particle size and moisture content are constant (Jervis, 1977). Since these are neither known nor kept constant a further discussion is not warranted.

3.1.3 Ultrasonic methods

As shown in Fig. 2, the Ultrasonic Doppler Velocimeter (UDV) employs two piezo-electric (PZT) crystals to transmit and receive an ultrasonic beam into and from the pipeline. The UDV has been chosen as the technique for measuring bed-load velocities because it satisfies the requirements presented in Section 2. A discussion of this technique is presented in Section 4.

3.2 Cross-correlation method

The cross-correlation method of velocity measurement is an established concept but has only recently become commercially available for the industrial situation. (Thorn, Beck and Green, 1982)

Like the Doppler Ultrasonic technique, the cross-correlation technique is independent of fluid properties such as temperature, density and pressure. Also, the transducers used need cause little or no obstruction to the flow since ultrasonic transducers may be used. In addition the transducers do not need to be calibrated.

Disadvantages of the method are: (i) determining cross-correlation functions requires a dedicated processor to process the output signals. Large amounts of memory may be required to store the signals from the sensors. Careful algorithms must be employed to ensure reliability and accuracy; (ii) the response time is inherently much slower than the Doppler techniques due to the complicated processing required with large amounts of data to determine and then analyse the cross correlation function to obtain a valid maximum peak; (iii) the cross correlation technique is more complicated to implement than the Doppler Ultrasonic technique.

4. Design of the Doppler Ultrasonic Velocimeter to satisfy the requirements

4.1 Measurement of bed load velocity

To ensure that the bed load rather than the mean mixture velocity is measured two conditions should be met:

(i) The ultrasonic "beams" from the transmitter and receiver should be "focussed" at the bed load by suitable geometry of the mounting structure.

(ii) Since ultrasonic attenuation through slurry shows dependency on frequency (Hovem *et al*, 1979), a choice of frequency which is suitably high will ensure that the beam attenuates upon entering the slurry, resulting in reflections and hence detection of Doppler shift solely due to the bed load. At the

frequency choice of 1 MHz for the system, the experimental results (Section 5.2) proved that only the bed load velocity is detected.

4.2 Non-intrusive transducer and no pipe modification

The transducer mounting is attached outside the pipe wall by means of an epoxy resin bond or alternatively by taping it with silicone sealant applied to both surfaces to ensure an acoustic bond is maintained.

Pipe lines with inner linings which possess adverse ultrasonic transmission properties should have the lining material replaced in a section of pipeline where the transducers are attached. The material should have good wear properties and also allow ultrasonic penetration. Wear and ultrasonic tests have been carried out on a selection of polyurethane materials. A polyether polyurethane was chosen as it exhibits excellent wear properties and allows sufficient transmission of ultrasound at the operating frequency of 1 MHz.

4.3 Linearity and repeatability

Linearity and repeatability can be assured even though factors such as the concentration and size of the bed load particles may vary. For all practical high concentration mining slurry transportation conditions, the concentration and size of the bed load particles will be adequate for operation of the system. Since the Doppler technique is independent of these factors, repeatability can be assured.

4.4 Accuracy

Possible inaccuracy may be due to the finite ultrasonic beamwidth of the PZT crystals causing a spread of Doppler shifts. The width of the spreading about the peak of the Doppler spectrum (as defined in eqn. 1) is dependent on the beamwidth. The power spectral density of the Doppler shift signal is strongly related to the PZT beam pattern and can be observed in the spectrums presented in Fig. 4.

Differentiation of eqn. 1 gives the relation between bandwidth df_D, due to Doppler spreading and the beamwidth of the crystal $d\theta$ where $d\theta$ is defined as:

$$d\theta = \sin^{-1}\left(0.61 \frac{\lambda}{r}\right) \qquad (2)$$

(See, for example, Camp, 1970)

where λ is the wavelength of the beam ($\lambda = \frac{c}{f}$ with c the speed of sound of the beam and f the frequency of the beam) and r is the radius of the crystals.

$$df_D = \frac{f_T v}{c} (\sin \theta_t + \sin \theta_r)\, d\theta \qquad (3)$$

Eqn. 3 can be divided by eqn. 1 to give

$$df_D/f_D = \left(\frac{\sin \theta_t + \sin \theta_r}{\cos \theta_t + \cos \theta_r}\right) d\theta \qquad (4)$$

The effect of the bandwidth, df_D of the Doppler frequency on its instantaneous measurement can be analysed based on theoretical studies by Schultheiss *et al* (1954). From Schultheiss, the probability density function of instanteous frequency has approximately the same width as the width of the power spectrum. In particular, the standard deviation of instantaneous frequency equals half the bandwidth of the signal. This means that the standard deviation of a single instantaneous Doppler frequency measurement will be half the value of the ratio df_D/f_D of eqn. (4).

To minimize the standard deviation of the instantaneous Doppler frequency

measurement (and hence to improve the accuracy in determining the Doppler frequency) we should:

(i) minimize df_D/f_D by minimizing θ_t and θ_r as much as physically possible.

(ii) minimize df_D/f_D by having a narrower beamwidth (eqn. 2). For a fixed frequency (1 MHz) and radius of crystal (5mm), the choice of material for the mounting structure should be chosen with a low speed of sound, c.

(iii) average the processing of the Doppler frequency spectrum to a voltage over a period of time. The electronics of the system allows for an adjustable average period to be set to up to 1 second. With a larger averaging period, the accuracy is higher but the response time is longer.

4.5 Detection from typical bed loads encountered in the mining industry

If the Doppler Ultrasonic technique can be used in the application of detection of blood flow by obtaining reflections from blood corpuscles, then it can detect reflections from all typical mining slurries with ease.

4.6 Independence of the properties of the transporting fluid

The Doppler Ultrasonic technique should be completely independent of the properties of the transporting fluid. Fluid properties such as its density, pressure and temperature will affect the speed of sound of the fluid, c'. (c' within a fluid increases as pressure increases and as temperature decreases, in general, any change which affects density or compressibility causes a corresponding change in c'). Speed of sound in the fluid may intuitively be thought to influence the Doppler frequency shift. However, in eqn. 1, c is fixed and dependent only on the physical characteristic of the mounting structure. From Snell's Law of Refraction, $\frac{\cos \theta_t}{c}$ of the mounting structure as defined in eqn. 1 will equal $\frac{\cos \theta_t'}{c'}$ in the fluid (where θ_t' is the angle between the transmitted ultrasonic beam in the fluid and the direction of the velocity of the particles). A variation in c' in the fluid will cause a corresponding change in θ_t' to satisfy Snell's Law: $\frac{\cos \theta_t}{c} = \frac{\cos \theta_t'}{c'}$. The same applies to θ_r within the mounting structure and θ_r' within the fluid.

4.7 Short response time

The electronics required to send an ultrasonic beam into the fluid, amplify and demodulate the received signal and extract the Doppler frequency which is then electronically analysed, operates very quickly. The response time required to obtain an indication of the bed load is very short (< 1 second) and this time is ideal for the implementation of the control system to the pumps.

4.8 Minimal maintenance

Since the system contains no moving parts or parts which wear, maintenance is anticipated to be very low.

5. Experimental results and discussion

5.1 Experimental Test Rigs

Two test rigs were used to conduct tests on the instrument.

(i) The main Hydrotransport Research Unit 140 mm diameter perspex section of pipeline (Lazarus and Sive, 1984) containing a sand water slurry was used for testing the UDV. The sliding bed load contained a volumetric concentration of 50%. The slurry rate was controlled with a variable speed pump so that a velocity profile could be achieved with the bed load remaining

stationary. The transducer was attached by taping it to the outside and underneath the pipeline with a layer of silicone sealant acting as an ultrasonic bond. The bed load could be varied between stationary to velocities of approximately 4 m/s.

(ii) A simulation of a moving bed load travelling at a fixed, known velocity was created using a simulation test rig as shown in Fig. 3. The simulation consisted of a 330 mm diameter disc driven by a variable speed D.C. motor. The lower quarter of the disc was submerged in a perspex tank of water. The rim of the disc was coated in sand to model the bed load and to act as a good reflector of the ultrasonic beam. The velocity of the disc could be varied from 0.45 m/s to 1.42 m/s and could be accurately determined. The transducer was bonded to the outside of the tank directly under the lowest point of the disc.

5.2 Results and discussion

Results from the 140 mm pipeline showed that the Velocimeter appeared to be operating correctly. At stationary bed loads, while the sand above the bed load could visibly be seen to be moving (see Fig. 1), the velocimeter gave a correct indication of zero. As the velocity of the bed load was increased, so the reading on the Velocimeter increased.

To investigate the linearity and accuracy of the instrument, the simulation test rig, simulating a moving bed load was used. The disc was set to fixed velocities, between 0 m/s and 1.42 m/s as tabulated (Table 1). The following results were obtained:

(i) The frequency spectrum of the Doppler shift frequency obtained from the demodulated received signal. The spectrums were plotted with the frequency axis extending to 2 kHZ. The peak of the spectrum, the Doppler shift frequency, is designated with a cross (x) on the plot. The x value gives the value of the frequency of the peak. These spectrums are presented in Fig. 4.1 to 4.6.

From the spectrums it can be seen that as the disc velocity increases, so the spectrum spreads out. From eqn. 3, the spreading of the Doppler frequency, df_D is dependent on the velocity, v.

At higher velocities of the disc, the spectrums start exhibiting peaks at frequencies below the expected Doppler frequency as seen in Fig. 4.5 and 4.6. This is due to bubbles occurring under the disc when its velocity increases. These bubbles travel slower than the sand particles on the rim of the disc and so present frequency peaks due to their velocity.

(ii) Readings were taken from the voltmeter display on the Velocimeter. The voltage is obtained from the electronic processing of the demodulated signal to determine the peak frequency of the Doppler shift spectrum. This voltage is tabulated in Table 1 for the range of disc velocities.

Figs. 5 and 6 are graphs of the Doppler frequency peak and the output voltage of the velocimeter for the range of disc velocities.

Fig. 5 is linear as indicated by eqn. 1. Fig. 6 shows that at higher disc velocities, the output voltage loses linearity. This is due to the electronic processing of the Doppler frequency to obtain a voltage proportional to the mean frequency spectrum. The spectrum at high disc velocities contains peaks at lower frequencies due to the Doppler shift from the slower moving bubbles, which cause the output voltage to decrease. This effect is not expected to occur in the measurement of the bed load velocity in a slurry filled pipeline as there should be no slower moving bubbles present below the bed load.

6. Conclusion

A prototype of an instrument for measuring bed load velocity of high concentration slurry has been developed. The instrument is based on the Doppler shift technique and uses ultrasound as its source of energy. The Ultrasonic Doppler Velocimeter (UDV) may be used for:

(i) minimizing head loss gradient thereby increasing hydraulic efficiency.
(ii) reducing the wear rate in systems transporting abrasive materials by monitoring the bed load and transporting the material at or near the limit deposit velocity.
(iii) its application to the theoretical and analytical study of pipe blockage.
(iv) a control sensor to provide feedback to the system pumps thereby preventing possible pipe blockage.

A list of various requirements that the system should possess have been presented. These requirements appear to have all been satisfied with the system design. Results taken from a test rig pipeline and a simulation of a moving bed load of various velocities show that the instrument appears to function correctly to give an accurate indication of bed load velocity.

References

1. Albright, R.J., "Relationship of Doppler ultrasonic scattered signal characteristics to flow and beam parameters", *J.Acoust. Soc. Am.*, Vol. 59, No. 4, April 1976, pp. 786-789.
2. Atkinson, P. and Woodcock, J.P., "Doppler Ultrasound and its use in clinical measurement", *Medical Physics Series*, Academic Press, 1982.
3. Brody, W.R. and Meindl, J.D., "Theoretical Analysis of the CW Doppler Ultrasonic Flowmeter", *IEEE Trans. on Biomed. Eng.*, Vol. BME-21, No. 3, May 1974, pp.183-192.
4. Camp, L., "Underwater Acoustics", Wiley-Interscience, 1970.
5. Denbigh, P.N., "Ship velocity determination by Doppler and correlation techniques", *IEEE Proceedings*, Vol. 131, Part F, No. 3, June 1984, pp. 315-326.
6. Di Pietro, D.M. and Meindl, J.D., "Optimal System Design for an Implantable CW Doppler Ultrasonic Flowmeter", *IEEE Trans. on Biomed. Eng.*, Vol BME-25, No. 3, May 1978, pp. 255-263.
7. Faddick, R., Pouska, G., Connery, J., Di Napoli, L., Punis, G., Connery J., Di Napoli, L., Punis, G., "Ultrasonic Velocity Meter", *Hydrotransport 6, 6th Int. Conf. on the Hydraulic Transport of Solids in Pipes*, Canterbury, England. September 1979, pp.113-124.
8. Flax, S.W., Webster, J.G., Updike, S.J., "Statistical Evaluation of the Doppler Ultrasonic Blood Flowmeter", *ISA Trans.*, Vol. 10, No. 1, 1971, pp. 1-20.
9. Green, P.S., "Spectral Broadening of Acoustic Reverberation in Doppler-Shift Fluid Flowmeters", *J. Aroust. Soc. Am.*, Vol. 36, No. 7, July 1964, pp. 1383-1390.
10. Hampton, L.D., "Acoustic Poroperties of Sediments", *J. Acoust. Soc. Am.*, Vol. 42, No. 4, 1976, pp.882-890.
11. Hovem, J.M., Ingram, G.D., "Viscous Attenuation of Sound in Saturated Sand", *J. Acoust. Soc. Am.*, Vol. 66, No. 6, Dec. 1979, pp.1807-1812.
12. Jervis, B.W., "Microwave Doppler-effect Particle Flow Measurement", IEEE *Trans. Industr. Electron. Control Instrum.*, IECI-24, pp.322-327.
13. Lazarus, J.H. and Sive, A.W., "A Novel Balanced Beam Tube Viscometer and the Rheological Characterisation of High Concentration Fly Ash Slurries", *9th Int. Conf. on the Hydraulic Transport of Solids in Pipes*, Rome, Italy, Oct. 1984, pp.207-226.
14. Leitner, J.R., "Slurry Flowmetering Using Correlation Techniques", *PhD Thesis* 1979, University of Cape Town.
15. Lynworth, L.C., "Clamp-on Ultrasonic Flowmeters", *Instrumentation Technology*, Sept. 1975, pp.37-44.

16. Lynworth, L.C., "Non-intrusive Ultrasonic Measurement of Flow Velocity and Mass Flow Rate", *Flow-Its Measurement and Control in Science and Industry*, Vol.1, Part 2, pp. 417-924. (Editor: Dowdell, R.B.)
17. McShane, J.L., "Ultrasonic Flowmeter Basics", *Instrumentation Technology*, Jul. 1971, pp.45-48.
18. Sanderson, M.L., Hemp, J., "Ultrasonic Flowmeters - A Review of the State-of-the-Art", *Int. Conf. On Advances in Flow Measurement Techniques*, Coventry, England, September 1981, pp.157-178 (Editor: Dowdell, R.B.)
19. Schultheiss, P.M., Wogrin, C.A., Zweig, F., "Short-Time Frequency Measurement of Narrow-Band Random Signals in the Presence of Wide-Band Noise", *J. of Applied Physics*, Vol. 25, No. 8, Aug. 1954, pp. 1025 - 1036.
20. Scott, M.J., "Doppler Ultrasonic Flowmeters", CME, Oct. 1978, pp. 51-54.
21. Scrivener, O., Reitzer, H., Hazzab, A., Idrissi, A., "Optical and Ultrasonic Instruments for Mixture Flow Investigation", *Hydrotransport 10, 10th International Conference on the Hydraulic Transport of Solids in Pipes*, Innsbruck, Austria, October 1986, pp. 275-282.
22. Thompson, H.D. and Stevenson, W.J., (Editors) "Laser Velocimetry and Particle Sizing", *Hemisphere Publishing Corporation*, 1978.
23. Thorn, R., Beck, M.S., Green, R.G., "Non-Intrusive Methods of Velocity Measurement in Pneumatic Conveying", *J. Phys. E. Sci. Instru.*, Vol. 15, 1982, pp. 1131-1138.
24. Wells, P.N.T., "Biomedical Ultrasonics", *Medical Physics Series*, Academic Press, 1977.

Table 1 : Table of Peak Doppler frequency and output voltage from the Velocimeter for various disc velocities.

Disc Velocity (m/s)	Peak Doppler Frequency (Hz)	Output Voltage (v)
0.00	0	0.00
0.45	255	0.88
0.52	325	1.04
0.71	465	1.41
0.82	555	1.60
1.02	685	1.98
1.22	830	2.26
1.42	935	2.54

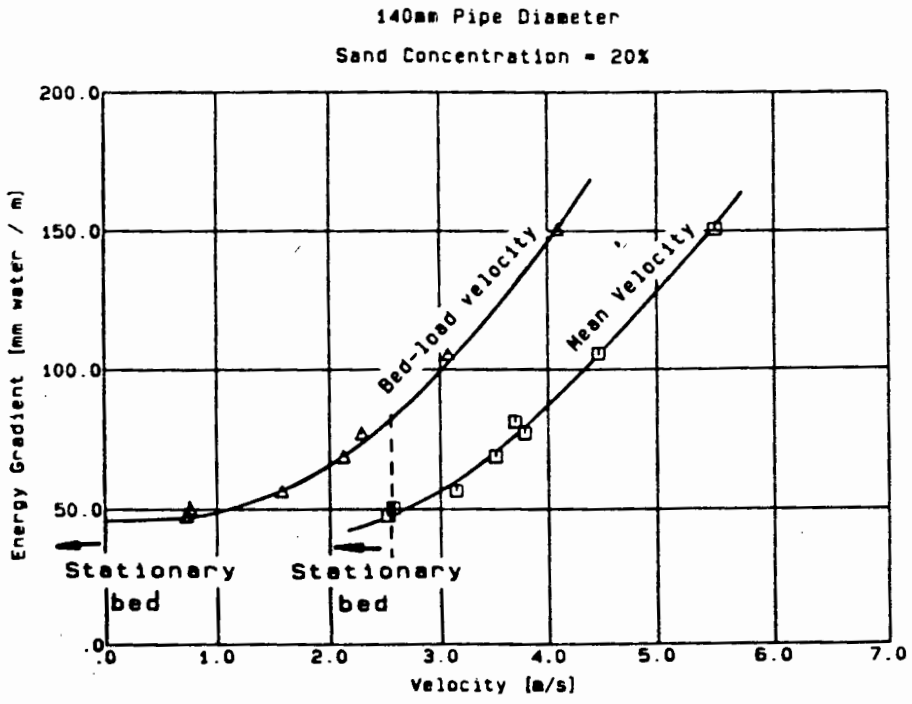

Figure 1 : Friction head loss gradient as a function of mean mixture velocity and bed load velocity.

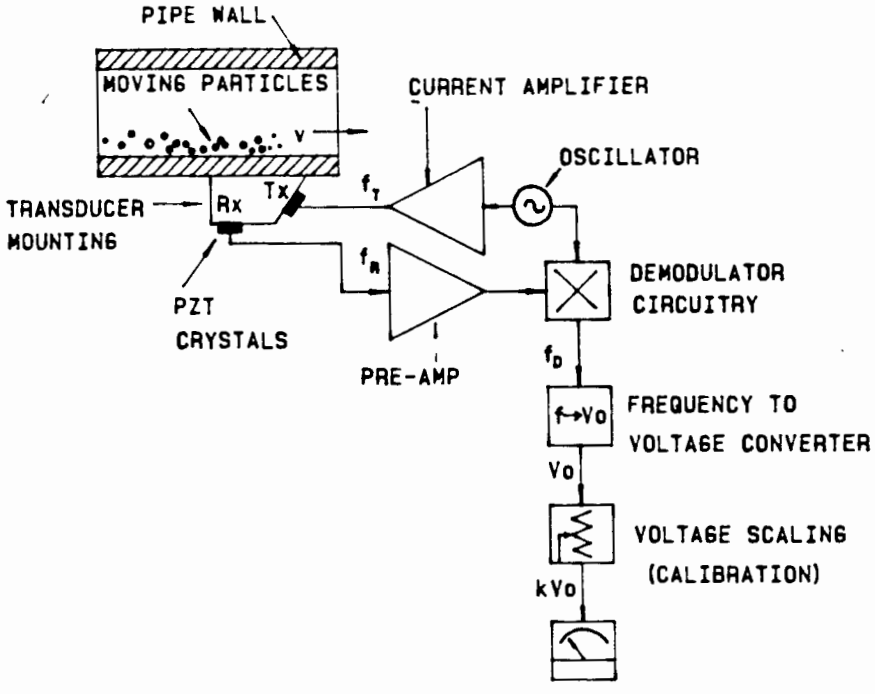

Tx	: Transmitter
Rx	: Receiver
f_T	: Frequency of Transmitted Signal
f_R	: Frequency of Received Signal
f_D	: Doppler Shift Frequency
v	: Bed-load Particle Velocity
Vo	: Voltage
k	: Constant

Figure 2 : Diagrammatic representation of the Ultrasonic Doppler Bed Load Velocimeter

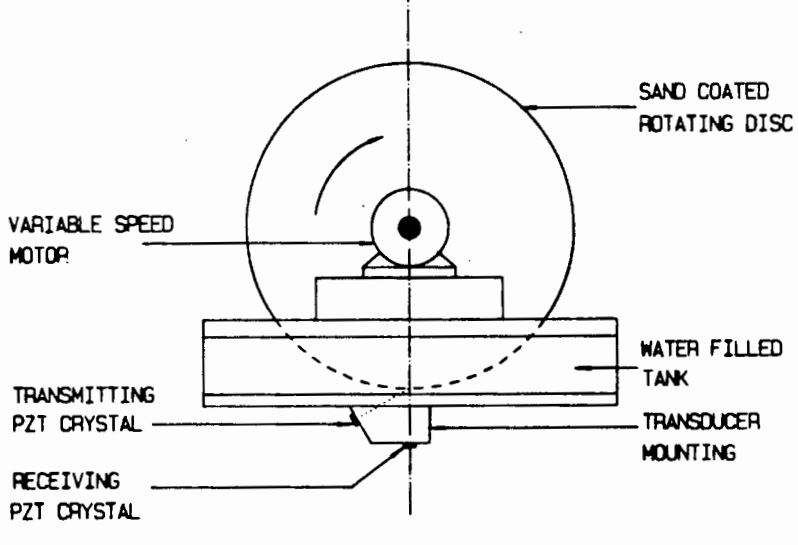

Figure 3 : Simulation Test-Rig consisting of a rotating disc at a fixed, known velocity.

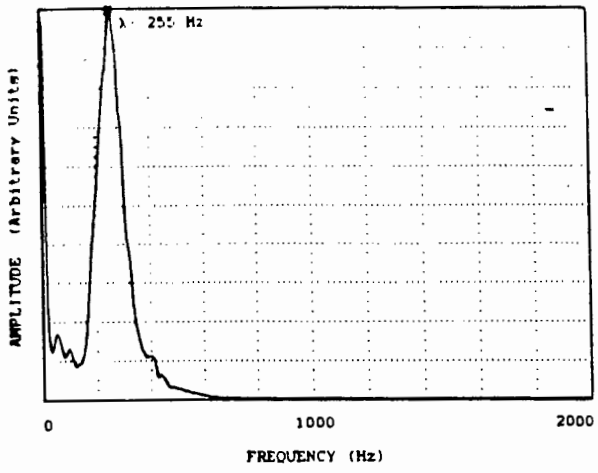

Figure 4.1 : Disc velocity = 0.45 m/s

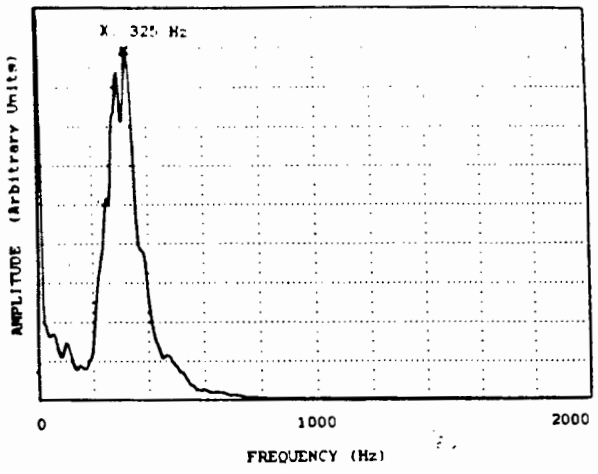

Figure 4.2 : Disc velocity = 0.52 m/s

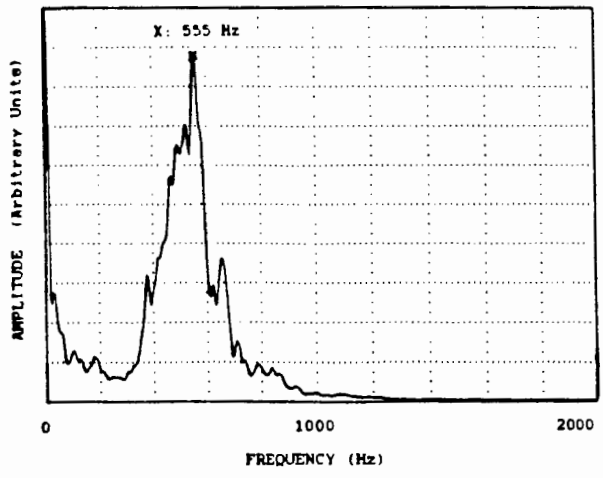

Figure 4.3 : Disc velocity = 0.82 m/s

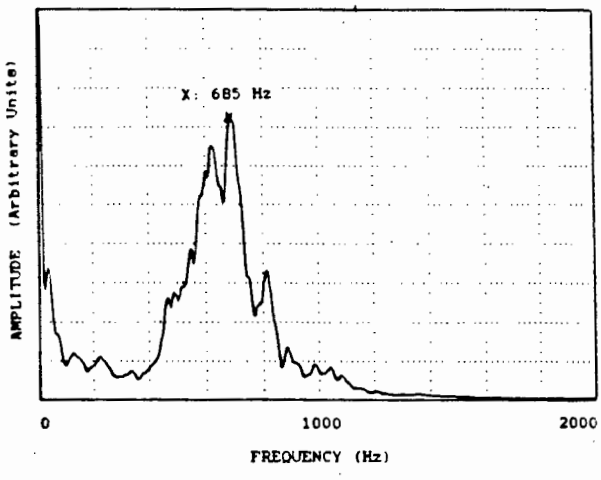

Figure 4.4 : Disc velocity = 1.02 m/s

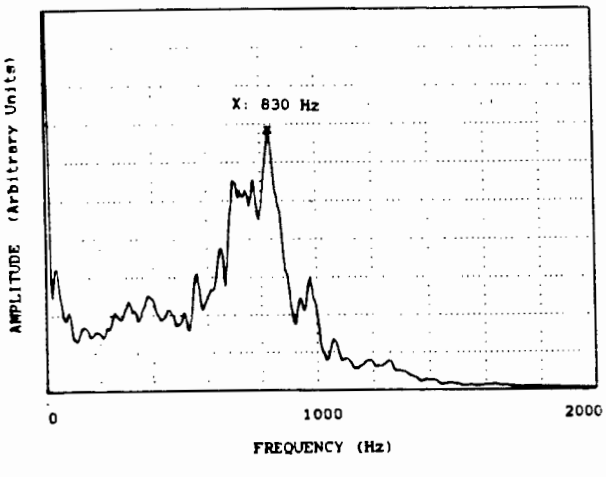

Figure 4.5 : Disc velocity = 1.22 m/s

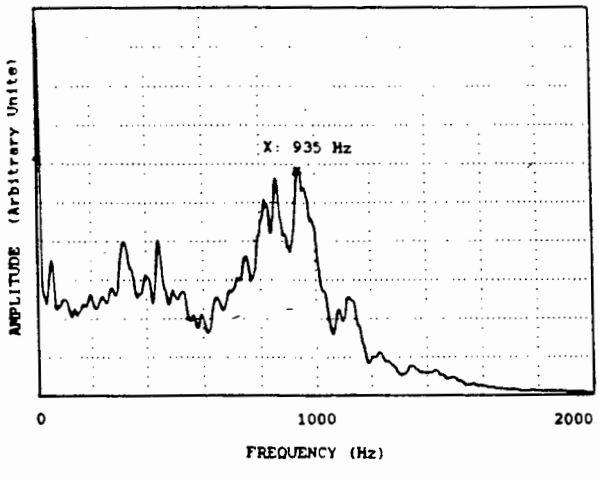

Figure 4.6 : Disc velocity = 1.42 m/s

Figures 4.1 - 4.6 : Doppler shift frequency spectrums for various disc velocities.

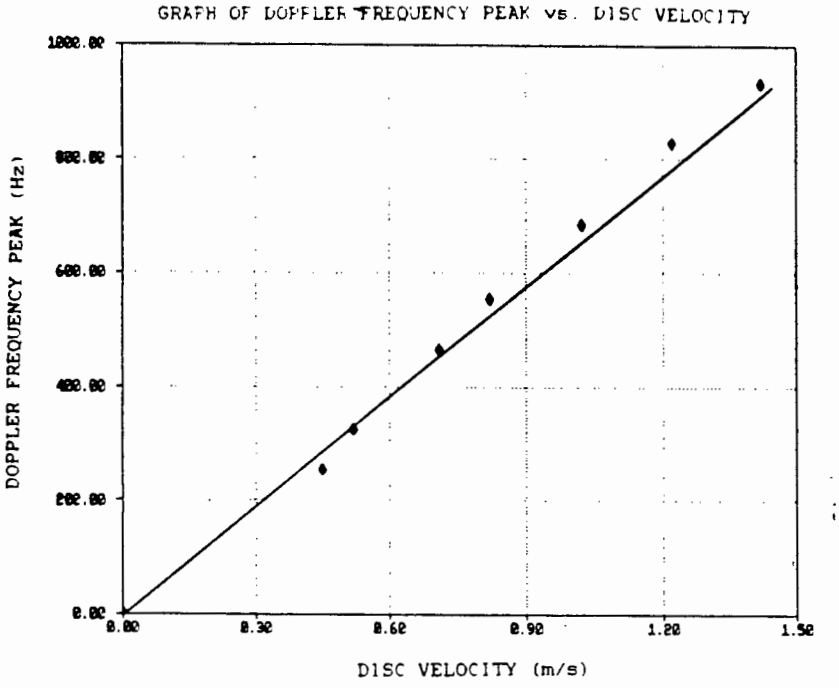

Figure 5 : Graph of Doppler frequency peak as a function of disc velocity.

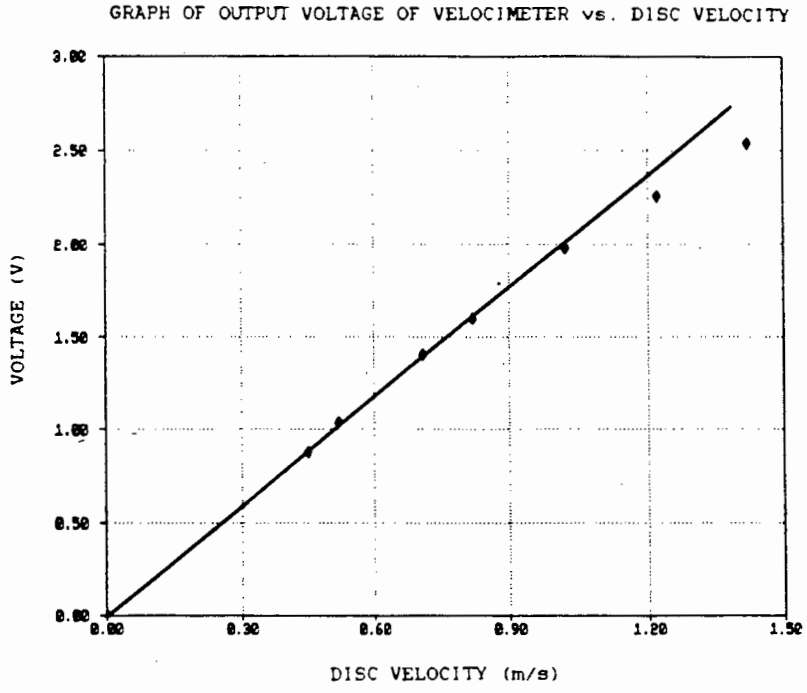

Figure 6 : Graph of output voltage of Velocimeter as a function of disc velocity.

APPENDIX B

DERIVING VARIOUS FOCUSING CONSTANTS

DERIVING VARIOUS FOCUSING CONSTANTS

Part 1: Deriving h_E from h

Refer to Fig. B1, which is identical to Fig. 6.6. Assume a material (the transducer window, with an ultrasonic velocity defined by c_{TW}) is in contact with another medium (the slurry, with an ultrasonic velocity defined by c_{SL}). If a beam propagates from the transducer window into the slurry material then refraction will occur at the interface of these two mediums. Assume two beams (one from a Tx. the other from a Rx.) intersect at a location within the slurry at a perpindicular height from the interface defined by h.

Another point within the slurry can be defined as an effective location with an effective perpindicular height defined by h_E (see Fig. B1). This is the location of the intersection of the same beams if the ultrasonic velocity within the slurry were identical to the ultrasonic velocity within the transducer window material and no refraction occured.

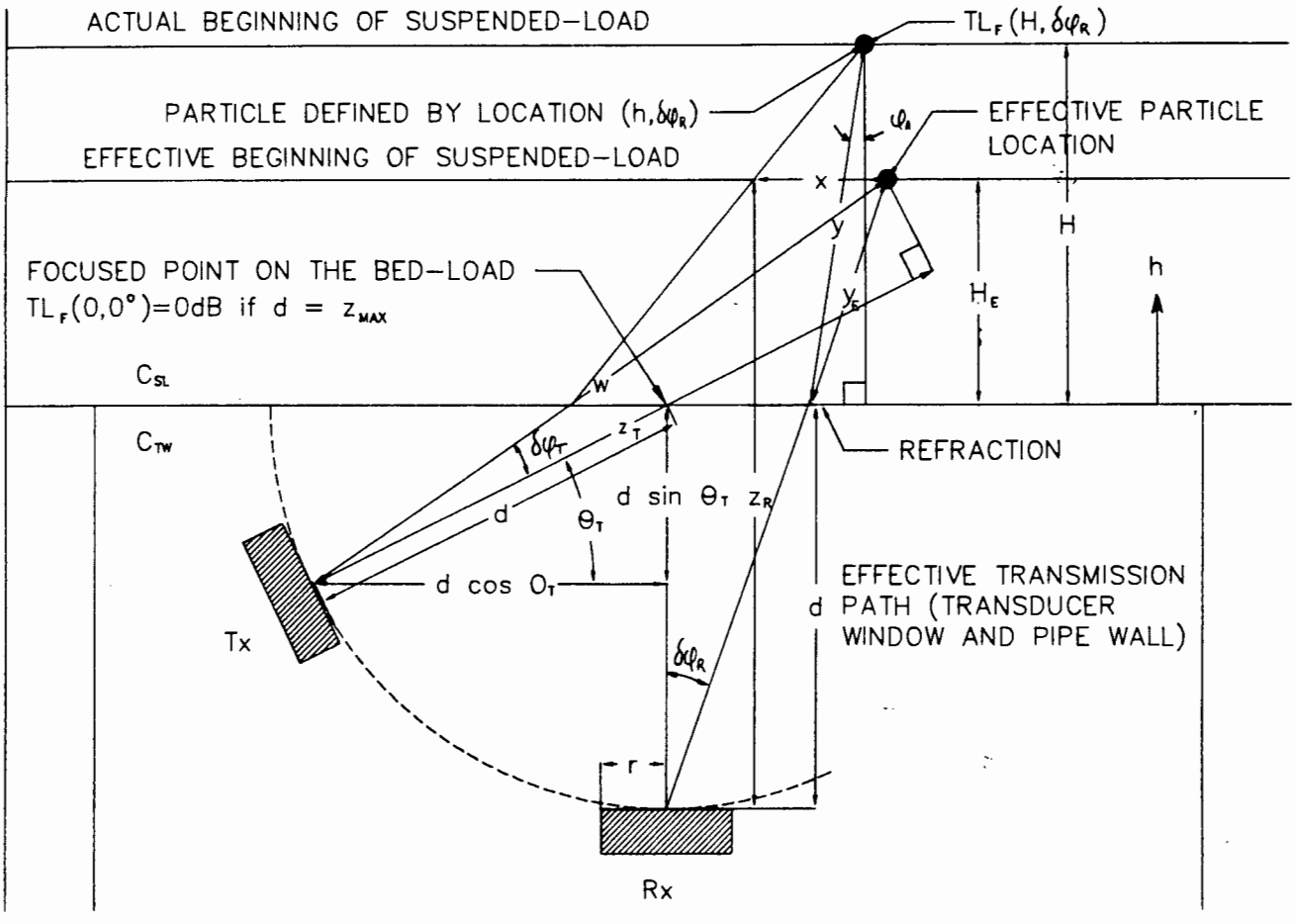

Fig. B.1 Actual and Effective particle locations within the slurry

Let the actual distance that the Rx. beam travels within the slurry layer to the intersection point be defined by y. The distance to the effective particle location [y_E] is related to y by the ratio of the ultrasonic velocities as follows:

$$y_E = c_{SL}/c_{TW} \cdot y \qquad (B.1)$$

The direction that the Rx. beam travels in the transducer window relative to the crystal normal is defined by $\delta\varphi_R$. Within the slurry layer, the direction of the same beam is defined by say φ_A. The angles $\delta\varphi_R$ and φ_A are related according to Snell's Law as follows:

$$\frac{\sin \delta\varphi_R}{\sin \varphi_A} = \frac{c_{TW}}{c_{SL}} \qquad (B.2)$$

The heights h and h_E can be exressed as follows:

$$y = h/\cos \varphi_A \qquad (B.3)$$

$$y_E = h_E/\cos \delta\varphi_R \qquad (B.4)$$

If y in Eqn. B.3 and y_E in Eqn B.4 are substituted into Eqn. B.4 then:

$$\frac{h_E}{\cos \delta\varphi_R} = \frac{c_{SL} \cdot h}{c_{TW} \cdot \cos \varphi_A} \qquad (B.5)$$

Now solve for φ_A from Eqn. B.2 and substitute into Eqn. B.5 and solve for h_E:

$$h_E = \frac{c_{SL} \cdot h \cdot \cos \delta\varphi_R}{c_{TW} \cdot \cos [\sin^{-1} \{(c_{SL}/c_{TW}) \sin \delta\varphi_R\}]} \qquad (B.6)$$

<u>Part 2: Deriving $\delta\varphi_T$ in terms of the focusing parameters:</u>

Refer again to Fig. B1. The point x can be expressed as follows:

$$x = (d+h_E) \tan \delta\varphi_R \qquad (B.7)$$

The angle $(\theta_T - \delta\varphi_T)$ can be expressed as follows:

$$\tan\ (\theta_T - \delta\varphi_T) = \frac{h_E + d \sin \theta_T}{d \cos \theta_T + (d+h_E) \tan \delta\varphi_R} \qquad (B.8)$$

Now solve for $\delta\varphi_T$:

$$\delta\varphi_T = \theta_T - \tan^{-1} \left[\frac{h_E + d \sin \theta_T}{d \cos \theta_T + (d+h_E) \tan \delta\varphi_R} \right] \qquad (B.9)$$

Part 3: Deriving z_T in terms of the focusing parameters:

Refer to Fig. B1 again, the z_T can be expressed in terms of length w as follows:

$$z_T = w \cos \delta\varphi_R \qquad (B.10)$$

Express w in terms of the focusing parameters:

$$w = \frac{h_E + d \sin \theta_T}{\sin\ (\theta_T - \delta\varphi_T)} \qquad (B.11)$$

Now solve for z_T:

$$z_T = \frac{(h_E + d \sin \theta_T) \cos \delta\varphi_T}{\sin\ (\theta_T - \delta\varphi_T)} \qquad (B.12)$$

APPENDIX C

ULTRASONIC DOPPLER BED-LOAD VELOCIMETER

HARDWARE TECHNICAL DESCRIPTION

CONTENTS

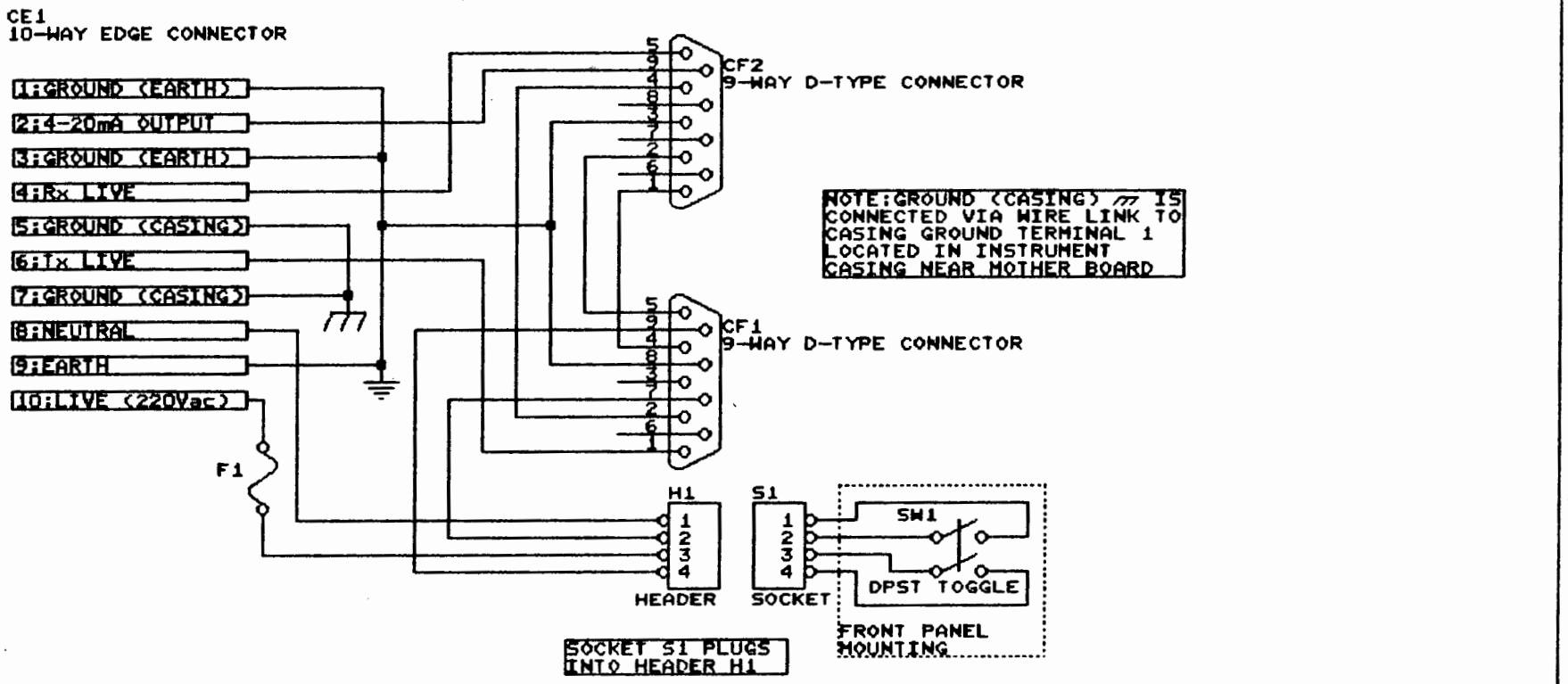

MARK LAZARUS		
ULTRASONIC DOPPLER BED LOAD VELOCIMETER		
Title: MOTHER BOARD CIRCUIT		
Size: A	Document Number: 1	REV: 1
Date: June 28, 1989	Sheet 1 of 10	

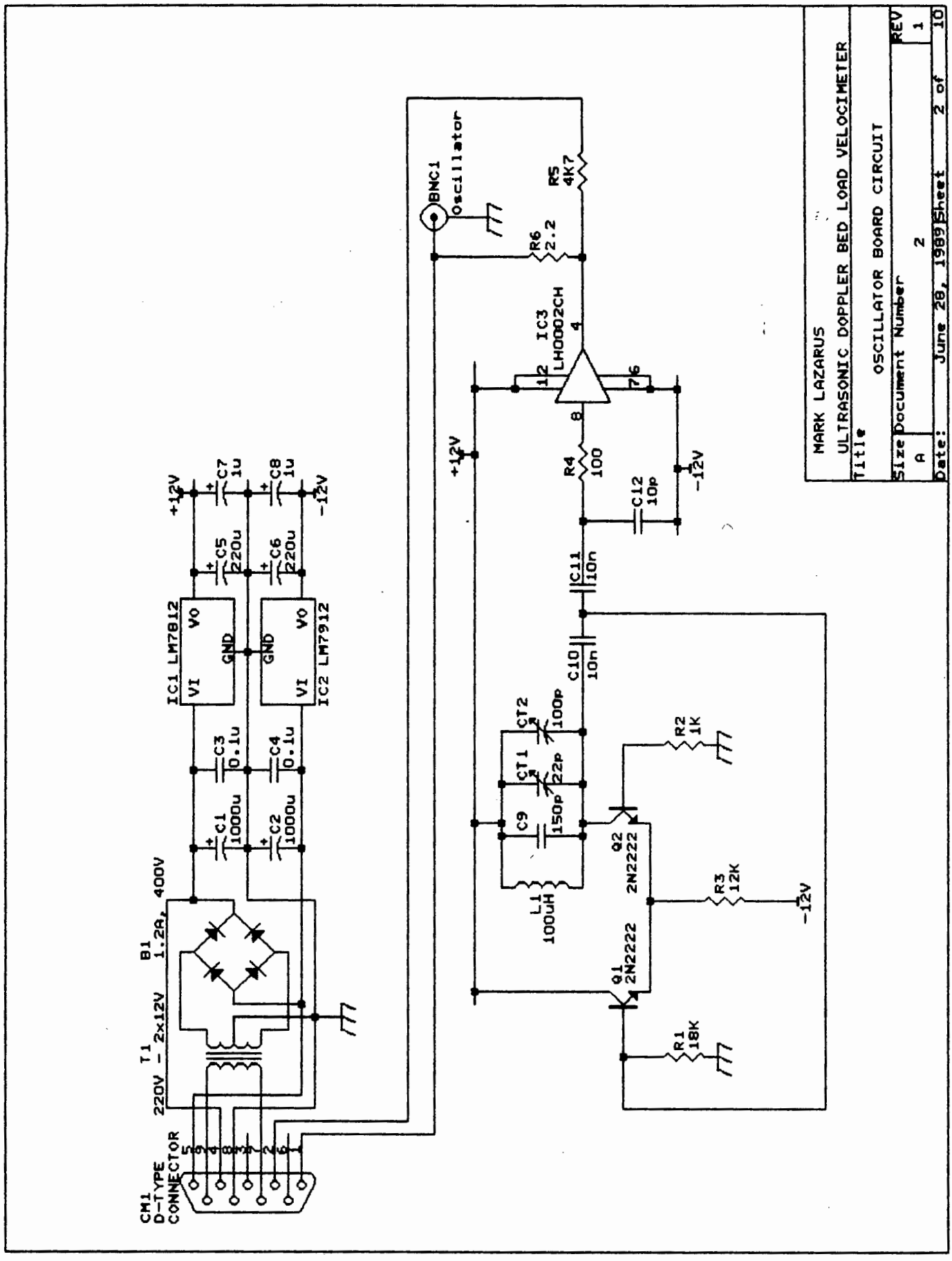
MARK LAZARUS
ULTRASONIC DOPPLER BED LOAD VELOCIMETER
Title
OSCILLATOR BOARD CIRCUIT
Size
A
Document Number
2
REV
1
Date: June 28, 1989
Sheet 2 of 10
CN1 D-TYPE CONNECTOR
T1 220V - 2x12V
B1 1.2A, 400V
IC1 LM7812
IC2 LM7912
IC3 LH0002CH
BNC1 Oscillator
Q1 2N2222
Q2 2N2222
L1 100uH
C1 1000u
C2 1000u
C3 0.1u
C4 0.1u
C5 220u
C6 220u
C7 1u
C8 1u
C9 150p
C10 10n
C11 10n
C12 10p
CT1 22p
CT2 100p
R1 18K
R2 1K
R3 12K
R4 100
R5 4K7
R6 2.2
+12V
-12V
VI
VO
GND

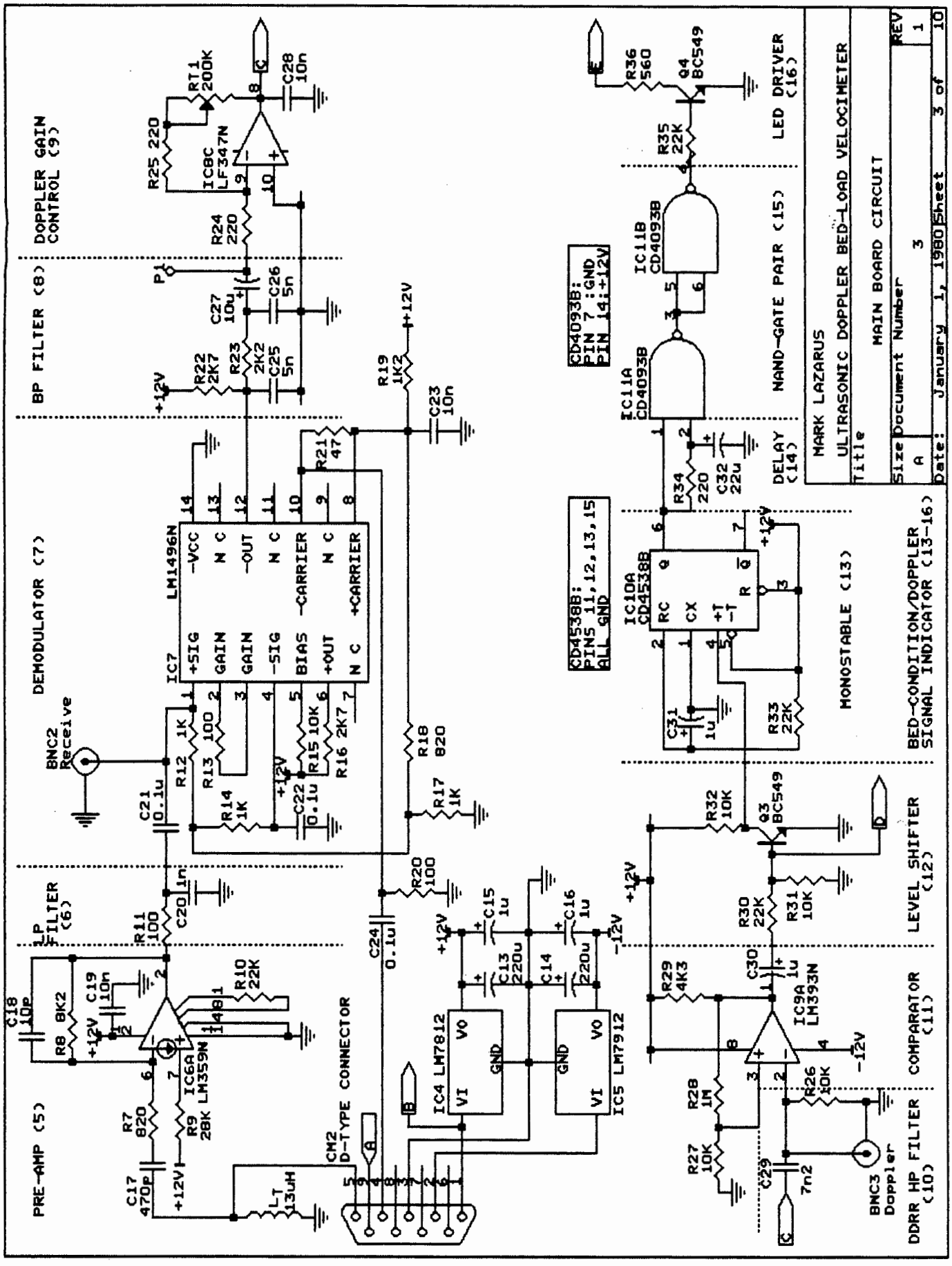
PRE-AMP (5)
LP FILTER (6)
DEMODULATOR (7)
BP FILTER (8)
DOPPLER GAIN CONTROL (9)
DDRR HP FILTER (10)
COMPARATOR (11)
LEVEL SHIFTER (12)
MONOSTABLE (13)
DELAY (14)
NAND-GATE PAIR (15)
LED DRIVER (16)
BED-CONDITION/DOPPLER SIGNAL INDICATOR (13-16)
IC7 LM1496N
IC6A LM359N
IC8C LF347N
IC9A LM393N
IC10A CD4538B
IC11A CD4093B
IC11B CD4093B
IC4 LM7812
IC5 LM7912
CD4538B: PINS 11,12,13,15 ALL GND
CD4093B: PIN 7 :GND PIN 14:+12V
CM2 D-TYPE CONNECTOR
BNC2 Receive
BNC3 Doppler
MARK LAZARUS
ULTRASONIC DOPPLER BED-LOAD VELOCIMETER
MAIN BOARD CIRCUIT
Size A
Document Number 3
REV 1
Date: January 1, 1980 Sheet 3 of 10

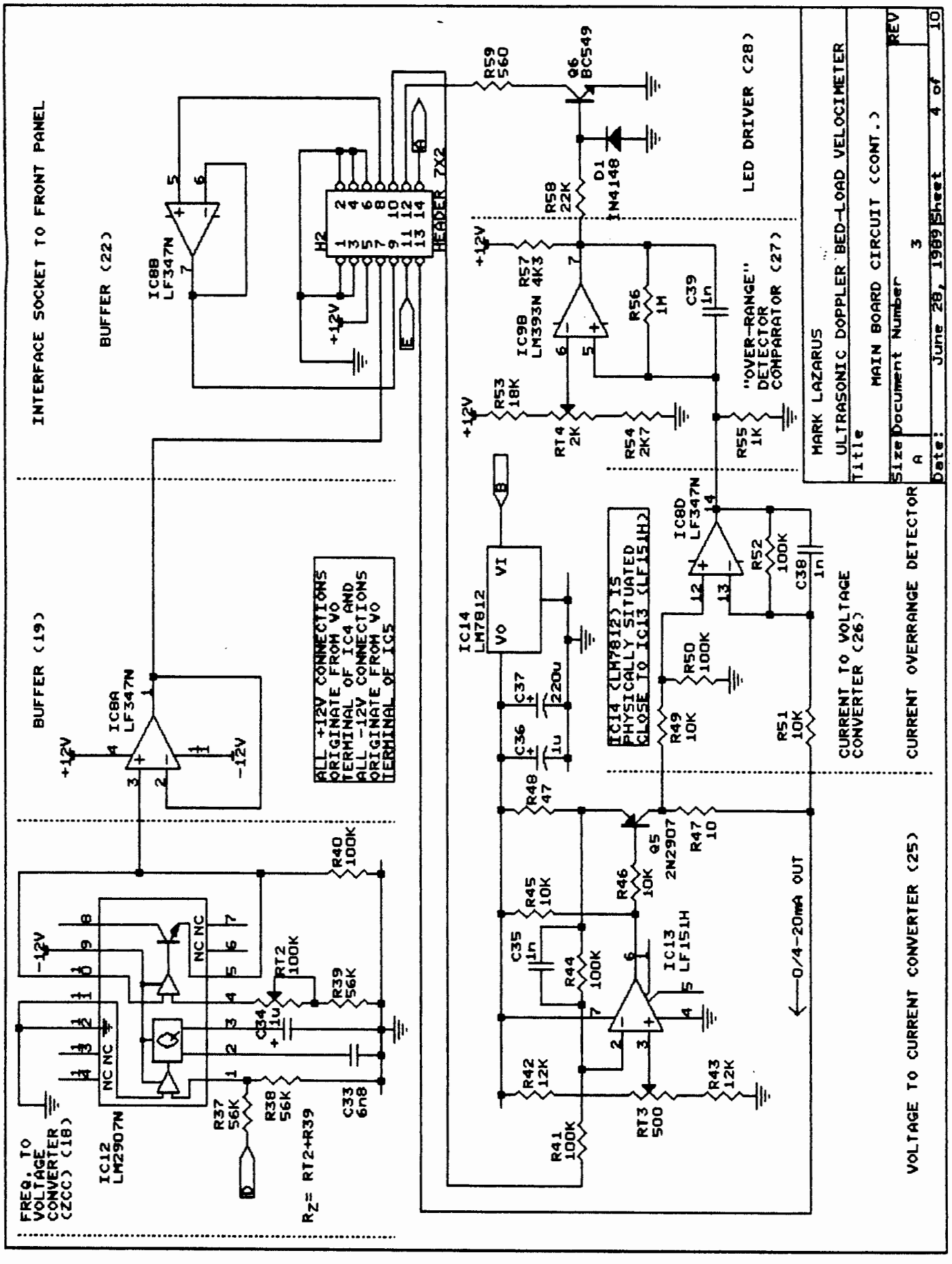
INTERFACE SOCKET TO FRONT PANEL
BUFFER (22)
BUFFER (19)
LED DRIVER (28)
"OVER-RANGE" DETECTOR COMPARATOR (27)
CURRENT TO VOLTAGE CONVERTER (26)
CURRENT OVERRANGE DETECTOR
VOLTAGE TO CURRENT CONVERTER (25)
FREQ. TO VOLTAGE CONVERTER (ZCC) (18)
ALL +12V CONNECTIONS ORIGINATE FROM VO TERMINAL OF IC4 AND ALL -12V CONNECTIONS ORIGINATE FROM VO TERMINAL OF IC5
IC14 (LM7812) IS PHYSICALLY SITUATED CLOSE TO IC13 (LF151H)
IC8A LF347N
IC8B LF347N
IC8C LF347N
IC8D LF347N
IC9B LM393N
IC12 LM2907N
IC13 LF151H
IC14 LM7812
HEADER 7X2
D1 IN4148
Q5 2N2907
Q6 BC549
R37 56K
R38 56K
R39 56K
R40 100K
R41 100K
R42 12K
R43 12K
R44 100K
R45 10K
R46 10K
R47 10
R48 47
R49 10K
R50 100K
R51 10K
R52 100K
R53 18K
R54 2K7
R55 1K
R56 1M
R57 4K3
R58 22K
R59 560
RT2 100K
RT3 500
RT4 2K
C33 6n8
C34 1u
C35 1n
C36 1u
C37 220u
C38 1n
C39 1n
0/4-20mA OUT
R_Z= RT2+R39
MARK LAZARUS
ULTRASONIC DOPPLER BED-LOAD VELOCIMETER
Title MAIN BOARD CIRCUIT (CONT.)
Size A
Document Number 3
REV
Date: June 28, 1989 Sheet 4 of 10

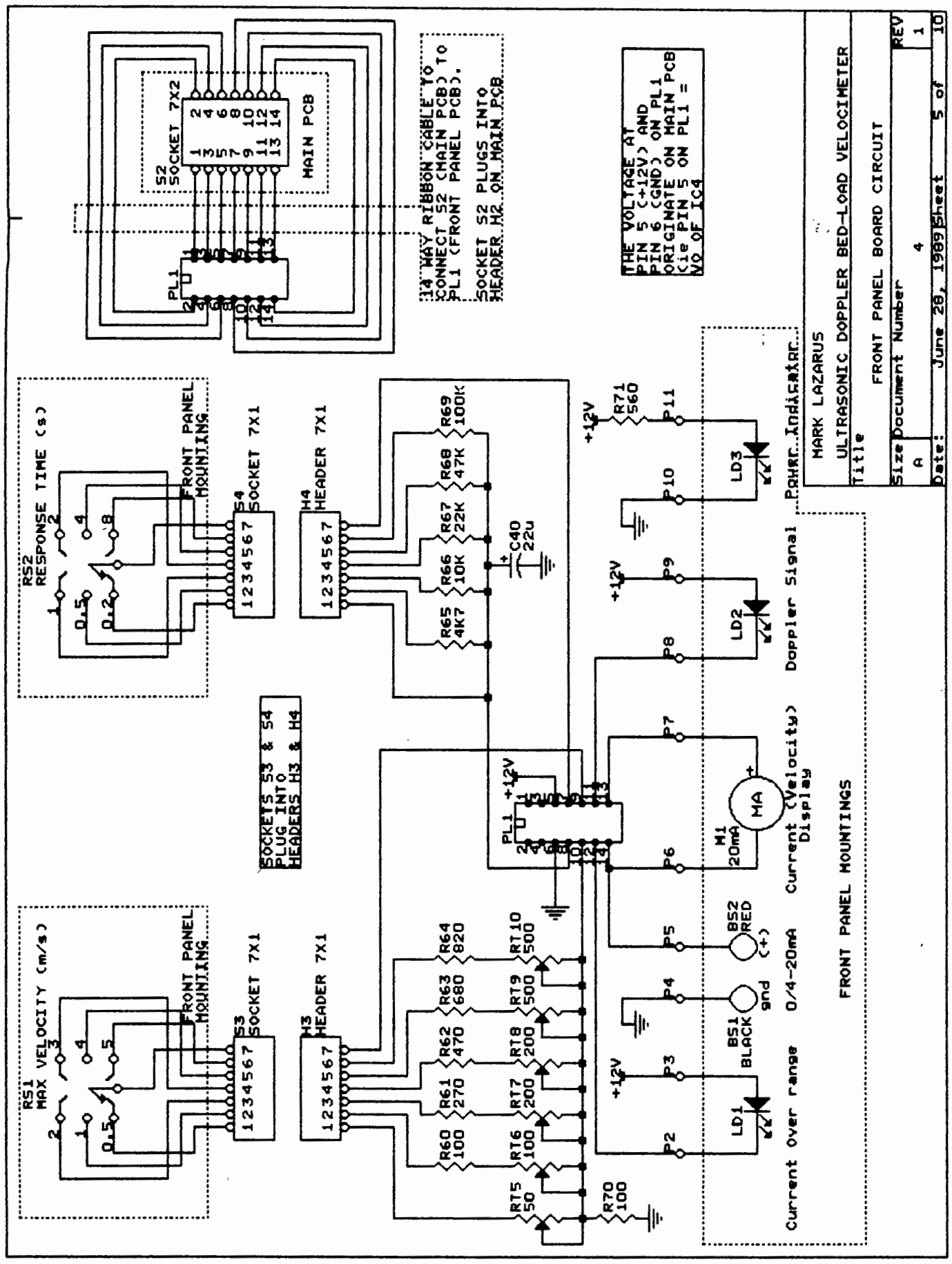
S2
SOCKET 7X2
1 3 5 7 9 11 13
2 4 6 8 10 12 14
MAIN PCB
PL1
14 WAY RIBBON CABLE TO CONNECT S2 (MAIN PCB) TO PL1 (FRONT PANEL PCB).
SOCKET S2 PLUGS INTO HEADER H2 ON MAIN PCB
THE VOLTAGE AT PIN 5 (+12V) AND PIN 6 (GND) ON PL1 ORIGINATE ON MAIN PCB (ie PIN 5 ON PL1 = VO OF IC4
RS2
RESPONSE TIME (s)
0.5
0.2
FRONT PANEL MOUNTING
S4
SOCKET 7X1
1234567
H4
HEADER 7X1
R69 100K
R68 47K
R67 22K
R66 10K
R65 4K7
C40 22u
+12V
R71 560
P11
P10
P9
P8
P7
P6
P5
P4
P3
P2
LD3
LD2
LD1
Power Indicator
Doppler Signal
M1
20mA
MA
Current (Velocity) Display
BS2
RED
(+)
BS1
BLACK
gnd
0/4-20mA
Current Over range
SOCKETS S3 & S4 PLUG INTO HEADERS H3 & H4
PL1
RS1
MAX VELOCITY (m/s)
S3
SOCKET 7X1
H3
HEADER 7X1
R64 820
R63 680
R62 470
R61 270
R60 100
RT10 500
RT9 500
RT8 200
RT7 200
RT6 100
RT5 50
R70 100
FRONT PANEL MOUNTINGS
MARK LAZARUS
ULTRASONIC DOPPLER BED-LOAD VELOCIMETER
Title
FRONT PANEL BOARD CIRCUIT
Size
A
Document Number
4
REV
1
Date: June 28, 1989
Sheet 5 of 10

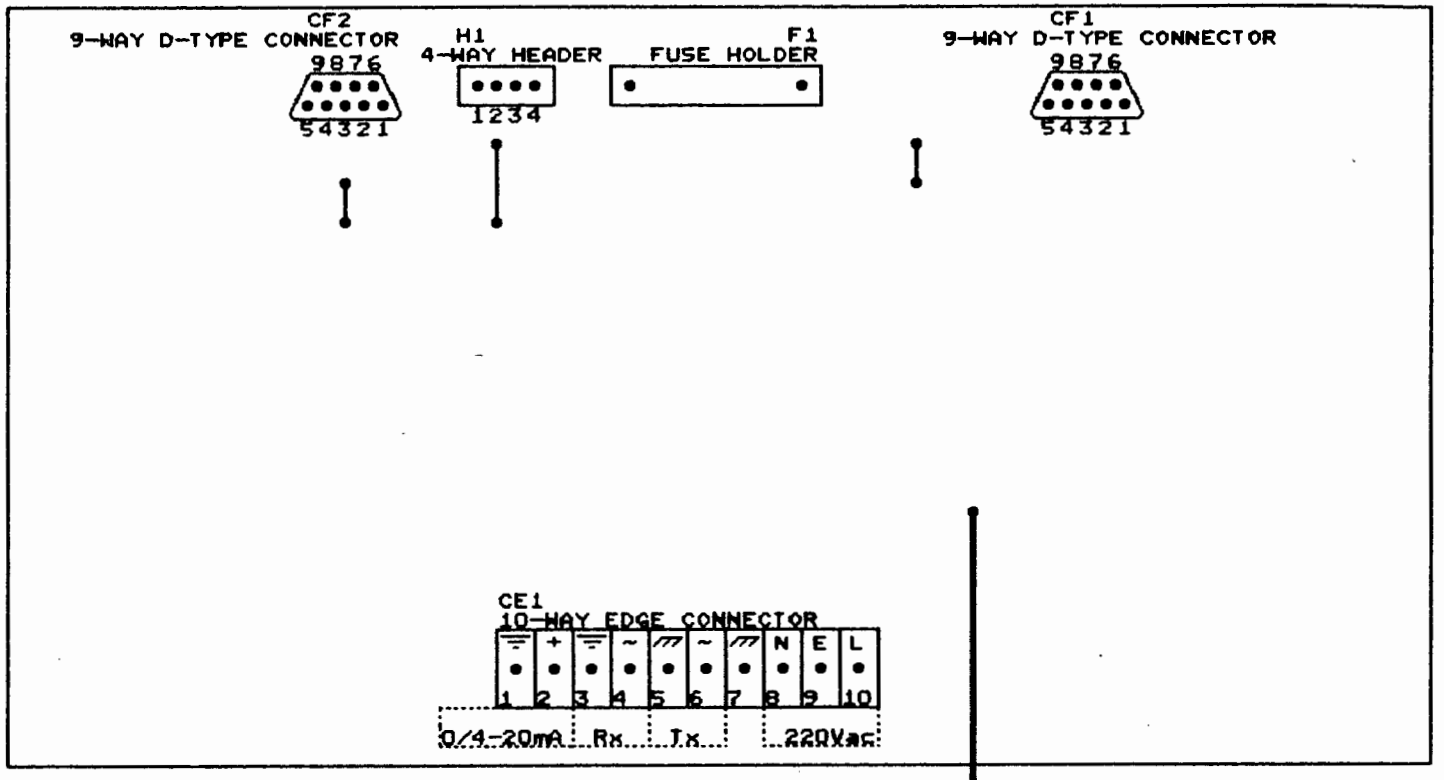

CASING GROUND TERMINAL 1
IS LOCATED IN INSTRUMENT
CASING NEAR MOTHER BOARD

MARK LAZARUS		
ULTRASONIC DOPPLER BED-LOAD VELOCIMETER		
Title: MOTHER BOARD COMPONENT LAYOUT		
Size: A	Document Number: 5	REV
Date: June 28, 1989	Sheet 6 of 10	

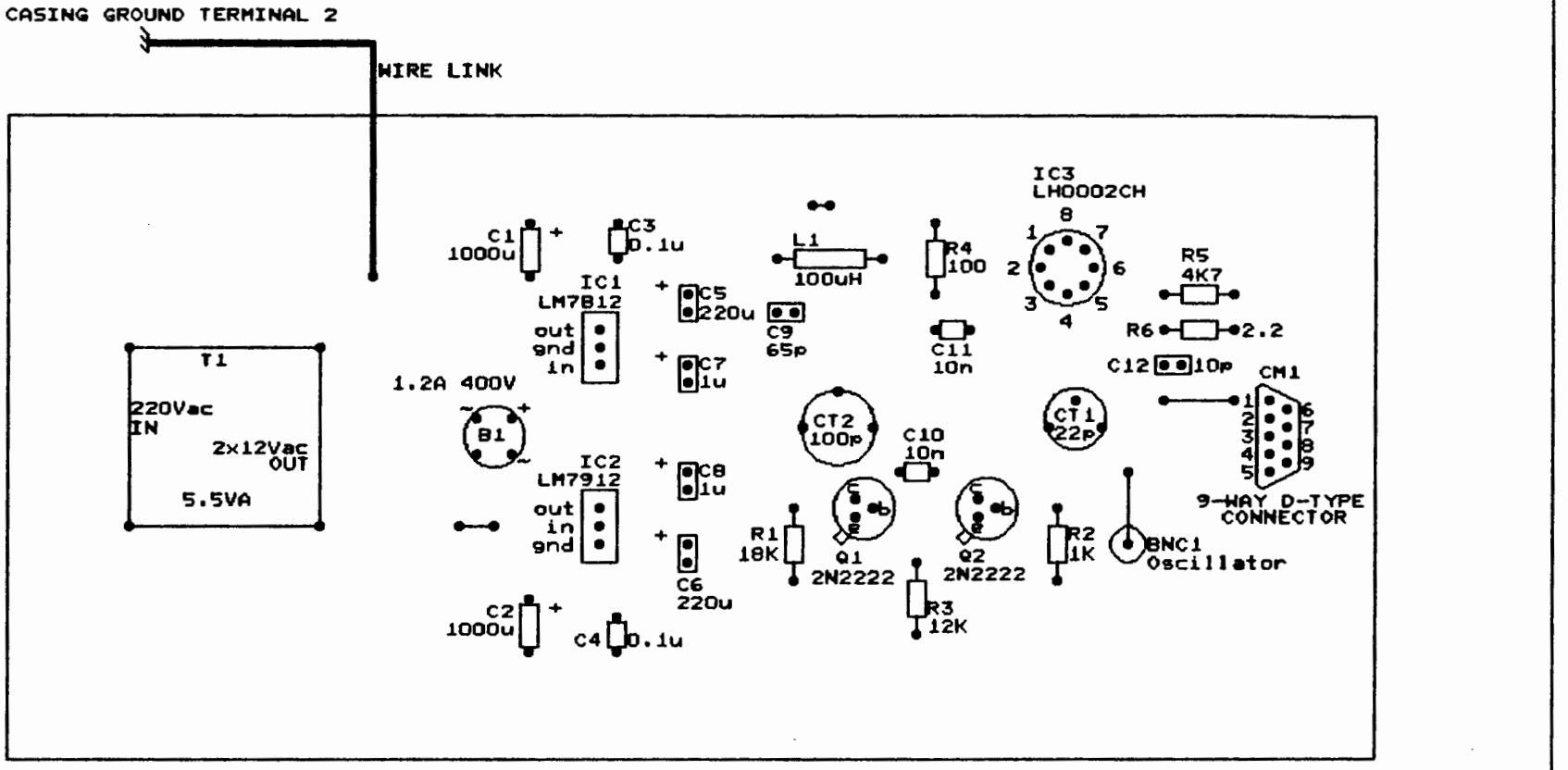

CASING GROUND TERMINAL 2
IS LOCATED ON MOUNTING PLATE
IN INSTRUMENT CASING
NEAR OSCILLATOR BOARD

MARK LAZARUS		
ULTRASONIC DOPPLER BED-LOAD VELOCIMETER		
Title: OSCILLATOR BOARD COMPONENT LAYOUT		
Size: A	Document Number: 6	REV: 1
Date: June 28, 1989	Sheet: 7 of 10	

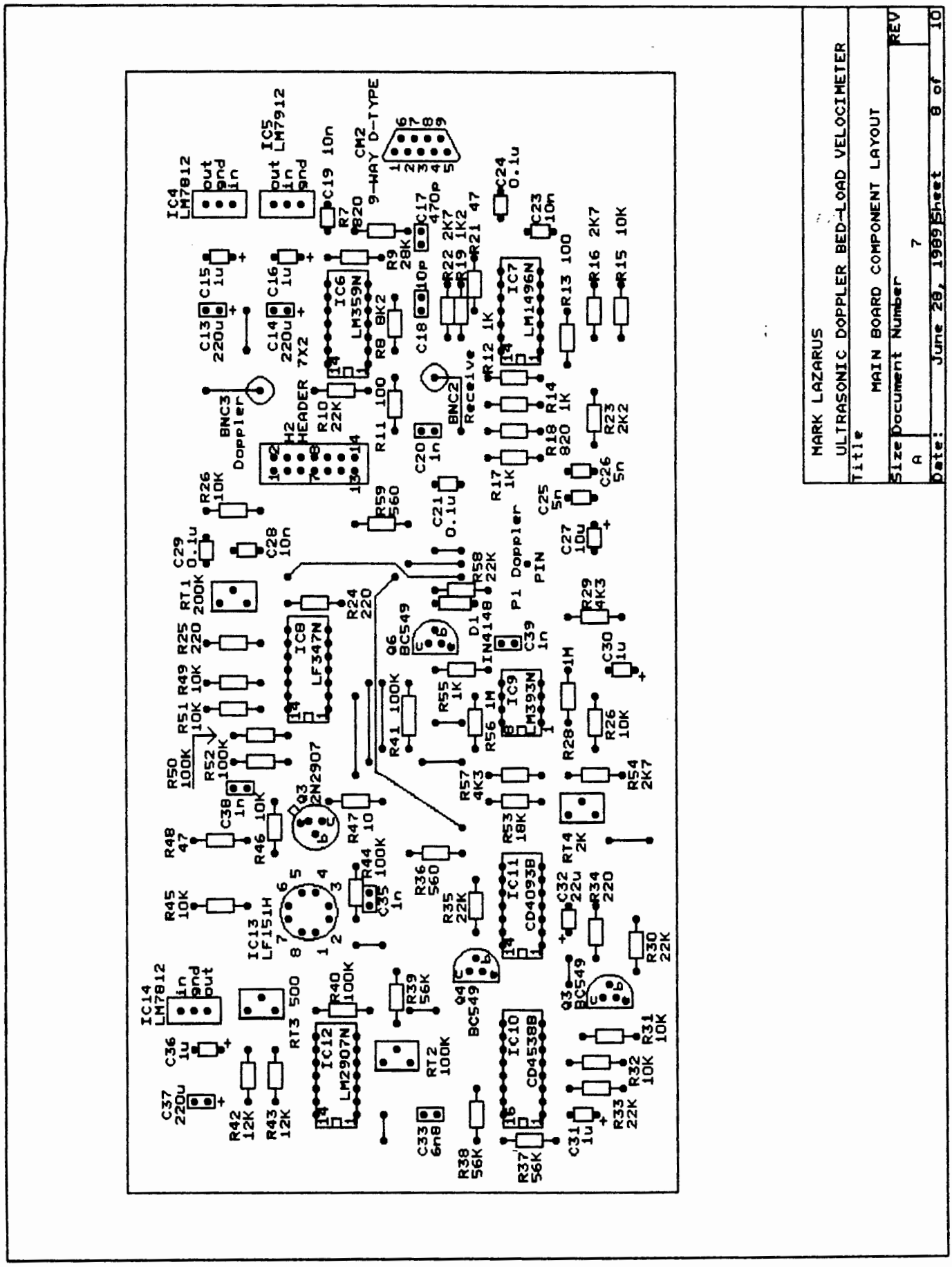
MARK LAZARUS
ULTRASONIC DOPPLER BED-LOAD VELOCIMETER
Title
MAIN BOARD COMPONENT LAYOUT
Size
A
Document Number
7
REV
Date: June 28, 1989 Sheet 8 of 10
IC4 LM7812
IC5 LM7912
CN2 9-WAY D-TYPE
IC6 LM359N
IC7 LM1496N
IC8 LF347N
IC9 LM393N
IC10 CD4538B
IC11 CD4093B
IC12 LM2907N
IC13 LF151H
IC14 LM7812
BNC2 Receive
BNC3 Doppler
H2 HEADER 7X2
P1 Doppler PIN
Q3 2N2907
Q4 BC549
Q6 BC549
D1 IN4148
RT1 200K
RT2 100K
RT3 500
RT4 2K

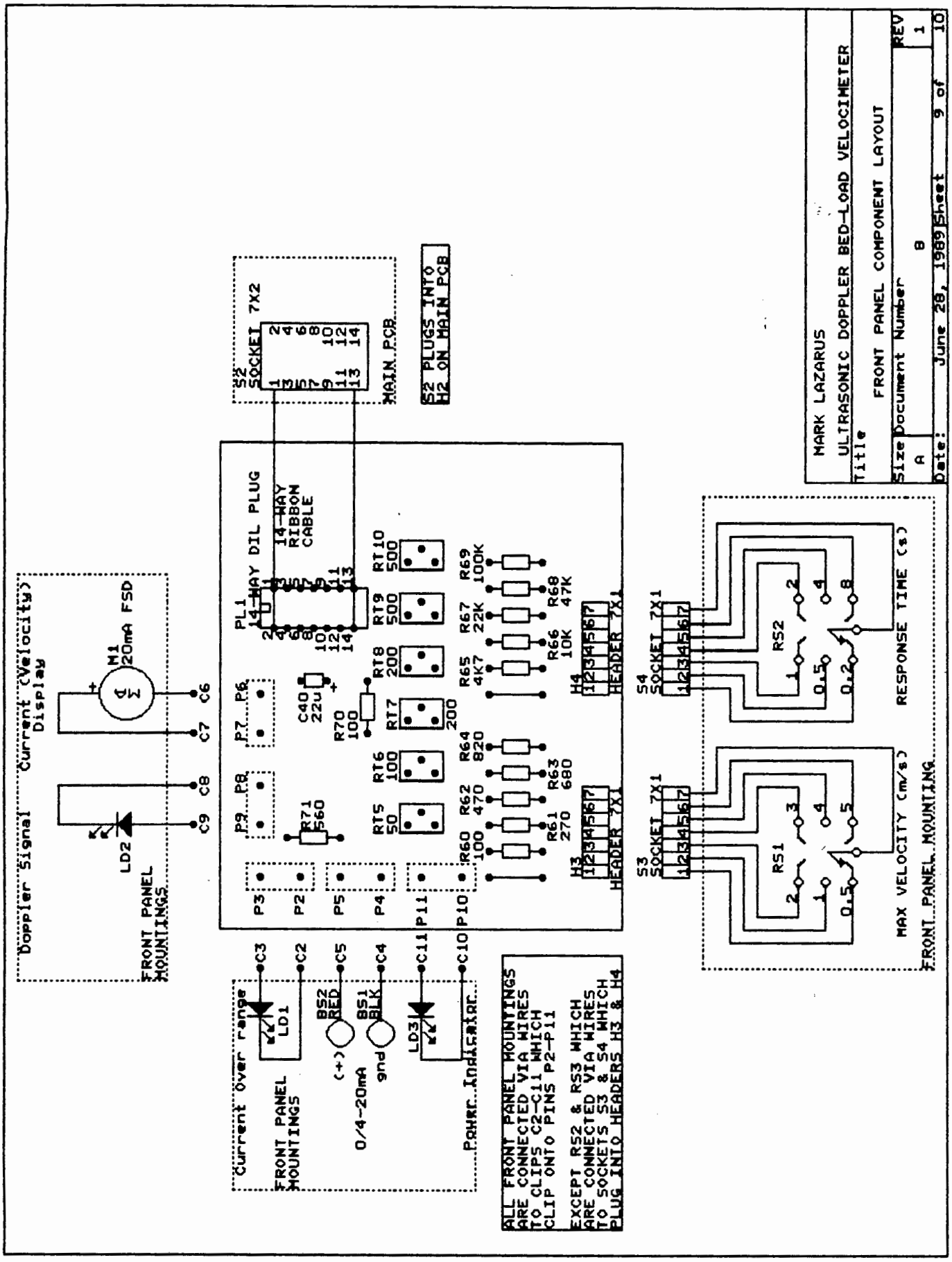
Doppler Signal Current (Velocity) Display
M1 20mA FSD
LD2
FRONT PANEL MOUNTINGS
C6 C7 C8 C9
P9 P8 P7 P6
P3 P2 P5 P4 P11 P10
R71 560
RT5 50
RT6 100
RT7 200
RT8 200
RT9 500
RT10 500
R70 100
C40 22u
R60 100
R62 470
R64 820
R61 270
R63 680
R65 4K7
R66 10K
R67 22K
R68 47K
R69 100K
PL1 14-WAY DIL PLUG
14-WAY RIBBON CABLE
S2 SOCKET 7X2
MAIN PCB
S2 PLUGS INTO H2 ON MAIN PCB
H3 HEADER 7X1
H4 HEADER 7X1
S3 SOCKET 7X1
S4 SOCKET 7X1
RS1
RS2
MAX VELOCITY (m/s)
RESPONSE TIME (s)
FRONT PANEL MOUNTING
Current over range
LD1
FRONT PANEL MOUNTINGS
C3 C2 C5 C4 C11 C10
BS2 RED (+)
BS1 BLK gnd
0/4-20mA
LD3
Power Indicator
ALL FRONT PANEL MOUNTINGS ARE CONNECTED VIA WIRES TO CLIPS C2-C11 WHICH CLIP ONTO PINS P2-P11
EXCEPT RS2 & RS3 WHICH ARE CONNECTED VIA WIRES TO SOCKETS S3 & S4 WHICH PLUG INTO HEADERS H3 & H4
MARK LAZARUS
ULTRASONIC DOPPLER BED-LOAD VELOCIMETER
Title
FRONT PANEL COMPONENT LAYOUT
Size A
Document Number
B
REV 1
Date: June 28, 1989
Sheet 9 of 10

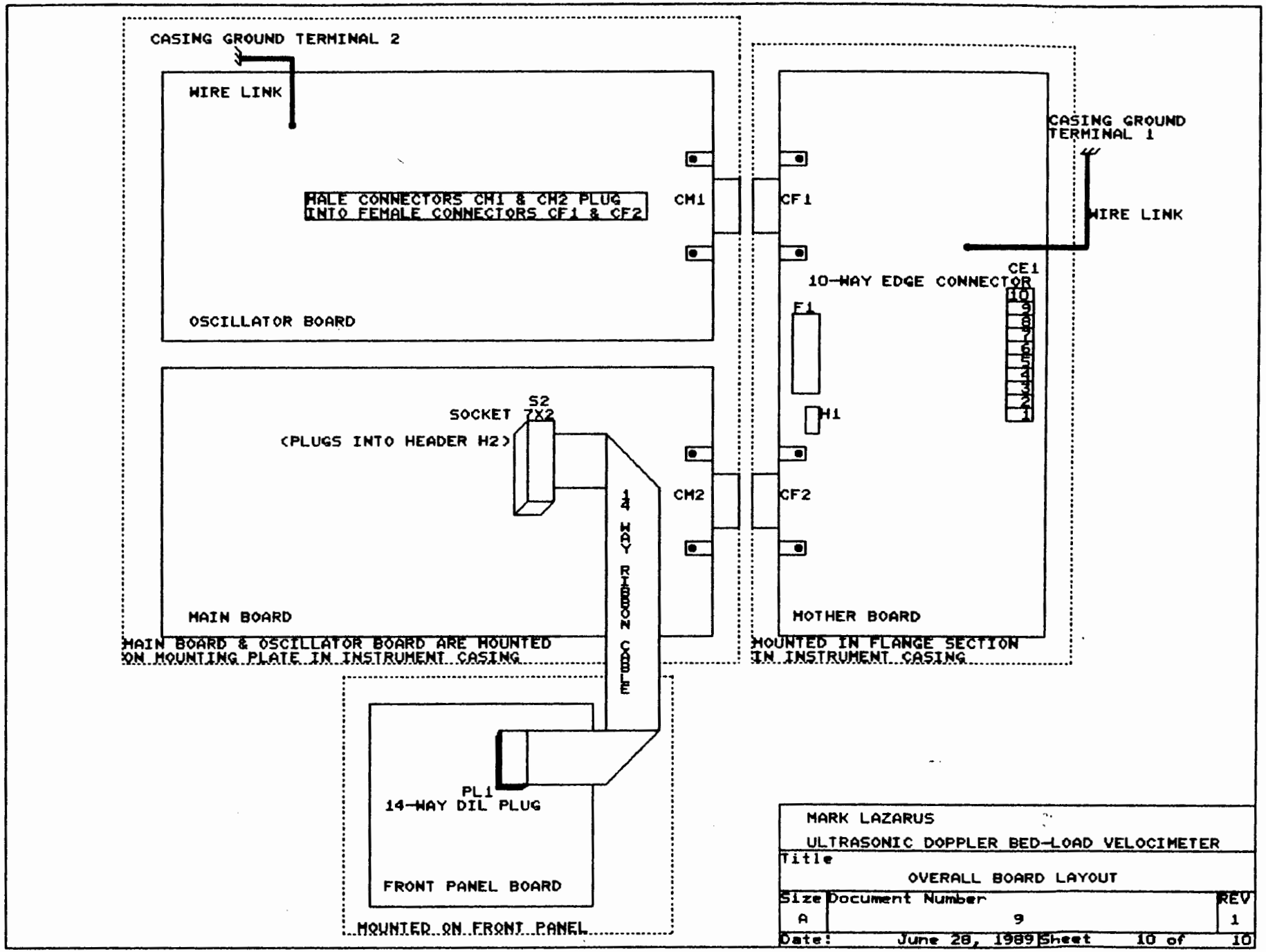

MARK LAZARUS		
ULTRASONIC DOPPLER BED-LOAD VELOCIMETER		
Title: OVERALL BOARD LAYOUT		
Size: A	Document Number: 9	REV: 1
Date: June 28, 1989	Sheet 10 of 10	

ULTRASONIC DOPPLER BED-LOAD VELOCIMETER COMPONENT LISTING

Note: Abbreviations used in the LOC(ation) column are as follows:

MAIN = Components on MAIN Circuit Board
OSC = Components on OSCILLATOR Circuit Board
FRONT = Components on FRONT PANEL Circuit Board
PANEL = Components Mounted on FRONT PANEL Plate

1. RESISTORS

Note: (1) All Resistors are carbon, 1/4 W, 10%, unless otherwise stated.
(2) Rz = RT2 + R39

REF.	VALUE	LOC.	REF.	VALUE	LOC.
R1	18K	OSC	R36	560	MAIN
R2	1K	OSC	R37	56K	MAIN
R3	12K	OSC	R38	56K	MAIN
R4	100	OSC	R39	200K	MAIN
R5	4K7	OSC	R40	100K	MAIN
R6	2.2	OSC	R41	100K	MAIN
R7	820	MAIN	R42	12K (1%)	MAIN
R8	8K2	MAIN	R43	12K (1%)	MAIN
R9	28K	MAIN	R44	100K	MAIN
R10	22K	MAIN	R45	10K	MAIN
R11	100	MAIN	R46	10K	MAIN
R12	1K	MAIN	R47	10	MAIN
R13	100	MAIN	R48	47	MAIN
R14	1K	MAIN	R49	10K	MAIN
R15	10K	MAIN	R50	100K	MAIN
R16	2K7	MAIN	R51	10K	MAIN
R17	1K	MAIN	R52	100K	MAIN
R18	820	MAIN	R53	18K	MAIN
R19	1K2	MAIN	R54	2K7	MAIN
R20	100	MAIN	R55	1K	MAIN
R21	47	MAIN	R56	1M	MAIN
R22	2K7	MAIN	R57	4K3	MAIN
R23	2K2	MAIN	R58	22K	MAIN
R24	220	MAIN	R59	560	MAIN
R25	220	MAIN	R60	100	FRONT
R26	10K	MAIN	R61	270	FRONT
R27	10K	MAIN	R62	470	FRONT
R28	1M	MAIN	R63	680	FRONT
R29	4K3	MAIN	R64	820	FRONT
R30	22K	MAIN	R65	4K7	FRONT
R31	10K	MAIN	R66	10K	FRONT
R32	10K	MAIN	R67	22K	FRONT
R33	22K	MAIN	R68	47K	FRONT
R34	220	MAIN	R69	100K	FRONT
R35	22K	MAIN	R70	100	FRONT

2. CAPACITORS

REF.	VALUE	VOLTAGE	TYPE	BOARD
C1	1000u	25V	electrolytic	OSC
C2	1000u	25V	electrolytic	OSC
C3	0.1u	63V	polyester (WIMA)	OSC
C4	0.1u	63V	polyester (WIMA)	OSC
C5	220u	25V	electrolytic	OSC
C6	220u	25V	electrolytic	OSC
C7	1u	35V	tantalum	OSC
C8	1u	35V	tantalum	OSC
C9	150p		ceramic	OSC
C10	10n	63V	polyester (WIMA)	OSC
C11	10n	63V	polyester (WIMA)	OSC
C12	10p		ceramic	OSC
C13	220u	25V	electrolytic	MAIN
C14	220u	25V	electrolytic	MAIN
C15	1u	35V	tantalum	MAIN
C16	1u	35V	tantalum	MAIN
C17	470p		ceramic	MAIN
C18	10p		ceramic	MAIN
C19	10n	63V	polyester (WIMA)	MAIN
C20	1n		ceramic	MAIN
C21	0.1u	63V	polyester (WIMA)	MAIN
C22	0.1u	63V	polyester (WIMA)	MAIN
C23	10n	63V	polyester (WIMA)	MAIN
C24	0.1u	63V	polyester (WIMA)	MAIN
C25	5n	100V	polyester (WIMA)	MAIN
C26	5n	100V	polyester (WIMA)	MAIN
C27	10u	25V	electrolytic	MAIN
C28	10n	63V	polyester (WIMA)	MAIN
C29	7n2		ceramic	MAIN
C30	1u	25V	electrolytic	MAIN
C31	1u	35V	tantalum	MAIN
C32	22u	16V	tantalum	MAIN
C33	3n		ceramic	MAIN
C34	1u	35V	tantalum	MAIN
C35	1n		ceramic	MAIN
C36	1u	35V	tantalum	MAIN
C37	220u	25V	electrolytic	MAIN
C38	1n		ceramic	MAIN
C39	1n		ceramic	MAIN
C40	22u	16V	tantalum	FRONT

3. TRIMMER RESISTORS (POTENTIOMETERS)

REF.	VALUE	BOARD	DESCR.	REF.	VALUE	BOARD	DESCR.
RT1	200K	MAIN	Dop. Gain	RT6	100	FRONT	vMAX trim
RT2	100K	MAIN	Calibrate	RT7	200	FRONT	vMAX trim
RT3	500	MAIN	Ios adj.	RT8	200	FRONT	vMAX trim
RT4	2K	MAIN	Vref adj.	RT9	500	FRONT	vMAX trim
RT5	50	FRONT	vMAX trim	RT10	500	FRONT	vMAX trim

4. SEMI-CONDUCTORS (TRANSISTORS & DIODES & LEDs)

REF.	VALUE	TYPE	BOARD
Q1	2N2222	NPN	OSC
Q2	2N2222	NPN	OSC
Q3	2N2907	PNP	MAIN
Q4	BC549	NPN	MAIN
Q5	BC549	NPN	MAIN
Q6	BC549	NPN	MAIN
D1	IN4148		MAIN
LD1	20mA, 5mm	(RED)	PANEL
LD2	20mA, 5mm	(RED)	PANEL
LD3	20mA, 5mm	(RED)	PANEL
LD4	20mA, 5mm	(RED)	PANEL

5. INTEGRATED CIRCUITS

REF.	VALUE	DESCRIPTION	BOARD
IC1	LM7812	+12V Series Voltage Regulator	OSC
IC2	LM7912	-12V Series Voltage Regulator	OSC
IC3	LH0002CH	Hybrid Current Amplifier	OSC
IC4	LM7812	+12V Series Voltage Regulator	MAIN
IC5	LM7912	-12V Series Voltage Regulator	MAIN
IC6	LM359N	Programmable Current Mode (Norton) A	MAIN
IC7	LM1496N	Balanced Modulator-Demodulator	MAIN
IC8	LF347N	Quad JFET Input Operational Amplifie	MAIN
IC9	LM393N	Low Power Low Offset Comparator	MAIN
IC10	CD4538B	Dual Monostable Multivibrator	MAIN
IC11	CD4093B	Quad 2-Input NAND Schmidt Trigger	MAIN
IC12	LM2907N	Frequency to Voltage Converter	MAIN
IC13	LF151H	JFET Input Operational Amplifier	MAIN
IC14	LM7812	+12V Series Voltage Regulator	MAIN

6. MISCELLANEOUS

REF.	DESCRIPTION	BOARD
CE1	10-Way Edge Connector (5.08mm pitch)	MOTHER
CF1	9-Way D-Type Female Edge Connector	MOTHER
CF2	9-Way D-Type Female Edge Connector	MOTHER
F1	20 mm Fuse Holder	MOTHER
H1	4-Way Locking Straight Header (2.54mm pitch)	MOTHER
S1	4-Way Socket (2.54mm pitch)	MOTHER
B1	Diode Bridge Rectifier 1.2A, 400V	OSC
BNC1	BNC Socket, 50ê, Chassis-mount	OSC
CM1	9-Way D-Type Male Edge Connector	OSC
CT1	Trimmer Capacitor 1.8 - 22 pF	OSC
CT2	Trimmer Capacitor 7 - 100 pF	OSC
L1	Inductor 100uH	OSC
T1	Transformer 220V - 2 x 12V, 2 x 225mA, 5.4VA	OSC
BNC2	BNC Socket, 50Ω, Chassis-mount	MAIN
BNC3	BNC Socket, 50Ω, Chassis-mount	MAIN
H2	14-Way Straight Ribbon Cable Header	MAIN
L	Inductor 13uH	MAIN
P1	PC Pin, Double Sided, 1.5mm Diameter	MAIN
S2	14-Way Ribbon Cable Socket	MAIN
C2-C11	Slide-on Clip Terminal	FRONT
H3	7-Way Locking Straight Header (2.54mm pitch)	FRONT
H4	7-Way Locking Straight Header (2.54mm pitch)	FRONT
P2-P11	PC Pin, Double Sided, 1.5mm Diameter	FRONT
PL1	14-Way DIL Ribbon Cable Plug	FRONT
S3	7-Way Socket (2.54mm pitch)	FRONT
S4	7-Way Socket (2.54mm pitch)	FRONT
BS1	Banana Socket (Black), 4mm	PANEL
BS2	Banana Socket (Red), 4mm	PANEL
M1	20mA Panel Meter	PANEL
RS1	6-Way Rotary Switch	PANEL
RS2	6-Way Rotary Switch	PANEL
SW1	DPST Toggle Switch	PANEL

I. DESCRIPTION OF TRIMMER RESISTORS (POTENTIOMETERS)

Note: All Trimmer Resistors have been adjusted under Laboratory test conditions to ensure that the Ultrasonic Doppler Bed-load Velocimeter (UDBV) provides an accurate indication of the Bed-load particle velocity (or pipe-wall particle velocity, depending on location of transducer) for Rossing's 450mm, polyurethane lined, Tailings line, if the transducer is attached to the specially designed spoolpiece.

There is no need for further adjustments of the Trimmer Resistors.

1. REFERENCE	LOCATION	NAME
RT1	MAIN BOARD	Doppler Gain

FUNCTION: Adjusts gain setting of the Demodulated Doppler signal so that only Bed-Load particle motion is detected.

SETTING: If set too high then Doppler signals due to particle motion above the bed-load will be detected. If adjusted too low then Bed-load particle motion will not be detected.

An Hydraulic test-rig is required for set-up procedure. RT1 is turned to its maximum setting (fully Clockwise). A condition within the test-rig is set up so that the insipient settling bed-load velocity is achieved while particles above the bed are in motion. RT1 is now reduced (by turning Anti-clockwise) until the Doppler Signal LED (see Operators Manual Ver 2.0) just begins to be extinguished.

2. REFERENCE	LOCATION	NAME
RT2	MAIN BOARD	Calibration Setting

FUNCTION: Adjusts conversion between the Doppler frequency and the voltage output of the frequency to voltage converter (IC12) ie. the calibration of the UDBV.

SETTING: Adjustment is made by using an independant method of measuring the bed-load velocity of slurry in a test-rig. This method is the Cross-correlation method with Resistivity Probes. The

Bed-load velocities detected this way for a range of mean velocities is used to set the Calibration Setting. This setting has been made for the Ultrasonic Transducer of the UDBV attached to a sample of Rossing's Tailings Spoolpiece.

3. REFERENCE	LOCATION	NAME
RT3	MAIN BOARD	0/4 mA Setting

FUNCTION: Adjusts Current Output corresponding to a zero Bed-load Velocity condition.

SETTING: Adjustment is made by sensing the Current Output with an ammeter. Adjustment can be made with the transducer unconnected. The adjustment is made so that the Current Output of the UDBV is 4 mA.

4. REFERENCE	LOCATION	NAME
RT4	MAIN BOARD	Over Range Setting

FUNCTION: Adjusts the trigger value that will cause the Over Range LED to light up.

SETTING: Adjustment is made so that the Over Range LED lights up when the Current Output equalls or exceeds 20 mA.

5. REFERENCE	LOCATION	NAME
RT5-10	FRONT BOARD	v_{MAX} Setting

FUNCTION: Adjusts the scaling of the Output Current for different v_{MAX} (Front Panel) settings.

RT5 adjusts the Current scaling when v_{MAX} = 0.5m/s
RT6 " " " " " " 1 m/s
RT7 " " " " " " 2 m/s
RT8 " " " " " " 3 m/s
RT9 " " " " " " 4 m/s
RT10 " " " " " " 5 m/s

SETTING: Adjustment is made by providing a fixed test frequency from a signal generator to the Doppler Pin (P1, Main Board). First Vmax is set to 0.5 m/s. The frequency is adjusted so that the Output Current is exactly 20 mA. The test

frequency corresponds to a Doppler signal from a 0.5 m/s Bed-load velocity.

To adjust RT6, the v_{MAX} setting is set to 1 m/s. The Output Current should be:

$(16 \cdot v_{BED} / v_{MAX}) + 4 = (16 \cdot 0.5 / 1) + 4 = 12$ mA; (see Operators Manual, Ver 2.0). Trimmer Resister, RT6 is then adjusted so that the Output Current is 12 mA.

To adjust RT7, the v_{MAX} setting is set to 2 m/s. The Output Current should be:

$(16 \cdot 0.5) / 2) + 4 = 8$ mA. RT7 is then adjusted so that the Output Current is 8 mA.

The same applies to RT8, RT9 and RT10. To adjust RT8, RT9 and RT10 respectively, v_{MAX} is set to 3,4 and 5 m/s respectively. The respective Output Currents for each case should be 6.666mA, 6 mA and 5.60 mA.

II. DESCRIPTION OF TRIMMER CAPACITORS

1. REFERENCE	LOCATION	NAME
CT1	OSCILLATOR BOARD	Fine Tuning

FUNCTION: Adjusts the tuning of the transmitter oscillator frequency for fine tuning, in the range ±20kHz.

OPERATION: Turn Clockwise to increase operating frequency and Anti-clockwise to decrease.

2. REFERENCE	LOCATION	NAME
CT2	OSCILLATOR BOARD	Course Tuning

FUNCTION: Adjusts the tuning of the transmitter oscillator frequency for course tuning, in the range ±120kHz.

OPERATION: Turn Clockwise to increase operating frequency and Anti-clockwise to decrease.

III. DESCRIPTION OF BNC SOCKETS

Note: The BNC sockets provide test points on the circuit boards. They may be connected via a coaxial cable to be observe test signals on an oscilloscope. The transducer (and transducer coaxial cables) may be disconnected while conducting tests.

1. REFERENCE	LOCATION	NAME
BNC1	OSCILLATOR BOARD	Transmitted Signal

FUNCTION: Test point for transmitter signal from Oscillator Board.

OPERATION: For correct operation this signal should be oscillating at between 850 kHz and 1150 kHz. The frequency of oscillation may be adjusted by adjusting either trimmer capacitors on the Oscillator Board. (see Section II above).

The peak to peak amplitude of the oscillating signal should be approximately 15V pp.

2. REFERENCE	LOCATION	NAME
BNC2	MAIN BOARD	Received Signal

FUNCTION: Test point of Received Signal on Main Board.

OPERATION: For correct operation, with transducers disconnected, this signal should resemble the transmitted signal frequency with a considerably smaller amplitude. The amplitude should be approximately 150-250mV peak to peak.

3. REFERENCE	LOCATION	NAME
BNC3	MAIN BOARD	Doppler Signal

FUNCTION: Test point of demodulated Doppler signal.

OPERATION: This test point is used in conjunction with PC Pin, P1, on the Main Board. This pin should be driven by a signal from a signal generator to simulate a Doppler signal. The signal injected to P1 should be set to between 100Hz and 5kHz with an amplitude of approximately 40mV.

The signal at BNC3 can be observed on an oscilloscope. It should be an amplified and filtered version of the signal being injected at P1. The gain of the amplifier has been set up to be 350.

By varying the frequency injected by the signal generator, so the frequency of the signal at BNC3 should vary. Also, the Current Output from the UDBV may be sensed and observed to vary in accordance with the frequency of the injected signal.

Other circuit modules may also be checked by this method. For example, the Doppler Signal LED (Front panel) should flash at frequencies bellow 30Hz. It should be fully on at frequencies exceeding 30 Hz.

APPENDIX D

AN EXAMPLE OF THE "QUATRO" SPREADSHEET USED FOR DETERMINING THE BEAM INTENSITY AT LOCATIONS WITHIN THE SLURRY FROM WHICH THE PENETRATION CONSTANT CAN BE CALCULATED FOR VARIOUS FOCUSING PARAMETERS

TRANSDUCER CONSTANTS				
freq.	vel.	radius	vel rat.	wave no.
f_T {kHz}	c_{TW} {m/s}	r {mm}	c_{SL}/c_{TW}	k
1000	2400	5	0.75	2618

FOCUSING PARAMETERS		
path len	Tx	b.w.
d {mm}	θ	ø
20	30	17

h {mm}: 2.00

Attenuation (α) {dB/mm}: -0.26
Atten. Loss AT {dB}: -1.56

$\delta\varphi_R$ {°}	$\delta\varphi_T$ {°}	$\delta f_D / f_D$ {ratio}	DI_F {dB}	AI_F {dB}	I(H)/I(0) {ratio}	TL_P {dB}
-17.01	-16.85	1.46	-95.6	-4.7	0.000000	-101.91
-13.61	-13.45	1.38	-27.4	-5.1	0.000389	-34.10
-10.21	-10.50	1.29	-13.8	-5.5	0.008036	-20.95
-6.81	-7.92	1.21	-6.6	-5.9	0.039326	-14.05
-3.40	-5.63	1.12	-2.5	-6.3	0.091452	-10.39
-0.00	-3.58	1.03	-0.7	-6.7	0.126917	-8.96
3.40	-1.73	0.95	-0.6	-7.0	0.119091	-9.24
6.81	-0.03	0.86	-2.7	-7.4	0.067575	-11.70
10.21	1.53	0.78	-6.7	-7.7	0.025058	-16.01
13.61	2.99	0.70	-14.5	-8.1	0.003843	-24.15
17.01	4.35	0.62	-53.3	-8.4	0.000000	-63.25

APPENDIX E

Circuit Diagram of cross-correlator Interface circuitry

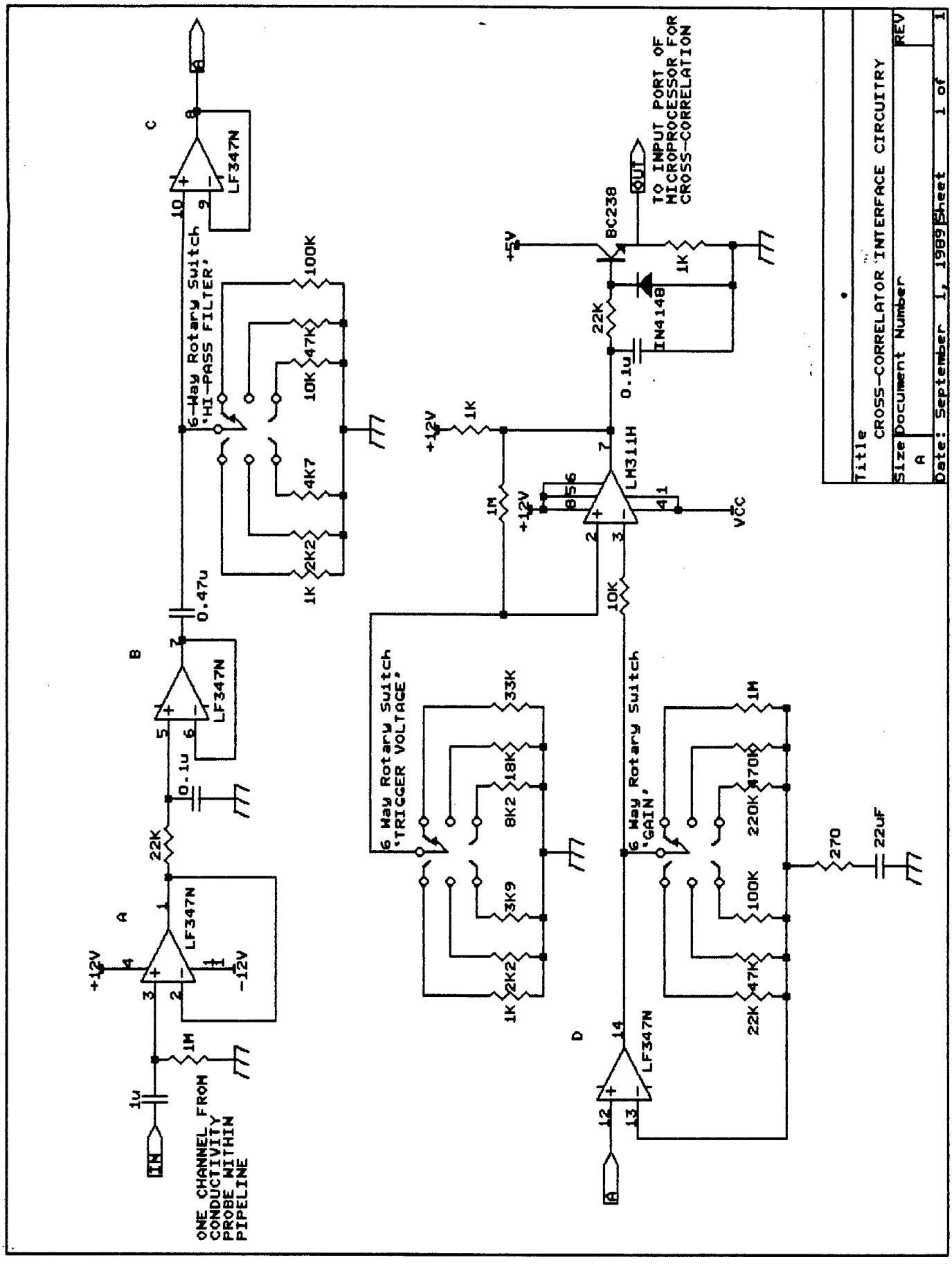
ONE CHANNEL FROM CONDUCTIVITY PROBE WITHIN PIPELINE
IN
1u
1M
LF347N
A
+12V
-12V
22K
0.1u
LF347N
B
0.47u
6-Way Rotary Switch 'HI-PASS FILTER'
100K
47K
10K
4K7
2K2
1K
LF347N
C
OUT
6 Way Rotary Switch 'TRIGGER VOLTAGE'
33K
18K
8K2
3K9
2K2
1K
6 Way Rotary Switch 'GAIN'
1M
470K
220K
100K
47K
22K
LF347N
D
270
22uF
+5V
BC238
1K
22K
IN4148
0.1u
TO INPUT PORT OF MICROPROCESSOR FOR CROSS-CORRELATION
+12V
1K
1M
LM311H
VCC
10K
Title
CROSS-CORRELATOR INTERFACE CIRCUITRY
Size
A
Document Number
REV
Date: September 1, 1989
Sheet 1 of 1

APPENDIX F

Table of Results from Cross-Correlator and from UDBV (before calibration and after calibration) as functions of the mean mixture velocity

RESULTS FROM THE UDBV AND THE CROSS-CORRELATOR FOR CALIBRATION

The table below (table F.1) tabulates readings taken from the UDBV and from the cross-correlator for a range of mean mixture velocities in the 140mm diameter PVC test loop in the Hydrotransport Research of the Civil Engineering Department. The tests were conducted with a slurry having a transport volumetric concentration of papproximately 50%. The solid particle material was ordinary sand quartz with a mean solid particle diameter of approximately 500μm.

The mean mixture velocity was measured with a Khrone Magnetic meter and is tabulated in the first colum of Table F.1 The second column are the position of the peaks of the cross-correlator averaged for approximately six readings. Column three converts the peak position to a bed-load velocity using Eqn. 7.2 Column four are the average output current [Iout] readings taken from the UDBV before calibration. The setting of v_{MAX} is 2m/s. The offset current [Ios] is set to 4mA, so that the conversion from Iout to v_{BED} is as follows (see Operators manual, Appendix G):

$$v_{BED} = 2 \cdot (Iout-4) \; / \; 16 \qquad (F.1)$$

The last column in Table F.1 are the readings taken from the UDBV after being calibrated and converted to v_{BED}'. It is expressed as v_{BED}' to signify that the readings are calibrated. The calibration in this case is simply:

$$v_{BED}' = 1.7 \cdot v_{BED} \qquad (F.2)$$

MAGNETIC METER	CROSS-CORRELATOR		ULTRASONIC DOPPLER BED-LOAD VELOCIMETER		
v_M	Peak	v_{BED}	Iout	v_{BED}	v_{BED}'
2.00	No peak	0.00	4.00	0.00	0.00
2.10	42.00	0.89	6.00	0.25	0.42
2.22	38.94	0.96	8.64	0.58	0.99
2.43	33.08	1.13	9.92	0.74	1.25
2.48	30.90	1.21	10.40	0.80	1.36
2.59	27.09	1.38	10.64	0.83	1.41
2.74	24.92	1.50	11.28	0.91	1.55
2.83	23.22	1.61	11.60	0.95	1.61
3.00	19.88	1.88	12.80	1.10	1.87
3.08	18.69	2.00	12.96	1.12	1.90
3.19	18.15	2.06	13.28	1.16	1.97
3.23	17.97	2.08	13.60	1.20	2.04
3.36	17.31	2.16	14.24	1.28	2.18
3.40	16.99	2.20	14.40	1.30	2.21
3.57	15.45	2.42	14.72	1.34	2.28
3.61	15.26	2.45	14.88	1.36	2.31

Table F.1 Data of bed-load velocities taken with cross-correlator and with UDBV for various mean velocities

The bed-load velocities [v_{BED}] measured with the cross-correlator (column 3) and v_{BED}', the calibrated measurement from the UDBV (column six) are plotted as a function of the mean mixture velocity [v_M] (column one) in Fig. 7.6 and are seen to resemble each other closely as expected.

APPENDIX G

OPERATORS MANUAL

ULTRASONIC DOPPLER BED-LOAD VELOCIMETER [Ver 2.0]

OPERATORS MANUAL

I. GENERAL INFORMATION

The instrument provides an accurate and rapid indication of the bed-load particle velocity of slurry transported down Rossing's lined, steel tailings line. The instrument consists of an Electronic Processing Unit connected to the transducer via two coaxial cables. The transducer is attached by means of either Silicone Sealant (temporary or permanent) or Araldite Epoxy (permanent) to a specially designed Polyurethane-lined, steel spool-piece. The system is calibrated to measure the exact bed-load particle velocity with this spool-piece and provide an indication of the velocity by means of a 4-20 mA output current which may be remotely sensed.

II. INSTALLATION

With reference to Fig. 1, the detachable terminal block under the front gland of the Electronic Processing Unit consists of 10 terminals for external connections:

1 : Ground
2 : Positive — 4 - 20 mA output current

3 : Ground
4 : Live — Receiver

5 : Ground
6 : Live — Transmitter

7 : Ground (No connection)

8 : Neutral
9 : Earth
10 : Live — 220 Vac Mains

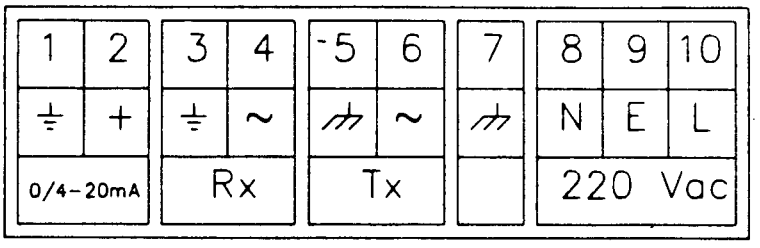

NB! 1. SWITCH OFF AT MAINS BEFORE REPLACING FUSE!!
2. 0/4-20mA CURRENT IS SENSED AT EITHER TERMINALS 1&2 OR AT FRONT PANEL SOCKETS.

Fig. 1. Terminal Block Connections

1. Mains Power Lead

Ensure that the mains power lead is connected to terminals 8 (Neutral : blue), 9 (Earth : yellow/green), 10 (Live : red) of the terminal block. Mains Supply is 220 Vac. (< 5A).

2. Transducer

Ensure that the transducer comprising the receiver (Rx) and transmitter (Tx) is connected to the Electronic Processing Unit via two 50 Ω co-axial cables (20 metres in length) as follows:

One end of each co-axial cable is connected to each BNC socket on the transducer, the other end of each is connected to the terminal block.

Note: The transmitter and receiver BNC sockets on the transducer may be interchanged ie. EITHER BNC socket may be used as the transmitter and receiver.

Receiver ground (outer shield of co-ax) to terminal 3.
Receiver live (inner core of co-ax) to terminal 4.

Transmitter ground (outer shield) to terminal 5.
Transmitter live (inner core) to terminal 6.

3. 4-20 mA Output Current Sensing

The instrument converts a bed-load velocity into a current. The current may be sensed by any ammeter (multimeter) capable of measuring currents in the range of 0 to 20 mA. Sensing is at EITHER:

(i) 4-20 mA output current sockets on front panel (red: +ve, black: gnd)

(ii) Between terminals 1 (gnd) and 2 (+ve) on the terminal block.

Notes:

1. Ensure that the impedance of the cable or wire of the positive and ground connections is less than 500 Ω in total.

2. The current may be sensed at EITHER 3 (i) or (ii) above.

3. If voltage remote sensing is required, then a resistor may be tied between either of the current out connections. The resistor value must be less than 500 Ω providing a maximum voltage output range from 0 V to 10 V referenced to ground of the instrument.

4. If a voltage remote sensing arrangement is used then ensure that the 'Over-Range' LED indicator on the front panel (see III 5.3) does not illuminate. This is especially important when a large resistor (≈ 500 Ω) is being used. The voltage output must not exceed 10 V. If the voltage output does exceed 10 V then either:

   (i) use a lower value resistor.

   (ii) adjust the 'Max Velocity' setting on the front panel (see III 4.1) to a larger value.

III. INSTRUMENT DETAILS

The instrument details pertain to switches, sockets, indicators and the analogue panel meter etc. located on the front panel of the instrument as illustrated in Fig. 2.

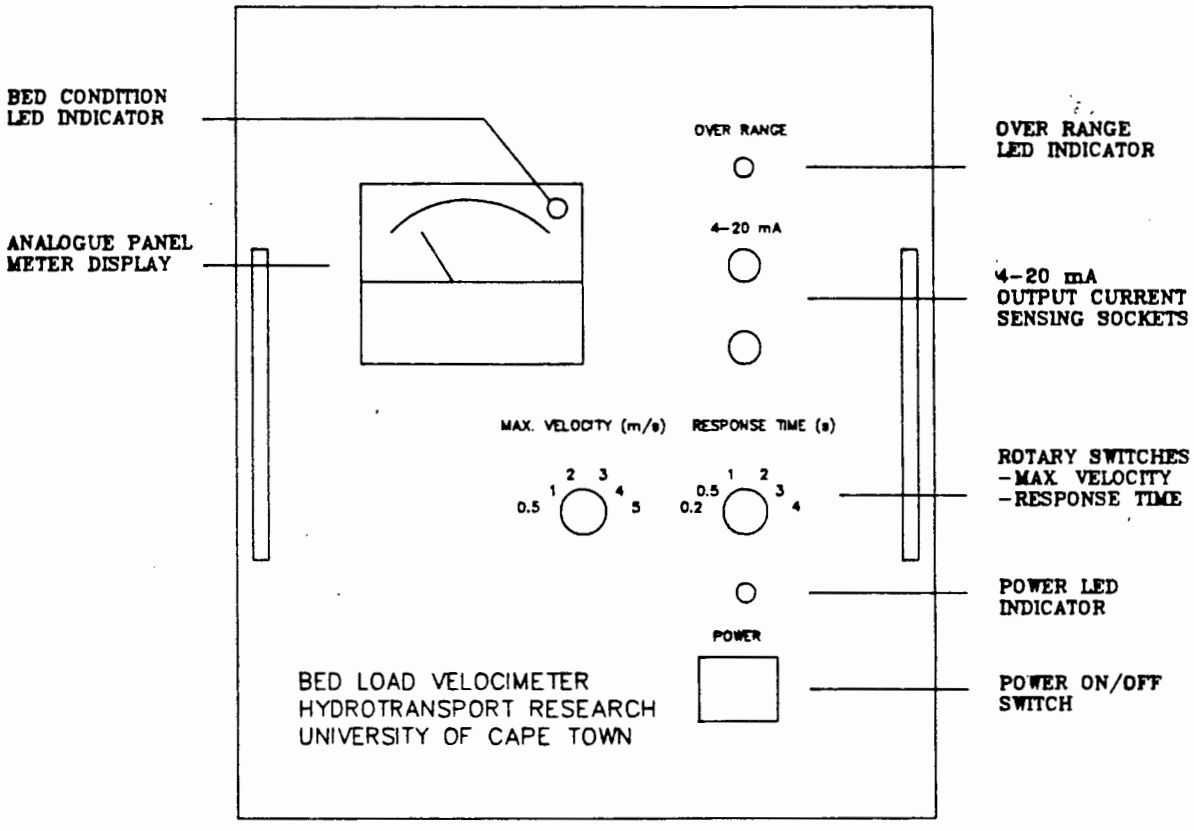

Fig. 2. Front Panel Layout

1. Power Switch

On / Off Mains power switch.

Note: When switching instrument on, allow approximately 30 minutes 'warm-up' time before accurate results are taken.

2. 4-20 mA Output Current Sensing Sockets

The instrument provides an output current to represent a bed-load velocity. The output current may be sensed at the 4-20 mA sockets.

A 4 mA output current always represents a zero bed-load velocity. A 20 mA output current represents the maximum detectable velocity. This maximum detectable velocity may be adjusted with the 'Max Velocity' Rotary Switch (see III 4.1). For example, if the 'Max Velocity' is set to 2 m/s then a 20 mA output current represents 2 m/s.

The bed-load velocity (v_{BED}) may be calculated from the ouput current (Iout) as follows (where v_{MAX} is the 'Max Velocity' setting):

$$v_{BED} = \frac{(\text{Iout} - 4\ \text{mA})}{16\ \text{mA}} \times v_{MAX}$$

eg. if Iout = 12 mA and Vmax is set to 2 m/s then the bed-load velocity (v_{BED}) is equal to:

$$V_{BED} = \frac{(12\ \text{mA} - 4\ \text{mA})}{16\ \text{mA}} \times 2\ \text{m/s} = 1\ \text{m/s}$$

Note: When determining the bed-load velocity from the output current (Iout), 4 mA must be subtracted from Iout to account for the 4 mA offset for a zero bed-load velocity. Also, Iout ranges from 4 to 20 mA which is a span of 16 mA, hence the division by 16 mA in the above equations.

3. Analogue Panel Meter Display

The analogue panel meter provides a display of the 4-20 mA ouput current as a percentage of the full scale deflection (FSD) of the meter. FSD (100%) represents a 20 mA output current.

Any output current in the range of 0 to 20 mA is represented as a percentage. If Iout is the output current, then the meter displays this current as a percentage as follows:

$$\text{Meter \%} = \frac{\text{Iout}}{\text{20 mA}} \times 100\%$$

eg. if Iout = 10 mA then Meter % is equal to:

$$\text{Meter \%} = \frac{\text{10 mA}}{\text{20 mA}} \times 100\% = 50\%$$

The 4 mA output current for a zero bed-load velocity (ie. stationary bed) is represented by 20% as follows:

$$\text{Meter \%} = \frac{\text{4 mA}}{\text{20 mA}} \times 100\% = 20\%$$

4. Rotary Switches

Two rotary-switches allow adjustments to be made in the measurement of the bed-load velocity.

4.1. Max Velocity (m/s) Setting

The 'Max Velocity' setting provides for six disrete maximum velocity settings as follows:

0.5, 1, 2, 3, 4, 5 m/s.

It allows bed-load velocities that lie in different ranges to be accurately determined. The 'Max Velocity' should be set to a value exceeding the highest expected bed-load velocity. Higher values allow a wider range of velocities to be measured. Lower values allow a particular bed-load velocity to be more accurately determined.

4.2. Response Time (s) Setting

The 'Response Time' setting provides for six discrete response time settings as follows:

0.2, 0.5, 1, 2, 4, 8 seconds

A longer (slower) response time performs more velocity averages, wheras a shorter (quicker) response time provides a quicker response to changing bed-load

velocities. A quicker response time is usually used to 'observe' a pulsating bed.

5. LED Indicators

Three Light Emitting Diode (LED) indicators represent the status of the instrument.

5.1. Power

The Power LED will illuminate when the system obtains power from the mains.

5.2. Bed Condition

The 'Bed Condition' LED provides information about the bed-load.

(i) The LED will be extinguished when a stationary bed exists (ie bed particles are settled).

(ii) The LED will flash when the bed begins to settle.

A slower rate of flashing signifies longer periods of settling.
A quicker rate of flashing signifies more bed-load particles beginning to move.

(iii) The LED will illuminate when all the bed-load particles are in motion.

5.3. Over-range

The 'Over-range' LED provides information about the current output from the instrument. For correct operation, this LED indicator should be extinguished at all times. If it is illuminated it signifies that an output current exceeding 20 mA is being provided by the instrument. To prevent this current over-range condition from occuring, the 'Max Velocity' Rotary switch (see III 4.1) should be set to a higher value.

APPENDIX H

INDUSTRIAL VERSION OF THE UDBV INSTALLED AND TESTED AT ERGO, ROSSING URANIUM AND THE CHAMBER OF MINES

Fig. H.2 Photograph of the inside of the UDBV

Fig. H.1 Photograph of

Industrial version of the UDBV